Mechanistic Studies of Surface-Confined Electrochemical Proton Coupled Electron Transfer

A Thesis Submitted to

The College of Graduate Studies and Research

In Partial Fulfillment of the Requirements

For the Degree of Doctor of Philosophy

In the Department of Chemistry

University of Saskatchewan

By

Wenbin Zhang

Department of Chemistry

University of Saskatchewan

Permission to Use

In presenting this thesis in partial fulfillment of the requirements for a Postgraduate degree from the University of Saskatchewan, I agree that the Libraries of this University may make it freely available for inspection. I further agree that permission for copying of this thesis in any manner, in whole or in part, for scholarly purposes may be granted by the professor Ian J. Burgess who supervised my thesis work or, in his absence, by the Head of the Department or the Dean of the College in which my thesis work was done. It is understood that any copying or publication or use of this thesis or parts thereof for financial gain shall not be allowed without my written permission. It is also understood that due recognition shall be given to me and to the University of Saskatchewan in any scholarly use which may be made of any material in my thesis.

Requests for permission to copy or to make other use of material in this thesis in whole or part should be addressed to:

The Head
Department of Chemistry
University of Saskatchewan
Saskatoon, Saskatchewan S7N 5C9
Canada

Abstract

Mechanistic studies of electrochemical proton coupled electron transfer (PCET) have attracted attention for many decades due to their importance in many fields ranging from electrocatalysis to biology. However, mechanistic research is confined to only a few groups, and challenges in this field can be found in both theory and experiment. The contributions to mechanistic studies of electrochemical PCET reaction in this thesis can be categorized under the following two headings: 1) mechanistic studies of an aminobenzoquinone modified monolayer system with multiple electron/proton transfer reaction; 2) studies that attempt to develop the relationship between thermochemical data and electrochemical PCET mechanism.

An aminobenzoquinone modified monolayer showing nearly ideal electrochemical behavior and high stability was successfully prepared and used as a model system for the mechanistic study of electrochemical multiple electron/proton transfer. This model system has been proposed to undergo a 2e3H transfer at low pH electrolyte and a 2e2H transfer at high pH electrolyte. Two non-destructive electrochemical techniques (cyclic voltammetry and chronocoulmetry) have been applied for the measurement of apparent standard rate constant as a function of pH. Both pH dependent apparent formal potential and pH dependent apparent standard rate constant have been used to determine the charge transfer mechanism of this monolayer system.

Under the assumption of an operative PCET mechanism (i.e. electron transfer step is the rate determining step), a theoretical description of this system has been developed based on the refinement and extension of previous models. By combining this extended theoretical model with pH dependent apparent formal potential and apparent standard rate constant, charge transfer pathways have been determined and shown to be consistent with the observed pH dependent electrochemical response, in

addition, the determined pathways in this aminobenzoquinone modified monolayer are similar to previous reported pathways for benzoquinone freely dissolved in aqueous buffered electrolyte.

A series of analytical expressions built in this thesis demonstrate that the parameters that differentiate stepwise mechanisms from concerted mechanisms can be classified into two aspects: thermodynamic parameters, namely acid dissociation constants, standard formal potentials; and kinetic parameters, namely standard rate constants, standard transfer coefficients. Although attempts to understand the relation between controlling parameters and electrochemical PCET mechanism (stepwise versus concerted) has been reported previously by some groups, there are still lots of unresolved aspects requiring further investigation. In this thesis, an important conclusion has been drawn which is that for the stepwise mechanism, an apparent experimentally observable kinetic isotope effect (KIE) can be induced by solvent isotope induced variation of acid dissociation constants, which contradicts previous understanding that the experimental measurement of an apparent KIE can only arise when the system is controlled by a concerted mechanism. Additionally, for the first time, values of apparent KIE, which were measured for the aminobenzoquinone modified monolayer system with stepwise PCET mechanism, were successfully explained by variation in acid dissociation constants, not by variation in standard rate constants.

Based on theoretical prediction, a nitroxyl radical modified bilayer showing one electron one proton transfer reaction has been prepared in an effort to afford experimental verification. After applying similar analytical procedures as those for the aminobenzoquinone modified monolayer system, this bilayer system has been shown to follow the concerted 1e1H transfer pathway in high pH electrolytes. These latter contributions provide evidence that further development in this field will eventually lead to a comprehensive theory that can use known thermochemical variables to fully predict PCET mechanism.

Acknowledgements

I would like to sincerely acknowledge my supervisor, Professor Ian J. Burgess, for giving me this opportunity to work on this interesting Ph.D. project. I would like to express my appreciation to his consistent support, his excellent guidance and especially his infinite patience with my thesis writing. It was really a pleasure to work with him and this experience will benefit not only for my future research ambitious but also my future teaching skill.

I would also like to thank all the members of my advisory committee: Professor Andrezej Baranski, Professor Richard Bowles and Professor Yuanming Pan for their invaluable suggestions and advice which has helped me complete this project. I also want to give the special gratitude to my external examiner Professor Hua-Zhong (Hogan) Yu from Simon Fraser University. His invaluable advice on my research project is much appreciated.

My sincere thanks to all the former and present members of the Burgess Group: Vivek, Scott, Tyler, Michelle, Jessica, Kevin, Brook and Morag for their contributions to a friendly working atmosphere. Special thanks to all the Lab managers: Dr. Alexandra Bartole-Scott, Dr. Swarnam Ravindran and Dr. Valarie Mackenzie. As a former physics student, I really believe teaching chemistry in the lab is an excellent experience.

Thanks to Natural Sciences and Engineering Research Council of Canada and University of Saskatchewan for the consistent financial support. It has been a great pleasure to pursue my Ph.D. research in Saskatoon.

Finally, I would like to express my deepest gratitude to my parents and my sisters for their unwavering love, support and encouragement throughout my life.

Dedication

To my parents,

张祖松

&

彭木秀

With love

To study the phenomena of nature in order to acquire knowledge

（格物致知）

-Book of Rites (~43BCE)

Table of Contents

List of Figures

List of Tables

List of Schemes

List of Abbreviations, Symbols and Ematical Terms

aBQ: aminobenzoquinone

AC: alternating current

AUT: 11-amino-1-undecanethiol

CV: cyclic voltammetry

cc: concerted

cpet: concerted proton coupled electron transfer

C_{18}TEMPO: 4-octadecaneamido- 2, 2'-6, 6'-tetramethyl-1-piperidynyloxy radical

DOS: density of states

ept: electron-proton transfer

ET: 1-ethanethiol

HAT: hydrogen atom transfer

HT: 1-hexanethiol

MBA: 4-mercaptobenzoic acid

MOA: 8-mercaptooctanoic acid

OT: 1-octanethiol

pet: proton-electron transfer

PCET: proton coupled electron transfer

sw: stepwise

TEMPO: 2, 2'-6, 6'-tetramethylpiperidine-1-oxyl radical

TEMPOH: 2, 2'-6, 6'-tetramethylpiperidine-1-oxyl hydroxylamine

$M\cdots HZ_j$: associated complex preceding concerted PCET charge transfer, M represent the species involving in the PCET reaction

$MH\cdots Z_j^-$: associated complex following concerted PCET charge transfer

F: faradic constant

f: Faraday's constant divided by molar thermal energy, i.e. F/RT

q: charge

k_B: the Boltzmann constant

i: current

Γ: surface concentration of species in overall PCET reaction

θ : fractional amount of oxidized redox centres on the electrode surface

υ : scan rate

ε_f : Fermi level

λ : reorganization energy

λ_i : reorganization energy of internal coordinates

λ_{ET} : reorganization energy of electron transfer in solvent

λ_{PT} : reorganization energy of proton transfer in solvent

α : transfer coefficient

α_i : standard transfer coefficient for single electron transfer

$\alpha_{cpet,j}$: standard transfer coefficient for simple 1e1H concerted PCET process involving proton donor species j

$k_{c:}$ cathodic reaction rate constant

$k_{a:}$ anodic reaction rate constant

$\Delta G^{\neq}$: activation energy

$\Delta G_a^{\#}$: activation energy of the anodic reaction

$\Delta G_{0a}^{\#}$: activation energy of the anodic reaction under equilibrium condition

$\Delta G_c^{\#}$: activation energy of the cathodic reaction

$\Delta G_{0c}^{\#}$: activation energy of the cathodic reaction under equilibrium condition

In the following terms, A and B represent species participating in the overall PCET reaction

$\alpha_{app,AB}^{sw,std}$: apparent standard transfer coefficient for global stepwise PCET from A to B

$\alpha_{app,AB}^{sw,c}$: apparent cathodic transfer coefficient for global stepwise PCET from A to B

$\alpha_{app,AB}^{sw,a}$: apparent anodic transfer coefficient for global stepwise PCET from A to B

$\alpha_{app,AB}^{cc,std}$: apparent standard transfer coefficient for global concerted PCET from A to B

$\alpha_{app,AB}^{cc,c}$: apparent cathodic transfer coefficient for global concerted PCET from A to B

$\alpha_{app,AB}^{cc,a}$: apparent anodic transfer coefficient for global concerted PCET from A to B

$\alpha_{app,AB}^{a}$: apparent anodic transfer coefficient for global mixed stepwise and concerted PCET from A to B

$\alpha_{app,AB}^{std}$: apparent standard transfer coefficient for global mixed stepwise and concerted PCET from A to B

$\alpha_{app,AB}^{c}$: apparent cathodic transfer coefficient for global mixed stepwise and concerted PCET from A to B

α_{app}^{std} or $\alpha_{app}(\eta = 0)$: apparent (observable) standard transfer coefficient for an aminobenzoquinone modified monolayer system

E: external potential

E_{pa}: anodic peak potential

E_{pc}: cathodic peak potential

$E^{0/}$: formal potential

$E_i^{0/}$: formal potential for simple electron transfer step i

$E_{cpet,j}^{0/}$: formal potential for simple 1e1H concerted PCET process involving proton donor species j

$E_{cpet,AB}^{0/,sw}$: apparent formal potential for global stepwise PCET from A to B

$E_{cpet,AB}^{0/,cc}$: apparent formal potential for global concerted PCET from A to B

$E^{0/}_{app,AB}$: apparent formal potential for global mixed stepwise and concerted PCET from A to B

η: overpotential

η_i: standard overpotential for single electron transfer *i*

$\eta_{cpet,j}$: standard overpotential for simple 1e1H concerted PCET process involving proton donor species *j*.

$\eta^{sw}_{app,AB}$: apparent overpotential for global stepwise PCET from A to B

$\eta^{cc}_{app,AB}$: apparent overpotential for global concerted PCET from A to B

$\eta_{app,AB}$: apparent overpotential for global mixed stepwise and concerted PCET from A to B

$k_{s,i}$: standard rate constant for single electron transfer step *i*

$k_{c,i}$: cathodic rate constant for single electron transfer step *i*

$k_{a,i}$: anodic rate constant for single electron transfer step *i*

$k^{cpet}_{s,j}$: standard rate constant for simple 1e1H concerted PCET process involving proton donor species *j*

$k^{sw,std}_{app,AB}$: apparent standard rate constant for global stepwise PCET from A to B

k^{std}_{app}: apparent (observable) standard rate constant for the experimental systems

$k^{c,a}_{app}$: apparent (observable) rate constant (cathodic and anodic) for an aminobenzoquinone modified monolayer system

$k^{sw,c}_{app,AB}$: apparent cathodic rate constant for global stepwise PCET from A to B

$k^{sw,a}_{app,AB}$: apparent anodic rate constant for global stepwise PCET from A to B

$k^{cc,std}_{app,AB}$: apparent standard rate constant for global concerted PCET from A to B

$k^{cc,c}_{app,AB}$: apparent cathodic rate constant for global concerted PCET from A to B

$k_{app,AB}^{cc,a}$: apparent anodic rate constant for global concerted PCET from A to B

$k_{app,AB}^{a}$: apparent cathodic rate constant for global mixed stepwise and concerted PCET from A to B

$k_{app,AB}^{std}$: apparent standard rate constant for global mixed stepwise and concerted PCET from A to B

$k_{app,AB}^{a}$: apparent anodic rate constant for global mixed stepwise and concerted PCET from A to B

$K_{a,j}$: acid dissociation constant for *j*th proton donor species involving simple 1e1H concerted PCET process

$K_{I,j}$: equilibrium constant for formation of *j*th preceding complex involving simple 1e1H concerted PCET process

$K_{II,j}$: equilibrium constant for formation of *j*th following complex involving simple 1e1H concerted PCET process

K_a : acid dissociation constant for single proton transfer step a of the PCET reagent

Chapter 1: Introduction and Literature Review

1.1 General Introduction

Mechanistic studies of an important charge process, namely electrochemical proton coupled electron transfer (PCET), are the main subject of this thesis. Due to its broad applications in diverse fields ranging from catalysis to biology, PCET has attracted intensive attention for many decades[1-16]. Hydrogen atom transfer, is now considered a subclass of PCET, and was studied much earlier than the first proposal of the PCET concept[16-23]. An important concern relevant to this fundamental physical chemical reaction is the determination of its mechanism, and this is the overarching goal of this body of work. In this introduction and literature review, the PCET reaction will be formally defined and illustrated through various important examples, in additions, the kinetics of elementary steps in a PCET reaction will be described using the Butler-Volmer equation and Marcus Density of State theory.

1.2 Proton Coupled Electron Transfer

It shouldn't be surprising to raise the concept of "electron transfer" without any advanced explanation in an electrochemical thesis since the electron transfer reaction has fundamental interest and broad application in chemical science and is an integral subject to the electrochemist. Over the past decades, electron transfer studies have started to be extended from one body systems (simple electron transfer) to many body systems (ion coupled electron transfer) in areas spanning from theory to industrial applications. Due to its broad existence in nature, the so called proton coupled electron transfer (PCET) reaction, which involves the overall transfer of both protons and electrons, has become one of the most interesting examples of a many bodied electron transfer process. PCET reactions of interest include the conversion of water to oxygen and hydrogen[24-26] (solar energy conversion) and the reverse reaction, the reduction of oxygen which couples electrons and protons to produce water[27-30] (fuel

cell reaction). These simple examples illustrate how the coupling of electron and proton transfer is a crucial component in energy conversion processes.

In 1981, Meyer and co-workers were the first scientists to propose the concept of proton coupled electron transfer[31]. It is interesting to note that their reduction reaction (defined as the first example of proton coupled electron transfer reaction) was found to be from metal complex systems, which are well known to play a significant role in the development of electron transfer studies[32]. For historical accuracy it should be noted that the hydrogen atom transfer (HAT) reaction was actually discussed in the literature prior to 1981, but as will be discussed in detail, HAT can be treated as a subclass of PCET. According to Mayer's definition[13;14], HAT is the transfer of a hydrogen radical, which is formally equivalent to a proton and an electron. This transfer can proceed through two possibilities; one where the proton and the electron are accepted into the same bond (Eqn. (1.1)). Alternatively it is possible to imagine a situation where a proton and an electron are accepted at separate locations of the same species. For example, transition metal complexes that abstract H· from various substrates can accept the electron at an oxidizing metal center (M^{m+}) and add the proton at a basic ligand (L:)(Eqn. (1.2)).

$$X\bullet + H\text{-}R \rightarrow X\text{-}H + R\bullet \qquad (1.1)$$

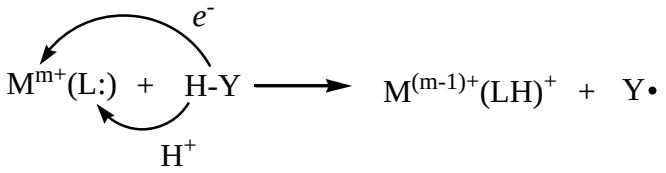

(1.2)

Equation 1.1 represents what would be considered a HAT whereas Equation 1.2 would not. However, it is clear that the bookkeeping is identical for both reactions, and as each reaction represents a formal transfer of a proton and an electron, each would be an example of PCET.

The continued and growing interest in PCET was illustrated at the first international conference on proton coupled electron transfer from biology to catalysis,

which was held in Paris, France in late 2011. The topics included important subjects such as catalysis, small molecule activation, biology, biochemistry, spectroscopy, mechanisms, energy conversion and energy storage. The large breadth of disciplines discussed in Paris demonstrates the ubiquitous nature of PCET reactions which can be further illustrated in the following short discussion. Many PCET events can be observed in biological reactions, such as in DNA and redox protein processes [1;4-7;33-35]. On the production of radicals by radiation in DNA, proton transfer reactions occur firstly because the formation of holes or the addition of an electron to a nucleobase strongly affects the acid dissociation constants of the nucleobases by orders of magnitude. The resulting species undergoes rapid proton coupled electron transfer reactions to form the final radicals. PCET events are crucial for the formation of ion radicals after the exposure of high energy radiation to DNA[6]. Another interesting biological reaction involving PCET takes place in protein redox machines[1], such as photosystem II and ribonucleotide reductase. To understand their inner workings, model systems of tyrosine and phenols appended with bases have been employed to study PCET reactions involving intramolecular proton transfer in aqueous solutions. The results have proved their importance in the design and construction of artificial photosynthetic machines to produce clean fuel from sunlight and water.

PCET also plays an important role in many industrial applications, for example, in terephthalic acid production induced by C-H oxidation of para-xylene [21-23], one of most important steps is the peroxyl radical removal of $H\bullet$ from the C-H bond. This crucial step is an obvious example of hydrogen atom transfer. Additionally, PCET reactions are crucial for the operation of both fuel cells and solar cells, a prototypical example of the former being the direct methanol fuel cell[28;29;36]. The production of charge from this system is from two half-cell reactions, the anodic reaction involves methanol oxidation to form carbon dioxide by transferring six protons and six electrons, and the cathodic reaction is oxygen consumption to produce water with the accepting of six protons and six electrons. It can be concluded that the overall reactions at both the anode and the cathode are proton coupled electron transfer reactions. Also in the energy conversion area, the design of new catalysts for

conversion between water and oxygen is extremely crucial for economic interests [25;26;37-46], as well as for fundamental research[47-57]. It should be kept in mind that the water splitting reaction is a PCET process and understanding the details of such reactions are very important in catalyst design. Any insight into the mechanism of these PCET reactions that can be gained from fundamental studies offers the potential to tremendously impact this important field and the area of energy conversion.

In studies of electron transfer reactions, redox molecules can be used as the electron donor/acceptor, with non-polarized electrodes serving as the complement acceptor/donor. As for the proton acceptor/donor, it is well known that any Brønsted-Lowry acid can act as a proficient proton donor and its conjugative base as the corresponding proton acceptor for the reverse reaction. If a redox molecule shuttles electrons in PCET, the driving force of such PCET reactions can only be controlled by fundamentally changing of the nature of the participating species. However, in another case, a metal electrode can be used as the electron donor/acceptor and the relating electron transfer reaction can be defined as a heterogeneous electron transfer reaction whose driving force can be easily and continuously varied by controlling the applied potential. Recently a semiconducting metal oxide was started to be used as the electron donor/acceptor in the PCET studies[58], and this first example was provided by Mayer and his co-workers. They basically combined zinc oxide nanoparticles with stable radicals to perform PCET reactions in which electrons come from the conduction band of the semiconductor materials and protons are present at the surface of the semiconductor nanocrystals. Using a semiconductor as the electron acceptor/donor for PCET reactions is intriguing considering its applications in solar energy conversion. The form of proton coupled heterogeneous electron transfer as shown in Scheme 1.1 has now been defined as electrochemical proton coupled electron transfer and the study of these types of PCET reactions is the subject of this thesis. Meanwhile, in this thesis, the proton is considered to be provided by water or hydronium ions depending on the solution pH. Despite the attentions of several high-profile electrochemical researchers, most notably Finklea in the United States and Costentin in France, there is still very little

known about the mechanism of electrochemical PCET.

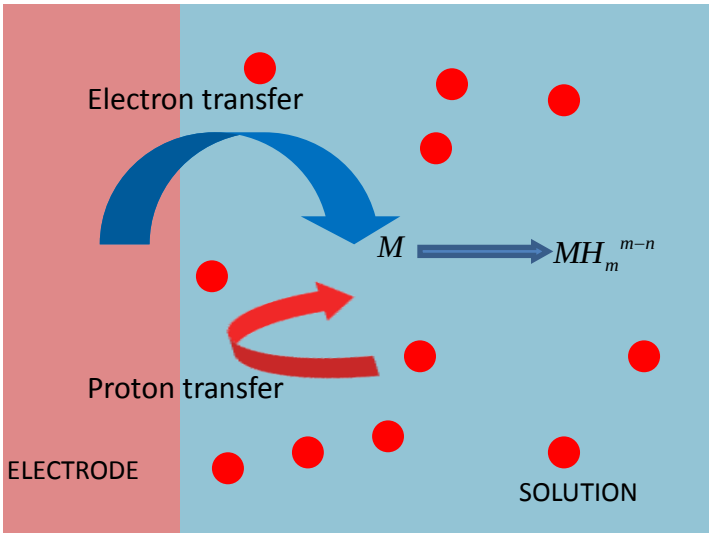

Scheme 1.1: Schematic representation of electrochemical proton coupled electron transfer.

Theoretical and computational considerations of the PCET reaction have been performed by Cukier's group[2; 16] and Hames-Schiffer's group[9-12; 18; 59-61]. Both of them have derived quantum mechanical models that provide rate constant expressions for one subcase of 1e1H transfer reactions, in which both an electron and a proton transfer during a single kinetic step, however, the above theoretical models are greatly limited by the fact that there are experimental inaccessible. To verify many of their conclusions, the Marcus theory of cross relation, in which the rate constant can be calculated by the self-exchange rate constant and the equilibrium constant, has been proved by Mayer and his co-workers[13;17;62-64] to be able to predict the rate constant of hydrogen atom transfer reaction. More interestingly, this Marcus cross relation which can be obtained from electron transfer theory is experimental accessible. Very recently, Meyer and his co-workers presented thermochemical data for acid dissociations, standard formal potentials of a range of PCET reagents[13], and then were able to show that the thermodynamic parameters are strongly correlated to PCET

mechanisms. To be more specific, a concept, bond dissociation free energy (BDFE), which is a function of pK_a and $E^{0/}$, was proposed to be able to offer qualitative insight to the determination of the PCET mechanism for any given reagent. It should be pointed out that the theoretical consideration described above is very disordered and up to now, no one has been able to provide an experimental accessible model for general PCET reactions.

In comparison with the extensive studies of other subcases of PCET particularly hydrogen atom transfer, investigations of electrochemical PCET reaction in both theory and experiment are very limited to date. Most contributions are from the groups of Liu[115-117], Laviron[15; 65-75], Finklea[76; 77] and Costentin[78-84]. Liu and his co-workers presented the fabrication and electrochemical characterization of an azobenzene monolayer with high surface coverage, which is probably the first system showing surface-confined electrochemical PCET behavior[115-117]. In this system, the overall charge transfer reaction involved two-electron, two-proton transfer and was observed between pH 3.2 and pH 8.6. Apparent standard rate constants were calculated by voltammetric measurements and a "V" shape was derived to describe the relationship between apparent standard rate constants and pH. However, the reaction mechanism of this system is very hard to determine due to the strong interaction between adjacent azobenzene molecules. In Costentin's group, the concerted one electron/one proton (1e1H) mechanism (CPET), defined as where one electron and one proton transfer during the same kinetic step, was fully discussed in both theory and experiment. In the theoretical aspect, they were able to prove that concerted 1e1H transfer can be treated as electronically non-adiabatic electron transfer reactions. It was stated that the term non-adiabatic electron transfer represents the case of weak electronic coupling of the electron donor and acceptor in comparison with the reorganization energy and thus the electron donor and the electron acceptor remain their identity. The theoretical treatment for concerted 1e1H transfer has been proved in experimental systems by Costentin and co-workers, who have measured the rate constants of many redox molecules in bulk solution systems using cyclic voltammetry. Theoretical consideration of stepwise mechanism was initialized by

Laviron and then modified by Finklea. Experimentally, Finklea's group was the first one to study electrochemical PCET reaction using electroactive monolayer systems. They have built two 1e1H monolayer systems: galvinol modified monolayer and osmium aquo-complex modified monolayer. It is regrettable that Finklea and his co-workers weren't able to show the complete kinetic analysis for the above two monolayer systems, even for those simple 1e1H systems, although Finklea is the first one to build a theory of stepwise PCET mechanism for redox coupled attached on metal electrodes[76].

In the above discussions of electrochemical PCET, both stepwise and concerted mechanism were mentioned but without explicit statements. Both mechanisms in the 1e1H case can be shown in Scheme 1.2, where M is the redox molecule and HZ is the proton donor. In the electrochemical PCET reaction with stepwise mechanism, electron transfer is the rate determining step and proton transfer doesn't play any contribution in the kinetics. There are two stepwise pathways: proton transfer followed by electron transfer (pet), or electron transfer followed by proton transfer (ept). The relative contributions of the ept and pet pathways depend on the pH of the electrolytes. Concerted proton coupled electron transfer (CPET) mechanism can be simply described by a single kinetic step involving both one proton transfer and one electron transfer. It is clear that above statements aren't enough to be used for the derivation of rate constant expressions, especially with the consideration of the possibility of different proton donors/acceptors for concerted mechanism. More specific pathways for concerted mechanism will be discussed later on in this thesis. It can be expected that for any electrochemical PCET reaction including one electron one proton transfer, as well as multiple electron and proton transfer, the derivation of the rate constant expression should rely on the elementary steps of single electron transfer and concerted 1e1H kinetics, and those will be described in the following section of this chapter.

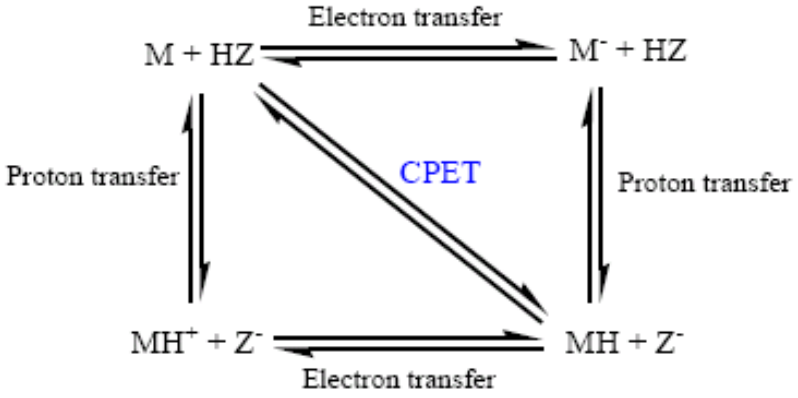

Scheme 1.2: Four member square scheme showing 1e1H PCET transfer mechanism.

1.3 Electron Transfer and Chemically Modified Monolayers

Any event where an electron moves from a chemical species or an atom to another chemical species or atom is called as electron transfer, and the movement of electrons induces a current. In electrochemistry, an anode reaction is one where electrons are passed from redox species in solution or adsorbed on the electrode to the external circuit. A cathode reaction is one where electrons are transferred from an external circuit to redox species in solution or adsorbed on the electrode.

As shown in Scheme 1.3, a one electron transfer process can be described by the donor (D)-barrier (B)-acceptor (A) structure. In this DBA structure, both electron donor and acceptor can be redox molecules or one can be an electrode. The types of barriers include different supporting electrolyte (aqueous, organic solvent or ionic liquid), carbon chains, and even weakly conductive materials. Depending on the barrier, an electron transfer process can be discussed in terms of either an inner sphere electron transfer or an outer sphere electron transfer. For the former, the participating redox couples (electron donor and acceptor) are connected by a covalent linkage, however, for the outer sphere electron transfer, the electron is forced to move through space from the electron donor to the electron acceptor as the electron donor and acceptor are not chemically connected. In this thesis, the electrons move between

redox molecules on the electrolyte side of the interface and the solid metal electrode, in which both electron donor and acceptor remain separate after the electron transfer event.

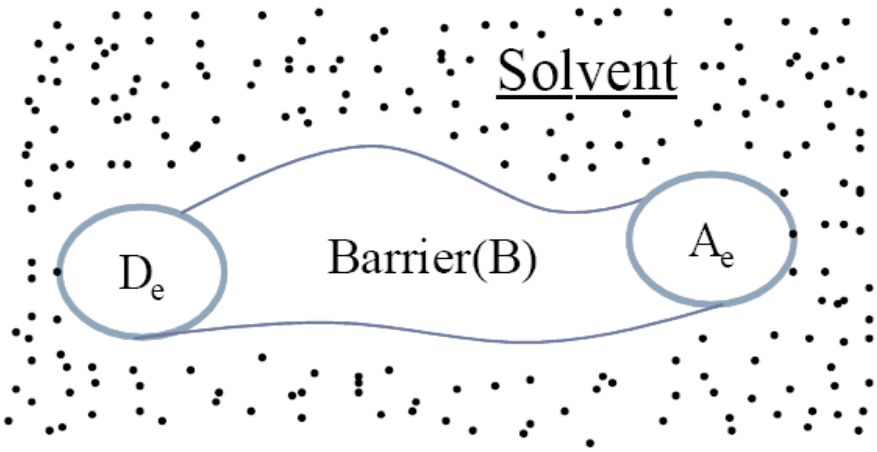

Scheme 1.3: Schematic depiction of a general donor/barrier/acceptor system.

In comparison with redox couples in the bulk of solution, the kinetic analysis of redox couples attached to electrodes is much easier because the total concentrations of reduced chemical species and oxidized chemical species remains constant under any applied potential, and calculations of rate constants are unencumbered by mass-transfer effects. The signals from electrochemical instruments are directly related with the electron transfer process. The above description suggests the building of redox molecule modified electrode in this thesis, and one experimental challenge is the design of strategies that can produce chemically modified monolayers with the attachment of redox couples.

Chemical modification of an electrode with metal particles and semiconductor particles has been used for the purpose of electrocatalysis[85-93]. Several polymers were shown to assemble onto electrode surfaces using various modification techniques[94-97], such as ion exchange reactions, coordination of redox molecules through intermolecular forces, and surface polymerization of redox species. The resulting thickness of polymers ranges from nanometers to micrometers. The inner structure of this polymer modified electrode is homogeneous, which may be important for the

fundamental studies of electron transfer coupled ion transportation from electrolyte. It has also been reported that electrostatic forces and/or hydrophobic forces can be used to form chemically modified monolayers[98-102]. Preparation techniques have been well reviewed elsewhere[101], and won't be revisited in this thesis. Due to their ease of fabrication, redox-active self-assembled monolayers (SAMs)[118] were chosen as the means to prepare PCET active monolayers in this thesis. A representative SAM structure is shown in Scheme 1.4. As it is shown, organic molecules are attached onto substrates and form close-packed arrangements which are largely driven by van der waal interactions.

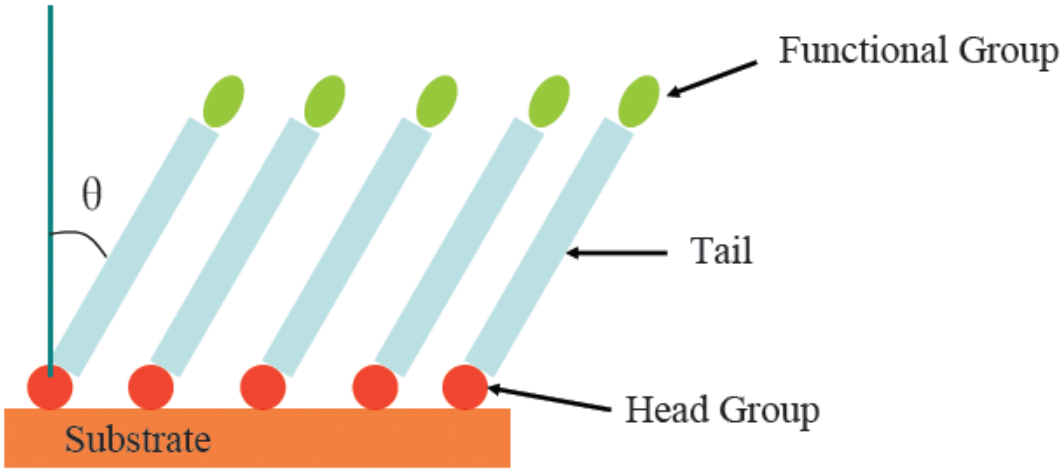

Scheme 1.4: Representation of a SAM structure.

A SAM usually consists of a substrate, a head group, a tail and a functional group. Due to its chemical inertness, gold was chose as the substrate for the chemically modification. More importantly, Au was chosen because of the strong affinity between Au and the thiol group. Thiols, which are the most important reagent in the development of SAMs, spontaneously generate covalent bonds between gold and the sulfur-containing head group. Infrared spectroscopy studies have proved that the alkanethiol chains are, on average, tilted from the surface normal by 30 ± 10^{o} on Au (111)[119; 120]. The resulting Au-S bond has a bond energy of 167-209 kJ/mol[101], which provides the high stability needed for experimental objectives. Different functional

groups (e.g. amine group, carboxylic group, quinone group) are assembled onto the electrode due to their applications in fundamental research and industry.

1.4 Electron Transfer Kinetics

Two mechanisms for the electrochemical PCET reaction, namely the stepwise and concerted pathways, have been introduced above. In the stepwise mechanism, the electron transfer steps are the rate determining steps. For example, for stepwise 1e1H transfer reaction, the rate constant for the whole PCET reaction is determined by the mixture of two single electron transfer steps upon protonation/deprotonation. It can be easily expected that for multiple proton and electron transfers, there will be more than two single electron transfer steps in the determination of an apparent rate constant (the experimental measurable rate constant for the whole PCET reaction). Clearly, for the stepwise mechanism, one only needs to slightly modify existing electron transfer models to describe the kinetics of the PCET reaction. Two such models exist for simple electron transfer reactions; one described by the Butler-Volmer equation[103;104] and the other based on Marcus theory[105-108]. The Butler-Volmer equation is named after chemists John Alfred Valentine Butler and Max Volmer, and this semi-empirical equation describes how the electrical current depends on the applied electrode potential. This current-potential relationship, which can be directly obtained from experimental measurement, provides an expression for the heterogeneous rate constant. Marcus theory was developed by Rudolph A. Marcus in the 1960s to calculate the rate constants of electron transfer reactions, and led to a Nobel Prize being award to Marcus in 1992. The details and descriptions of both the Butler-Volmer equation and Marcus theory will be shown in the following section, as well as the mathematical relationship between these two models. It is worth to mention beforehand that understanding electron transfer kinetics is crucial to the derivation of rate constant expressions of both stepwise and concerted mechanisms.

1.4.1 The Butler-Volmer Equation

The first phenomenological model of electrode reaction kinetics, what is now

known as the Butler-Volmer (B-V) equation, was proposed by Butler in 1924 and then modified by Volmer in 1930. The B-V equations is based on the Arrhenius equation, which was proposed by van't Hoff and then shown by Arrhenius to be a simple, but remarkably meaningful means for the calculation of a chemical reaction rate constant. This equation served as the basis for the most successfully description of electron transfer kinetics for about one hundred years until being superceded with the development of quantum mechanics.

The elementary reaction for the subsequent discussions is shown in Equation (1.3)

$$Ox + e \underset{k_a}{\overset{k_c}{\rightleftarrows}} \mathrm{Re}d \tag{1.3}$$

where k_c and k_a are the cathodic and anodic reaction rate constants, respectively.

The overall rate of electron transfer v is related to the net current by the following Eqn. (1.4)

$$v = \frac{i}{FA} = \frac{i_a - i_c}{FA} = k_a \Gamma_{\mathrm{Re}d} - k_c \Gamma_{Ox} \tag{1.4}$$

Where $\Gamma_{\mathrm{Re}d}$ and Γ_{Ox} represent the concentrations of reduced species and oxidized species, respectively. In a system where the redox couples are dissolved in aqueous solutions, both $\Gamma_{\mathrm{Re}d}$ and Γ_{Ox} at different potentials depend at least partially on mass-transport mechanisms and are related to the known initial concentration of redox molecules in the bulk of solution. However, for systems where the redox couples are attached to electrodes, the total concentration of reduced and oxidized species stays constant at any potential.

The Arrhenius equation is shown in Eqn. (1.5), in which k is the electron transfer rate constant, $\Delta G^{\neq}$ is the activation energy, R is the universal gas constant, A is the pre-exponential factor and T is the temperature.

$$k = A \exp(-\frac{\Delta G^{\neq}}{RT}) \tag{1.5}$$

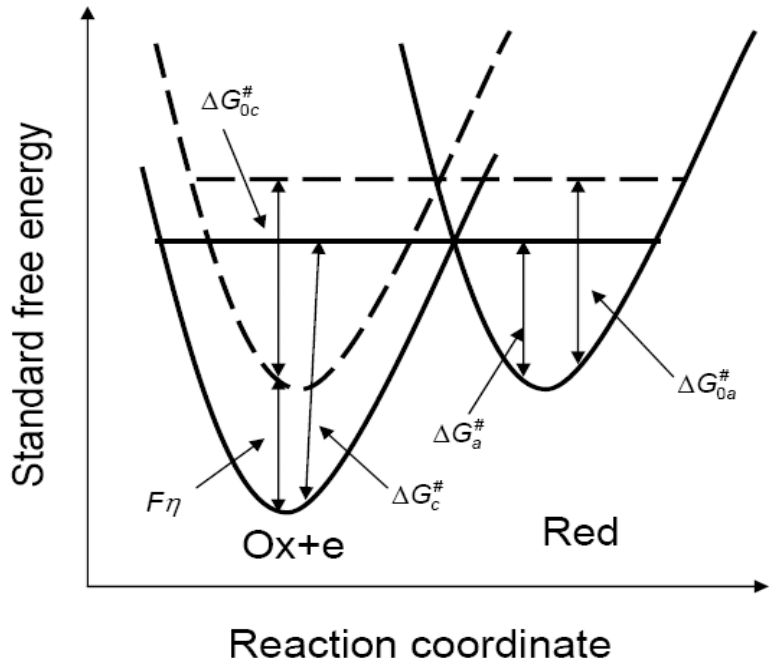

Figure 1.1: Effects of change in potential on the energy barrier for an electron transfer reaction.

A potential diagram for reaction (1.3) is shown in Figure 1.1. The standard free energy of reactant/product upon electron transfer without any applied potential as a function of reaction coordinate is shown by the solid line of Figure 1.1. As shown, electron transfer is thermodynamically unfavoured at the initial state. Standard free energy of the oxidized species becomes larger with increasing external potential, while more and more electrons reside in the bands of oxidized species. The standard free energy of oxidized species is indicated by a dashed line when electron transfer reaches equilibrium. Meanwhile, standard free energy of reactant equals that of the product. At this equilibrium condition, the cathodic rate constant is the same as the anodic rate constant, and is defined as the standard rate constant of an electron transfer reaction. The value of standard rate constant k_s depends on the nature of the electron transfer system. The standard formal potential $E^{0\prime}$ is defined as the applied potential at equilibrium conditions relative to the reference electrode. An overpotential, η, is calculated by the subtraction of the standard formal potential from the applied potenital, as shown in Eqn. (1.6).

$$\eta = E - E^{0/} \tag{1.6}$$

In order to complete the derivation of rate constant expressions based on Eqn. (1.5), the Gibbs free energy will be extended as below. Figure 1.1 shows the relationship between the energy barrier of the anodic reaction $\Delta G_a^{\#}$ and that of the cathodic reaction $\Delta G_c^{\#}$:

$$F\eta + \Delta G_{0c}^{\#} - \Delta G_{0a}^{\#} = \Delta G_c^{\#} - \Delta G_a^{\#}$$

If we define that $\Delta G_c^{\#} - \Delta G_{0c}^{\#} = \alpha F\eta$ (1.7a)

It follows that $\Delta G_{0a}^{\#} - \Delta G_a^{\#} = (1-\alpha)F\eta$ (1.7b)

Where $\Delta G_{0a}^{\#}$ and $\Delta G_{0c}^{\#}$ are the energy barriers for the anodic reaction and the cathodic reactions under equilibrium conditions, and α is the transfer coefficient.

As explained by Eqn. (1.7), the transfer coefficient α, or symmetry factor, indicates the conversion ability from potential to free energy for both the anodic part and cathodic part. This value of transfer coefficient is dependent on the symmetry of the energy barrier for the oxidized species and the reduced species, as shown in Figure 1.2. The standard transfer coefficient of an electron transfer reaction, which is the value of transfer coefficient at zero overpotential, is often assumed to be ½ in many kinetic analyses.

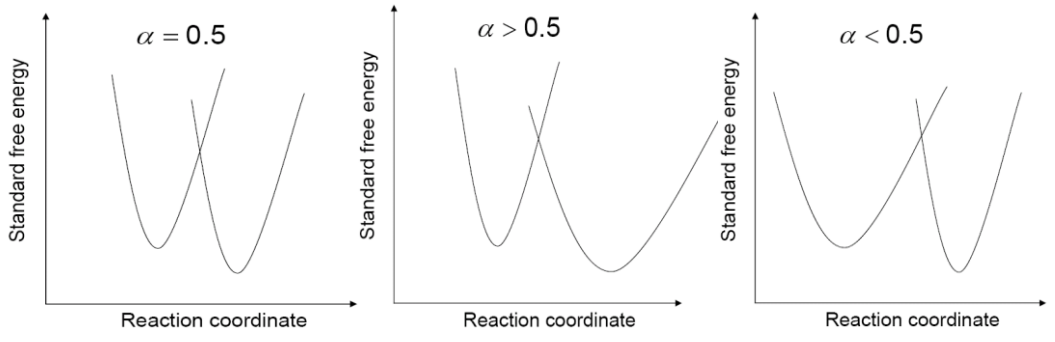

Figure 1.2: Schematic representative of energy barrier symmetry for different transfer coefficients (α=0.5, α>0.5, and α<0.5).

Combining Eqn. (1.5) with Eqn. (1.7), the rate constant expressions for both the cathodic reaction and the anodic reaction become:

$$k_a = A_a \exp(-\frac{\Delta G_a^{\#}}{RT}) = A_a \exp(-\frac{\Delta G_{0a}^{\#}}{RT}) \exp(\frac{(1-\alpha)F\eta}{RT}) \quad (1.8a)$$

$$k_c = A_c \exp(-\frac{\Delta G_c^{\#}}{RT}) = A_c \exp(-\frac{\Delta G_{0c}^{\#}}{RT}) \exp(\frac{-\alpha F\eta}{RT}) \quad (1.8b)$$

Therefore, the standard rate constant for $\eta = 0$ can be expressed by:

$$k_s = A_a \exp(-\frac{\Delta G_{0a}^{\#}}{RT}) = A_c \exp(-\frac{\Delta G_{0c}^{\#}}{RT}) \quad (1.9)$$

The expressions for k_a and k_c can be rewritten as:

$$k_c = k_s \exp(-\alpha f\eta) \quad (1.10a)$$

$$k_a = k_s \exp((1-\alpha) f\eta) \quad (1.10b)$$

Where $f = \frac{F}{RT} = 38.92V^{-1}$ at 25℃

The resulting plots from Eqn. (1.10) are called Tafel plots, and can be used to determine transfer coefficients from experimental results.

The Butler-Volmer equation, which shows the current-potential relationship, is then obtained by combining Eqns. (1.4), (1.5) and (1.8)

$$i = FAk_s(\Gamma_{Red} \exp((1-\alpha) f\eta) - \Gamma_{Ox} \exp(-\alpha f\eta)) \quad (1.11)$$

The above equation has been proven in many electron transfer reactions. As will be shown in Chapter 3, Eqn. (1.11) provides a means to calculate both standard rate constants and transfer coefficients using the measurement of cyclic voltammetry.

1.4.2 Marcus Density of State Theory

Although the Butler-Volmer equation has been successfully applied to many experimental systems, it is still a very crude model because the participant parameters in that equation don't reflect the nature of an electron transfer system. As shown in Eqn. (1.10), the only controlling parameters for the cathodic and anodic rate constants

are the standard rate constant and the transfer coefficient. In the aspect of microscopic observation, important parameters such as the structure of the redox molecule, the electrode structure, and the nature and organization of the solvent should all affect the rate of electron transfer. Clearly these parameters are not reflected in Eqns. (1.10) or (1.11). Therefore it is necessary to build an alternative theoretical framework, which includes these microscopic parameters. The theory which will be described started with the work of Gurney and was then incorporated with that of Gerischer and Marcus[121; 122], and is commonly now referred to as Marcus DOS theory. In general, this model can be demonstrated in terms of nuclear configuration potential energy diagrams, electronic configuration potential energy diagrams and electron distribution functions. It also provides a theoretical framework that can predict the relationship between microscopic energies and macroscopic energies.

In solid state physics, band theory is usually used to interpret the electronic structure of metals. From the principles of quantum mechanics, energy states of electrons in atomic orbitals are discrete. One mole of metal consists of 10^{23} order of electrons, this huge amount of electrons leads to the overlap of individual energy states and results in the formation of a continuum or band of energy levels. For example, an "s" energy state of one atom can combine with its counterparts in neighboring atoms to form an "s" band. For the energy bands in a metal, semiconductor or insulator, the highest occupied band is the termed the valence band and the lowest unoccupied band is defined as the conduction band. The valence band of platinum is a mixture of "s" orbitals and "d" orbitals, and for gold and silver their valence band is built from only "s" atomic orbitals. A very important concept in band theory, is the density of state which describes the number of similar energy states (either occupied or unoccupied) per energy interval. The functional form of a solid's DOS is dependent on the structure and composition of the material.

Probability is a requisite concept in the description of the occupation of electrons in different band energies. The Fermi level refers to the band with 50% probability of electron occupation. In the absence of any thermal activation, the Fermi level will equal the highest energy level in the valence band. For semiconductor and insulator,

the electron occupying probability of the conduction band is closes to 0 and that of the valence band is close to 1. The electron transfer process must occur in those energy bands which are near the Fermi level, and the Fermi-Dirac distribution described below has been used to calculate the probability that a single state of energy would contribute/accept an electron during a redox process. From the Fermi-Dirac function (Eqn. (1.12)), it is clear to see that the probability is determined by the applied potential, *E*, and the Fermi energy of the electrode.

$$f(\varepsilon) = \frac{1}{1+\exp(\frac{\varepsilon}{k_B T})} \quad \text{(Cathodic reaction)}$$

$$f(\varepsilon) = \frac{\exp(\frac{\varepsilon}{k_B T})}{1+\exp(\frac{\varepsilon}{k_B T})} \quad \text{(Anodic reaction)} \qquad (1.12)$$

In which ε is the energy with respect to the Fermi level ε_f at which the electron is transferred, and k_B is the Boltzmann's constant.

For a redox molecule, since the oxidant and reductant have the same nuclear configuration, i.e. for a vertical transition according to Marcus theory, a Gaussian function can be used to describe its density of states and is shown in Eqn. (1.13).

$$G(\varepsilon,\ \lambda,\ \eta) = (4\pi\lambda k_B T)^{-1/2} \exp(\frac{-(\varepsilon-\lambda-e\eta)^2}{4\lambda k_B T}) \quad \text{(Density of acceptor states for } k_c\text{)}$$

$$G(\varepsilon,\ \lambda,\ \eta) = (4\pi\lambda k_B T)^{-1/2} \exp(\frac{-(\varepsilon+\lambda-e\eta)^2}{4\lambda k_B T}) \quad \text{(Density of donor states for } k_a\text{)} \qquad (1.13)$$

In which λ is the reorganization energy and η is the overpotential with respect to formal potential $E^{0/}$.

Eqn. (1.13) shows that the density of states is a function of the reorganization energy and the overpotential. The reorganization energy is the transfer energy of the redox molecule and its surrounding solvent from one equilibrium structure to another equilibrium structure without the involvement of charge transfer.

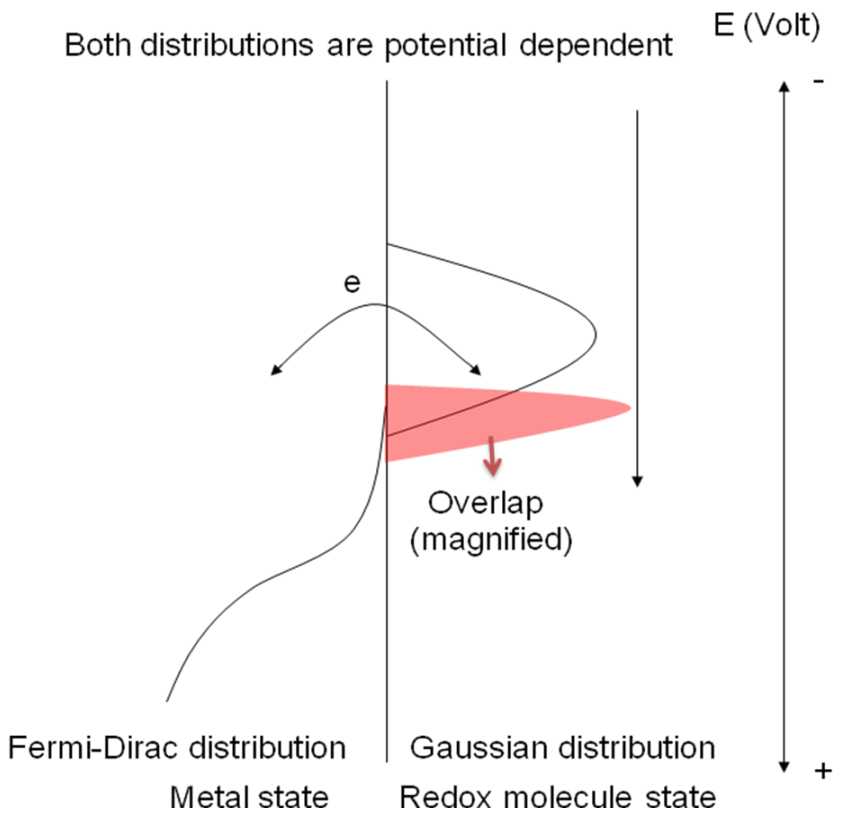

Figure 1.3: Electron transfer process shown by the overlap between the Fermi-Dirac distribution of metal states and a Gaussian distribution of redox molecule states.

For a cathodic reaction, the electron transfers from an occupied state of the electrode to an acceptor state of the redox molecule in the solution or on the surface, and vice versa for an anodic reaction. As shown in Figure 1.3 and Eqns.(1.12) and (1.13), both the cathodic rate constant and the anodic rate constant are expressed by the overlap between all possible energy states around the Fermi level of the electrode and all energy states of the redox molecule (Eqn. (1.14)). It is obvious that higher positive potential induces lower overlap between metal donor states and Ox acceptor states, which results in a smaller cathodic rate constant and a larger anodic rate constant.

$$k_{c,a} = Z\int G(\varepsilon,\ \lambda,\ \eta) f(\varepsilon) d\varepsilon \qquad (1.14)$$

Z is the electronic coupling factor, which is usually assumed to be energy state independent.

There is no need of integration under the simplifying assumption that the transfer

is confined to occur only at the Fermi energy. In such cases Eqn. (1.14) can be simplified to:

$$k_{c,a} = P\exp(\frac{-(\lambda \pm F\eta)^2}{4\lambda RT}) \tag{1.15}$$

where P is the constant, and it is only dependent on the nature of system.

1.4.3 Relationship between the Butler-Volmer Equation and Marcus Theory

The B-V equation can easily be applied to experimental systems because its expression is very analytical (albeit more empirical) in nature. Quantum mechanical principles are used to derive the Marcus DOS theory and arrive at a mathematical expression that views an electron transfer reaction in microscopic terms. Both Chidsey[109;110] and Forster et al[100] have presented compelling evidence that Marcus theory is significantly better than the classic Butler-Volmer equation in describing electron transfer over a board range of driving forces. The standard transfer coefficient in the Butler-Volmer equation is normally assumed to be 0.5, and deviations between the Marcus theory and the Butler-Volmer equation can be observed for low reorganization energy experimental systems. To achieve agreement between the two theoretical models, Finklea proposed that the transfer coefficient should be dependent on both overpotential and the reorganization energy[77]. He derived a fifth-order polynomial expression (Eqn. (1.16)) in order to accurately calculate transfer coefficients at different overpotentials.

$$\alpha(\eta) = 0.5 + a\eta + b\eta^3 + c\eta^5 \tag{1.16}$$

Table 1.1: Transfer coefficients for α(η) as a function of reorganization energy λ (adapted from reference)[77]

***λ*/eV**	**0.5 eV**	**0.7 eV**	**0.9 eV**	**1.2 eV**	**2.0 eV**
a	4.141×10^{-1}	3.082×10^{-1}	2.466×10^{-1}	1.899×10^{-1}	1.179×10^{-1}
b	-7.376×10^{-2}	-1.926×10^{-2}	-8.049×10^{-3}	-3.238×10^{-3}	-2.580×10^{-4}
c	9.882×10^{-3}	-9.978×10^{-3}	-3.785×10^{-3}	-8.334×10^{-4}	-2.788×10^{-3}

Table 1.1 shows the values of polynomial coefficients for the transfer coefficient at different reorganization energies. At high overpotential (e.g. 2.0 V), the transfer coefficient at small overpotential range is close to 0.5, which may significantly simplify experimental analysis and theoretical consideration. However, for small reorganization energy systems, it is more reasonable to describe the transfer coefficient as a function of overpotential and reorganization energy, so that it should be variable in any kinetic analysis. For the particular case where the electron transfer is confined to the Fermi level, the expression for the transfer coefficient can be derived from Eqn. (1.15), and it is shown in Eqn. (1.17). The α coefficients obtained from this equation are much larger than the α coefficients in Table 1.1, so that it is recommend to use Table (1.1) not Eqn. (1.17) to calculate the transfer coefficient obtained from Marcus DOS theory.

$$\alpha(\eta) = 0.5 + \frac{\eta}{4\lambda} \tag{1.17}$$

1.4.4 Kinetics of Concerted 1e1H Transfer

To fully understand the charge transfer mechanism of multiple proton and electron transfer, the kinetics of the concerted 1e1H transfer also needs to be introduced. There are four diabatic states for 1e1H concerted mechanism depending on the coupling strength between the electron donor and the electron acceptor or proton donor and proton acceptor, namely, electronically adiabatic PT and ET, electronically non-adiabatic PT and ET, and electronically adiabatic PT-non-adiabatic ET and electronically non-adiabatic PT-adiabatic ET. The electrochemical approach to concerted mechanism inherently assumes an electron transfer through the electrode/electrolyte interface and the usual theoretical description of heterogeneous electron transfer involving a coupling between two non-adiabatic states since the strength of the electronic coupling between the electron donor and electron acceptor is weak. In most cases, it is reasonable to assume that the proton donor and acceptor are connected by a hydrogen bond, which means that proton transfer is adiabatic. In other words, the rate-limiting steps involve two hydrogen bonded intermediates which both

electron and proton transfer in a single concerted step.

Figure 1.4 shows the potential energy diagram of a concerted 1e1H transfer reaction. Although roughly 2000 times heavier than an electron, a proton is still light enough to tunnel through a significant barrier, leading to a small proton transfer probability. In most practical cases where CPET takes place within an intermolecular hydrogen-bonded complex, the proton activation barrier is much larger than the proton vibrational ground state. However, the resonance energy is small compared to the proton activation barrier, so that the proton will be transferred by the tunneling mechanism. Based on the above discussion, electrochemical intermolecular CPET reactions can be categorized as electronically non-adiabatic electron transfer reactions[78;79;82], so that Marcus DOS theory can be used to describe the rate constant expression of this concerted 1e1H transfer.

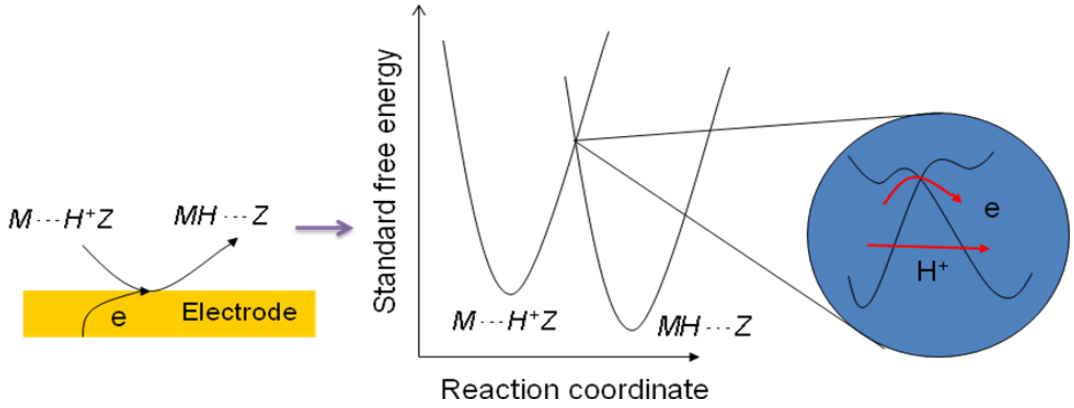

Figure 1.4: Adapted potential energy profiles for a concerted 1e1H transfer[78]

The rate constant expression for the concerted 1e1H transfer mechanism was derived by combining Eqn. (1.12), Eqn. (1.13) and Eqn. (1.14). As described in Eqn. (1.18), the independent parameters including λ and Z show different physical meaning in comparison with those parameters in the rate constant expression for simple electron transfer.

$$k_{c,a} = Z\int_{-\infty}^{+\infty}(4\pi\lambda k_B T)^{-1/2}\exp(\frac{-(\varepsilon \pm \lambda - e\eta)^2}{4\lambda k_B T})\frac{\exp\left(\frac{\varepsilon}{2}\pm\frac{\varepsilon}{2}\right)}{k_B T}}{1+\exp(\frac{\varepsilon}{k_B T})}d\varepsilon \quad (1.18)$$

The reorganization energy λ includes the internal reorganization λ_i, which is for the reorganization of internal coordinates, and two solvent ones λ_{ET} and λ_{PT} (the reorganization energy of electron transfer and proton transfer in solvent respectively). The internal reorganization energy can be estimated from quantum mechanical calculations, and the two solvent ones can be calculated from a simple electrostatic force model. *Z* is the pre-exponential factor, which is a function of electronic coupling constant, reorganization energy, and other parameters, proton barrier and quantum energy scale for the localization of the proton donor-acceptor vibrational wave function. A detailed expression of *Z* can be derived from simple quantum mechanics, and requires knowledge of the adiabatic proton potential profile at the transition state. An intrinsic kinetic isotope effect can be predicted from the expression for the pre-exponential factor due to its strong dependence on the parameters that affect proton tunneling.

Eqn. (1.18) has been successfully used for the kinetic analysis of many experimental systems. Meanwhile, mathematically it is reasonable to covert Eqn. (1.18) to an exponential expression, and this conversion can largely simplify the related theoretical analysis. However, the current discussion in the literature on theoretical considerations of concerted mechanism is still limited, and a general expression for concerted ion coupled electron transfer mechanism will be required in the future.

To summarize the theoretical consideration of both simple electron transfer kinetics and concerted 1e1H transfer kinetics, it can be concluded that the rate constant expressions of both mechanisms can be expressed as exponential functions. This conclusion is very useful since, in principles, it leads to the expectation that it

should be possible to derive the analytical expressions describing the rate constants for multiple electrons and protons transfer reactions.

1.5 Overview of the Thesis

This thesis consists of seven chapters. A brief introduction to the research background is given in Chapter 1 and the details of the experimental section including electrochemical techniques are provided in Chapter 2. Chapter 3 describes a preparation method used to form a nearly ideal aminobenzoquinone modified monolayer, which shows two electron, three proton transfer at low pH electrolyte and two electron, two proton transfer at high pH electrolyte. The discussion of proton coupled electron transfer mechanism based on extended stepwise mechanism is shown in Chapter 4. In Chapter 5, the influence of acid dissociation, standard formal potential and standard rate constant on apparent kinetic isotope effect for both stepwise and concerted mechanism is discussed in theory. Additionally the experimental measured values of apparent kinetic isotope effect of an aminobenzoquinone modified monolayer system are analyzed within the context of the theoretical discussion. Chapters 3, 4 and 5 basically give a mechanistic study of electrochemical proton coupled electron transfer on a self-assembled monolayer system. These chapters combine experimental methods and theoretical model development. In Chapter 6, a nitroxyl radical modified bilayer is prepared and it shown to be a one electron, one proton transfer system. Preliminary kinetic analysis of this electrochemical system is described in this chapter. In the last chapter, the contribution of the thesis to electrochemical mechanistic study of proton coupled electron transfer reaction is addressed and the scope for further research is suggested.

Although it has been explored for many decades, PCET field is still relative young, especially for its subcase: electrochemical PCET. New contributions for electrochemical PCET field have been rare over many decades, even though new developments in theory and experiment are required considering the importance of this field. The contributions of this thesis to electrochemical PCET can be summarized in the following two points:

1. Multiple electron and proton transfers:

It is understandable that previous experimental systems of electrochemical PCET are centered on 1e1H case due to its simplicity in mechanistic analysis [82;84;111]. *However, the investigation of multi-electron, multi-proton transfer is also vital for the study of complex biological processes of respiration and photosynthesis, as well as the design of catalysts for various energy conversion processes like water splitting, hydrogen evolution and carbon fixation. Although significantly more challenging, it is important to begin to target multi-electron, multi-proton PCET reactions for experimental studies. Quinones are well known to play an important role in many biological reactions and represent a model system for both fundamental interest and industrial application*[48; 112-114]. *The study of quinone PCET is however usually greatly complicated by strong intermolecular interactions (including possible dimerization) and degradation side reactions that often accompany quinone PCET. To minimize the complexity of kinetic analysis, in this thesis, a nearly ideal benzoquinone modified monolayer system, was constructed. This represents the first ideal multi-electron, multi-proton transfer reaction electrochemical system to be fully investigated as a model system for PCET mechanistic studies. Chapters 3 and 4 detail the thermodynamic and kinetic information provided by electrochemical studies and also provides the related theoretical framework upon which the analysis has been built. Finally, the charge transfer pathways for this aminobenzoquinone modified monolayer system have been derived.*

2. Relationship between thermochemical data and charge transfer mechanism:

It has been introduced that there are two possible charge transfer mechanisms for electrochemical PCET reactions: the stepwise mechanism and the concerted mechanism. Differentiating these two mechanisms and determining the related controlling parameters has been a long standing issue. In other words, determining the relationship between thermodynamic parameters (e.g. standard formal potential, acid dissociation constant), kinetic parameters and charge transfer mechanisms is crucial in the electrochemical PCET field. It is highly ambitious to attempt to solve this long standing issue during the course of a PhD thesis considering its complexity.

In this thesis, only the influence of thermochemical data on the PCET mechanism will be discussed. A theoretical model predicting the electrochemical behavior of PCET reactions under exclusive control of the stepwise and the concerted mechanisms has been refined and then extended to the prediction of apparent kinetic isotope effects (KIE) in terms of thermodynamic contribution (Chapter 5). Results show that unexpectedly an apparent KIE should be observed in electrochemical PCET when pure electron transfer represents the rate determining step (stepwise mechanism). This result leads to a need to re-interpret previous reports of apparent KIEs. From this analytical framework, one new insight is that a large pK_a difference between the species in a redox couple greatly favours the role of the concerted mechanism. This provided the motivation to prepare a nitroxyl radical modified electrode to test this hypothesis, and a detailed discussion of this system will be shown in Chapter 6.

Reference List

(1) Dempsey, J. L.; Winkler, J. R.; Gray, H. B. *Chem.Rev.* **2010**, *110*, 7024-7039.

(2) Cukier, R. I.; Nocera, D. G. *Annu.Rev.Phys.Chem.* **1998**, *49*, 337-369.

(3) Huynh, M. H.; Meyer, T. J. *Chem.Rev.* **2007**, *107*, 5004-5064.

(4) Reece, S. Y.; Nocera, D. G. *Annu.Rev.Biochem.* **2009**, *78*, 673-699.

(5) Kaila, V. R. I.; Verkhovsky, M. I.; Wikström, M. *Chem.Rev.* **2010**, *110*, 7062-7081.

(6) Kumar, A.; Sevilla, M. D. *Chem.Rev.* **2010**, *110*, 7002-7023.

(7) Hammes-Schiffer, S.; Soudackov, A. V. *J.Phys.Chem.B* **2008**, *112*, 14108-14123.

(8) Mayer, J. M. *Annu.Rev.Phys.Chem.* **2004**, *55*, 363-390.

(9) Hammes-Schiffer, S. *Acc.Chem.Res.* **2001**, *34*, 273-281.

(10) Hammes-Schiffer, S.; Iordanova, N. *Biochimica et Biophysica Acta (BBA) - Bioenergetics* **2004**, *1655*, 29-36.

(11) Hammes-Schiffer, S.; Hatcher, E.; Ishikita, H.; Skone, J. H.; Soudackov, A. V. *Coord. Chem. Rev.* **2008**, *252*, 384-394.

(12) Hammes-Schiffer, S.; Stuchebrukhov, A. A. *Chem.Rev.* **2010**, *110*, 6939-6960.

(13) Warren, J. J.; Tronic, T. A.; Mayer, J. M. *Chem.Rev.* **2010**, *110*, 6961-7001.

(14) Mayer, J. M.; Rhile, I. J. *Biochimica et Biophysica Acta (BBA) - Bioenergetics* **2004**, *1655*, 51-58.

(15) Laviron, E. *J. Electroanal. Chem.* **1981**, *130*, 23-29.

(16) Cukier, R. I. *Biochimica et Biophysica Acta (BBA) - Bioenergetics* **2004**, *1655*, 37-44.

(17) Roth, J. P.; Yoder, J. C.; Won, T. J.; Mayer, J. M. *Science* **2001**, *294*, 2524-2526.

(18) Hammes-Schiffer, S. *ChemPhysChem* **2002**, *3*, 33-42.

(19) Mayer, J. M. *Acc.Chem.Res.* **1998**, *31*, 441-450.

(20) Siegbahn, P. E. M.; Eriksson, L.; Himo, F.; Pavlov, M. *J.Phys.Chem.B* **1998**, *102*, 10622-10629.

(21) Partenheimer, W. *Catalysis Today* **1995**, *23*, 69-158.

(22) Partenheimer, W. *Adv.Synth.Catal.* **2009**, *351*, 456-466.

(23) Kuivila, H. G.; Walsh, E. J. *J.Am.Chem.Soc.* **1966**, *88*, 571-576.

(24) Nocera, D. G. *Inorg.Chem.* **2009**, *48*, 10001-10017.

(25) Pijpers, J. J. H.; Winkler, M. T.; Surendranath, Y.; Buonassisi, T.; Nocera, D. G. *Proc. Natl. Acad. Sci.* **2011**, *108*, 10056-10061.

(26) Concepcion, J. J.; Jurss, J. W.; Brennaman, M. K.; Hoertz, P. G.; Patrocinio, A. O.; Murakami Iha, N. Y.; Templeton, J. L.; Meyer, T. J. *Acc.Chem.Res.* **2009**, *42*, 1954-1965.

(27) Mano, N.; Mao, F.; Heller, A. *J.Am.Chem.Soc.* **2003**, *125*, 6588-6594.

(28) Cracknell, J. A.; Vincent, K. A.; Armstrong, F. A. *Chem.Rev.* **2008**, *108*, 2439-2461.

(29) Dohle, H.; Mergel, J.; Stolten, D. *J. Power Sour.* **2002**, *111*, 268-282.

(30) Fishilevich, S.; Amir, L.; Fridman, Y.; Aharoni, A.; Alfonta, L. *J.Am.Chem.Soc.*

2009, *131*, 12052-12053.

(31) Binstead, R. A.; Moyer, B. A.; Samuels, G. J.; Meyer, T. J. *J.Am.Chem.Soc.* **1981**, *103*, 2897-2899.

(32) Taube, H. *Angew.Chem.Int.Ed.Engl.* **1984**, *23*, 329-339.

(33) Zhang, M. T.; Hammarström, L. *J.Am.Chem.Soc.* **2011**, *133*, 8806-8809.

(34) Hatcher, E.; Soudackov, A. V.; Hammes-Schiffer, S. *J.Am.Chem.Soc.* **2004**, *126*, 5763-5775.

(35) Okamura, M. Y.; Paddock, M. L.; Graige, M. S.; Feher, G. *Biochimica et Biophysica Acta (BBA) - Bioenergetics* **2000**, *1458*, 148-163.

(36) Sundmacher, K. *Ind.Eng.Chem.Res.* **2010**, *49*, 10159-10182.

(37) Yin, Q.; Tan, J. M.; Besson, C.; Geletii, Y. V.; Musaev, D. G.; Kuznetsov, A. E.; Luo, Z.; Hardcastle, K. I.; Hill, C. L. *Science* **2010**, *328*, 342-345.

(38) Kanady, J. S.; Tsui, E. Y.; Day, M. W.; Agapie, T. *Science* **2011**, *333*, 733-736.

(39) Symes, M. D.; Surendranath, Y.; Lutterman, D. A.; Nocera, D. G. *J.Am.Chem.Soc.* **2011**, *133*, 5174-5177.

(40) Dogutan, D. K.; McGuire, R.; Nocera, D. G. *J.Am.Chem.Soc.* **2011**, *133*, 9178-9180.

(41) Liu, F.; Cardolaccia, T.; Hornstein, B. J.; Schoonover, J. R.; Meyer, T. J. *J.Am.Chem.Soc.* **2007**, *129*, 2446-2447.

(42) Nakagawa, T.; Bjorge, N. S.; Murray, R. W. *J.Am.Chem.Soc.* **2009**, *131*, 15578-15579.

(43) Surendranath, Y.; Dincã, M.; Nocera, D. G. *J.Am.Chem.Soc.* **2009**, *131*, 2615-2620.

(44) Wasylenko, D. J.; Ganesamoorthy, C.; Henderson, M. A.; Koivisto, B. D.; Osthoff, H. D.; Berlinguette, C. P. *J.Am.Chem.Soc.* **2010**, *132*, 16094-16106.

(45) McAlpin, J. G.; Stich, T. A.; Ohlin, C. A.; Surendranath, Y.; Nocera, D. G.; Casey, W. H.; Britt, R. D. *J.Am.Chem.Soc.* **2011**, *133*, 15444-15452.

(46) Kanan, M. W.; Nocera, D. G. *Science* **2008**, *321*, 1072-1075.

(47) Suntivich, J.; May, K. J.; Gasteiger, H. A.; Goodenough, J. B.; Shao-Horn, Y. *Science* **2011**, *334*, 1383-1385.

(48) Barber, J. *Inorg.Chem.* **2008**, *47*, 1700-1710.

(49) Minguzzi, A.; Fan, F. R.; Vertova, A.; Rondinini, S.; Bard, A. J. *Chem.Sci.* **2012**, *3*, 217-229.

(50) Betley, T. A.; Wu, Q.; Van Voorhis, T.; Nocera, D. G. *Inorg.Chem.* **2008**, *47*, 1849-1861.

(51) Yagi, M.; Kaneko, M. *Chem.Rev.* **2000**, *101*, 21-36.

(52) Chen, Z.; Concepcion, J. J.; Jurss, J. W.; Meyer, T. J. *J.Am.Chem.Soc.* **2009**, *131*, 15580-15581.

(53) Bediako, D. K.; Lassalle-Kaiser, B.; Surendranath, Y.; Yano, J.; Yachandra, V. K.; Nocera, D. G. *J.Am.Chem.Soc.* **2012**.

(54) Rüttinger, W.; Dismukes, G. C. *Chem.Rev.* **1997**, *97*, 1-24.

(55) Meyer, T. J.; Huynh, M. H. V.; Thorp, H. H. *Angewandte Chemie International Edition* **2007**, *46*, 5284-5304.

(56) Gagliardi, C. J.; Vannucci, A. K.; Concepcion, J. J.; Chen, Z.; Meyer, T. J. *Energy Environ.Sci.* **2012**.

(57) Yano, J.; Kern, J.; Sauer, K.; Latimer, M. J.; Pushkar, Y.; Biesiadka, J.; Loll, B.;

Saenger, W.; Messinger, J.; Zouni, A.; Yachandra, V. K. *Science* **2006**, *314*, 821-825.

(58) Hayoun, R.; Whitaker, K. M.; Gamelin, D. R.; Mayer, J. M. *J.Am.Chem.Soc.* **2011**, *133*, 4228-4231.

(59) Hammes-Schiffer, S. *J.Phys.Chem.Lett.* **2011**, *2*, 1410-1416.

(60) Venkataraman, C.; Soudackov, A. V.; Hammes-Schiffer, S. *J.Phys.Chem.C* **2008**, *112*, 12386-12397.

(61) Hammes-Schiffer, S. *Acc.Chem.Res.* **2009**, *42*, 1881-1889.

(62) Yoder, J. C.; Roth, J. P.; Gussenhoven, E. M.; Larsen, A. S.; Mayer, J. M. *J.Am.Chem.Soc.* **2003**, *125*, 2629-2640.

(63) Mayer, J. M. *Acc.Chem.Res.* **1998**, *31*, 441-450.

(64) Mayer, J. M. *Acc.Chem.Res.* **2010**, *44*, 36-46.

(65) Laviron, E. *J. Electroanal. Chem.* **1974**, *52*, 395-402.

(66) Laviron, E.; Roullier, L. *J. Electroanal. Chem.* **1980**, *115*, 65-74.

(67) Laviron, E. *J. Electroanal. Chem.* **1980**, *109*, 57-67.

(68) Laviron, E. *J. Electroanal. Chem.* **1981**, *124*, 1-7.

(69) Laviron, E. *J. Electroanal. Chem.* **1981**, *122*, 37-44.

(70) Laviron, E. *J. Electroanal. Chem.* **1981**, *124*, 9-17.

(71) Laviron, E. *J. Electroanal. Chem.* **1983**, *146*, 1-13.

(72) Laviron, E. *J. Electroanal. Chem.* **1983**, *146*, 15-36.

(73) Laviron, E. *J. Electroanal. Chem.* **1984**, *164*, 213-227.

(74) Laviron, E. *J. Electroanal. Chem.* **1984**, *169*, 23-28.

(75) Laviron, E. *J. Electroanal. Chem.* **1984**, *169*, 29-46.

(76) Finklea, H. O. *J.Phys.Chem.B* **2001**, *105*, 8685-8693.

(77) Finklea, H. O. *J.Electroanal.Chem.* **2001**, *495*, 79-86.

(78) Costentin, C.; Robert, M.; Savéant, J. M. *J.Electroanal.Chem.* **2006**, *588*, 197-206.

(79) Costentin, C.; Robert, M.; Savéant, J. M. *J.Am.Chem.Soc.* **2006**, *128*, 4552-4553.

(80) Costentin, C.; Robert, M.; Savéant, J. M. *J.Am.Chem.Soc.* **2007**, *129*, 9953-9963.

(81) Costentin, C.; Robert, M.; Savéant, J. M. *J.Am.Chem.Soc.* **2007**, *129*, 5870-5879.

(82) Costentin, C. *Chem.Rev.* **2008**, *108*, 2145-2179.

(83) Costentin, C.; Donati, L.; Robert, M. *Chem.Eur.J.* **2009**, *15*, 785-792.

(84) Costentin, C.; Robert, M.; Savéant, J. M. *Chem.Rev.* **2010**, *110*, R1-R40.

(85) Bediako, D. K.; Lassalle-Kaiser, B.; Surendranath, Y.; Yano, J.; Yachandra, V. K.; Nocera, D. G. *J.Am.Chem.Soc.* **2012**.

(86) Dinc , M.; Surendranath, Y.; Nocera, D. G. *Proc. Natl. Acad. Sci.* **2010**, *107*, 10337-10341.

(87) Dogutan, D. K.; McGuire, R.; Nocera, D. G. *J.Am.Chem.Soc.* **2011**, *133*, 9178-9180.

(88) Jurss, J. W.; Concepcion, J. C.; Norris, M. R.; Templeton, J. L.; Meyer, T. J.

Inorg.Chem. **2010**, *49*, 3980-3982.

(89) Kamat, P. V. *J.Phys.Chem.Lett.* **2011**, *2*, 242-251.

(90) Kamat, P. V. *J.Phys.Chem.Lett.* **2012**, *3*, 663-672.

(91) Li, Y.; Cox, J. T.; Zhang, B. *J.Am.Chem.Soc.* **2010**, *132*, 3047-3054.

(92) Surendranath, Y.; Lutterman, D. A.; Liu, Y.; Nocera, D. G. *J.Am.Chem.Soc.* **2012**.

(93) Tian, N.; Zhou, Z. Y.; Sun, S. G.; Ding, Y.; Wang, Z. L. *Science* **2007**, *316*, 732-735.

(94) Lukkari, J.; Kleemola, K.; Meretoja, M.; Kankare, J. *Chem.Commun.* **1997**, 1099-1100.

(95) Sadki, S.; Schottland, P.; Brodie, N.; Sabouraud, G. *Chem.Soc.Rev.* **2000**, *29*, 283-293.

(96) Stern, E.; Jay, S.; Bertram, J.; Boese, B.; Kretzschmar, I.; Turner-Evans, D.; Dietz, C.; LaVan, D. A.; Malinski, T.; Fahmy, T.; Reed, M. A. *Anal.Chem.* **2006**, *78*, 6340-6346.

(97) Hu, D.; Peng, C.; Chen, G. Z. *ACS Nano* **2010**, *4*, 4274-4282.

(98) Bent, S. F. *ACS Nano* **2007**, *1*, 10-12.

(99) Fendler, J. H. *Chem.Mater.* **2001**, *13*, 3196-3210.

(100) Forster, R. J.; Faulkner, L. R. *J.Am.Chem.Soc.* **1994**, *116*, 5453-5461.

(101) Love, J. C.; Estroff, L. A.; Kriebel, J. K.; Nuzzo, R. G.; Whitesides, G. M. *Chem.Rev.* **2005**, *105*, 1103-1170.

(102) Ulman, A. *Chem.Rev.* **1996**, *96*, 1533-1554.

(103) Butler, J. A. V. *Trans.Faraday Soc.* **1924**, *19*, 734-739.

(104) Butler, J. A. V. *Trans.Faraday Soc.* **1924**, *19*, 729-733.

(105) Oldham, K. B.; Myland, J. C. *J.Electroanal.Chem.* **2011**, *655*, 65-72.

(106) Marcus, R. A. *J.Electroanal.Chem.* **1997**, *438*, 251-259.

(107) Marcus, R. A. *Can.J.Chem.* **1959**, *37*, 155-163.

(108) Marcus, R. A. *Annu.Rev.Phys.Chem.* **1964**, *15*, 155-196.

(109) Chidsey, C. E. D.; Bertozzi, C. R.; Putvinski, T. M.; Mujsce, A. M. *J.Am.Chem.Soc.* **1990**, *112*, 4301-4306.

(110) Chidsey, C. E. D. *Science* **1991**, *251*, 919-922.

(111) Costentin, C.; Louault, C.; Robert, M.; Savéant, J. M. *Proc. Natl. Acad. Sci.* **2009**, *106*, 18143-18148.

(112) Osyczka, A.; Moser, C. C.; Dutton, P. L. *Trends Biochem Sci* **2005**, *30*, 176-182.

(113) Mayer, J.; Rhile, I.; Larsen, F.; Mader, E.; Markle, T.; DiPasquale, A. *Photosyn. Res.***2006**, *87*, 3-20.

(114) Feher, G.; Allen, J. P.; Okamura, M. Y.; Rees, D. C. *Nature* **1989**, *339*, 111-116.

(115) Wang, Y. Q.; Yu, H. Z.; Cheng, J. Z.; Zhao, J. W.; Cai, S. M.; Liu, Z. F. *Langmuir* **1996**, *12*, 5466-5471.

(116) Yu, H. Z.; Wang, Y. Q.; Cheng, J. Z.; Zhao, J. W.; Cai, S. M.; Inokuchi, H.; Fujishima, A.; Liu, Z. F. *Langmuir* **1996**, *12*, 2843-2848.

(117) Yu, H. Z.; Wang, Y. Q.; Cheng, J. Z.; Zhao, J. W.; Cai, S. M.; Inokuchi, H.;

Fujishima, A.; Liu, Z. F. *J. Electroanal. Chem.* **1995**, *395*, 327-330.

(118) Eckermann, A. L.; Feld, D. J.; Shaw, J. A.; Meade, T. J. *Coord. Chem. Rev.* **2010**, *254*, 1769-1802.

(119) Rojas, M. T.; Koeniger, R.; Stoddart, J. F.; Kaifer, A. E. *J.Am.Chem.Soc.* **1995**, *117*, 336-343.

(120) Porter, M. D.; Bright, T. B.; Allara, D. L.; CHIDSEY, C. E. D. *J.Am.Chem.Soc.* **1987**, *109*, 3559-3568.

(121) Matthews, D. *Aust.J.Chem.* **1995**, *48*, 1843-1852.

(122) Matthews, D. *Aust.J.Chem.* **1994**, *47*, 2171-2186.

Chapter 2: Experimental Techniques and Data Analysis

2.1 Materials

All chemicals expect 11-amino-1-undecanethiol (AUT), which was ordered from Assemblon (99% pure), were obtained from Sigma-Aldrich, and all chemicals used without purification except for 1,4-benzoquinone (Alfa Aesar), which was purified by sublimation at reduced pressure and slightly elevated temperatures (~50℃). After the process of sublimation (Scheme 2.1), the yellow, pure 1, 4-benzoquinone was formed on the surface of a cold-finger, leaving the black impurity in the bottom of sample container.

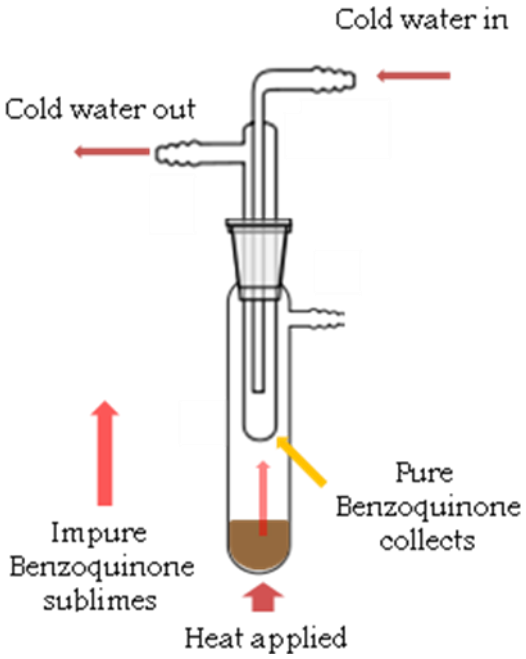

Scheme 2.1: Cold-finger used for sublimation of benzoquinone.

All thiol solutions were made in 95% ethanol. To make the buffer electrolytes and ensure their same ionic strength, the electrolyte used in Chapters 3 and 4 was prepared from 0.1M $NaClO_4$ (≥99.0%, Fluka) and 5mM sodium phosphate buffer. Another electrolyte used in Chapters 5 and 6 was made from 0.1M $NaClO_4$ (≥ 99.0%, Fluka) and 0.04M Britton-Robinson buffer, which consist of acetic acid, phosphoric acid and boric acid, and the pH of this electrolyte was adjusted using sodium

hydroxide for high pH or perchloric acid for low pH. All electrolytes were made using 18.2 MΩ cm Millipore water or 99.9% deuterium oxide for the solvent isotope effect study. The methods of modifying the redox molecules onto a gold electrode including the synthesis of a redox surfactant will be described in the following chapters.

All potentials reported in this thesis are measured with respect to the KCl saturated silver/silver chloride (Ag/AgCl) electrode, which is -0.197V biased from the standard hydrogen electrode. This reference electrode is homemade. AgCl was electrodeposited onto polished Ag electrode in 0.1M HCl by holding the potential at 0.7V. A coil of gold wire with high surface area, which had been treated with freshly prepared piranha solution (a 3:1 mixture of sulfuric acid and hydrogen peroxide) and then flame annealed before each experiment, was used as a counter electrode. Working electrodes were gold bead electrodes, which were formed by melting the end of a gold wire (1 mm diameter, 99.9%) in hydrogen-oxygen flame. Before melting, the gold wire was cleaned by immersing it in freshly prepared piranha solution for 10 minutes followed by sonication in Milli-Q water for 5 minutes. After forming the gold bead at the end of the gold wire, it was quenched in Milli-Q water and then etched in aqua regia to remove any trace amount of surface impurities. The as prepared electrode was used as the working electrode by immersing the spherical segment as a whole into the electrolyte solution. Before any electrochemical test, the suitability of the working electrode was assessed by running voltammetry in 0.1M $HClO_4$ to ensure all affecting impurities have been removed. Alternatively, a mechanically polished gold electrode in a hanging meniscus arrangement will be used and described in Chapter 6 as the working electrode.

2.2 Electrochemical Set up

All the electrochemistry experiments were performed by a computer controlled system, consisting of a HEKA PG590 potentiostat (HEKA, Mahone Bay, NS, Canada). Data were collected using a multifunction DAQ card (PCI 6251 M Series, National Instruments) and in-house software written in the LabVIEW environment.

The three electrode system, including reference electrode, working electrode and

counter electrode, was used for all electroanalytical measurements. The reference electrode is to act as reference in measuring and controlling the electrode's potential, which is measured between the working electrode and the reference electrode. The counter electrode passes all the current needed to balance the current observed at the working electrode, and the current recorded flows between the working electrode and counter electrode.

The electrochemical cell was made of glass and had a solution capacity of 30 ml. It consists of two parts: the bottom part is the electrolyte container with a 30 mm ground joint at the top and a 10mm joint at the side to connect a side-arm glass container that houses the reference electrode. The main electrochemical cell and the reference electrode need to be well connected with the electrolyte but without having the Cl^- ions from the reference electrode enter the working compartment. This is accomplished by welting a ground glass stopcock with electrolyte solution. The stopcock isolates the reference and working compartments but maintains ionic conductivity. The top joint is fitted to a glass cover which has five ground joints on the top. One joint is connected to the glass bubbler for the outlet of argon. Two joints are used to allow argon purge of the electrolyte solution and one of them is for the purging inside the electrolyte, and the other is placed on the top of electrolyte surface to remove the air above the electrolyte. The remaining two joints are used for the counter and working electrodes. The electrochemical cell was enclosed in a faraday cage, a grounded conductive shield made of copper mesh, to protect the electrochemical setup against electromagnetic interference from external sources.

The electrochemical cell was washed in a hot acid bath containing a 1:3 mixture of nitric acid and sulfuric acid, and then washed with Milli-Q water of resistivity 18.2MΩ and again soaked in fresh Milli-Q water for about 6 hrs before use. All other glassware used for preparing all solutions needed for electrochemical measurements was also washed in the same manner.

2.3 Cyclic Voltammetry and Apparent Formal Potential

Cyclic voltammetry (CV) is one of the most versatile electroanalytical

techniques[1], which can be used for qualitative diagnosis and quantitative measurement of electrode reactions[1]. A CV measurement is performed by scanning linearly the potential of a stationary working electrode in an unstirred electrolyte. The employed triangular potential waveform is shown in Fig. 2.1a, and the voltage scan rate equals to the absolute value the slope of the line. Depending on the experimentalistic specific objective, single or multiple cycles can be applied. The current flowing across the interface is recorded as a function of the electrode potential, and the resulting plot of current versus potential is termed a cyclic voltammogram. For a system with the redox couple assembled on the electrode surface, a representative CV is shown in Figure 2.1b. This CV is different from that for the case of a redox couple freely dissolved in the electrolyte where the voltammetry is strongly influenced by diffusion control. In those systems, the peak current is dictated by the rate at which redox molecules arrive at the electrode surface through mass-transport phenomena. Diffusion control is seen at large overpotentials and the peak current scales with the square root of the potential scan rate. For surface bound redox molecule systems, the current is controlled only by the rate of electron transfer, so that peak heights obtained from CVs are linear with potential scan rates. The absence of diffusion controlled currents also means that at large overpotentials, there will be no Faradaic current flowing through the interface and, assuming a potential independent monolayer capacitance, the background charging current should be constant over the entire CV.

It can be expected that concentrations of reduced species and oxidized species at the electrode surface vary as a function of the applied external potentials. The apparent formal potential is the average of peak potential of the anodic reaction and that of the cathodic reaction. The total current includes the faradic current and the non-faradic current. Non-faradic current, also called “capacitive” or “double layer” current, is the current flowing through the electrochemical cell that is charging/discharging the electrical double layer capacitance. The faradic current is caused by the charge transfer occurring at electrode surface, and specifically in this thesis, the charge transfer is the proton coupled electron transfer. The non-faradic current needs to be

removed in order to discuss the kinetic contribution of the PCET reaction occurring at the chemically modified electrode.

As introduced in Chapter 1, a theoretical current-potential relation has been introduced by Butler-Volmer equation and Marcus DOS theory, in which the current from the charge transfer reaction is a function of overpotential, scan rate, standard rate constant, transfer coefficient and other parameters. Therefore in experiment, the voltammograms recorded at different potentials and scan rates can be used to calculate the values of rate constant and transfer coefficient. For a proton coupled electron transfer process, the acid dissociation constant of the proton transfer can be calculated by the adjustment of pH in the measurement of the voltammograms. To sum up, cyclic voltammetry provides a rapid and convenient way for the extraction of both thermodynamic and kinetic information of a PCET system.

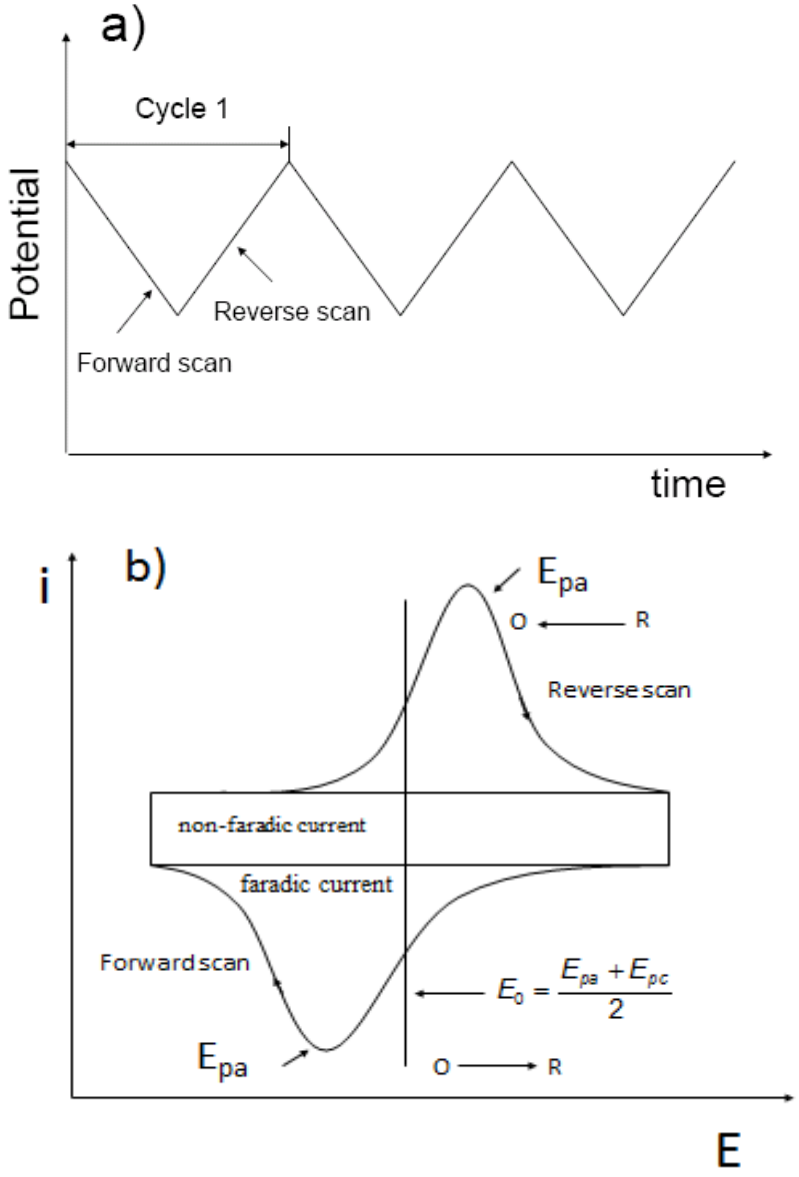

Figure 2.1: a) Potential-time signal in a cyclic voltammetry experiment; b) A representative CV for a reversible $O + ne \rightleftharpoons R$ (O: Oxidant, R: Reductant) redox process on an electroactive surface system showing faradic and non-faradic current.

In this section, the theoretical treatment of the voltammogram with the only contribution from faradic current [2; 3]will be discussed. The following discussion will also be limited to the case of the redox molecule attached to an electrode. The theoretical model was built by the finite difference simulation method, in which the voltammetric scans at a series of discrete small-amplitude potential steps over fixed time intervals whose duration depends on sweep rate.

Based on the finite difference simulation method, the current at each time or potential interval is proportional to the amount of electroactive material that is oxidized/reduced in response to each potential step, and thus the derivation of a dimensionless current is shown as follows:

$$i_{\text{dimensionless}} = \frac{\Delta f}{\Delta E / (\frac{RT}{F})} \tag{2.1}$$

where Δf is the change of the fractional degree of oxidation during a given interval, ΔE is the potential increment for each interval, which is related to the scan rate ν, and $\upsilon = \Delta E/t$.

For the apparent cathodic/anodic rate constant at any overpotential, the single electron transfer reaction can be represented by:

$$Ox + e \underset{k_a}{\overset{k_c}{\rightleftharpoons}} \text{Red}$$

t_0	f_n	1-f_n
$t + t_0$	f_{n+1}	1-f_{n+1}

t is the time interval, which corresponds to the potential interval by scan rate. t_0 is the reaction time before one new interval.

Based on a first order reaction, one obtains:

$$-\frac{df_n}{dt} = k_c f_n - k_a(1 - f_n), \tag{2.2}$$

The above Eqn. (2.2) can be rewritten as:

$$\frac{-1}{k_a + k_c} \frac{d\left((k_a + k_c) f_n - k_a\right)}{(k_a + k_c) f_n - k_a} = dt \tag{2.3}$$

In which f_n is the fractional degree of oxidation in a given time (or potential) interval. Expressions for cathodic rate constant k_c and anodic rate constant k_a of single electron transfer reaction are:

$$k_c = k_s \exp(-\alpha f \eta) \tag{2.4}$$

$$k_a = k_s \exp((1-\alpha) f \eta) \tag{2.5}$$

Where k_s is the standard rate constant, η is the overpotential, α is the standard transfer

coefficient and $f = \frac{F}{RT}$.

After integration of Eqn. (2.3), one obtains:

$$\ln\left((k_a + k_c) f_n - k_a\right)\Big|_{f_n}^{f_{n+1}} = -(k_a + k_c)t\Big|_{t_0}^{t+t_0} \tag{2.6}$$

Therefore:

$$\frac{(k_a + k_c) f_{n+1} - k_a}{(k_a + k_c) f_n - k_a} = e^{-(k_a + k_c)t} \tag{2.7}$$

The expression for the change of the fraction degree of oxidation is:

$$f_{n+1} - f_n = \left(\frac{k_a}{k_a + k_c} - f_n\right)\left(1 - e^{-(k_a + k_c)t}\right) \tag{2.8}$$

It is reasonable to define that fractional degree of oxidation under equailibrium condition $f_{nernst} = \frac{k_a}{k_a + k_c}$

Therefore Eqn. (2.8) can also be written as:

$$f_{n+1} - f_n = \left(f_{nernst} - f_n\right)\left(1 - e^{-(k_a + k_c)t}\right) \tag{2.9}$$

Finally, the equation for the dimensionless current can be shown as follows:

$$i_{\text{dimensionless}} = \frac{\left(f_{nernst} - f_n\right)\left(1 - e^{-(k_a + k_c)t}\right)}{\Delta E \,/\, (\frac{RT}{F})} \tag{2.10}$$

The above Eqn. (2.10) was derived for single electron transfer steps and can be extended to multi-electron transfer reaction. In this thesis, voltage scan rate, standard rate constant and standard transfer coefficient dependent voltammograms with the only contribution from faradic current will be provided from Eqn. (2.10) and discussed.

As shown in Fig. (2.2), the potential separations of cathodic peaks and anodic peaks increase with increasing scan rates. This figure demonstrates that the more charge, which is obtained by numerical integration of the current with respect to the potential, will be accumulated with the slowing of the scan rate. For the purpose of kinetic measurement of an aminobenzoquinone system, scan rates dependent voltammograms were measured and as expected, the measurements provided similar

results as those shown in Figure (2.2).

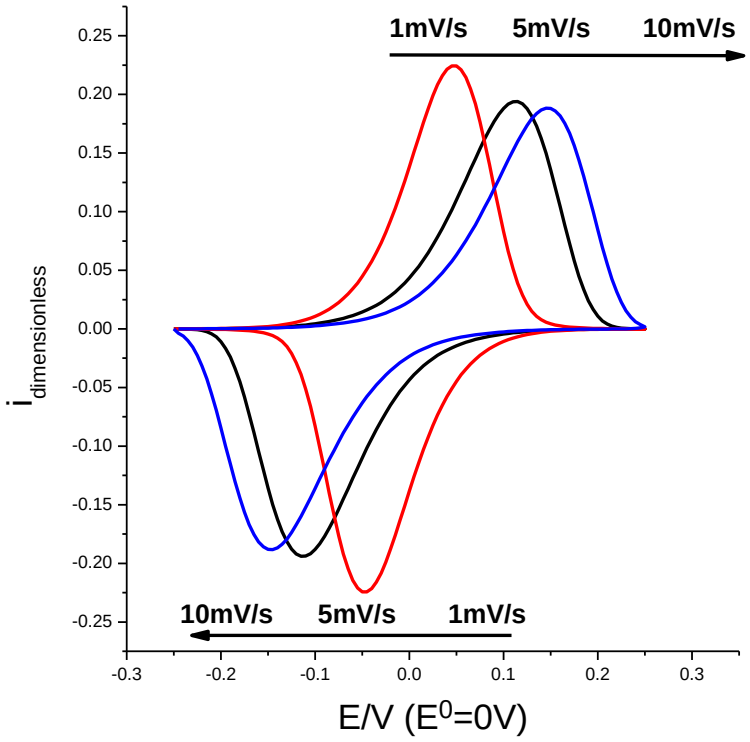

Figure 2.2: Simulated CVs as a function of scan rates (1 mV/s, 5 mV/s and 10 mV/s) with $\alpha=0.5$ and $k_s=0.01$.

Figure 2.3 demonstrates voltammograms for three systems with different standard rate constants. A direct observation from this figure is that the potential separations between cathodic peaks and anodic peaks is largely affected by the standard rate constants, and with the increasing of standard rate constants, these peak separations recorded at the same scan rate should increase under the assumption of identical transfer coefficients.

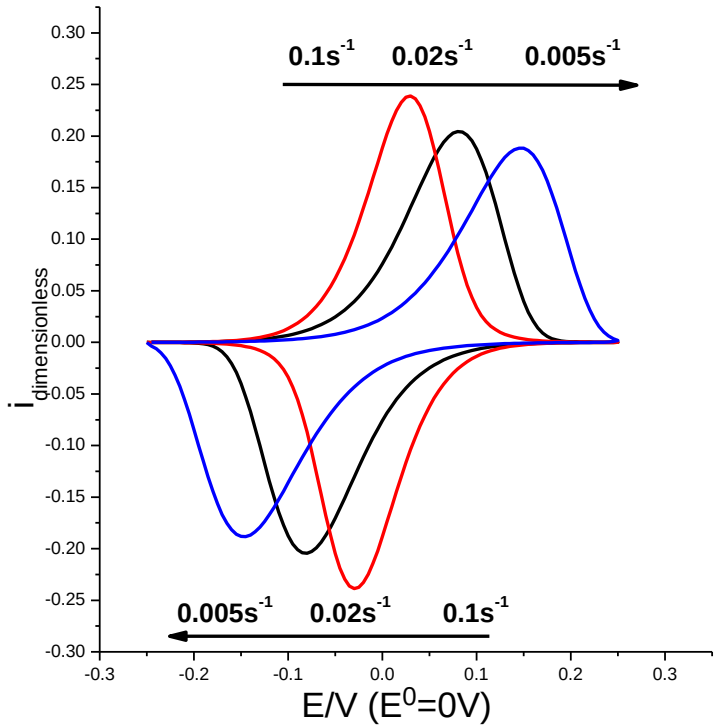

Figure 2.3: Standard rate constants ($0.005s^{-1}$, $0.02s^{-1}$ and $0.1s^{-1}$) and resulting simulated CVs with $\alpha=0.5$ and $\upsilon=5$ mV/s.

In order to investigate the influence of standard transfer coefficients on the shape of voltammograms, CVs under the conditions of $\alpha=0.3$, 0.5 and 0.7 have been shown in Fig. 2.4 with constant values for all other parameters. To show the comparison of the shapes in a good manner, these three CVs are integrated to one graph without labeling the potential axis. It can be observed that the degree of asymmetry of cathodic/anodic peaks is strongly dependent on the standard transfer coefficient. Symmetric cathodic and anodic peaks are shown in the Fig. 2.4 when $\alpha=0.5$, however, remarkable asymmetry is found for the standard transfer coefficient of 0.3 or 0.7. When $\alpha=0.3$, the anodic peak is much broader than the cathodic peak, and the anodic peak is much more narrow than the cathodic peak in the case of $\alpha=0.7$.

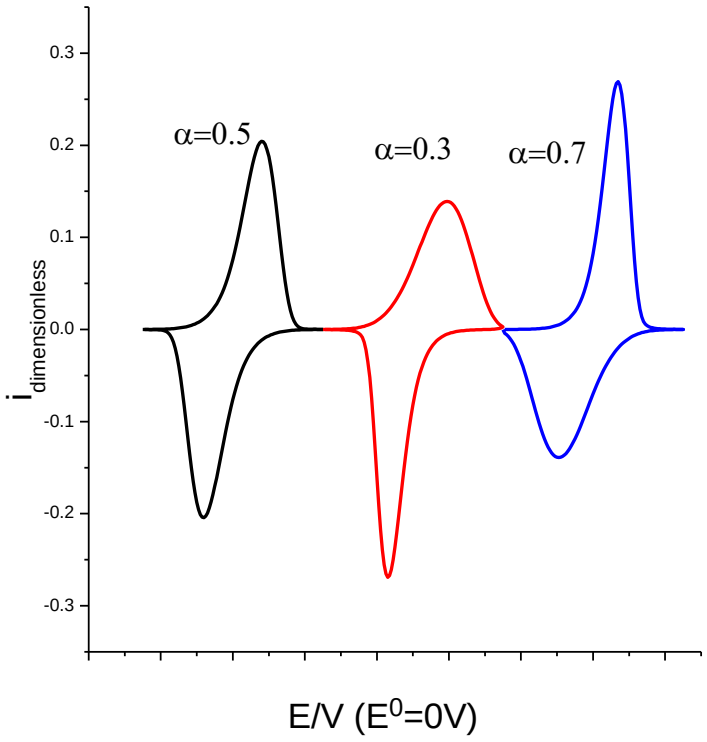

Figure 2.4: Simulated CVs as a function of standard transfer coefficient (α=0.3, 0.5 and 0.7) with constant standard rate constant and scan rate (υ=5 mV/s, k_s=0.02s^{-1}).

2.4 Chronocoulometry

As a controlled-potential technique, chronocoulometry is the measurement of the current respond to an applied potential[1]. The basic premise involved in this technique is that the potential of the working electrode is stepped from a value at which no faradic reaction occurs to another value at which faradic reaction may occur. The stepped potential and its holding time are set on the basis of different objectives. Specifically, the electrode potential is preset at a limiting negative potential denoted as E_{base} in relation to the formal potential, where all of redox molecules are in the reduced state. Then the working electrode potential is stepped to a more positive value E_v and for a period of time, where thermodynamically the charge transfer reaction should occur. The last step of one set of charge measurement is that the electrode

potential steps back to E_{base}, where all redox molecules are returned back to reduced state after a short period of time of μs considering the large overpotential involved in this step. During the potential stepping from E_c to E_{base}, the current flowing across the interface is acquired and then integrated to obtain charge information as a function of different holding times at E_v. The calculated value of the charge can be easily converted to the surface concentration of reduced species or oxidized species. Schematic diagrams of the different chronocoulometric experiments are shown in Figures 2.5 and 2.6.

In order to determine the chronocoulometric response of the systems described in this thesis under equilibrium conditions, the program shown in Figure 2.5a is performed. The time spent at each value of E_v is sufficiently long enough to ensure the ratio of oxidized and reduced forms of the redox couple is that dictated by the Nernst equation. The resulting charge density as function of potential can be divided into three ranges (Figure 2.5c). In range 1, the charge is from non-faradic current only, and this charge is linear with potential due to the constant capacitance of the monolayer. With the potential increasing to the occurrence of anodic reaction, within range 2, the measured charge is attributed to both the faradic current and non-faradic current, therefore the slope in this range is larger than that in range 1. At range 3, all the anodic reaction has been done and the charge contains the total faradic charge and the potential dependent non-faradic charge. The slope in this range should be the same as that in the first range.

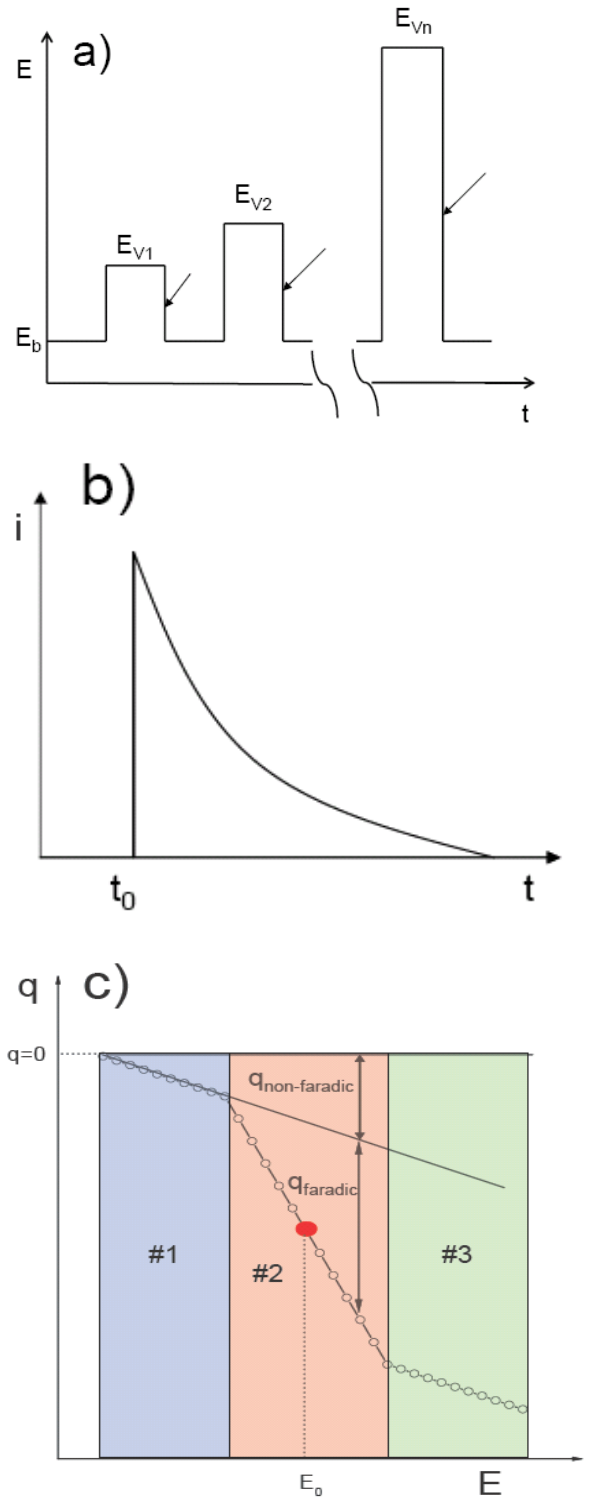

Figure 2.5: Schematic diagram of the chronocoulometric experiment: a) variation of potential during the step sequence, b) current transient collected upon a step from a variable potential to the base potential, c) charge density as a function of electrode potential, a point in this plot is from the integration of a single current transient at the corresponding potential.

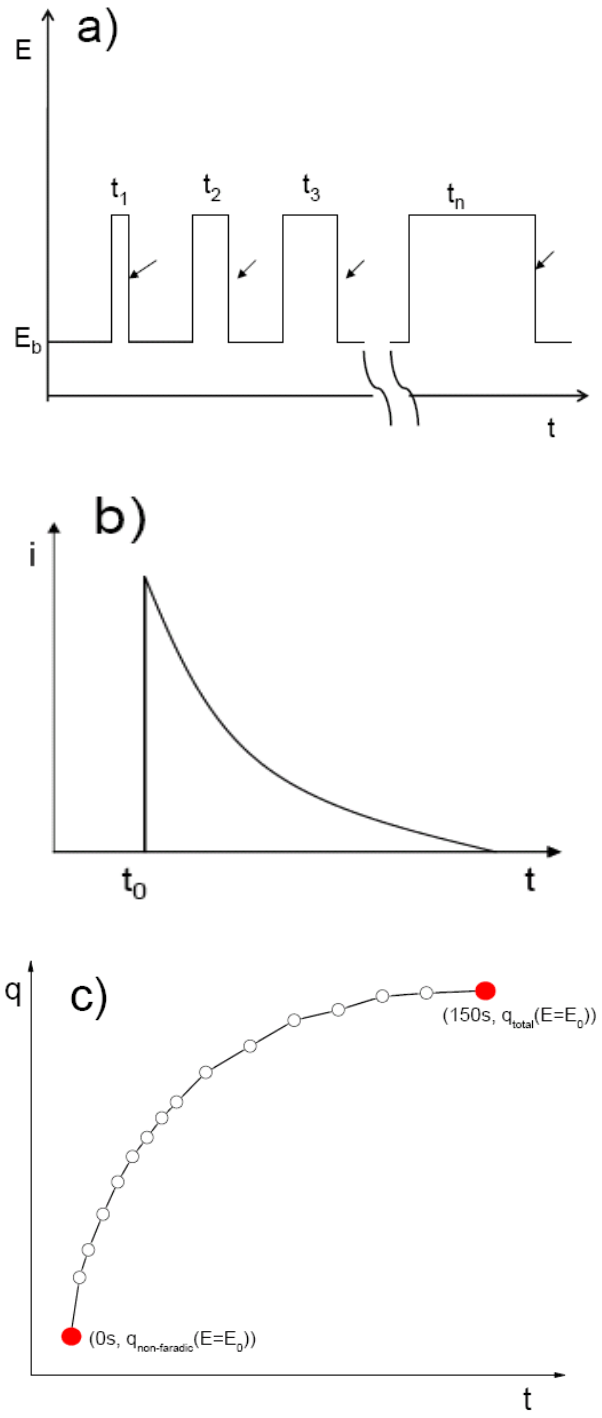

Figure 2.6: Schematic diagram of the chronocoulometric experiment: a) variation of time during the step sequence, b) current transient collected upon a step from formal potential to the base potential at variable time, c) charge density as a function of electrode potential, a point in this plot is from the integration of a single current transient at the corresponding potential.

Time dependent charge measurement is performed (Figure 2.6) in order to study PCET kinetics. The standard rate constant is measured when the holding potential is set to the apparent formal potential, which is calculated from CVs or potential dependent charge measurements under equilibrium condition. In these experiments, the potential is toggled between E_b and $E_{0.}$ The time spent at E_0 is increased to allow increasing amounts of oxidation to occur. Once again, the current transient is integrated on the step from E_0 to E_b. The low capacitance of the monolayer means the time required to change the double layer is much smaller than the time required for extensive charge transfer. As shown in Figure 2.6, the measured charge initially is only from non-faradic current at apparent formal potential, which can be obtained from the measurement shown in Figure 2.5. The collected charge at the apparent formal potential, which represents the surface concentration of reduced species, becomes larger with increasing holding time. The curve at transient (Figure 2.6c) shows an exponential function of time dependent charge density. The maximum holding time in the thesis is estimated to be 150s, which is sufficient to oxidize all of redox molecules because the estimated standard rate constant for the aminobenzoquinone modified monolayer system is around $0.1s^{-1}$.

2.5 Solvent Isotope Effect

99.9%D_2O instead of Millipore H_2O is used to prepare deuterium based electrolyte for the studies of apparent kinetic isotope effects. Electrolyte acidity measurements were carried out using a pH meter from Alfa Aesar and a standard glass electrode. The electrode was calibrated using standard aqueous buffers beforehand. The pH reading directly from D_2O by pH meter is called "pH^*". In theory, the pH electrode response is based on the equilibrium between ions in solution and groups on the surface of the membrane of the electrode. Similar to the definition of *pH*, *pD* is a measure of acidity or basicity of a deuterium solution. The relationship between *pD* and *pH* for 0.1M electrolyte can be expressed by[4]: $pD = 1.076 \times pH$.

In these experiments, the *pH* meter was used to measure the concentration of deuterium ion in electrolyte and provide the values of pH^*. The following equation

given from literature is used to show the relationship between pH^* and pH in 0.1M electrolyte[4]:

$$pH^* = 1.076 \times pH - 0.45 \tag{2.11}$$

While the relationship of pK_a in light water and heavy water is:

$$pK_a(H_2O^*) = 1.076 \times pK_a(H_2O) - 0.45 \tag{2.12}$$

Where $pK_a\ (H_2O^*)$ is the acid dissociation constant with respect to pH^*.

In this thesis, the so called "isotope effect" includes the H/D replacement induced changes of acid dissociation constant, standard rate constant, standard formal potential and apparent standard rate constant, and the change of apparent standard rate constant is called "apparent kinetic isotope effect", which will be proved to be useful in the mechanistic discussion of proton coupled electron transfer reaction.

2.6 Apparent Parameters

An elementary step, also called an elementary reaction or an elementary process, expresses how the reactants form products in a single reaction event. The equation in an elementary step represents the reaction at the molecular level, and the related parameters are termed as standard parameters. In the PCET reaction, the elementary steps will be a single electron transfer step and a single proton transfer step. For an electron transfer step, the standard parameters include a standard rate constant, a standard formal potential and a standard formal potential.

In chemical kinetics, the overall reaction is usually defined by the combination of a number of elementary steps. In this thesis, the PCET reaction should be treated as an overall reaction not an elementary reaction, therefore the observed parameters can't directly reflect the nature of PCET reagents in most cases. These experimental measurable parameters are defined by apparent parameters and will be expressed by the standard parameters. Three apparent parameters: apparent standard rate constant, apparent formal potential and apparent standard transfer coefficient are mainly considered in this thesis for a PCET reaction.

Reference List

(1) Joseph Wang *Analytical Electrochemistry*2001; pp 28-62.

(2) Weber, K.; Creager, S. E. *Anal.Chem.* **1994**, *66*, 3164-3172.

(3) Nahir, T. M.; Clark, R. A.; Bowden, E. F. *Anal.Chem.* **1994**, *66*, 2595-2598.

(4) Krezl, A.; Bal, W. *J. Inorg. Biochem.* **2004**, *98*, 161-166.

Chapter 3: Coupled Electron/Proton Transfer Studies of Aminobenzoquinone Modified Monolayers

Reproduced in part with permission from [Zhang, W.; Rosendahl, S. M.; Burgess, I. J. *J.Phys.Chem.C* **2010**, *114*, 2738-2745.]

3.1 Introduction

Quinones and their charge transfer behavior have been investigated in experiment and in theory for many decades. They are involved in many biological electron transport processes[1-4] such as photosynthetic reactions and mitochondrial adenosine triphosphate (ATP) synthesis, and quinones are often used as mild oxidizing agents and as dehydrogenating reagents, particularly for aromatization and in the production of hydrogen peroxide. The redox behavior of quinone/hydroquinone under controlled potential has been studied in aqueous solution (buffered and unbuffered conditions) and in organic solvents[5; 6] (Scheme3.1), which largely improves the understanding of heterogeneous electron transfer process and electrochemical proton coupled electron transfer process. Two sequential one electron transfer reductions to form the quinone dianion have been observed in aprotic organic solvents like dimethylformamide. The addition of water can strongly affect this redox behavior due to water induced hydrogen bonding network and greater solvent polarity. In aqueous solution without the presence of buffer species, reduction of quinone will consume protons at the electrode surface in a very small time scale and build up an effectively higher pH at the electrode/electrolyte interface compared with that in the bulk of solution. The overall reaction determined from experimental measurement is more likely two electron reductions followed by possible chemical reactions. In general for aqueous solutions with high buffer capacity, quinone undergoes two

electron transfers and two proton transfers to become dihydroquinone since the interfacial pH can be maintained at the same level as the pH in bulk solution. Additionally, the homogeneous charge transfer behavior of quinones has been studied as a model system to help improve the understanding of general PCET reactions.

(a) Buffered H_2O or unbuffered with $[H^+]>[Q]$

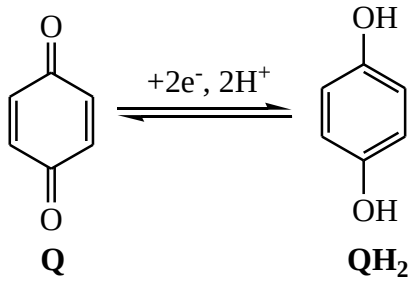

(b) Unbuffered H_2O with $[H^+]<[Q]$

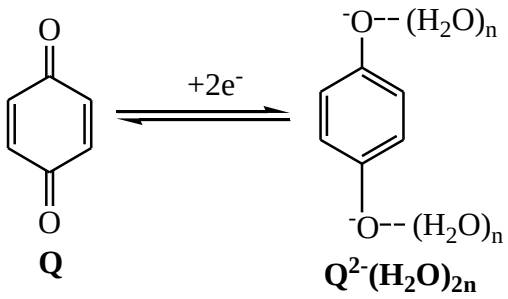

(c) Aprotic solvents

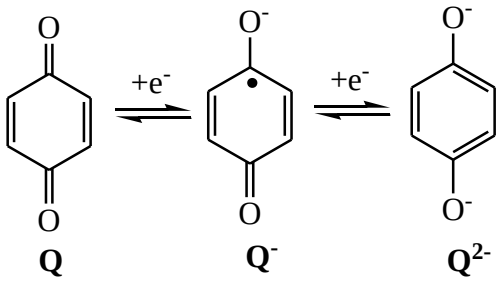

Scheme 3.1: Proposed quinone reduction reactions, adapted from[6].

Self-assembled monolayers on metal electrodes that contain quinone redox centers (or their hydroquinone analogues) have been successfully built over the past twenty years. Most previous quinone-containing monolayer systems were formed using gold-sulfur chemistry[7-16]. Such monolayer systems are very attractive due to the following reasons. Firstly, kinetic analysis of the electrochemical behavior of surface

confined redox molecules is much easier than that of redox molecules in bulk solution, as has been introduced in Chapter 1. Secondly, self-assembled monolayer systems allow for control of charge transfer rates by changing the localized environment such as the distance between redox probe and electrode and the monolayer composition. Oligo(phenylene vinylene) (OPV)s with a hydroquinone moiety and a thiol anchor group have been synthesized and directly assembled onto gold electrodes, and the apparent rate constants as a function of pH for this system have been measured by cyclic voltammetry[13;14]. Results showed that rate constants were on the order of $1s^{-1}$ and ca. 100-fold faster than for the same H_2Q functionality confined to the surface via alkane tethers. Moreover, rate constants were independent of the length of the OPV bridge in the same pH electrolyte. Hong and Park reported upon a system with a quinone/hydroquinone terminus separated from the thiol-Au surface by a 12 carbon methylene chain[9; 10]. This system exhibited very slow kinetics (apparent standard rate constant, k_{app}^{std} = 3.6 x 10^{-4} s^{-1}). Similarly, 2-(-11-mercaptoundecyl) hydroquinone SAMs built by Ye et al showed very slow PCET process in acidic electrolytes, which was evidenced by very large peak separations in recorded cyclic volatmmograms (CVs)[15]. Comparably small apparent standard rate constants have been reported for slightly shorter chained (eight CH_2 units) quinone SAM as well as for long chained anthroquinone (AQ) monolayers. Nevertheless, Abhayawardhana and Sutherland have very recently reported a k_{app}^{std} ~10 s^{-1} for an AQ monolayer with a 10-carbon alkyl spacer[7]. This is roughly three orders of magnitude faster than the reported apparent standard rate constants mentioned above. Experimental evidence indicates that the apparent standard rate constant is strongly dependent on the bonding environment and molecular structure of the redox active moiety. Precise control of the localized environment and the distances involved in the charge transfer between the electron acceptor and donor can be performed to adjust the charge transfer kinetics. Additionally, simple electrochemical techniques like cyclic voltammetry have the capability to measure apparent rate constants and apparent formal potentials as a function of pH. However,

none of these aforementioned studies have looked at the fundamental PCET mechanism in quinone modified monolayer redox systems. These types of studies require experimental measurements of apparent rate constants, apparent formal potentials and apparent transfer coefficients as a function of pH. Furthermore, an ideal surface system is essential to minimize the complexity of kinetic analysis. An ideal electrochemical PCET system is one where there are no intermolecular interactions between neighboring surface redox species. All of the previously reported surface PCET systems (not just quinones) suffer from strong intermolecular interactions and are unsuitable for mechanistic analyses. In this chapter, the preparation of a nearly ideal aminobenzoquinone modified monolayer will be described and characterized to prove its ideality for studying charge transfer behavior. By modifying a method first reported by Lukkari et al[17], and later refined by Novák and co-workers[16], it was possible to build a monolayer system where the quinone surface concentration is sufficiently dilute enough to provide nearly ideal electrochemical behaviour. This has been proved by charge measurement under equilibrium conditions. Secondly, through the use of both voltammetry and chronocoulometry, values of the apparent rate constant as a function of pH have been extracted as a function of pH. Additionally, the pH dependent apparent formal potential and the apparent transfer coefficient have been obtained for this ideal system from cyclic voltammetry measurements.

3.2 Experimental

Both the required chemical reagents and the electrochemical techniques employed (cyclic voltammetry and chronocoulometry) have been introduced in Chapter 2. This experimental section focuses on the preparation procedure for fabricating the aminobenzoquinone modified monolayer.

After the cleaning procedure reported in Chapter 2, the gold bead electrode was rinsed with ethanol and then immersed in the thiol ethanolic solution. This solution consists of either 0.1mM AUT and 1.5mM OT (two component SAMs) or 0.1 mM AUT (single component SAMs). To improve the formation of the amine terminated monolayer, ammonium hydroxide was added to the incubating solution to reach

pH~11. After 1 hour of incubation in this high pH ethanolic solution, the resulting SAM was rinsed with ethanol to remove possible non-covalent bonding thiol and then immediately placed in a freshly prepared 5mM benzoquinone ethanolic solution for 3 minutes at 50 ℃. The proposed reaction mechanism is demonstrated in Scheme 3.2. Amine group attacks the electrophilic position of the benzoquinone forming an amino-hydroquinone. Free benzoquinone will oxidize the amino hydroquinone in the ethanolic solution to form aminobenzoquinone. It can be predicted from this mechanism that if there is high surface density of amino groups on the electrode, an adjacent amine group can attack at another position on the benzoquinone. After the surface Michael addition-like reaction, the electrode was removed from ethanolic solution, and then rinsed with ethanol followed by Millipore water. The resulting aminobenzoquinone modified monolayer electrode was dried with a stream of argon before being placed in the electrochemical cell.

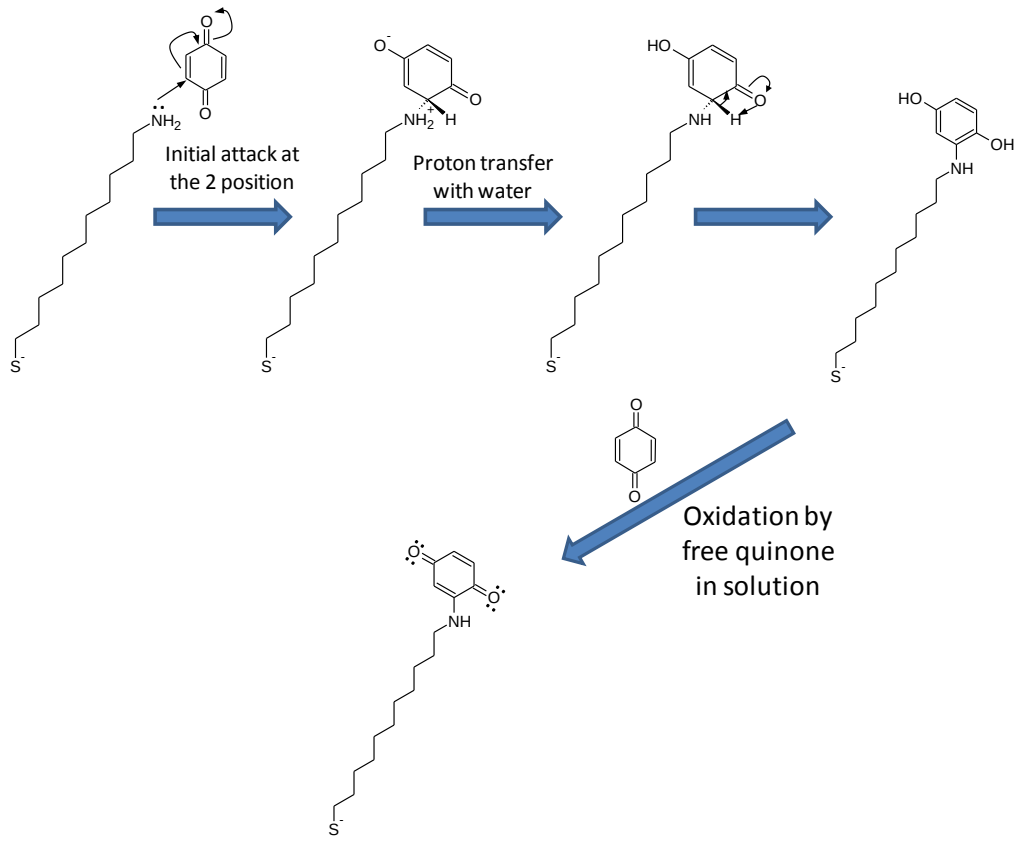

Scheme 3.2: Proposed reaction mechanism of formation of quinone modified monolayer.

3.3 Results and Discussion

3.3.1 General Cyclic Voltammetry Features

For single component SAMs, the cleaned gold electrode was incubated in 1.5 mM ammonium hydroxide ethanolic solutions of 11-aminoundecylthiol (AUT) (pH~11). The resulting SAM covered electrode was further modified by placing it in a freshly prepared benzoquinone ethanolic solution. CVs for this type of SAM in pH 4.5 phosphate buffer electrolytes were characteristic of the dotted line shown in Figure 3.1. This voltammogram reveals two redox couples with about 300mV separation of apparent formal potentials, which is consistent with previous reports on similar benzoquinone derivatized SAMs[16]. Novák and co-workers have been able to demonstrate that the surface reaction between amine terminated SAMs and benzoquinone in ethanolic solution can induce multiple binding motifs. Nucleophilic attack of the amine to one position of benzoquinone produces singly-bound aminobenzoquinone derivatives. However, as shown in Scheme 3.3, a terminal amine of an adjacent SAM molecule can further attack another position of the bound quinone and result in a disubstituted aminobenzoquinone.

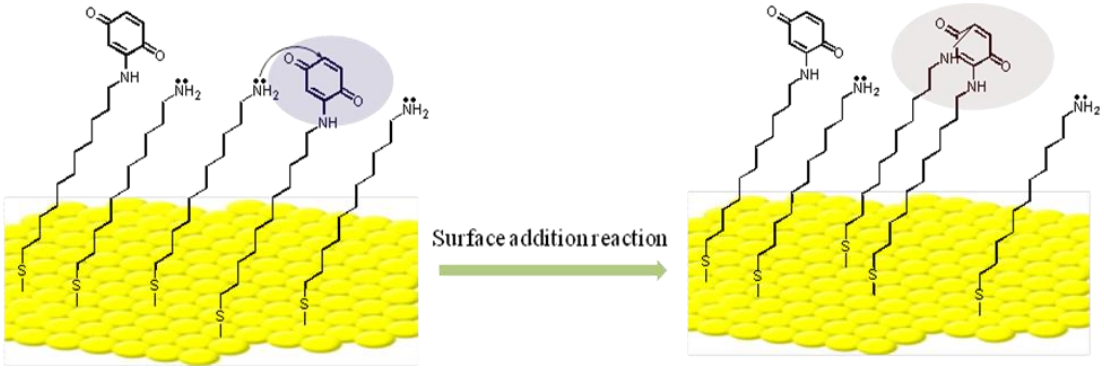

Scheme 3.3: The formation of disubstituted aminobenzoquinone modified monolayer at gold electrode surface.

Following the explanation of Novák and co-workers[16], each addition reaction shifts the formal potential cathodically because of increasing electron density on the quinone center. The cyclic voltammogram (Figure 3.1) for the one component SAM

reveals a much higher loading of disubstituted compared to singly-bound aminobenzoquinone. This is probably due to the high concentration of amine groups on the surface. Meanwhile, even at very slow scan rates (1 mV/s) all four peaks displayed peak half-widths greater than ~90mV, which are well in excess of the theoretical 45 mV predicted for an ideal two electron transfer (the theoretical explanation will be provided below). This non-ideal electrochemical behavior can be expected for surfaces with strongly interacting redox-centers. The uncertain heterogeneity of such systems complicates the interpretation of kinetic studies where the measured parameters are averages of a wide distribution of microenvironments, each with their own characteristic standard heterogeneous rate constant for electron transfer and acid dissociation constants for proton transfer. Therefore it is necessary to isolate each redox center in an effort to create a more ideal, single substituted aminobenzoquinone modified monolayer system.

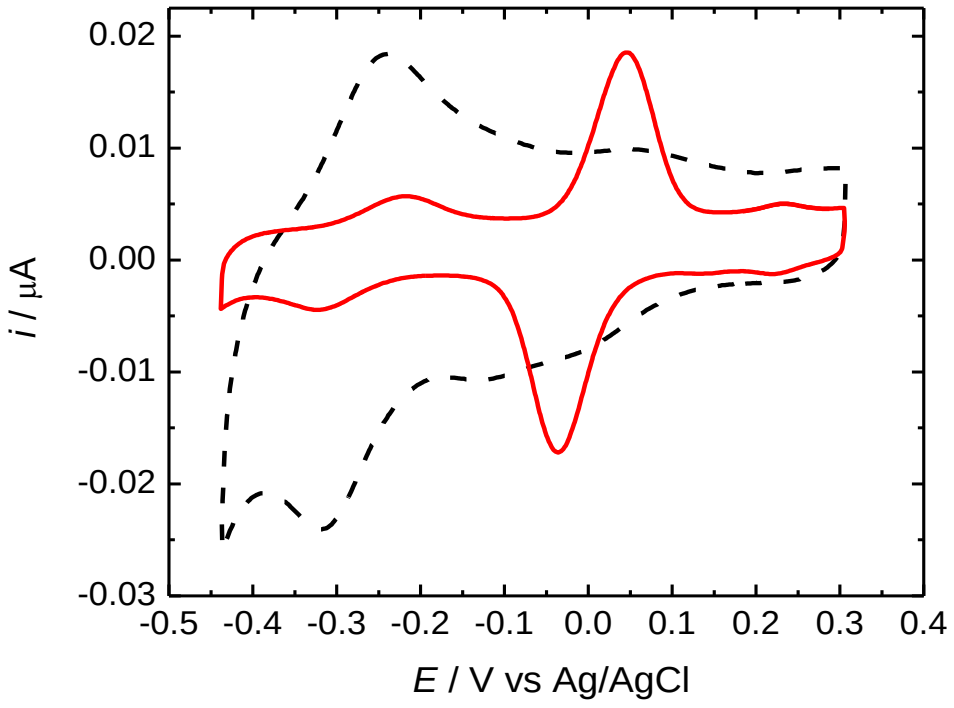

Figure 3.1: Cyclic voltammograms in pH 4.5 phosphate buffer electrolyte recorded at 5 mV/s for quinone derivatized self-assembled monolayers formed from ethanolic solutions of 1.5 mM AUT (----) and a 15:1 mixture (1.5 mM total thiol concentration) of OT:AUT (——).

The electrochemical behavior of surface monolayer systems with varying extent of intermolecular interactions was studied by Laviron and others[18-22]. Laviron built an approach to diagnose the interaction of surface electroactive groups by applying a Frumkin-like interaction potential to the current-potential response of potential sweep methods. In this model, Laviron focused exclusively on non-idealities caused by lateral interactions, which is characterized by different values of an interaction coefficient. He concluded that with increasing values of the interaction coefficient, the full width half maximum (FWHM) of the resulting voltammograms (*i*-*E* curves) under equilibrium conditions becomes bigger, and in the absence of intermolecular potentials, the FWHM equals 90.6/*n*, where *n* is the numbers of electrons involved in the overall charge transfer step. It is possible to extract the charge transfer rate constant of a non-ideal electroactive monolayer system. However, this kinetic analysis involves many independent parameters, which complicate the analytical procedures and lowers the reliability of the measure rate constant values. Additionally, as it is difficult to reproduce the same interaction coefficient in experimental preparation of monolayer systems it is preferable to eliminate intermolecular reactions of redox couples at the electrode surface. In doing so, it has been recently proven that some sophisticated techniques such as scanning tunneling spectroscopy were able to measure the electrochemical behavior of a single molecule[23;24]. A different method to ensure the elimination of intermolecular reaction was used for the aminobenzoquinone monolayers studied in this thesis. In this method, an inert thiol (octanethiol) was co-assembled with AUT by incubating the gold electrode in a mixture of the two thiols[25-29]. Octanethiol (OT) has been chosen as the diluting inert thiol for the following reasons, 1) octanethiol forms vertical monolayer after short time incubation, and 2) the methyl terminated OT can ensure that the quinone centers extended beyond the hydrophobic core of the monolayer. Meanwhile, the hydrophobic, van der Waals interaction between the methylene carbons causes the thiol chain to tilt in order to maximize the interaction between the chains and lower the overall surface energy. The most suitable ratio between OT and AUT was determined to be 15:1 by experiment, with a total thiol concentration of 1.5mM. It

should be noted that the ratio in the incubating solution does not necessarily equal the mole fraction on the electrode[13; 14]. The chosen ratio and overall thiol concentration ensure enough loading of benzoquinone at the gold electrode surface and the charge transfer behavior is close to ideal. The method of reductive desorption has been used to measure the surface coverage of covalently bonded self-assembled monolayers on metal surfaces. It has been reported that surface coverage values for long-chain alkanethiols assembled on gold electrodes have been measured to be around 8.5×10^{-10} mol/cm^2 [62;63]. For the mixed OT/AUT systems used herein, it is reasonable to estimate that the total thiol surface coverage of the mixed monolayer attached on polycrystalline gold electrode will be very close to the aforementioned thiol. Meanwhile, integration of background subtracted voltammograms (e.g. Figure 3.2) indicates that the amount of mono-substituted aminobenzoquinone is around 10^{-12} mol/cm^2. Therefore, the ratio the benzoquinone loading on this mixed monolayer system is ~0.1%, which indicates that the redox active molecules are well diluted on the electrode surface. Additionally, the yield of the Michael-like surface reaction can be estimated to be about 1.5% by assuming that the concentration of AUT attached to the surface is the same (1:15) as that in the solution.

A representative 5 mV/s CV for two component SAMs (AUT and OT) followed by the interfacial reaction with benzoquinone in pH 4.5 phosphate buffer is shown as the solid line in Figure 3.1. Similar to the dashed line for the AUT only monolayer system, the two component monolayer system gives three reduction peaks, and the most pronounced one is centered at 0V, and can be assigned to the redox behavior of the mono-substituted benzoquinone species. A weaker redox pair is observed at -0.3 V, which is from the di-substituted benzoquinone species[12]. Additionally, one can note that in some instances a minor third redox couple was observed at more positive potentials (0.2V) and with much smaller peak currents. This third redox pair has been attributed to quinones non-covalently attached to the mono-substituted species. This was easily verified by the fact that prolonged rinsing of the electrode lead to the complete disappearance of this third redox pair. It seems likely that the majority redox component present on the mixed monolayer is the mono-substituted benzoquinone

species, which is the preferred system targeted for investigation. The loading of quinone on this mixed monolayer is smaller than that on the single AUT monolayer (based on the integration of CVs) which is reasonable given the lower concentration of amino groups on the surface. However, this difference is much smaller than that predicted from the 15:1 ratio of mixed thiol in the bulk solution. Because of the differences in the monolayer assembling rates and the thermodynamic equilibria the resulting mole ratio of thiols on gold surface is not the same as the mole fraction of those in the incubating solution, and the estimated ratio is lower than 15:1 because often a longer chain thiol like AUT will replace a relatively shorter chain thiol like OT during the incubation step. This can be explained by the fact that increasing the chain length increases the thermodynamic stability of aliphatic monolayers. In the surface Michael addition-like reaction of the AUT only monolayer, both the formation of a hydrogen bonding network due to the close proximity of the amine groups and the steric hindrance can significantly decrease the surface concentrations of active amine groups. Consequently, the efficiency of the surface reaction to form mono-substituted aminobenzoquinone modified monolayer is significantly lower. In comparison, isolated amine groups found on the mixed OT/AUT monolayer are more reactive, and give higher yields (10% by crude calculation from the integration of the background corrected voltammograms) of the quinone functionalized monolayer.

CVs at different scan rates (10 mV/s, 20 mV/s, 50 mV/s, 100 mV/s, and 200 mV/s, 500 mV/s) in pH 5.6 after background corrections are shown in Figure 3.2 (a). Figure 3.2 (b) plots the relationship between the maximum peak current intensity as a function of the scan rate. The linear relationship obtained in Figure 3.2 b indicates that the assembly of benzoquinone onto the electrode surface was successful. The mono-substituted aminobenzoquinone derivatized surface is stable in the electrolyte even with prolonged cycling of the electrode potential, although there is a slow attenuation of the peak intensity in electrolytes whose pH is higher than 9. The FWHM of the voltammograms recorded at the slowest scan rate (1mV/s) at different pH is 50-75mV, which is larger than the theoretically predicted 45mV for the two electron transfer expected under Nernstian conditions. In other words, the PCET

transfer rate of the mono-substituted aminobenzoquinone modified monolayer is so slow that 1 mV/s scan rate isn't able to create equilibrium conditions. It will be shown below that the potential step technique (chronocoulometry) can be used to reach equilibrium conditions and provides evidence of the near-ideality of the mono-substituted aminobenzoquinone monolayer system.

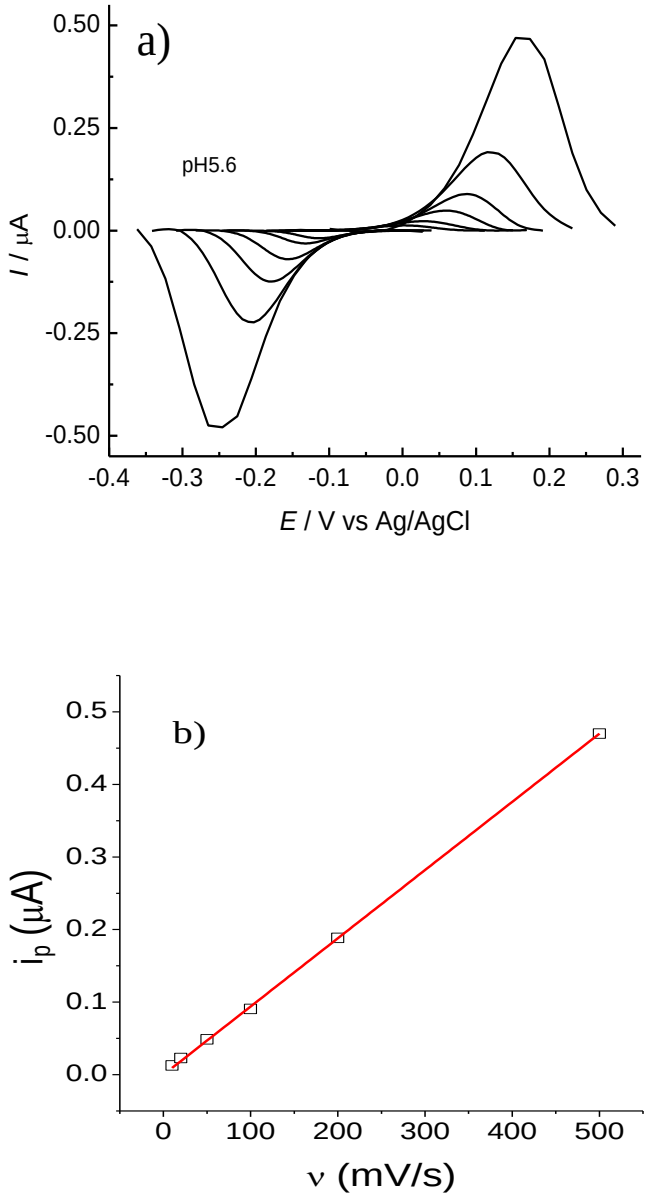

Figure 3.2: (a) Representative cyclic voltammograms (pH 5.6) at different scan rates (10 mV/s, 20 mV/s, 50 mV/s, 100 mV/s, and 200 mV/s, 500 mV/s), (b) scan rate versus peak current at pH5.6.

3.3.2 Evidence of Ideal Monolayer Behavior

An ideal monolayer system is defined as a system without intermolecular interactions between surface redox species. Often the adsorption of redox couples to the electrode is assumed to follow a Langmuir adsorption isotherm. The following discussion includes two parts: one is a theoretical prediction on the current-potential function of an ideal electron transfer reaction[30]; the other is for the chronocoulometric measurement of the mono-substituted aminobenzoquinone modified monolayer system.

1) Theoretical Electrochemical Behavior of an Ideal Electron Transfer System

For a multiple electron transfer reaction, the expression of current versus concentration of reduced and oxidized species is described by Eqn. (3.1).

$$Ox + ne \rightleftharpoons \mathrm{Red}$$

$$-\frac{\partial \Gamma_{Ox}(t)}{\partial t} = \frac{\partial \Gamma_{\mathrm{Red}}(t)}{\partial t} = \frac{i}{nFA} \tag{3.1}$$

Where $\Gamma_{Ox}(t)$ and $\Gamma_{\mathrm{Red}}(t)$ are the time dependent surface concentrations, F is the Faradary constant and A is the electrode surface area.

Concentrations of reduced and oxidized species under equilibrium conditions can be expressed by the Nernst equation:

$$\frac{\Gamma_{Ox}(t)}{\Gamma_{\mathrm{Red}}(t)} = \exp\left[\frac{nF}{RT}\left(E - E^0\right)\right] \tag{3.2}$$

And $\Gamma_{Ox}(t) + \Gamma_{\mathrm{Red}}(t) = \Gamma_{tot}$

By combining Eqn. (3.1) with Eqn. (3.2), the relation between current and potential can be expressed by Eqn. (3.3).

$$i = \frac{n^2F^2}{RT}\frac{\upsilon A\Gamma_{tot}\exp\left[\frac{nF}{RT}\left(E - E^{0'}\right)\right]}{\left\{1+\exp\left[\frac{nF}{RT}\left(E - E^{0'}\right)\right]\right\}^2} \tag{3.3}$$

Where Γ_{tot} is the total surface concentration, $\upsilon = \frac{dE}{dt}$ is the scan rate.

After differentiation of Eqn. (3.3), one can obtain an expression for the maximum peak height:

$$i_p = \frac{n^2F^2}{4RT}\upsilon AT_{tot} \tag{3.4}$$

Eqn. (3.4) shows that for an electroactive surface system, the intensity of the peak current should be linear with the scan rate. This is different for the case of a redox couple in bulk solution where the peak current intensity is proportional to the square root of the scan rate[30].

From Eqn. (3.3), the expression for the full width half maximum can be derived and shown by Eqn. (3.5).

$$\Delta E_{p,1/2} = 3.53\frac{RT}{nF} \tag{3.5}$$

In which *n* is the number of electrons.

It can be calculated that for an ideal two electron transfer reaction, the FWHM should be 45.9mV. Therefore to test if a charge transfer reaction is influenced by intermolecular interaction, Eqn. (3.5) should be used. Under equilibrium conditions, an ideal mono-substituted aminobenzoquinone modified monolayer should give a FWHM of 45.9mV in the measured voltammogram, since it is well known that quinone undergoes two electron transfer in aqueous buffer solution.

2) Chronocoulometry measurements of the mono-substituted aminobenzoquinone modified monolayer

As described above, the kinetics of the interfacial benzoquinone reduction is so slow that the equilibrium condition of this system can't be achieved by a cyclic voltammetry measurement with the lowest accessible scan rate of 1mV/s. Other electrochemical techniques like chronocoulometry were explored to achieve equilibrium conditions. The details of chronocoulometric measurements have been described in Chapter 2, and the required apparent formal potentials were determined from the 1 mV/s voltammograms.

Briefly, the working electrode was initially biased at a potential, E_{rest}, ~ 0.2 – 0.3V negative of the apparent formal potential of the mono-substituted redox couple.

Care was taken to ensure that this potential was positive of the residual signal arising from di-substituted benzoquinones. At E_{rest} all mono-substituted redox centres will be in the fully reduced form. The potential was then stepped to a more positive potential, E_{var}, and held for 120 seconds which is long enough to achieve the fraction of oxidation mandated by the Nernst equation. The potential was then stepped back to E_{rest} and the resulting current transient was measured for 250 ms. E_{rest} is a sufficiently negative enough overpotential that all oxidized species formed in the forward step can easily be reduced within the 250 ms window even with standard heterogeneous rate constants on the order of 10^{-2} s^{-1} (see Equation (1.10) and the following Equation (3.12a)). The transient is numerically integrated to provide the difference in the total charge, ΔQ, between E_{rest} and E_{var}. This procedure was then repeated for increasingly positive values of E_{var} in 15 mV steps. The total charge measured consists of contributions from both Faradaic and capacitive processes

$$\Delta Q = \Delta q_F + \Delta q_C \tag{3.6a}$$

where Δq_F represents the charge from electron transfer of the benzoquinone and Δq_C represents the background charge which is induced by non-faradic capacitive currents.

Figure 3.3a provides the results of double-step experiments in both pH 1.9 and pH 5.5 phosphate buffer electrolytes. At potentials well-removed from the formal potentials, ΔQ varies linearly with potential with a constant slope. This indicates that the interfacial capacitance associated with the hydrophobic core of the SAM is potential independent in agreement with the CV results. Furthermore, the linearity allows us to accurately correct the ΔQ values to give Δq_F as illustrated in Figure 3.3a. Figure 3.3b shows the fractional amount of oxidized redox centres as a function of potential which can be determined from the measured charge as follows;

$$\theta = \frac{\Gamma_{ox}}{\Gamma_{tot}} = \frac{\left(\Delta q_F\right)_E}{\left(\Delta q_F\right)_{tot}} \tag{3.6b}$$

Γ_{ox} is the surface concentration of the oxidized form of the mono-substituted benzoquinone. Γ_{tot} is the total surface concentration of mono-substituted redox centres

which is proportional to the total charge $(\Delta q_F)_{tot}$ associated with the complete conversion of the reduced species to its oxidized form. Numerical differentiation of Figure 3.3b yields a plot of $\frac{d\theta}{dE}$ *versus* E which is the equivalent of a linear sweep voltammogram under Nernstian conditions. Figure 3.3c provides such plots for the two pHs. Comparing with ~65mV from 1mV/s CV, the full-width half maxima for pH 1.9 and pH 5.5 were measured to be 50 mV and 51 mV respectively, proving that both redox waves correspond to nearly ideal two-electron processes with very slow rates of electron transfer. The above chronocoulometric measurements prove that the mono-substituted aminobenzoquinone modified monolayer shows nearly ideal electron transfer behaviour. The following section will concentrate on the extraction of thermodynamic and kinetic information from the voltammograms and the charge measurement.

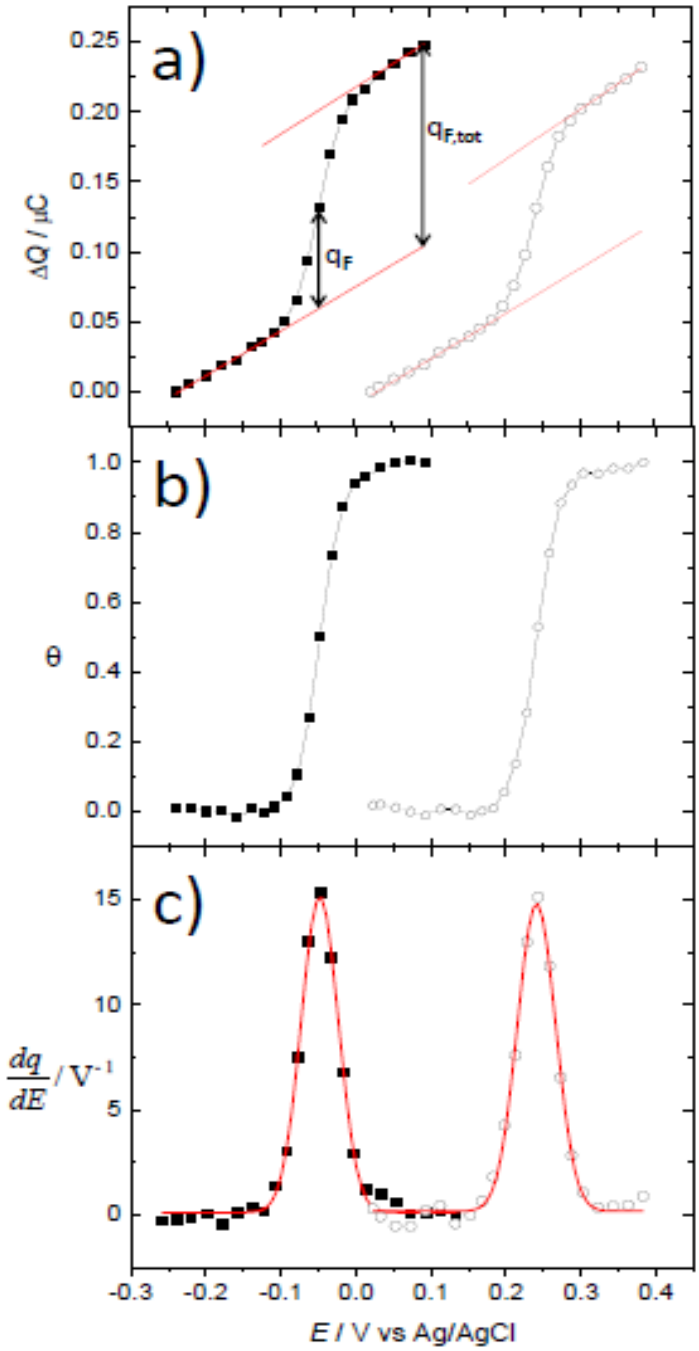

Figure 3.3: Results of chronocoluometry measurements for benzoquinone derivatized 15:1 (OT: AUT) mixed SAMs in sodium phosphate buffer electrolytes. Filled squares (■) correspond to experiments performed at pH 5.5 and open circles (○) correspond to pH 1.9. Panel a) Relative charge as a function of stepped potential. Panel b) Fractional composition of oxidized species as determined from the charge measurements. Panel c) Numerical differentiation of panel b (points) and resulting Gaussian fits (solid lines). FWHM of fits are 50 mV for pH 5.5 and 51 mV for pH 1.9.

3.3.3 Electrochemical Measured Thermodynamic and Kinetic Parameters

Electrode potential is an important adjustment parameter in the studies of ion coupled heterogeneous electron transfer reaction and has been used for the electrochemical PCET systems. For mechanistic studies of an aminobenzoquinone modified monolayer system, both cyclic voltammetry and chronocoulometry were used for the determination of parameters such as apparent standard rate constants, apparent formal potentials, and apparent standard transfer coefficients.

In PCET, pH is another important adjustment parameter due to the involvement of proton transfer. It can be noted here that the formal potential is related to the Gibbs free energy, so that pH dependent apparent formal potential can be regarded as thermodynamic information. Meanwhile, pH dependent apparent standard rate constants and apparent transfer coefficients can be regarded as kinetic information.

1) Influence of pH on Apparent Formal Potential

In order to calculate the number of transferred protons in this monolayer system, pH dependent cyclic voltammetry measurements in phosphate buffer solution with the same ionic strength have been performed and the resulting apparent formal potential versus pH has been plotted. The voltammograms recorded at 1 mV/s from pH 2.5 to pH 8.3 are shown in Figure 3.4. The monolayer system was freshly prepared for the measurement of each CV and the CVs have been offset on the current axis for comparison. It is difficult to ensure the same loading of benzoquinone on the surface on each electrode preparation due to the uncertainty of monolayer composition and surface reaction, and this is evidenced by the area under each half-cycle in the different CVs. Fortunately this uncertainty of surface concentrations won’t affect the following mechanistic studies. Qualitatively, it is obvious that the apparent formal potential is strongly pH dependent as redox couple peak positions shift anodically with decreasing electrolyte pH. Another pronounced result from these pH dependent CVs are the high degree of asymmetry between anodic peak and cathodic peak, which has been proven to relate to the values of the apparent transfer coefficient in the PCET kinetics from the description in Chapter 2.

More information on the electrochemical kinetics can be obtained from the voltammograms. For instance the degree of potential separation in the anodic and cathodic peaks is an indication of the apparent standard rate constant and the degree of asymmetry represents the value of apparent standard transfer coefficient. In Chapter 2, a theoretical model has been introduced for a quasi-reversible reaction and it has been concluded that the larger potential separation is, the smaller the apparent standard rate constant will be. In addition, the apparent standard transfer coefficient can be predicted to be smaller than 0.5 when the cathodic peak is broader than the anodic peak, and conversely, if the anodic peak is broader than the cathodic peak, the corresponding apparent standard transfer coefficient will be larger than 0.5.

The asymmetry becomes more pronounced with increasing scan rate at any investigated pH. At the same scan rate, the voltammograms are most symmetric at pH 5 but become increasingly more asymmetric with both increasing and decreasing pH. The highest recorded pH can't be greater than 9 due to the observed lower loading and degradation of the voltammetric peaks for the mono-substituted aminobenzoquinone at the electrode surface. This is most likely caused by decomposition of the quinone[31], hydrolysis of the carbon-nitrogen bond or the conversion from mono-substituted quinone to the disubstituted quinone.

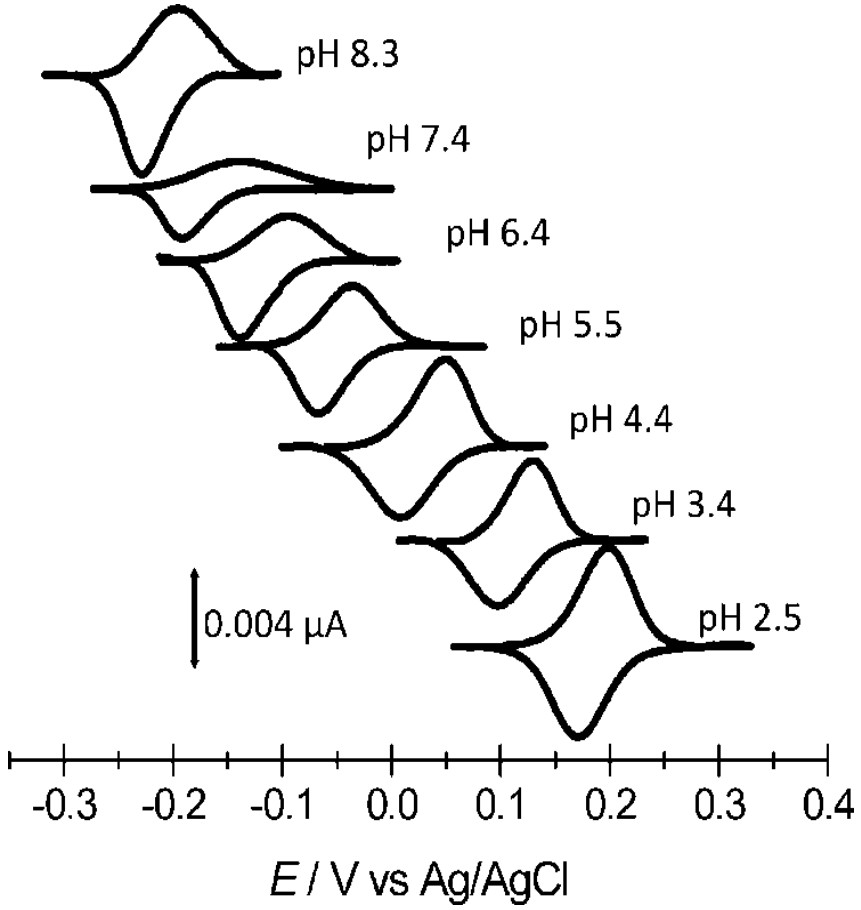

Figure 3.4: Baseline corrected 1 mV/s CVs of benzoquinone derivatized 15:1 (OT:AUT) mixed SAMs in 0.1M $NaClO_4$ + 5 mM phosphate buffer electrolytes, the pH of which is indicated next to each curve. The CVs have been displaced along the ordinate axis for clarity.

Pourbaix diagrams, which plot equilibrium or formal potential versus pH, are one form of a thermochemical map and an elegant application of the Nernst equation. The slope of the line in a Pourbaix diagram can be used to indicate the proton/electron stoichiometry of a PCET reaction. A detailed analysis of Pourbaix diagrams will be shown in Chapter 4, and will show that the slope (in mV/pH) should equal $-58m/n$ where m is the number of the protons and n is the number of the electrons involved in the overall charge transfer. Figure 3.5 demonstrates that between 2<pH<4.5, the slope is -88mV/pH and between 4.5<pH<8.5, the slope is -58mV/pH. The chronocoulometric measurement has already informed us that the mono-substituted aminobenzoquinone modified monolayer undergoes two electron transfers. Based on

the Pourbaix slope, it seems that there are three protons being transferred for the quinone/hydroquinone redox couple in low pH electrolyte. This is very surprising given the expected redox behavior of the quinone moiety (see Scheme 3.1). The nature of the third proton transfer will be verified in following Chapter 4 by combining experimental results with theoretical model. The overall reaction from pH 4.5 to pH 8.5 is the conversion from mono-substituted amino-benzoquinone modified monolayer to mono-substituted amino-dihydroquinone modified monolayer after the accepting of two electrons and two protons, as indicated in Scheme 3.3. Below pH 4.5 by simple consideration of the Nernst equation, the slope of -88mV/pH indicates 2e3H transfer. The proposed third protonation is centered on the amine group tethering the benzoquinone[32] (Scheme 3.4). This mechanism would be consistent with Abhayawardhana and Sutherland's proposed electric-field driven proton transfer of the aryl amine for an aminoanthraquinone self-assembled monolayer[7]. Such field-assisted proton transfer processes have been observed in redox inactive SAMs containing carboxylic acid functional groups[33-37].

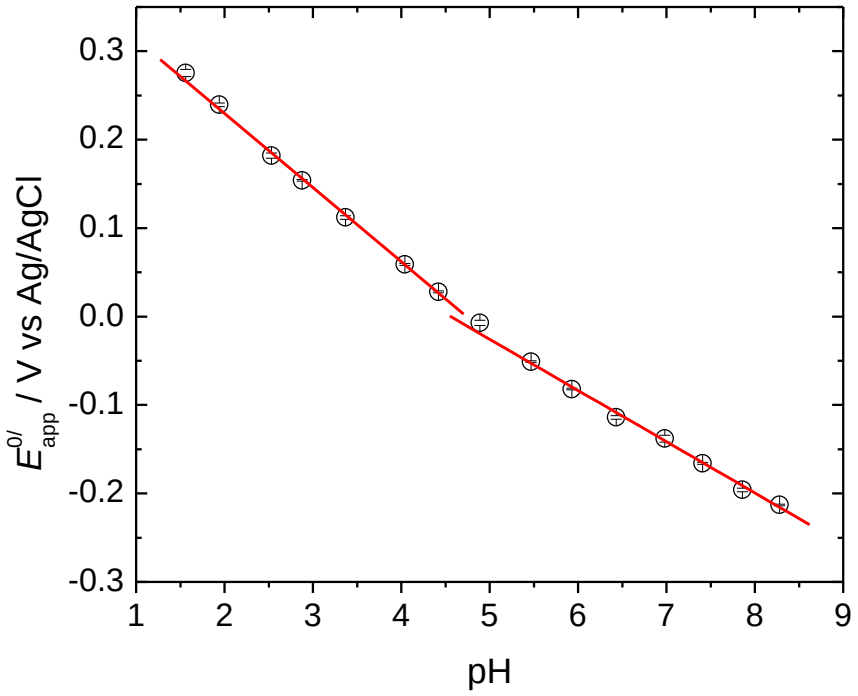

Figure 3.5: Formal potential of benzoquinone derivatized 15:1 (OT:AUT) mixed SAMs in 0.1M $NaClO_4$ + 5 mM phosphate buffer electrolytes as a function of pH. The formal potential was estimated as the midpoint of the cathodic and anodic peak potentials in very slow scan (1 mV/s) CVs.

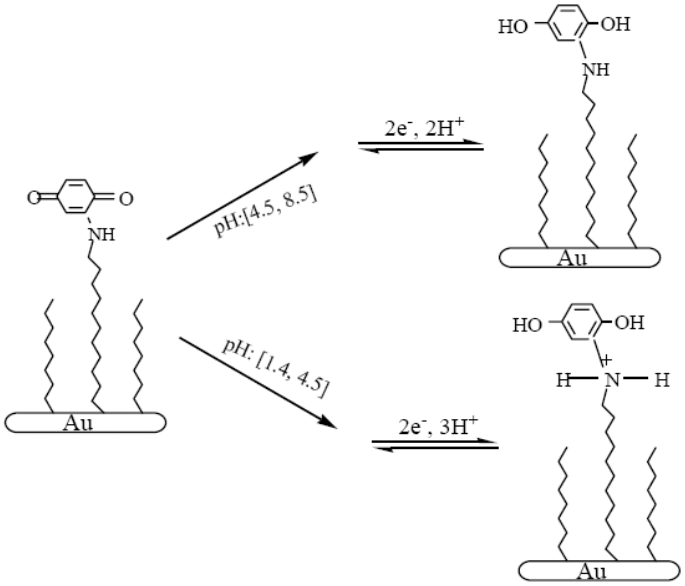

Scheme 3.4: Proposed overall reaction of aminobenzoquinone modified monolayer.

2) Influence of pH on Apparent Standard Rate Constant (Cyclic Voltammetry and Chronocoulometric Measurement)

Based on Eqn. (2.10), the discussion on both the apparent standard rate constant and the apparent standard transfer coefficient from the voltammograms has been shown qualitatively. In the following section, the values of the pH dependence of the apparent standard rate constants as measured by cyclic voltammetry and chronocoulometry will be shown.

For a multiple proton and electron transfer reaction, it is difficult to measure the rate constant and the transfer coefficient for each single electron transfer experimentally. The measured kinetic parameters, which are termed the apparent rate constant and apparent transfer coefficient, are for the overall PCET reaction. As introduced in Chapter 2, both apparent rate constant and apparent transfer coefficient for multi-electron, multi-proton transfer reaction are functions of standard rate constant and standard transfer coefficient of single electron transfer. With the assumption of a stepwise 2e2H transfer mechanism, Laviron and then Finklea were able to derive a mathematical model that predicts a "W" shape for the apparent standard rate constant versus pH[38;39]. The details of this model will be explored in Chapter 4. As discussed in Chapter 2, the peak separation between the cathodic peak and the anodic peak in a CV provides a qualitative estimation of the apparent standard rate constant. Figure 3.6 plots the pH dependent potential separation for the mono-substituted aminobenzoquinone modified monolayer, A "W" shape can be clearly observed with a local maximum around pH 5.5 and local minima at pH 4 and pH 7.5.

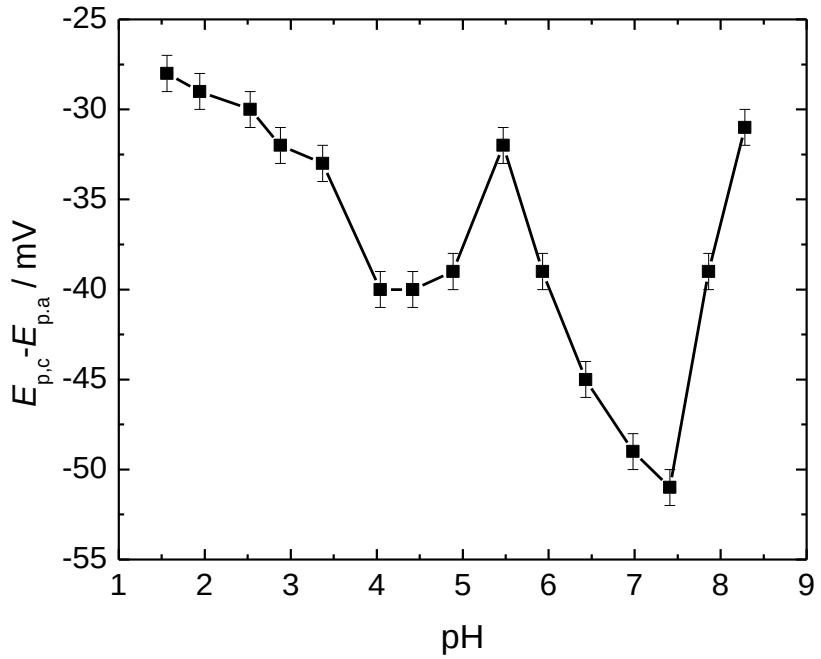

Figure 3.6: Potential separation between the cathodic and anodic peaks as determined from 1mV/s voltammograms. CVs were run in 0.1M $NaClO_4$ + 5 mM phosphate buffer electrolytes.

Many electrochemical techniques have been used to determine the values of apparent standard rate constants, including cyclic voltammetry[40-43], alternating current (AC) voltammetry[44;45], and chronocoulometry[46-50]. The AC voltammetry method was unable to be employed for this study because the very small k_{app}^{std} values require measurements at inaccessibly low frequencies. Perhaps the most commonly used approach to obtain heterogeneous rate constants for electron transfer from voltammograms in redox-active SAMs is the Laviron approach[51-56]. In this method, the potentials of the cathodic and anodic peaks are measured as a function of scan rate, υ. Kinetic parameters may be obtained from Equations 3.7 and 3.8

$$E_{pc} = E^{0/} - \frac{RT}{\alpha nF}\ln\left(\frac{\alpha nF\upsilon}{RTk_{app}^{std}}\right) \tag{3.7}$$

$$E_{pa} = E^{0/} - \frac{RT}{(1-\alpha)nF}\ln\left(\frac{(1-\alpha)nF\upsilon}{RTk_{app}^{std}}\right) \tag{3.8}$$

Where E_{pc} and E_{pa} are the potentials of the cathodic and anodic peaks, n is the number

of electrons transferred, and α is the transfer coefficient. By plotting E_p-$E^{0/}$ versus ln(υ) for both the anodic and cathodic branches and extrapolating the linear portion (which occurs when $\left|E - E_p\right| > {}^{100mV}/_{n}$) back to the *x*-axis intercept (E_{pc} or $E_{pa} = E^{0/}$), υ_a and υ_c, which are called as the critical scan rates, can be obtained and then used for the calculation of apparent standard rate constant (Eqn. (3.9)). Ideally, the apparent standard rate constants and apparent standard transfer coefficients obtained from the two branches of the CVs are self-consistent.

$$k_{app}^{std} = \frac{\alpha nF\upsilon_c}{RT} = \frac{(1-\alpha)nF\upsilon_a}{RT} \tag{3.9}$$

Inherent in this approach is the assumption of a constant value of α at all peak potentials which move further from the formal potential with increasing scan rate. This assumption is not valid for PCET reactions where α_{app}^{std} is potential dependent based on the observation of shape of the voltammograms. This is evidenced in Figure 3.7 where Laviron plots are presented for pH 3 and pH 7. At the higher pH, the anodic branch is quite linear but the cathodic branch fits to a 2nd order polynomial, and the situation is reversed for the lower pH. Any attempt to fit the data to a linear function should result in serious error when extracting values for α_{app}^{std} and k_{app}^{std} and for this reason the Laviron method was deemed unsuitable for these studies and a method to determine k_{app}^{std} without extrapolation of data from large overpotentials was sought.

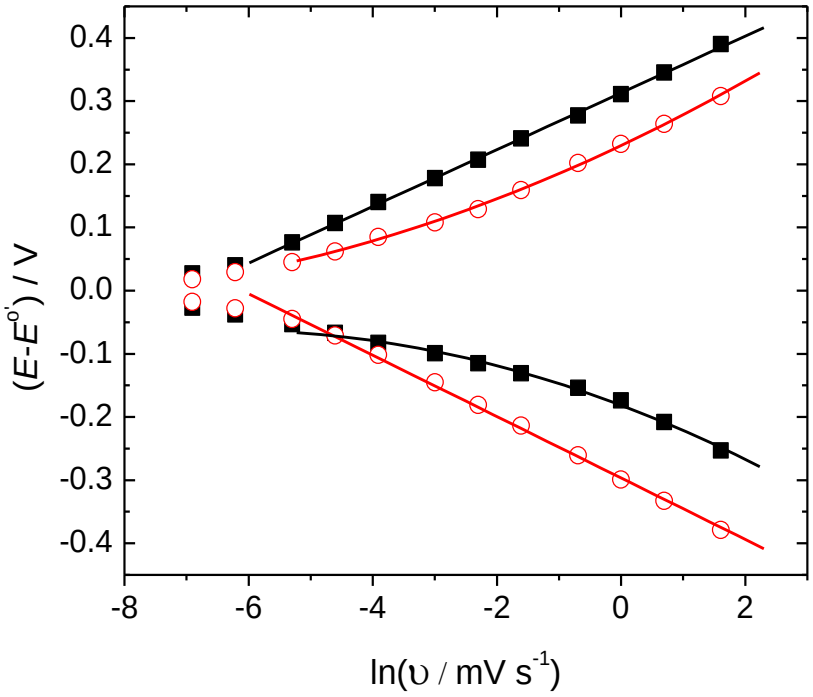

Figure 3.7: Laviron plots for the anodic and cathodic branches of voltammograms recorded in pH 7 (■) and pH 3 (○) phosphate buffer electrolytes. Solid lines are either linear or second order polynomial fits for data where $|E\text{-}E^{0\prime}| > 0.05$V.

Finklea has described an alternative method[40;57], which is able to calculate the apparent standard rate constant from the voltammogram without using scan rate dependent experiments. This method involves isolating the Faradaic current from the double layer charging currents and integrating the corrected voltammogram to obtain the surface concentrations of reduced and oxidized forms. After applying the Butler-Volmer equation to this PCET system, one can obtain

$$i = FAk_{app}^{std}\left(\Gamma_{ox}\exp\left[-\frac{\alpha F}{RT}\left(E-E_0\right)\right]-\Gamma_{red}\exp\left[\frac{(1-\alpha)F}{RT}\left(E-E_0\right)\right]\right) \qquad (3.10)$$

Meanwhile, the total concentration of reduced and oxidized species during the PCET event keeps constant

$$\Gamma_{ox}+\Gamma_{red}=\Gamma_{tot}$$

Thus Eqn. (3.10) can be rewritten as:

$$i = FAk_{app}^{std}\left(\Gamma_{ox}\exp\left[-\frac{\alpha F}{RT}\left(E-E_0\right)\right]-\left(\Gamma_{tot}-\Gamma_{ox}\right)\exp\left[\frac{(1-\alpha)F}{RT}\left(E-E_0\right)\right]\right)$$

At the apparent formal potential the apparent standard rate constant and the Faradaic, $i_{F,\eta}$=0, are related as follows

$$k_{app}^{std} = \frac{i_{F,\eta=0}}{q_{F,tot}\left[1-2f_{\eta=0}\right]}. \tag{3.11}$$

For systems that exhibit very large or very small potential separation in their CVs, Eqn. (3.11) is not reliable to calculate the apparent standard rate constant, since even a small error in the determination of the apparent formal potential can lead to large error in the apparent standard rate constant. For the condition of small potential separation, $i_{F,\eta=0}$ is so close to zero that the apparent standard rate constant is unable to be calculated. On the other hand, for the condition of large potential separation, large uncertainly from the calculation of the apparent standard rate constant is caused by the very small value of $q_{F,tot}\left[1-2f_{\eta=0}\right]$.

In Eqn. (3.11), $f_{\eta=0}$ is the fraction of benzoquinone species reduced in the cathodic sweep from the positive limit to the formal potential. Equivalently, $f_{\eta=0}$ can be computed for an anodic scan by integrating this linear sweep from the negative potential limit to the formal potential. Thus, in a single voltammogram, k_{app}^{std} can be calculated for both the anodic and cathodic half cycles and an average value reported. In theory, the measurement can be performed for all scan rates as long as the peak separation is sufficiently large that the denominator does not approach zero but small enough that the Faradic current at η=0 is sufficiently above background. The latter issue was the most demanding for the aminobenzoquinone system and effectively prevented the use of all but the slowest scan rates (1 mV/s) for our kinetic analysis.

The slow kinetics of this system also allows for the employment of a chronocoulometric method developed in this thesis. If one writes the redox process in terms of generalized oxidized and reduced species,

$$\mathrm{Ox} + ne^- \underset{k_{app}^{a}}{\overset{k_{app}^{c}}{\rightleftharpoons}} \mathrm{Red}$$

θ represents the fractional amount of oxidized redox centers, and for this first

order reaction, the solution to the resulting differential equation for a potential step from θ=0 (E_{rest}) to $0 \leq \theta \leq 1$ (E_{step}) can be written in terms of the fractional amount of oxidized redox centres and the apparent rate constants of the cathodic (k_{app}^{c}) and anodic (k_{app}^{a}) half reactions at E_{step}.

$$\theta(t) = \frac{k_{app}^{a}}{k}\left[1 - e^{-kt}\right] \tag{3.12a}$$

In which $k = k_{app}^{a} + k_{app}^{c}$.

If E_{step} is chosen to be the formal potential then $k_{app}^{a} = k_{app}^{c} = k_{app}^{std}$ and the fractional concentration of oxidized centres will reach θ=0.5 after sufficient time. By varying the duration the potential is held at $E^{0/}$ one can determine $\theta(t)$ by integrating the current transient arising from stepping the potential back to E_{rest}. After correcting the total charge for background contributions (as described above) the measured charge $\left[\Delta q_F(t)\right]_E$ is converted to $\theta(t)$. The results of a typical experiment are shown in Figure 3.8, which shows that θ=1/2 is achieved after step durations on the order of 2 minutes at pH 7.5. Extraction of k_{app}^{std} is achieved *via* Eqn. (3.12b) and linear regression (see inset of Figure 3.8).

$$\ln\left[1 - 2\theta(t)\right] = -2tk_{app}^{std}. \tag{3.12b}$$

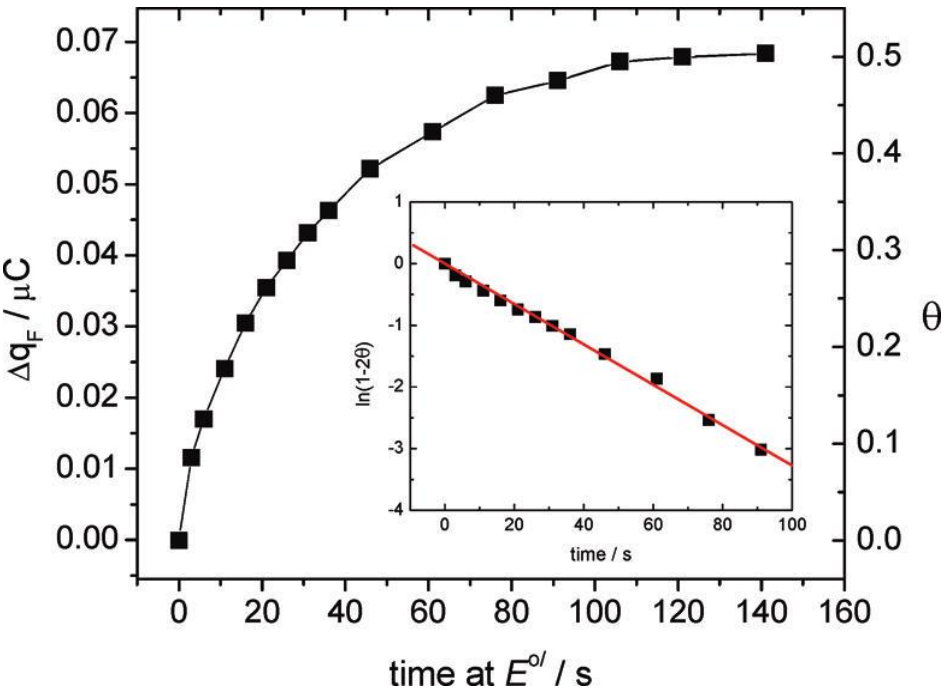

Figure 3.8: Kinetic results associated with a potential step from η = 0V to η = -0.3V as a function of hold time at the formal potential. Main plot: left axis is the measured Faradaic charge for each transient and the right axis is the corresponding fractional amount of the oxidized species. The inset shows the results of charge data linearization which can be used to extract the apparent heterogeneous rate constant, k_{app}^{std}.

Figure 3.9 shows the results of the kinetic measurements as a function of pH using the two approaches detailed above. The measured apparent standard rate constants range between ~0.1-0.01 s^{-1}. The calculated values are larger by about an order of magnitude than the values reported earlier for similar length quinone monolayer systems[15]. It should be noted that in previous studies, the kinetic information was extracted using the Laviron formulism which does not account for possible potential dependence of α_{app}. Quantitatively, the curve obtained from the potential step experiments is consistently larger than the data obtained from voltammetry. It is believed that this systematic discrepancy arises from uncertainties in determining and then applying the true formal potential during the double step experiments. For a two electron process, even small excursions from zero

overpotential lead to large differences between the rate constants and the standard rate constant. Even an offset as little as ±4 mV can lead to a nearly 20% change in the anodic and cathodic rate constants (Eqn. (3.12)). Furthermore, any difference between the actual stepped potential and the true apparent formal potential always results in an overestimate and never underestimate of k_{app}^{std} when the charge measurement described above is applied. Based on the above discussion, the open data points in Figure 3.9 can be considered as the upper bound of apparent standard rate constants. In theory, step potential experiments of a series of applied potential near the perceived formal potential can be performed to determine the accurate apparent formal potential based on the principle that the charge measured at the actual apparent formal potential should be half of the total faradic charge. Unfortunately, the preliminary attempts for those measurements failed because of the slow loss of electroactive species on the surface during the prolonged exposure in the electrolyte solution especially at high pH. Additionally, the error in charge measurement gets bigger when the applied potential becomes closer to the apparent formal potential. In fact, for the calculation from cyclic voltammetry, the uncertainties of formal potential also induce an error in the value of the apparent rate constant. For an anodic scan, positive errors in $E^{0/}$ will lead to overestimates of k_{app}^{std} and negative errors in $E^{0/}$ will give underestimates. Due to the asymmetry of the voltammograms, these errors will not be cancelled out by averaging the results of the anodic and cathodic scans due to the asymmetric behaviour of the voltammograms of this monolayer system.

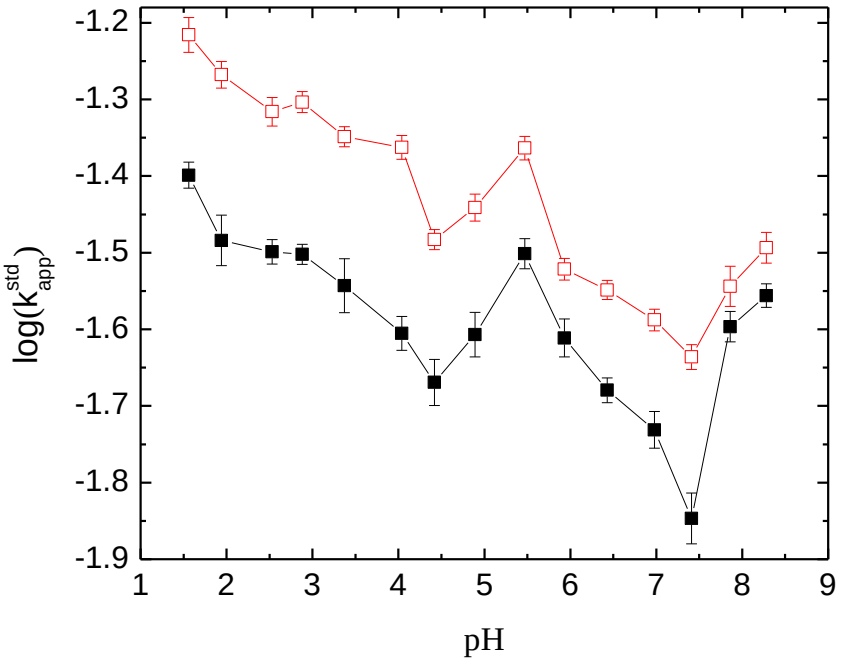

Figure 3.9: Semi-logarithmic plot of the apparent standard rate constant versus pH for the mono-substituted aminobenzoquinone monolayer. Data was obtained from cyclic voltammetry (open squares) and double-step chronocoulometry (solid squares).

The investigated pH in this monolayer system can't be extended to pH higher than 9 due to the possible decomposition of the aminobenzoquinone monolayer. Additionally, experiments cannot be performed below pH 1 because of the variation of ionic strength. However, in the range of experimentally accessible pH, the experimental data can be compared with Finklea's prediction for benzoquinone solution system with stepwise PCET mechanism. Qualitatively, the two techniques of cyclic voltammetry and chronocoulmetry provide very similar shape for apparent standard rate constant as a function of pH with approximately a 10% magnitude shift. The data also demonstrate that the apparent standard rate constant varies by nearly an order of magnitude in the range 1 < pH < 9. This is consistent with the spread of apparent standard rate constants calculated by Finklea over a similar pH range for simulation conditions pertinent to benzoquinone. It is clear that at pH 7.5, one can observe a minimum point for the apparent standard rate constant, which is close to the value predicted from Finklea's simulation results using known pK_a and E^0 values for

the benzoquinone solution system. The primary minimum at pH 7.5 is well defined in the data obtained using both techniques, while the secondary minimum is less pronounced than expected. Figure 3.6 demonstrates that the peak separation data is very consistent with the qualitative shape of the rate constant versus pH plot, and supports the existence of a secondary minimum centred at pH 4.5. In short, it can be concluded that both techniques provide a distorted "W" plot for k_{app}^{std} vs pH, which is predicted from Laviron and Finklea's simulated results for the 2e2H system. However, the plot is distorted from the perfect "W" plot expected from Finklea's model. The distortion may arise due to differences in the pK_a values and formal potential values between quinone in solution and quinone confined to the SAM/electrolyte interface. However, a more obvious explanation is that the third proton transfer is not accounted for in Finklea's model. The influence of this protonation on PCET kinetic and thermodynamic parameters will be fully discussed in Chapter 4.

3) Influence of pH on apparent transfer coefficient

The apparent transfer coefficient can be obtained for the scan rate dependent voltammetry measurement. Firstly from cyclic voltammetry measurement at different scan rates one can build a Tafel plot, which gives the relation between rate constants and overpotentials, for any given pH. Rate constants were calculated at potentials corresponding to 50% conversion (50% of redox couple oxidized or reduced)[43], providing only one measure of the anodic and cathodic rate constant per CV scan rate. At scan rates where 50% conversion occurred at $|\eta|$ > 50 mV, rate constants could be obtained for both the oxidative and reductive peaks and the appropriate limiting form of Eqn. (3.10).

$$k_{app}^{a} = k_{app}^{std} \exp(-\alpha f \eta) = \frac{2i_f(\eta)}{Q_{tot}} \quad \eta > 50 \text{ mV} \tag{3.13}$$

$$k_{app}^{c} = k_{app}^{std} \exp((1-\alpha) f \eta) = \frac{2i_f(\eta)}{Q_{tot}} \quad \eta < -50 \text{ mV} \tag{3.14}$$

The cathodic and anodic rate constants were plotted against overpotential to

yield Tafel slopes. The above equations have been used for calculation of the apparent transfer coefficient. Each scan rate yields two data points on this plot, one in the anodic branch (positive η) and one in the cathodic branch (negative η).

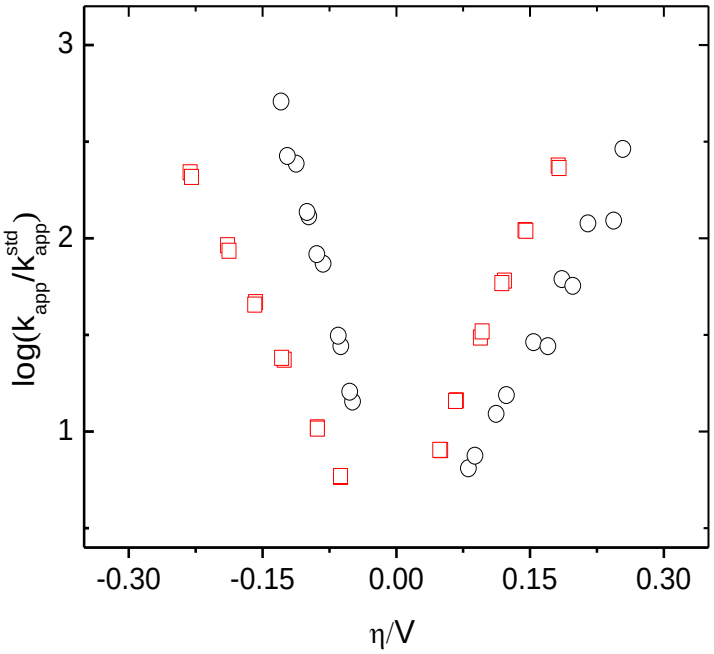

Figure 3.10: Experimental Tafel plots for the aminobenzoquinone monolayer system at pH 7 (○) and pH 4.1 (□).

By measuring CVs at different scan rates (the representative CVs for 10mV/s, 20mV/s, 50mV/s, 100mV/s and 200mV/s have been shown in Figure 3.2), the cathodic and anodic rate constants were calculated from Eqns. (3.13) and (3.14), and then Tafel plots were constructed and shown in Figure 3.10 for pH 4 and pH 7. As expected, the experimental Tafel data does not extend to sufficiently large enough overpotentials to display enough curvature from which the reorganization energy can be extracted.

However, the Tafel analysis does display pronounced asymmetry between the cathodic and anodic branches. This asymmetry manifests itself in the 10 mVs^{-1} CVs with broader voltammetric anodic (cathodic) peaks being observed when the anodic (cathodic) branch of the Tafel plot is less steep than its counterpart. It should be noted that the asymmetry is reversed between pH 4 and pH 7 in both the voltammetry and the Tafel plots. This asymmetry indicates that for this multi-proton, multi-electron

transfer process, the apparent standard transfer coefficients don't equal 0.5, which is the assumed value for standard transfer coefficient of a single electron transfer step. Interpolated to zero overpotential, one can obtain the apparent standard transfer coefficient at zero overpotential as a function of pH for this PCET monolayer system, which is shown in Figure 3.11. The plot shows an incomplete "V" shape and the values are between 0.4 and 0.72 and the minimum is observed around pH 4. The discussion of apparent transfer coefficients requires an in-depth understanding of this aminobenzoquinone modified monolayer system in many aspects. It is generally accepted that the standard transfer coefficient of single electron transfer step from either Butler-Volmer Equation or Marcus DOS theory equals 0.5. However, for this proton coupled two electron transfer experimental system, the measured apparent standard transfer coefficients at different pH obviously fluctuate around 0.5. According to Marcus DOS theory, transfer coefficients of single electron transfer step at non-zero overpotentials should depend on both the reorganization energy, as well as the overpotential[58-61]. Therefore, Tafel plots, namely overpotentials versus apparent transfer coefficient (Fig. 3.10), should be able to offer insight into the reorganization energy of the studied monolayer system. Because of the significance on the kinetic analysis, especially in a multiple proton and electron transfer reaction, these two points will be addressed in some details in Chapter 4.

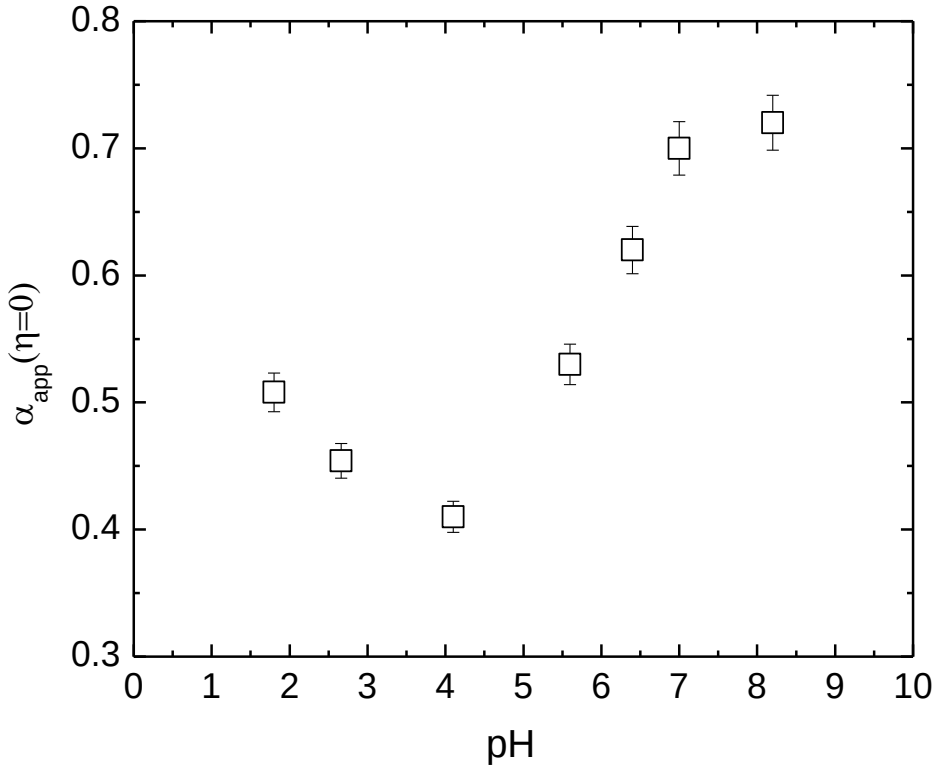

Figure 3.11: Experimental values of the apparent transfer coefficient at $\eta = 0$ (points with error bars) for the aminobenzoquinone monolayer system as a function of pH.

3.4 Summary and Conclusions

An aminobenzoquinone modified monolayer system has been prepared for the purpose of studying multiple electron and proton transfer. Near-ideal charge transfer behavior of this system has been provided by the initial assembly of a two component (OT and AUT) monolayer. Chronocoulometric measurements under equilibrium conditions provide evidence of the homogeneity of the redox centers in this modified layer. The system is well-suited for studies that can be used to test existing PCET theories. The dependence of the apparent formal potential on pH displays two linear regions, at high pH electrolyte between pH 3.5 and pH 8.5, the observed slope is -58mV, which is consistent with 2e2H transfer. With increasing acidity, another linear region, where the slope is -88mV/pH is observed. In low pH electrolytes, the number of electrons transferred is still two and therefore the Pourbaix diagram in this region

implies that a third proton is transferred during the aminobenzoquinone reduction. It is proposed that the third proton transfer is caused by the protonation of the amino group.

It has been shown from the cyclic voltammograms that the peak separation is variable with pH, which indicates that the apparent standard rate constant is also pH dependent. Two different techniques: cyclic voltammetry and double step charge measurements have used to measure the apparent standard rate constant. As opposed to the commonly employed Laviron approach, these two methods don't require the assumption of a potential independent transfer coefficient. A distorted "W" plot for the apparent standard rate constant as a function of pH arises from the calculations of both methods. This plot is similar to Finklea's prediction for stepwise 2e2H transfer.

In low pH electrolyte, the plot of apparent formal potentials versus pHs predicts 2e3H transfer not 2e2H transfer, therefore it is more reasonable to explain the experimental measureable thermodynamic and kinetic information in an extended theoretical framework. The final goal in the electrochemical characterization of this mono-substituted aminobenzoquinone modified monolayer system is to determine its electrochemical PCET mechanism. To do so, a theoretical model will be required for this purpose and shown in next chapter.

Reference List

(1) Osyczka, A.; Moser, C. C.; Dutton, P. L. *Trends Biochem Sci* **2005**, *30*, 176-182.

(2) Mayer, J.; Rhile, I.; Larsen, F.; Mader, E.; Markle, T.; DiPasquale, A. *Photosyn. Res.* **2006**, *87*, 3-20.

(3) Reece, S. Y.; Nocera, D. G. *Annu.Rev.Biochem.* **2009**, *78*, 673-699.

(4) Okamura, M. Y.; Paddock, M. L.; Graige, M. S.; Feher, G. *Biochimica et Biophysica Acta (BBA) - Bioenergetics* **2000**, *1458*, 148-163.

(5) Gupta, N.; Linschitz, H. *J.Am.Chem.Soc.* **1997**, *119*, 6384-6391.

(6) Quan, M.; Sanchez, D.; Wasylkiw, M. F.; Smith, D. K. *J.Am.Chem.Soc.* **2007**, *129*, 12847-12856.

(7) Abhayawardhana, A. D.; Sutherland, T. C. *J.Phys.Chem.C* **2009**, *113*, 4915-4924.

(8) Bulovas, A.; Dirvianskyté, N.; Talaikyté, Z.; Niaura, G.; Valentukonyté, S.; Butkus, E.; Razumas, V. *J.Electroanal.Chem.* **2006**, *591*, 175-188.

(9) Hong, H. G.; Park, W.; Yu, E. *J.Electroanal.Chem.* **1999**, *476*, 177-181.

(10) Hong, H. G.; Park, W. *Langmuir* **2001**, *17*, 2485-2492.

(11) Park, W.; Ahmed, J.; Kim, S. *Colloids and Surfaces B: Biointerfaces* **2009**, *68*, 120-124.

(12) Sarkar, S.; Sampath, S. *Langmuir* **2006**, *22*, 3388-3395.

(13) Trammell, S. A.; Seferos, D. S.; Moore, M.; Lowy, D. A.; Bazan, G. C.;

Kushmerick, J. G.; Lebedev, N. *Langmuir* **2006**, *23*, 942-948.

(14) Trammell, S. A.; Moore, M.; Lowy, D.; Lebedev, N. *J.Am.Chem.Soc.* **2008**, *130*, 5579-5585.

(15) Ye, S.; Yashiro, A.; Sato, Y.; Uosaki, K. *J.Chem.Soc., Faraday Trans.* **1996**, *92*, 3813-3821.

(16) Budavária, V.; Szu"csa, Á.; Somlai, C.; Nováka, M. *Electrochim. Acta* **2002**, *47*, 4351-4356.

(17) Lukkari, J.; Kleemola, K.; Meretoja, M.; Kankare, J. *Chem.Commun.* **1997**, 1099-1100.

(18) Alévèque, O.; Blanchard, P. Y.; Breton, T.; Dias, M. n.; Gautier, C.; Levillain, E.; Seladji, F. *Electrochem. Comm.* **2009**, *11*, 1776-1780.

(19) Alévèque, O.; Blanchard, P. Y.; Gautier, C.; Dias, M. n.; Breton, T.; Levillain, E. *Electrochem. Comm.* **2010**, *12*, 1462-1466.

(20) Aleveque, O.; Gautier, C.; Dias, M.; Breton, T.; Levillain, E. *Phys.Chem.Chem.Phys.* **2010**, *12*, 12584-12590.

(21) Laviron, E. *J.Electroanal.Chem.* **1981**, *122*, 37-44.

(22) Shiryaeva, I. M.; Collman, J. P.; Boulatov, R.; Sunderland, C. J. *Anal.Chem.* **2002**, *75*, 494-502.

(23) Petrangolini, P.; Alessandrini, A.; Navacchia, M. L.; Capobianco, M. L.; Facci, P. *J.Phys.Chem.C* **2011**, *115*, 19971-19978.

(24) Salvatore, P.; Glargaard Hansen, A.; Moth-Poulsen, K.; Bjornholm, T.; John Nichols, R.; Ulstrup, J. *Phys.Chem.Chem.Phys.* **2011**, *13*, 14394-14403.

(25) Bain, C. D.; Evall, J.; Whitesides, G. M. *J.Am.Chem.Soc.* **1989**, *111*,

7155-7164.

(26) Bain, C. D.; Whitesides, G. M. *J.Am.Chem.Soc.* **1989**, *111*, 7164-7175.

(27) Larsen, A. G.; Gothelf, K. V. *Langmuir* **2004**, *21*, 1015-1021.

(28) Lee, L. Y. S.; Sutherland, T. C.; Rucareanu, S.; Lennox, R. B. *Langmuir* **2006**, *22*, 4438-4444.

(29) Zhang, L.; Lu, T.; Gokel, G. W.; Kaifer, A. E. *Langmuir* **1993**, *9*, 786-791.

(30) Allen J.Bard Larry R.Faulkner *Electrochemical methods: fundamentals and applications*1980; pp 593-596.

(31) Sarr, D. H.; Kazunga, C.; Charles, M. J.; Pavlovich, J. G.; Aitken, M. D. *Environ.Sci.Technol.* **1995**, *29*, 2735-2740.

(32) Cameron, D. W.; Giles, R. G. F.; Pay, M. H. *Tetrahedron Lett.* **1970**, *11*, 2049-2050.

(33) Burgess, I.; Seivewright, B.; Lennox, R. B. *Langmuir* **2006**, *22*, 4420-4428.

(34) Fawcett, W. R.; Fedurco, M.; Kovacova, Z. *Langmuir* **1994**, *10*, 2403-2408.

(35) Pillay, J.; Agboola, B. O.; Ozoemena, K. I. *Electrochem. Comm.* **2009**, *11*, 1292-1296.

(36) Rosendahl, S. M.; Burgess, I. J. *Electrochim. Acta* **2008**, *53*, 6759-6767.

(37) Smith, C. P.; White, H. S. *Langmuir* **1993**, *9*, 1-3.

(38) Finklea, H. O. *J.Phys.Chem.B* **2001**, *105*, 8685-8693.

(39) Laviron, E. *J. Electroanal. Chem.* **1983**, *146*, 15-36.

(40) Finklea, H. O.; Haddox, R. M. *Phys.Chem.Chem.Phys.* **2001**, *3*, 3431-3436.

(41) Laviron, E. *J. Electroanal. Chem.* **1974**, *52*, 395-402.

(42) Laviron, E.; Roullier, L. *J. Electroanal. Chem.* **1980**, *115*, 65-74.

(43) Madhiri, N.; Finklea, H. O. *Langmuir* **2006**, *22*, 10643-10651.

(44) Creager, S. E.; Wooster, T. T. *Anal.Chem.* **1998**, *70*, 4257-4263.

(45) Bell, C. G.; Anastassiou, C. A.; O'Hare, D.; Parker, K. H.; Siggers, J. H. *Electrochim. Acta* **2012**, *64*, 71-80.

(46) Sucheta, A.; Rusling, J. F. *Electroanalysis* **1991**, *3*, 735-739.

(47) Sharp, M. *Electrochim. Acta* **1983**, *28*, 301-308.

(48) Sharp, M. *Electrochim. Acta* **1983**, *28*, 301-308.

(49) Orlik, M.; Gritzner, G. *J. Electroanal. Chem.* **2005**, *582*, 144-150.

(50) Žutic, V.; Svetlicic', V.; Lovric', M.; Ruzic, I.; Chevalet, J. *J. Electroanal. Chem.* **1984**, *177*, 253-268.

(51) Ranieri, A.; Battistuzzi, G.; Borsari, M.; Casalini, S.; Fontanesi, C.; Monari, S.; Siwek, M. J.; Sola, M. *J. Electroanal. Chem.* **2009**, *626*, 123-129.

(52) Argüello, J.; Leidens, V. L.; Magosso, H. r. A.; Ramos, R. R.; Gushikem, Y. *Electrochim. Acta* **2008**, *54*, 560-565.

(53) Vargo, M. L.; Gulka, C. P.; Gerig, J. K.; Manieri, C. M.; Dattelbaum, J. D.; Marks, C. B.; Lawrence, N. T.; Trawick, M. L.; Leopold, M. C. *Langmuir* **2009**, *26*, 560-569.

(54) Frasconi, M.; Boer, H.; Koivula, A.; Mazzei, F. *Electrochim. Acta* **2010**, *56*, 817-827.

(55) Laviron, E. *J. Electroanal. Chem.* **1979**, *101*, 19-28.

(56) Trammell, S. A.; Lowy, D. A.; Seferos, D. S.; Moore, M.; Bazan, G. C.; Lebedev, N. *J. Electroanal. Chem.* **2007**, *606*, 33-38.

(57) Haddox, R. M.; Finklea, H. O. *J.Electroanal.Chem.* **2003**, *550-551*, 351-358.

(58) Chidsey, C. E. D.; Bertozzi, C. R.; Putvinski, T. M.; Mujsce, A. M. *J.Am.Chem.Soc.* **1990**, *112*, 4301-4306.

(59) Chidsey, C. E. D. *Science* **1991**, *251*, 919-922.

(60) Finklea, H. O. *J.Electroanal.Chem.* **2001**, *495*, 79-86.

(61) Forster, R. J.; Faulkner, L. R. *J.Am.Chem.Soc.* **1994**, *116*, 5453-5461.

(62) Walczak, M. M.; Popenoe, D. D.; Deinhammer, R. S.; Lamp, B. D.; Chung, C.; Porter, M. D. *Langmuir* **1991**, *7*, 2687-2693.

(63) Widrig, C. A.; Chung, C.; Porter, M. D. *J. Electroanal. Chem.* **1991**, *310*, 335-359.

Chapter 4: Stepwise Proton Coupled Electron Transfer in Aminobenzoquinone Modified Monolayers

[Zhang, W.; Burgess, I. J. *Phys.Chem.Chem.Phys.* **2011**, *13*, 2151-2159.]
-Reproduced in part by permission of the PCCP Owner Societies

4.1 Introduction

Kinetic studies on electrochemical PCET system have been attracting intensive attention due to the importance of PCET in fundamental research and industrial applications[1-27]. As was discussed in Chapter 1, one important reaction in energy conversion is the oxidation of water to produce oxygen which involves four electrons and four protons transfer. The design of new catalysts to improve the conversion efficiency of this reaction requires deeper understanding of the mechanism of PCET[28-40]. The mechanism of multiple proton-coupled charge transfers is just an ensemble of individual stepwise and or concerted mechanisms. In the stepwise mechanism, the proton transfer reaches equilibrium very quickly and the electron transfer is assumed to be the rate determining step. For the concerted mechanism, the electron transfer and the proton transfer occur during the same elementary step and potentially high energy intermediates produced from discrete proton and electron transfers are avoided. Seminal work from Laviron nearly 30 years ago laid the foundation of the stepwise PCET mechanism using classical electron transfer theory[6-19]. Later, Finklea revisited Laviron's work and using Marcus DOS theory provided analytical expression for stepwise (SW)-PCET for one electron one proton (1e1H), one electron two proton (1e2H), two electron one proton (2e1H), and two electron two proton (2e2H) systems[2;3]. With the development of the concerted mechanism, Costentin and his co-workers derived a series of analytical expressions for the mixed (stepwise and concerted) mechanism of the 1e1H subcase.

Unfortunately, there are very few experimental systems that are suitable for mechanistic studies of electrochemical PCET, and the 1e1H oxidation of freely-dissolved phenols in organic solvents is the most investigated system[21;27;41]. In comparison with solution systems, monolayer systems are less complicated to study partly because they eliminate competing side reactions such as disproportionation and dimerization. The measurement of apparent standard rate constant is much easier in monolayer systems due to the removal of mass transport and double layer effects. Finklea and his co-workers focused their experimental efforts on monolayer systems[1;4;5]. In the last ten years, due to the difficulty in preparing convenient monolayers, Finklea's group only successfully developed two such systems: a galvinol modified monolayer and an osmium aquo complex modified monolayer system, and both systems show one electron, one proton transfer behavior. The pH dependent apparent standard rate constant and apparent formal potential of these systems have been provided using cyclic voltammetry. Unfortunately, there is a lack of mechanistic studies of those two electrochemical PCET systems to date. In order to develop an analytical method suitable to describe electrochemical PCET mechanism of the newly built monolayer system, in this chapter Laviron's model and Finklea's model[2;3;7;10;12-18], will be refined and extended to fulfill the theoretical requirements for the mono-substituted aminobenzoquinone modified monolayer system.

Using the strategy of covalently attaching 1, 4-benzoquinone (BQ) to a preformed amine terminated monolayer *via* Michael addition, Chapter 3 reported upon PCET in a nearly ideal monolayer. The determined dependence of the apparent standard rate constant (which describes the kinetics of the overall conversion) on electrolyte pH agreed only semi-qualitatively with 2e2H SW-PCET theory. In Chapter 3 it was proposed that the discrepancies observed in acidic solutions (pH < 4.5) may have been due to the additional protonation of the amino functionality. In this chapter, an extended theoretical framework is built which successfully justifies the hypothesis introduced in Chapter 3. Additionally, experimental measurements provided are in reasonable agreement with the proposed stepwise PCET mechanism and give realistic values for the various acid dissociation and standard rate constants. Finally, PCET

pathways of this aminobenzoquinone modified monolayer are derived.

4.2 Theory

The model described below was first built by Laviron and then modified by Finklea. Both discussed four specific cases of *n* electron *m* proton PCET where *n* and *m* can equal 1 or 2. . Here their work is summarized and then extended for two new cases $n = 1$, $m = 3$ and $n = 2$, $m = 3$. The resulting analytical expressions for the apparent standard rate constant can be used to simulate voltammograms.

4.2.1 Overview

Mechanistic studies of stepwise PCET starts with the building of a scheme of the possible intermediate species produced during PCET steps. The members of the scheme are decided by the number of transferred electron/proton(s). For example, for the 1e1H subcase, there are four members in a square scheme due to the involvement of four possible chemical species. Since the aminobenzoquinone modified monolayer was proposed to show 2e3H transfer in the low pH electrolyte, a 12-member scheme needs to be built for the discussion of this system. In the 12-member scheme there are nine possible acid/base reactions (shown by vertical transformations in Scheme 4.1) and eight formal potentials describing electron transfer equilibria (shown by horizontal transformations in Scheme 4.1). As shown in Scheme 4.1, the dissociation constants should decrease as one moves down a column of proton transfers and a series of single electron reductions are present moving left to right across a row. Thus, *M* and *C* correspond to the fully deprotonated/fully oxidized species and the fully protonated/fully reduced species respectively. Finklea has discussed the nine member square scheme that excludes the bottom row in Scheme 4.1 so that all but two of the possible square, ladder, and picket fence subsets of Scheme 4.1 have been previously described. Here two new subcases, namely 1e3H and 2e3H will be discussed.

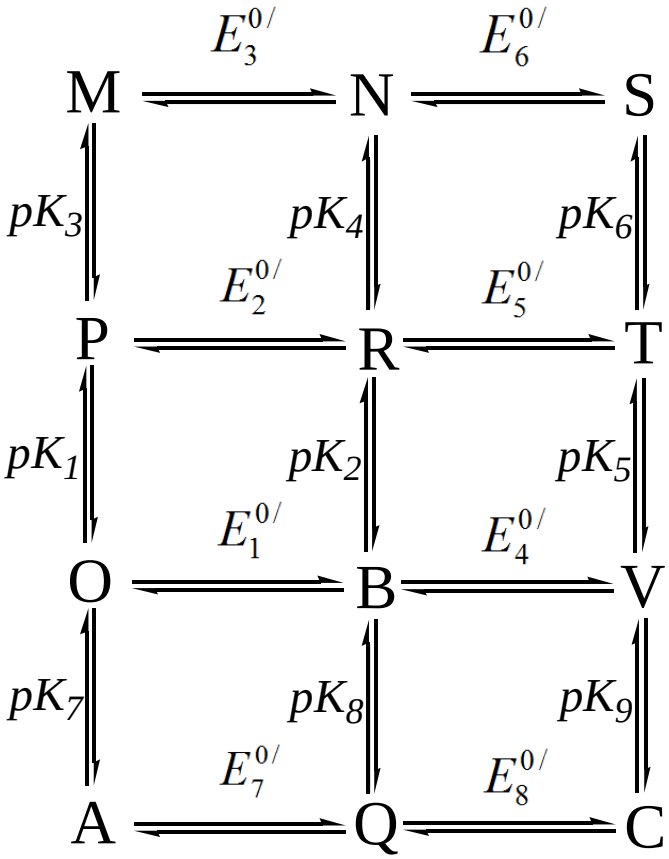

Scheme 4.1: 12-member scheme for two electron, three proton transfer.

The relationship between the two formal potentials in any 1e1H sub square is obtained by applying the Nernst equation. For example consider the four-membered scheme MNPR.

$M + e^- \rightleftharpoons N \qquad E_3^{0/}$

$P + e^- \rightleftharpoons R \qquad E_2^{0/}$

Applying the Nernst equation to each redox couple provides,

$$E = E_3^{0/} + \frac{RT}{F} \ln \frac{\Gamma_M}{\Gamma_N}$$

$$E = E_2^{0/} + \frac{RT}{F} \ln \frac{\Gamma_P}{\Gamma_R}$$

For a simple proton transfer process such as M↔P:

$$10^{-pK_3} = K_3 = \frac{\Gamma_M [H^+]}{\Gamma_P} \qquad (4.1)$$

Similarly for the other proton transfer reactions:

$$10^{-pK_4} = K_4 = \frac{\Gamma_N [H^+]}{\Gamma_R} \tag{4.2}$$

$$10^{-pK_6} = K_6 = \frac{\Gamma_S [H^+]}{\Gamma_T} \tag{4.3}$$

$$10^{-pK_5} = K_5 = \frac{\Gamma_T [H^+]}{\Gamma_V} \tag{4.4}$$

$$10^{-pK_2} = K_2 = \frac{\Gamma_P [H^+]}{\Gamma_B} \tag{4.5}$$

$$10^{-pK_1} = K_1 = \frac{\Gamma_P [H^+]}{\Gamma_O} \tag{4.6}$$

$$10^{-pK_9} = K_9 = \frac{\Gamma_V [H^+]}{\Gamma_C} \tag{4.7}$$

$$10^{-pK_8} = K_8 = \frac{\Gamma_B [H^+]}{\Gamma_Q} \tag{4.8}$$

$$10^{-pK_7} = K_7 = \frac{\Gamma_O [H^+]}{\Gamma_A} \tag{4.9}$$

Upon combining Eqns (4.1) and (4.2) with the corresponding Nernst equations, one can obtain:

$$E_3^{0/} = E_2^{0/} + \frac{RT}{F} \ln \frac{K_4}{K_3} \tag{4.10}$$

Similarly:

$$E_6^{0/} = E_5^{0/} + \frac{RT}{F} \ln \frac{K_6}{K_4} \tag{4.11}$$

$$E_1^{0/} = E_2^{0/} + \frac{RT}{F} \ln \frac{K_1}{K_2} \tag{4.12}$$

$$E_4^{0/} = E_5^{0/} + \frac{RT}{F} \ln \frac{K_2}{K_5} \tag{4.13}$$

$$E_7^{0/} = E_2^{0/} + \frac{RT}{F} \ln \frac{K_1 K_7}{K_2 K_8} \tag{4.14}$$

$$E_8^{0/} = E_5^{0/} + \frac{RT}{F}\ln\frac{K_2K_8}{K_5K_9} \tag{4.15}$$

For each individual electron transfer process (elementary step), an overpotential, η_i can be defined that relates the applied potential E to the i^{th} formal potential, $E_i^{0/}$

$$\eta_i = E - E_i^{0/} \tag{4.16}$$

with i = 1,2,3,…8.

Similarly, for the overall process of different subcases (1e1H, 1e2H…), their apparent overpotential $\eta_{app,XY}$ can be calculated by the corresponding apparent formal potential $E_{app,XY}^{0/}$:

$$\eta_{app,XY} = E - E_{\mathrm{app,XY}}^{0/} \tag{4.17}$$

Where X and Y are the letters defining the appropriate subcase. The apparent standard rate constant is measured at the zero apparent overpotential.

The rates of the cathodic ($k_{c,i}$) and anodic ($k_{a,i}$) electron transfer for each electron transfer step are assumed to follow the Tafel relationship.

$$k_{c,i} = k_{s,i}\exp\left[-\alpha_i f\eta_i\right] \tag{4.18}$$

$$k_{a,i} = k_{s,i}\exp\left[(1-\alpha_i) f\eta_i\right] \tag{4.19}$$

And for the overall PCET reaction, the corresponding Tafel relations are:

$$k_{app,XY}^{c} = k_{app,XY}^{std}\exp\left[-\alpha_{app,XY}^{c} f\eta_{app,XY}\right] \tag{4.20a}$$

$$k_{app,XY}^{a} = k_{app,XY}^{std}\exp\left[(1-\alpha_{app,XY}^{a}) f\eta_{app,XY}\right] \tag{4.20b}$$

where $f = \frac{F}{RT}$, $k_{s,i}$ is the standard rate constant for each electron transfer step, and $k_{app,XY}^{std}$ is the apparent standard rate constant for any required subclass of PCET reaction. The plots of apparent rate constant versus overpotential from above Eqns. are defined as the Tafel plot for either single electron transfer step or overall PCET reaction. At this point, no assumptions are made on whether or not the transfer

coefficients, α_i, depend on overpotential.

All sub-schemes include multiple pathways from which the principal component oxidized and reduced species can interconvert. Therefore, the experimentally measurable parameters are the apparent standard rate constant ($k_{app,XY}^{std}$) and *apparent* formal potential ($E_{app,XY}^{0/}$) where *X* and *Y* are the oxidized and reduced species in the overall electrochemical reaction. A detailed expression for apparent rate constants will be derived in the following section.

From measurements of the rate of conversion at different potentials one can also obtain an apparent transfer coefficient, $\alpha_{app,XY}^{c}$ and $\alpha_{app,XY}^{a}$ from simple rearrangement of the Tafel relationship.

$$\alpha_{app,XY}^{c} = \frac{\ln\left(\frac{k_{app,XY}^{std}}{k_{app,XY}^{c}}\right)}{nf\eta_{app,XY}} \tag{4.21a}$$

$$\alpha_{app,AB}^{a} = 1 - \frac{\ln\left(\frac{k_{app,XY}^{a}}{k_{app,XY}^{std}}\right)}{nf\eta_{app,XY}} \tag{4.21b}$$

Where *n* is number of electrons transferred in the overall process and $\eta_{app,XY} = E - E_{app,XY}^{0/}$ is the apparent overpotential.

The following discussion will be limited to the stepwise mechanism. It is assumed that all proton transfers are much faster than electron transfers in stepwise mechanism and thus the *path* of conversion is determined only by the relative rates of the electron transfers in any column in Scheme 4.1. The parameter $path_i$ is defined to be the ratio of the i^{th} cathodic rate constant to the sum of cathodic rate constants in a particular column

$$Path_i = \frac{k_i}{\sum_n k_n} \tag{4.22}$$

For example, there are four possible pathways for each 1e3H subcase. The discussion follows for the MNPROBAQ ladder but is equally applicable for the NSRTBVQC ladder. Assuming M to be the starting species (results obtained if M, O, or A are

chosen as the starting species are identical), each path for the generation of Q can be quantified. For example, $Path_2$ is defined by the rapid deprotonation of M, followed by a rate-limiting reduction to P which converts to Q in a series of very fast protonations.

$$Path_2 = \frac{k_{MPRBQ}}{k_{MNRBQ} + k_{MPOBQ} + k_{MPRBQ} + k_{MPOAQ}} = \frac{k_2}{k_3 + k_2 + k_1 + k}$$

The exact forms of $path_i$ are provided in the discussion of different subcases.

4.2.2 Analytical Expressions of Different Subcases (from 1e1H to 2e3H)

In this section, analytical expressions for the stepwise mechanism to different subcases will be derived for 1) the apparent formal potential of the overall process; 3) the apparent anodic and cathodic rate constants; 3) the pathway.

Subset for 1e1H

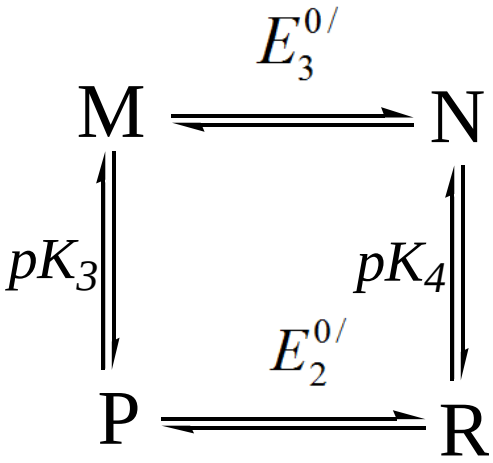

Scheme 4.2: Four membered square scheme for 1e1H subcase.

The overall reaction for the 1e1H is depicted by the four membered square scheme in Scheme 4.2 is: $M + H^+ + e \rightleftharpoons R$

The formal potential of the overall conversion of M to R is related to the applied potential, E by the Nernst equation

$$E = E_{app,MR}^{0/,sw} + \frac{RT}{F}\ln\left(\frac{\Gamma_{ox}}{\Gamma_{red}}\right) \tag{4.23}$$

Where $\Gamma_{ox} = \Gamma_M + \Gamma_P$ and $\Gamma_{red} = \Gamma_N + \Gamma_R$.

Using expressions for acid dissociations, Eqn. (4.23) can be re-written in terms of acid dissociation constants.

$$E_{app,MR}^{0/,sw} = E - \frac{RT}{F}\ln\left(\frac{\Gamma_M}{\Gamma_N}\right) - \frac{RT}{F}\ln\left(\frac{1+\frac{[H^+]}{K_3}}{1+\frac{[H^+]}{K_4}}\right) \tag{4.24}$$

A Nernstian relationship can also be written for the simple electron transfer event (*i.e.* direct passage from M → N) as follows

$$E_3^{0/} = E - \frac{RT}{F}\ln\left(\frac{\Gamma_M}{\Gamma_N}\right) \tag{4.25}$$

which can be substituted into Eqn. (4.24) to afford,

$$E_{app,MR}^{0/,sw} = E_3^{0/} - \frac{RT}{F}\ln\left(\frac{1+\frac{[H^+]}{K_3}}{1+\frac{[H^+]}{K_4}}\right) \tag{4.26}$$

Any square or ladder scheme involving only a single electron transfer eliminates the complicating issue of the formation of unstable intermediates such as semiquinones in aqueous solution. However, as will be shown, the kinetics of even the simplest of these schemes includes multiple pathways and hence the measured kinetic rate constants will be apparent rate constants.

Since we assume proton transfer is at equilibrium, the kinetics of the overall process are decided by the kinetics of the rate-limiting individual electron transfer processes

$$M + e \rightleftharpoons N$$

$$Rate_3 = \frac{dM}{dt} = -k_{s,3}\Gamma_M \exp\left(-\alpha_3 f \eta_3\right) + k_{s,3}\Gamma_N \exp\left[\left(1-\alpha_3\right) f \eta_3\right] \tag{4.27}$$

$$P + e \rightleftharpoons R$$

$$Rate_2 = \frac{dP}{dt} = -k_{s,2}\Gamma_P \exp\left(-\alpha_2 f \eta_2\right) + k_{s,2}\Gamma_R \exp\left[\left(1-\alpha_2\right) f \eta_2\right] \tag{4.28}$$

The observed apparent rate of electron transfer is the sum of the rates for the two half reactions MN and PR.

$$\begin{aligned} Rate_{app}^{MR} &= Rate_3 + Rate_2 = \frac{dM}{dt} + \frac{dP}{dt} \\ &= -k_{s,3}\Gamma_M \exp\left(-\alpha_3 f\eta_3\right) + k_{s,3}\Gamma_N \exp\left[\left(1-\alpha_3\right) f\eta_3\right] \\ &\quad -k_{s,2}\Gamma_P \exp\left(-\alpha_2 f\eta_2\right) + k_{s,2}\Gamma_R \exp\left[\left(1-\alpha_2\right) f\eta_2\right] \end{aligned} \tag{4.29}$$

The above Eqn. (4.29) can be rewritten as:

$$\begin{aligned} Rate_{app}^{MR} &= -k_{s,3}\Gamma_M \exp\left(-\alpha_3 f\eta_3\right) + k_{s,3}\frac{K_4\Gamma_R}{[H^+]} \exp\left[\left(1-\alpha_3\right) f\eta_3\right] \\ &\quad -k_{s,2}\frac{\Gamma_M[H^+]}{K_3} \exp\left(-\alpha_2 f\eta_2\right) + k_{s,2}\Gamma_R \exp\left[\left(1-\alpha_2\right) f\eta_2\right] \end{aligned} \tag{4.30}$$

Eqn. (4.30) can be separated into contributions for both the forward and reverse processes. For example, the rate expression for just the cathodic component is

$$\begin{aligned} Rate_{app,c}^{MR} &= -k_{app,MR}^{sw,c}\Gamma_{ox} \\ &= -k_{s,3}\Gamma_M \exp\left(-\alpha_3 f\eta_3\right) - k_{s,2}\frac{\Gamma_M[H^+]}{K_3} \exp\left(-\alpha_2 f\eta_2\right) \end{aligned} \tag{4.31}$$

where $\Gamma_{ox} = \Gamma_M + \Gamma_P = \Gamma_M\left(1+\frac{[H^+]}{K_3}\right)$.

Thus, from Eqn. (4.31) one obtains

$$k_{app,MR}^{sw,c} = \frac{k_{s,3}\exp\left(-\alpha_3 f\eta_3\right) + \frac{k_{s,2}[H^+]}{K_3}\exp\left(-\alpha_2 f\eta_2\right)}{1+\frac{[H^+]}{K_3}} \tag{4.32}$$

Expressions for the anodic apparent rate constant are achieved through a similar analysis,

$$k_{app,MR}^{sw,a} = \frac{\frac{k_{s,3}K_4}{[H^+]}\exp\left[(1-\alpha_3) f\eta_3\right] + k_{s,2}\exp\left[(1-\alpha_2) f\eta_2\right]}{1+\frac{K_4}{[H^+]}} \tag{4.33}$$

When the apparent formal potential is applied to the electrode, the apparent cathodic rate constant equals the apparent anodic rate constant, and is defined as the apparent

standard rate constant. The apparent standard rate constant for the 1e1H case can be derived:

$$k_{app,MR}^{sw,std} = \frac{k_{s,3}\left(\frac{1+\frac{[H^+]}{K_3}}{1+\frac{[H^+]}{K_4}}\right)^{\alpha_3} + \frac{k_{s,2}[H^+]}{K_3}\left(\frac{K_3+[H^+]}{K_4+[H^+]}\right)^{\alpha_2}}{1+\frac{[H^+]}{K_3}} = \frac{\frac{k_{s,3}K_4}{[H^+]}\left(\frac{1+\frac{[H^+]}{K_3}}{1+\frac{[H^+]}{K_4}}\right)^{\alpha_3-1} + k_{s,2}\left(\frac{K_3+[H^+]}{K_4+[H^+]}\right)^{\alpha_2-1}}{1+\frac{K_4}{[H^+]}} \tag{4.34}$$

Although the kinetically favoured pathway will be the same for both the anodic and cathodic processes, only the analysis of the overall reduction is presented below. Since the electron transfer step is the rate determining step, the rate at which the reaction proceeds sequentially from M→P→R is determined by the rate of conversion of P→R.

$$Rate_{P,R} = Rate_{M,P,R}$$

$$k_{MPR} = \frac{k_{s2}\exp(-\alpha_2 f\eta_2)\Gamma_P}{\Gamma_M} \tag{4.35}$$

For a simple four-membered scheme the only other pathway is M→N→R whose rate is given by

$$k_{MNR} = k_{MN} = k_{s,3}\exp(-\alpha_3 f\eta_3)$$

The expressions for k_{MPR} and k_{MNR} can then be used to determine a relative weighting for the pathways and the path with higher weighting is the dominant process.

$$Path_{MPR} = \frac{k_{MPR}}{k_{MNR}+k_{MPR}} = \frac{k_{s,2}\frac{[H^+]}{K_3}\exp(-\alpha_2 f\eta_2)}{k_{s,3}\exp(-\alpha_3 f\eta_3)+k_{s,2}\frac{[H^+]}{K_3}\exp(-\alpha_2 f\eta_2)}$$

$$Path_{MNR} = \frac{k_{MNR}}{k_{MNR}+k_{MPR}} = \frac{k_{s,3}\exp(-\alpha_3 f\eta_3)}{k_{s,3}\exp(-\alpha_3 f\eta_3)+k_{s,2}\frac{[H^+]}{K_3}\exp(-\alpha_2 f\eta_2)}$$

Chapter 2 described how voltammograms can be simulated given a standard rate constant and transfer coefficient using Eqn. (2.10). This equation can also be used to simulate voltammograms for PCET processes by substitution of the pertinent analytical expression for the apparent rate constant.

Subset for 1e2H

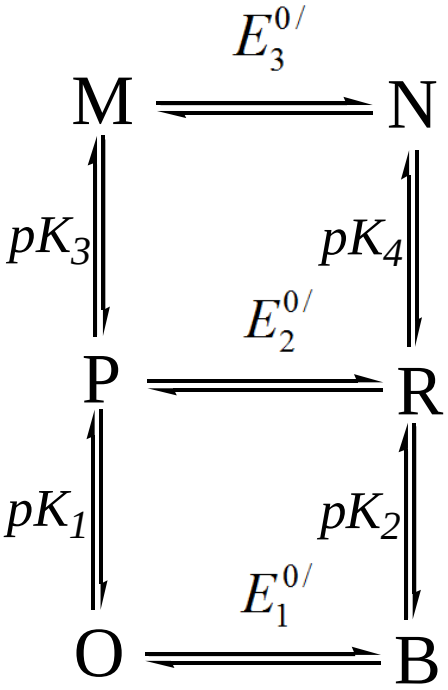

Scheme 4.3: Six membered ladder scheme for 1e2H subcase.

A six membered ladder scheme was used to describe this 1e2H transfer process. As shown in Scheme 4.3, the overall reaction to be considered is the conversion of M to B via the transfer of one electron and two protons, $M + e^- + 2H^+ \rightleftharpoons B$, for which the following form of the Nernst Equation can be written

$$E = E_{app,MB}^{0/,sw} + \frac{RT}{F}\ln\left(\frac{\Gamma_{ox}}{\Gamma_{red}}\right). \tag{4.36}$$

Expressions for acid dissociations can be used to build the following expressions for the total surface concentration of oxidized and reduced species

$$\Gamma_{ox} = \Gamma_M + \Gamma_P + \Gamma_O = \Gamma_P\left(\frac{K_3}{[H^+]} + 1 + \frac{[H^+]}{K_1}\right) \tag{4.37}$$

$$\Gamma_{red} = \Gamma_N + \Gamma_R + \Gamma_B = \Gamma_R \left(\frac{K_4}{[H^+]} + 1 + \frac{[H^+]}{K_2} \right) \tag{4.38}$$

which, in turn, can be substituted into Eqn. (4.36)

$$E = E_{app,MB}^{0/,sw} + \frac{RT}{F} \ln\left(\frac{\Gamma_P}{\Gamma_R} \right) + \frac{RT}{F} \ln\left(\frac{\left(\frac{K_3}{[H^+]} + 1 + \frac{[H^+]}{K_1} \right)}{\left(\frac{K_4}{[H^+]} + 1 + \frac{[H^+]}{K_2} \right)} \right) \tag{4.39}$$

As the second term on the right hand side of Eqn. (4.39) is equal to $E - E_2^{0/}$,

$$E_{app,MB}^{0/,sw} = E_2^{0/} - \frac{RT}{F} \ln\left(\frac{\left(\frac{K_3}{[H^+]} + 1 + \frac{[H^+]}{K_1} \right)}{\left(\frac{K_4}{[H^+]} + 1 + \frac{[H^+]}{K_2} \right)} \right) \tag{4.40}$$

There are three electron transfer reaction rates to consider for the 1e2H process

$$Rate_3 = \frac{dM}{dt} = -k_{s,3}\Gamma_M \exp\left(-\alpha_3 f \eta_3\right) + k_{s,3}\Gamma_N \exp\left[\left(1-\alpha_3\right) f \eta_3\right]$$
$$Rate_2 = \frac{dP}{dt} = -k_{s,2}\Gamma_P \exp\left(-\alpha_2 f \eta_2\right) + k_{s,2}\Gamma_R \exp\left[\left(1-\alpha_2\right) f \eta_2\right]$$
$$Rate_1 = \frac{dO}{dt} = -k_{s,1}\Gamma_O \exp\left(-\alpha_1 f \eta_1\right) + k_{s,1}\Gamma_B \exp\left[\left(1-\alpha_1\right) f \eta_1\right]$$

and the observed rate of M converting to B is the sum of the rates for the M↔N, P↔R and O↔B half reactions.

$$\begin{aligned} Rate_{obs}^{MB} = & -k_{s,3}\Gamma_M \exp\left(-\alpha_3 f \eta_3\right) + k_{s,3}\Gamma_N \exp\left[\left(1-\alpha_3\right) f \eta_3\right] \\ & - k_{s,2}\Gamma_P \exp\left(-\alpha_2 f \eta_2\right) + k_{s,2}\Gamma_R \exp\left[\left(1-\alpha_2\right) f \eta_2\right] \\ & - k_{s,1}\Gamma_O \exp\left(-\alpha_1 f \eta_1\right) + k_{s,1}\Gamma_B \exp\left[\left(1-\alpha_1\right) f \eta_1\right] \end{aligned} \tag{4.41}$$

By using expressions for acid dissociations, Eqn. (4.41) can be rewritten in terms of only one oxidized species, *P*, and one reduced species, *R*

$$\begin{aligned} Rate_{app}^{MB} = & -k_{s,3}\Gamma_P \frac{K_3}{[H^+]} \exp\left(-\alpha_3 f \eta_3\right) + k_{s,3}\Gamma_R \frac{K_4}{[H^+]} \exp\left[\left(1-\alpha_3\right) f \eta_3\right] \\ & - k_{s,1}\Gamma_P \frac{[H^+]}{K_1} \exp\left(-\alpha_1 f \eta_1\right) + k_{s,1}\Gamma_R \frac{[H^+]}{K_2} \exp\left[\left(1-\alpha_1\right) f \eta_1\right] \\ & - k_{s,2}\Gamma_P \exp\left(-\alpha_2 f \eta_2\right) + k_{s,2}\Gamma_R \exp\left[\left(1-\alpha_2\right) f \eta_2\right] \end{aligned} \tag{4.42}$$

Based on the expressions for the total coverage of oxidized species, the rate of cathodic components in Eqn. (4.42) becomes

$$\begin{aligned} Rate_{app.c}^{MB} = & -k_{s,3}\Gamma_P \frac{K_3}{[H^+]}\exp\left(-\alpha_3 f\eta_3\right) \\ & -k_{s,2}\Gamma_P \exp\left(-\alpha_2 f\eta_2\right) \\ & -k_{s,1}\Gamma_P \frac{[H^+]}{K_1}\exp\left(-\alpha_1 f\eta_1\right) \end{aligned} \tag{4.43}$$

Following in an analogous fashion as was done for the 1e1H subset leads to the following expressions for the anodic and cathodic apparent rate constants.

$$k_{app,MB}^{sw,c} = \frac{k_{s,3}\frac{K_3}{[H^+]}\exp\left(-\alpha_3 f\eta_3\right) + k_{s,2}\exp\left(-\alpha_2 f\eta_2\right) + k_{s,1}\frac{[H^+]}{K_1}\exp\left(-\alpha_1 f\eta_1\right)}{\left(\frac{K_3}{[H^+]} + 1 + \frac{[H^+]}{K_1}\right)} \tag{4.44}$$

$$k_{app,MB}^{sw,a} = \frac{k_{s,3}\frac{K_4}{[H^+]}\exp\left[\left(1-\alpha_3\right) f\eta_3\right] + k_{s,2}\exp\left[\left(1-\alpha_2\right) f\eta_2\right] + k_{s,1}\frac{[H^+]}{K_2}\exp\left[\left(1-\alpha_1\right) f\eta_1\right]}{\left(\frac{K_4}{[H^+]} + 1 + \frac{[H^+]}{K_2}\right)} \tag{4.45}$$

Using a similar procedure as the 1e1H case and assuming P is the starting species (this is for convenience as the same results are obtained if M or O is chosen as the starting species), each Path for the generation of B can be quantified.

$$\begin{aligned} Path_3 &= \frac{k_{PMNRB}}{k_{PMNRB} + k_{PRB} + k_{POB}} \\ &= \frac{k_{s,3}\frac{K_3}{[H^+]}\exp\left(-\alpha_3 f\eta_3\right)}{k_{s,3}\frac{K_3}{[H^+]}\exp\left(-\alpha_3 f\eta_3\right) + k_{s,2}\exp\left(-\alpha_2 f\eta_2\right) + k_{s,1}\frac{[H^+]}{K_1}\exp\left(-\alpha_1 f\eta_1\right)} \end{aligned}$$

$$\begin{aligned} Path_2 &= \frac{k_{PRB}}{k_{PMNRB} + k_{PRB} + k_{POB}} \\ &= \frac{k_{s,2}\exp\left(-\alpha_2 f\eta_2\right)}{k_{s,3}\frac{K_3}{[H^+]}\exp\left(-\alpha_3 f\eta_3\right) + k_{s,2}\exp\left(-\alpha_2 f\eta_2\right) + k_{s,1}\frac{[H^+]}{K_1}\exp\left(-\alpha_1 f\eta_1\right)} \end{aligned}$$

$$Path_1 = \frac{k_{POB}}{k_{PMNRB} + k_{PRB} + k_{POB}}$$

$$= \frac{k_{s,1}\frac{[H^+]}{K_1}\exp(-\alpha_1 f \eta_1)}{k_{s,3}\frac{K_3}{[H^+]}\exp(-\alpha_3 f \eta_3) + k_{s,2}\exp(-\alpha_2 f \eta_2) + k_{s,1}\frac{[H^+]}{K_1}\exp(-\alpha_1 f \eta_1)}$$

Subset for 1e3H

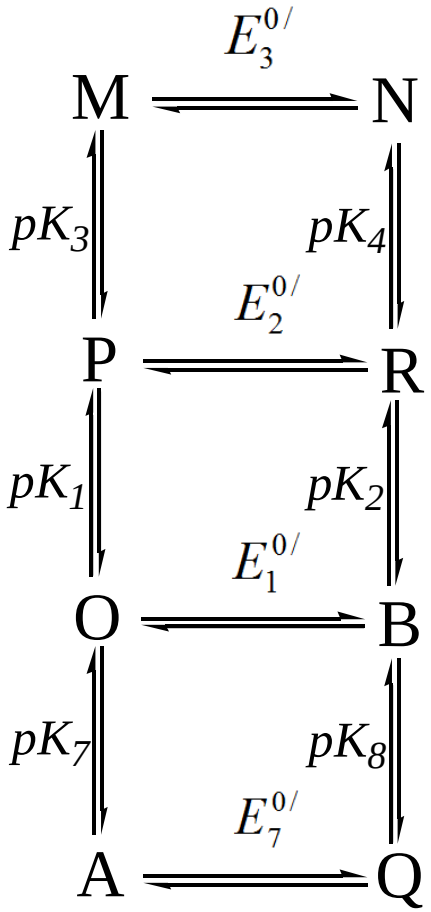

Scheme 4.4: Eight membered ladder scheme for 1e3H subcase.

The reaction to be considered is the conversion of M to Q via the transfer of one electron and three protons, $M + e^- + 3H^+ \rightleftharpoons Q$. An eight membered ladder scheme was used to describe this subcase. Starting from $E = E_{app,MQ}^{0/,sw} + \frac{RT}{F}\ln\left(\frac{\Gamma_{ox}}{\Gamma_{red}}\right)$, the

following expressions for the total surface concentrations of oxidized and reduced species can be easily derived.

$$\Gamma_{ox} = \Gamma_M + \Gamma_P + \Gamma_O + \Gamma_A = \Gamma_P \left(\frac{K_3}{[H^+]} + 1 + \frac{[H^+]}{K_1} + \frac{[H^+]^2}{K_1 K_7} \right) \tag{4.46}$$

$$\Gamma_{red} = \Gamma_N + \Gamma_R + \Gamma_B + \Gamma_Q = \Gamma_R \left(\frac{K_4}{[H^+]} + 1 + \frac{[H^+]}{K_2} + \frac{[H^+]^2}{K_2 K_8} \right) \tag{4.47}$$

Subsititution into the Nernst equation yields the following expression for the formal potential of a 1e3H transfer reaction.

$$E = E^{0/,sw}_{app,MQ} + \frac{RT}{F} \ln\left(\frac{\Gamma_P}{\Gamma_R} \right) + \frac{RT}{F} \ln\left(\frac{\left(\frac{K_3}{[H^+]} + 1 + \frac{[H^+]}{K_1} + \frac{[H^+]^2}{K_1 K_7} \right)}{\left(\frac{K_4}{[H^+]} + 1 + \frac{[H^+]}{K_2} + \frac{[H^+]^2}{K_2 K_8} \right)} \right) \tag{4.48}$$

As before, the second term of Eqn. (4.48) can be replaced by $E - E^{0/}_2$

$$E^{0/,sw}_{app,MQ} = E^{0/}_2 - \frac{RT}{F} \ln\left(\frac{\left(\frac{K_3}{[H^+]} + 1 + \frac{[H^+]}{K_1} + \frac{[H^+]^2}{K_1 K_7} \right)}{\left(\frac{K_4}{[H^+]} + 1 + \frac{[H^+]}{K_2} + \frac{[H^+]^2}{K_2 K_8} \right)} \right) \tag{4.49}$$

In addition to the three rate expressions previously shown for the 1e2H case, a fourth rate must be added for the interconversion between A and Q.

$$Rate_7 = \frac{dA}{dt} = -k_{s,7} \Gamma_A \exp\left(-\alpha_7 f \eta_7 \right) + k_{s,7} \Gamma_Q \exp\left[\left(1 - \alpha_7 \right) f \eta_7 \right] \tag{4.50}$$

The observed apparent rate for charge transfer is the sum of the rates for the four simple redox half reactions M↔N, P↔R, O↔B, and A↔Q.

$$\begin{aligned} Rate^{MQ}_{app} = & -k_{s,3} \Gamma_M \exp\left(-\alpha_3 f \eta_3 \right) + k_{s,3} \Gamma_N \exp\left[\left(1 - \alpha_3 \right) f \eta_3 \right] \\ & - k_{s,2} \Gamma_P \exp\left(-\alpha_2 f \eta_2 \right) + k_{s,2} \Gamma_R \exp\left[\left(1 - \alpha_2 \right) f \eta_2 \right] \\ & - k_{s,1} \Gamma_O \exp\left(-\alpha_1 f \eta_1 \right) + k_{s,1} \Gamma_B \exp\left[\left(1 - \alpha_1 \right) f \eta_1 \right] \\ & - k_{s,7} \Gamma_A \exp\left(-\alpha_7 f \eta_7 \right) + k_{s,7} \Gamma_Q \exp\left[\left(1 - \alpha_7 \right) f \eta_7 \right] \end{aligned} \tag{4.51}$$

Eqn. (4.51) can be recast through the use of the acid dissociation constants to eliminate all surface coverage other than those for species *P* and *R*.

$$
\begin{aligned}
Rate_{app}^{MQ} = & -k_{s,3}\Gamma_P \frac{K_3}{[H^+]}\exp\left(-\alpha_3 f\eta_3\right) + k_{s,3}\Gamma_R \frac{K_4}{[H^+]}\exp\left[\left(1-\alpha_3\right) f\eta_3\right] \\
& -k_{s,2}\Gamma_P \exp\left(-\alpha_2 f\eta_2\right) + k_{s,2}\Gamma_R \exp\left[\left(1-\alpha_2\right) f\eta_2\right] \\
& -k_{s,1}\Gamma_P \frac{[H^+]}{K_1}\exp\left(-\alpha_1 f\eta_1\right) + k_{s,1}\Gamma_R \frac{[H^+]}{K_2}\exp\left[\left(1-\alpha_1\right) f\eta_1\right] \\
& -k_{s,7}\Gamma_P \frac{[H^+]^2}{K_1K_7}\exp\left(-\alpha_7 f\eta_7\right) + k_{s,7}\Gamma_R \frac{[H^+]^2}{K_2K_8}\exp\left[\left(1-\alpha_7\right) f\eta_7\right]
\end{aligned}
\tag{4.52}
$$

Extracting from Eqn. (4.52) the terms containing Γ_P (i.e. those that contribute to the cathodic current) leads to an expression for the apparent rate of reduction.

$$
\begin{aligned}
Rate_{app,c}^{MQ} = & -k_{s,3}\Gamma_P \frac{K_3}{[H^+]}\exp\left(-\alpha_3 f\eta_3\right) - k_{s,2}\Gamma_P \exp\left(-\alpha_2 f\eta_2\right) \\
& -k_{s,1}\Gamma_P \frac{[H^+]}{K_1}\exp\left(-\alpha_1 f\eta_1\right) - k_{s,7}\Gamma_P \frac{[H^+]^2}{K_1K_7}\exp\left(-\alpha_7 f\eta_7\right)
\end{aligned}
\tag{4.53}
$$

which readily provides the following expressions for the apparent cathodic rate constants.

$$
k_{app,MQ}^{sw,c} = \frac{\frac{k_{s,3}K_3}{[H^+]}e^{(-\alpha_3 f\eta_3)} + k_{s,2}e^{(-\alpha_2 f\eta_2)} + \frac{k_{s,1}[H^+]}{K_1}e^{(-\alpha_1 f\eta_1)} + \frac{k_{s,7}[H^+]^2}{K_1K_7}e^{(-\alpha_7 f\eta_7)}}{\left(1+\frac{K_3}{[H^+]}+\frac{[H^+]}{K_1}+\frac{[H^+]^2}{K_1K_7}\right)} \tag{4.54}
$$

Similarly for apparent anodic rate constant

$$
k_{app,MQ}^{sw,a} = \frac{\frac{k_{s,3}K_4}{[H^+]}e^{\left[(1-\alpha_3) f\eta_3\right]} + k_{s,2}e^{\left[(1-\alpha_2) f\eta_2\right]} + \frac{k_{s,1}[H^+]}{K_2}e^{\left[(1-\alpha_1) f\eta_1\right]} + \frac{k_{s,7}[H^+]^2}{K_2K_8}e^{\left[(1-\alpha_7) f\eta_7\right]}}{\left(1+\frac{K_4}{[H^+]}+\frac{[H^+]}{K_2}+\frac{[H^+]^2}{K_2K_8}\right)} \tag{4.55}
$$

There are four possible pathways in this case and assuming *P* to be the starting species, we can use a similar procedure as shown in the 1e1H case.

$$
\begin{aligned}
Path_3 &= \frac{k_{PMNRBQ}}{k_{PMRNRBQ} + k_{PRBQ} + k_{POBQ} + k_{POAQ}} \\
&= \frac{\frac{k_{s,3}K_3}{[H^+]}e^{(-\alpha_3 f\eta_3)}}{\frac{k_{s,3}K_3}{[H^+]}e^{(-\alpha_3 f\eta_3)} + k_{s,2}e^{(-\alpha_2 f\eta_2)} + \frac{k_{s,1}[H^+]}{K_1}e^{(-\alpha_1 f\eta_1)} + \frac{k_{s,7}[H^+]^2}{K_1K_7}e^{(-\alpha_7 f\eta_7)}}
\end{aligned}
$$

$$Path_2 = \frac{k_{PRBQ}}{k_{PMNRBQ} + k_{PRBQ} + k_{POBQ} + k_{POAQ}}$$
$$= \frac{k_{s,2} e^{(-\alpha_2 f \eta_2)}}{\frac{k_{s,3} K_3}{[H^+]} e^{(-\alpha_3 f \eta_3)} + k_{s,2} e^{(-\alpha_2 f \eta_2)} + \frac{k_{s,1}[H^+]}{K_1} e^{(-\alpha_1 f \eta_1)} + \frac{k_{s,7}[H^+]^2}{K_1 K_7} e^{(-\alpha_7 f \eta_7)}}$$

$$Path_1 = \frac{k_{POBQ}}{k_{PMNBQR} + k_{PRBQ} + k_{POBQ} + k_{POAQ}}$$
$$= \frac{\frac{k_{s,1}[H^+]}{K_1} e^{(-\alpha_1 f \eta_1)}}{\frac{k_{s,3} K_3}{[H^+]} e^{(-\alpha_3 f \eta_3)} + k_{s,2} e^{(-\alpha_2 f \eta_2)} + \frac{k_{s,1}[H^+]}{K_1} e^{(-\alpha_1 f \eta_1)} + \frac{k_{s,7}[H^+]^2}{K_1 K_7} e^{(-\alpha_7 f \eta_7)}}$$

$$Path_7 = \frac{k_{POAQ}}{k_{PMNRBQ} + k_{PRBQ} + k_{POBQ} + k_{POAQ}}$$
$$= \frac{\frac{k_{s,7}[H^+]^2}{K_1 K_7} e^{(-\alpha_7 f \eta_7)}}{\frac{k_{s,3} K_3}{[H^+]} e^{(-\alpha_3 f \eta_3)} + k_{s,2} e^{(-\alpha_2 f \eta_2)} + \frac{k_{s,1}[H^+]}{K_1} e^{(-\alpha_1 f \eta_1)} + \frac{k_{s,7}[H^+]^2}{K_1 K_7} e^{(-\alpha_7 f \eta_7)}}$$

2e case

As introduced in Chapter 1, most of previous experimental systems belong to the 1e1H subcase, so that they don't demand the same theoretical discussion as in the proton coupled multi-electron transfer case. However, in Chapter 3, it was shown that the aminobenzoquinone monolayer system shows multi-electron (n=2) transfer over the entire range of investigated pHs. In order to determine the charge transfer mechanism of this monolayer system, Finklea's work on the theoretical consideration of two electron redox event will be refined and then used it as a basis for the theoretical model of proton coupled two electron transfer subcases.

Let *X*, *Y* and *Z* be three redox species where

$$X + e^- \rightleftharpoons Y \qquad E_a^{0/}$$
$$Y + e^- \rightleftharpoons Z \qquad E_b^{0/}$$

$$-\frac{dX}{dt} = k_{a,XY}\Gamma_Y - k_{c,XY}\Gamma_X$$
$$\frac{dZ}{dt} = k_{a,YZ}\Gamma_Z - k_{c,YZ}\Gamma_Y$$

Now assume that the intermediate oxidation state *Y* is unstable, and net 2e$^-$ transfer is observed. Therefore, the rate of loss of *X* must equal the rate of gain of *Z*.

$$-\frac{dX}{dt} = \frac{dZ}{dt}$$

Then $k_{a,XY}\Gamma_Y - k_{c,XY}\Gamma_X = k_{a,YZ}\Gamma_Z - k_{c,YZ}\Gamma_Y$

$$\Gamma_Y = \frac{k_{a,YZ}\Gamma_Z + k_{c,XY}\Gamma_X}{k_{a,XY} + k_{c,YZ}}$$

After eliminating Γ_Y from the expression for the rate of loss of *X*, an apparent rate constant can be derived

$$k_{a,XZ}\Gamma_Z - k_{c,XZ}\Gamma_X = -\left(\frac{dX}{dt}\right)_{app} = \frac{k_{a,XY}k_{a,YZ}}{k_{a,XY} + k_{c,YZ}}\Gamma_Z - \frac{k_{c,XY}k_{c,YZ}}{k_{a,XY} + k_{c,YZ}}\Gamma_X$$

The apparent cathodic rate constant is: $k_{c,XZ} = \frac{k_{c,XY}k_{c,YZ}}{k_{a,XY} + k_{c,YZ}}$ (4.56)

And the apparent anodic rate constant is: $k_{a,XZ} = \frac{k_{a,XY}k_{a,YZ}}{k_{a,XY} + k_{c,YZ}}$ (4.57)

The apparent formal potential for this 2e subcase is easily obtained from the Nernst equation:

$$E_{app,XZ}^{0/} = 0.5(E_a^{0/} + E_b^{0/}) \qquad (4.58)$$

By combining Eqn. (4.58) with Eqns. (4.56), (4.57) and the expressions for overpotential, the cathodic and anodic rate constants can be rewritten as follows

$$k_{app,XZ}^{sw,c} = \frac{k_{s,XY}\exp(-\alpha_{XY} f \eta_{XY}) k_{s,YZ}\exp(-\alpha_{YZ} f \eta_{YZ})}{k_{s,XY}\exp((1-\alpha_{XY}) f \eta_{XY}) + k_{s,YZ}\exp(-\alpha_{YZ} f \eta_{YZ})}$$
$$= \frac{k_{s,XY}\exp(-\alpha_{XY} f (E - E_a^{0/})) k_{s,YZ}\exp(-\alpha_{YZ} f (E - E_b^{0/}))}{k_{s,XY}\exp((1-\alpha_{XY}) f (E - E_a^{0/})) + k_{s,YZ}\exp(-\alpha_{YZ} f (E - E_b^{0/}))} \qquad (4.59)$$

$$k_{app,XZ}^{sw,a} = \frac{k_{s,XY}\exp((1-\alpha_{XY})f\eta_{XY})k_{s,YZ}\exp((1-\alpha_{YZ})f\eta_{YZ})}{k_{s,XY}\exp((1-\alpha_{XY})f\eta_{XY})+k_{s,YZ}\exp(-\alpha_{YZ}f\eta_{YZ})}$$
$$= \frac{k_{s,XY}\exp((1-\alpha_{XY})f(E-E_a^{0/}))k_{s,YZ}\exp((1-\alpha_{YZ})f(E-E_b^{0/}))}{k_{s,XY}\exp((1-\alpha_{XY})f(E-E_a^{0/}))+k_{s,YZ}\exp(-\alpha_{YZ}f(E-E_b^{0/}))} \quad . \tag{4.60}$$

For the overall two-electron transfer reaction, the rate constants can be expressed as:

$$k_{app,XZ}^{sw,c} = k_{app,XZ}^{sw,std}\exp(-2\alpha_{app,XZ}^{sw,c}f\eta_{app,XZ}^{sw}) \tag{4.61}$$

and

$$k_{app,XZ}^{sw,a} = k_{app,XZ}^{sw,std}\exp(2(1-\alpha_{app,XZ}^{sw,a})f\eta_{app,XZ}^{sw}) \tag{4.62}$$

Combining with the expression for the apparent formal potential for the overall reaction (Eqn. 4.58) one obtains:

$$k_{app,XZ}^{sw,c} = k_{app,XZ}^{sw,std}\exp(-2\alpha_{app,XZ}^{sw,c}f(E-0.5(E_a^{0/}+E_b^{0/}))) \tag{4.63}$$

$$k_{app,XZ}^{sw,a} = k_{app,XZ}^{sw,std}\exp(2(1-\alpha_{app,XZ}^{sw,a})f(E-0.5(E_a^{0/}+E_b^{0/}))) \tag{4.64}$$

When the first electron-transfer step is treated as the rate determining step, $k_{s,XY}\exp((1-\alpha_{XY})f(E-E_a^{0/})) \gg k_{s,YZ}\exp(-\alpha_{YZ}f(E-E_b^{0/}))$

Or $E \ll \dfrac{(1-\alpha_{XY})E_a^{0/}+\alpha_{YZ}E_b^{0/}-\dfrac{1}{f}\ln\left(\dfrac{k_{s,XY}}{k_{s,YZ}}\right)}{1-\alpha_{XY}+\alpha_{YZ}}$

Eqns. (4.63) and (4.64) reduce to:

$$k_{app,XZ}^{sw,c} = k_{s,XY}\exp(-f(E-E_a^{0/}))k_{s,YZ}\exp(-\alpha_{YZ}f(E-E_b^{0/})) \tag{4.65}$$

$$k_{app,XZ}^{sw,a} = k_{s,YZ}\exp((1-\alpha_{YZ})f(E-E_b^{0/})) \tag{4.66}$$

To compare with Eqns. (4.63) and (4.64), the above Equations are rewritten as:

$$k_{app,XZ}^{sw,c} = k_{s,YZ}\exp(-\alpha_{YZ}f(E-\frac{E_b^{0/}+E_a^{0/}}{2}))\exp((1-\alpha_{YZ})f\frac{E_a^{0/}-E_b^{0/}}{2}) \tag{4.67}$$

$$k_{app,XZ}^{sw,a} = k_{s,YZ}\exp((1-\alpha_{YZ})f(E-\frac{E_b^{0/}+E_a^{0/}}{2}))\exp((1-\alpha_{YZ})f\frac{E_a^{0/}-E_b^{0/}}{2}) \tag{4.68}$$

In comparison with Eqn. (4.65), for the cathodic part, it yields:

$$k_{app,XZ}^{sw,std} = k_{s,YZ}\exp((1-\alpha_{YZ})f\frac{E_a^{0/}-E_b^{0/}}{2})$$

And thus: $\alpha_{app,XZ}^{sw,c} = \frac{1-\alpha_{YZ}}{2}$ (4.69)

For the anodic part,

$$k_{app,XZ}^{sw,std} = k_{s,YZ} \exp((1-\alpha_{YZ}) f \frac{E_a^{0/} - E_b^{0/}}{2})$$

Therefore: $\alpha_{app,XZ}^{sw,a} = \frac{1+\alpha_{YZ}}{2}$ (4.70)

Conversely, if $k_{s,XY} \exp((1-\alpha_{XY}) f (E - E_a^{0/})) \ll k_{s,YZ} \exp(-\alpha_{YZ} f (E - E_b^{0/}))$,

Or: $E \gg \frac{(1-\alpha_{XY}) E_a^{0/} + \alpha_{YZ} E_b^{0/} - \frac{1}{f} \ln\left(\frac{k_{s,XY}}{k_{s,YZ}}\right)}{1-\alpha_{XY} + \alpha_{YZ}}$

Eqns. (4.59) and (4.60) become:

$$k_{app,XZ}^{sw,c} = k_{s,XY} \exp(-\alpha_{XY} f (E - E_a^{0/}))$$ (4.71)

$$k_{app,XZ}^{sw,c} = k_{s,XY} \exp((1-\alpha_{XY}) f (E - E_a^{0/})) \exp(f (E - E_b^{0/}))$$ (4.72)

The above Eqns. can be rewritten

$$k_{app,XZ}^{sw,c} = k_{s,XY} \exp(-\alpha_{XY} f (E - \frac{E_b^{0/} + E_a^{0/}}{2})) \exp(-\alpha_{XY} f \frac{E_b^{0/} - E_a^{0/}}{2})$$ (4.73)

$$k_{app,XZ}^{sw,a} = k_{s,XY} \exp((2-\alpha_{XY}) f (E - \frac{E_b^{0/} + E_a^{0/}}{2})) \exp(-\alpha_{XY} f \frac{E_b^{0/} - E_a^{0/}}{2})$$ (4.74)

Therefore, the standard rate constant becomes:

$$k_{app,XZ}^{sw,std} = k_{s,YZ} \exp((1-\alpha_{YZ}) f \frac{E_a^{0/} - E_b^{0/}}{2})$$ (4.75)

And the cathodic transfer coefficient:

$$\alpha_{app,XZ}^{sw,c} = \frac{\alpha_{XY}}{2}$$ (4.76)

Similarly, the anodic transfer coefficient:

$$\alpha_{app,XZ}^{sw,a} = 1 - \frac{\alpha_{XY}}{2}$$ (4.77)

Assuming $\alpha_{XY} = \alpha_{YZ} = 0.5$, the values of anodic and cathodic apparent transfer

coefficients are limited between 0.25 and 0.75.

Subset for 2e1H

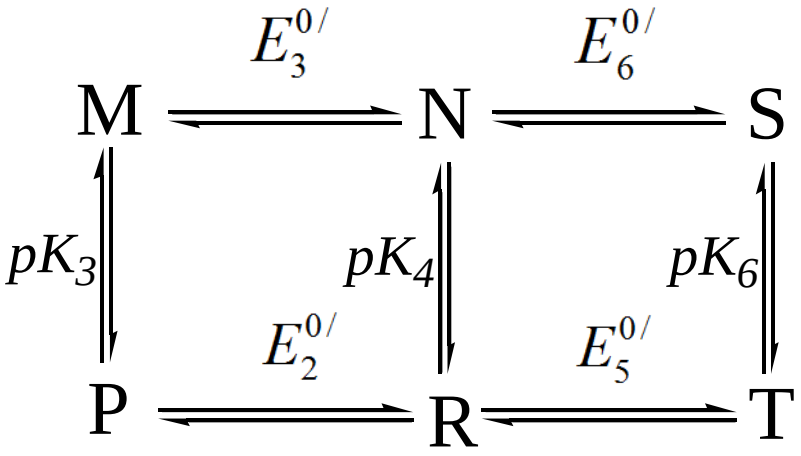

Scheme 4.5: Square scheme for 2e1H subcase.

The overall reaction is described by $M + 2e + 1H^+ \rightleftharpoons T$ is represented in the six membered "picket fence" shown in Scheme 4.5.

After applying the Nernst equation to this process one obtains:

$$E = E_{app,MR}^{0/,sw} + \frac{RT}{F}\ln\left(\frac{\Gamma_M + \Gamma_P}{\Gamma_N + \Gamma_R}\right) \tag{4.78}$$

$$E = E_{app,NT}^{0/,sw} + \frac{RT}{F}\ln\left(\frac{\Gamma_N + \Gamma_R}{\Gamma_S + \Gamma_T}\right) \tag{4.79}$$

and overall $$E = E_{app,MT}^{0/,sw} + \frac{RT}{2F}\ln\left(\frac{\Gamma_M + \Gamma_P}{\Gamma_S + \Gamma_T}\right) \tag{4.80}$$

Clearly:

$$\begin{aligned} 2E &= E_{app,MR}^{0/,sw} + E_{app,NT}^{0/,sw} + \frac{RT}{F}\ln\left(\frac{\Gamma_M + \Gamma_P}{\Gamma_S + \Gamma_T}\right) \\ 2E &= E_{app,MT}^{0/,sw} + \frac{RT}{F}\ln\left(\frac{\Gamma_M + \Gamma_P}{\Gamma_S + \Gamma_T}\right) \end{aligned} \tag{4.81}$$

Hence: $E_{app,MT}^{0/,sw} = 0.5\times(E_{app,MR}^{0/,sw} + E_{app,NT}^{0/,sw})$

As has been shown in the derivation for the 1e1H case, $E_{app,MR}^{0/,sw}$ and $E_{app,NT}^{0/,sw}$ can be

expressed as follows:

$$E_{app,MR}^{0/,sw} = E_3^{0/} - \frac{RT}{F}\ln\left(\frac{1+\frac{[H^+]}{K_3}}{1+\frac{[H^+]}{K_4}}\right) \tag{4.82}$$

$$E_{app,NT}^{0/,sw} = E_6^{0/} - \frac{RT}{F}\ln\left(\frac{1+\frac{[H^+]}{K_4}}{1+\frac{[H^+]}{K_6}}\right) \tag{4.83}$$

After substitution in Eqn. (4.81), the formal potential for the overall 2e1H reaction can be written

$$E_{app,MT}^{0/,sw} = 0.5(E_3^{0/} + E_6^{0/}) - \frac{RT}{2F}\ln\left(\frac{1+\frac{[H^+]}{K_3}}{1+\frac{[H^+]}{K_6}}\right). \tag{4.84}$$

It has been shown that the 2e process can be treated separately as two 1e processes with the assumption that the intermediate oxidation state is unstable. Therefore, as shown in Chapter 2, and the apparent anodic and cathodic rate constants, $k_{app,MT}^{sw,c}$ and $k_{app,MT}^{sw,a}$, are calculated using the following equations:

$$k_{app,MT}^{sw,a} = \frac{k_{app,MR}^{sw,a} k_{app,NT}^{sw,a}}{k_{app,MR}^{sw,a} + k_{app,NT}^{sw,c}} \tag{4.85}$$

$$k_{app,MT}^{sw,c} = \frac{k_{app,MR}^{sw,c} k_{app,NT}^{sw,c}}{k_{app,MR}^{sw,a} + k_{app,NT}^{sw,c}} \tag{4.86}$$

Expression for $k_{app,MR}^{sw,c}$ and $k_{app,MR}^{sw,a}$ are readily obtained by simple modifications of the expressions previously derived for the 1e1H subcase,

$$k_{app,MR}^{sw,a} = \frac{k_{s,3}\frac{K_4}{[H^+]}\exp\left[(1-\alpha_3)f\eta_3\right] + k_{s,2}\exp\left[(1-\alpha_2)f\eta_2\right]}{1+\frac{K_4}{[H^+]}} \tag{4.87}$$

$$k_{app,MR}^{sw,c} = \frac{k_{s,3}\exp(-\alpha_3 f\eta_3) + k_{s,2}\frac{[H^+]}{K_3}\exp(-\alpha_2 f\eta_2)}{1+\frac{[H^+]}{K_3}} \tag{4.88}$$

A similar consideration gives equivalent rate constant expressions for the other 1e1H square in Scheme 4.5

$$k_{app,NT}^{sw,c} = \frac{k_{s,6}\exp(-\alpha_6 f\eta_6) + k_{s,5}\frac{[H^+]}{K_4}\exp(-\alpha_5 f\eta_5)}{1+\frac{[H^+]}{K_4}} \tag{4.89}$$

$$k_{app,NT}^{sw,a} = \frac{k_{s,6}\frac{K_6}{[H^+]}\exp[(1-\alpha_6) f\eta_6] + k_{s,5}\exp[(1-\alpha_5) f\eta_5]}{1+\frac{K_6}{[H^+]}} \tag{4.90}$$

There are two columns here, and each column will contain two pathways. Assuming that P and R are the starting species for each column, and using a similar procedure for the 1e1H case, we can derive equations for different possible paths in the overall 2e1H conversion.

$$path2 = \frac{k_2}{k_2+k_3} = \frac{k_{MPR}}{k_{MN}+k_{MPR}} = \frac{k_{s,2}\frac{[H^+]}{K_3}\exp(-\alpha_2 f\eta_2)}{k_{s,3}\exp(-\alpha_3 f\eta_3) + k_{s,2}\frac{[H^+]}{K_3}\exp(-\alpha_2 f\eta_2)}$$

$$path3 = \frac{k_3}{k_2+k_3} = \frac{k_{MN}}{k_{MN}+k_{MPR}} = \frac{k_{s,3}\exp(-\alpha_3 f\eta_3)}{k_{s,3}\exp(-\alpha_3 f\eta_3) + k_{s,2}\frac{[H^+]}{K_3}\exp(-\alpha_2 f\eta_2)}$$

$$path6 = \frac{k_6}{k_6+k_5} = \frac{k_{NS}}{k_{NS}+k_{NRT}} = \frac{k_{s,6}\exp(-\alpha_6 f\eta_6)}{k_{s,6}\exp(-\alpha_6 f\eta_6) + k_{s,5}\frac{[H^+]}{K_4}\exp(-\alpha_5 f\eta_5)}$$

$$path5 = \frac{k_5}{k_6 + k_5} = \frac{k_{NRT}}{k_{NS} + k_{NRT}} = \frac{k_{s,5}\frac{[H^+]}{K_4}\exp(-\alpha_5 f\eta_5)}{k_{s,6}\exp(-\alpha_6 f\eta_6) + k_{s,5}\frac{[H^+]}{K_4}\exp(-\alpha_5 f\eta_5)}$$

Subset of 2e2H

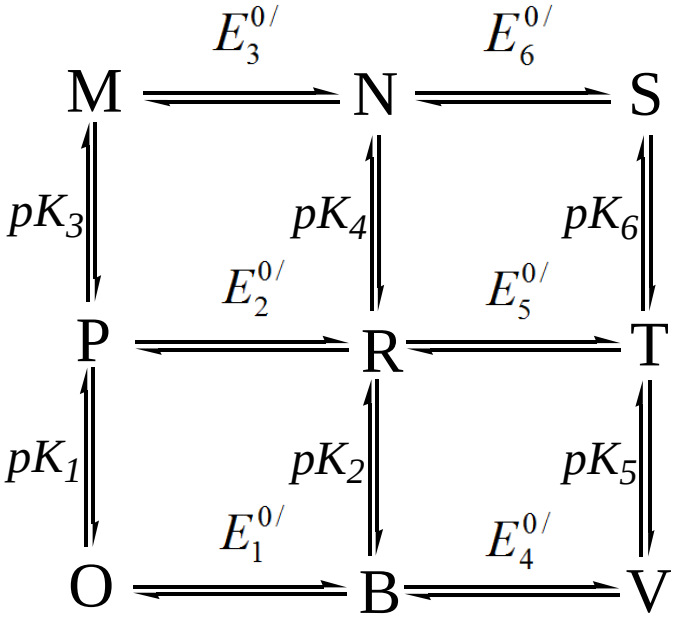

Scheme 4.6: Eight membered square scheme for 2e2H subcase.

A nine membered square scheme is used to describe the two-electron, two-proton transfer process for the conversion of species M to species V.

The overall process is: $M + 2e + 2H^+ \rightleftharpoons V$.

Application of the Nernst equation to the various electron transfer reactions within this scheme gives the following three expressions.

$$E = E_{app,MB}^{0/,sw} + \frac{RT}{F}\ln\left(\frac{\Gamma_M + \Gamma_P + \Gamma_O}{\Gamma_N + \Gamma_R + \Gamma_B}\right) \tag{4.91}$$

$$E = E_{app,NV}^{0/,sw} + \frac{RT}{F}\ln\left(\frac{\Gamma_N + \Gamma_R + \Gamma_B}{\Gamma_S + \Gamma_T + \Gamma_V}\right) \tag{4.92}$$

$$E = E_{app,MV}^{0/,sw} + \frac{RT}{2F}\ln\left(\frac{\Gamma_M + \Gamma_P + \Gamma_O}{\Gamma_S + \Gamma_T + \Gamma_V}\right) \tag{4.93}$$

Therefore, $2E = E_{app,MB}^{0/,sw} + E_{app,NV}^{0/,sw} + \frac{RT}{F}\ln\left(\frac{\Gamma_M + \Gamma_P + \Gamma_O}{\Gamma_S + \Gamma_T + \Gamma_V}\right)$

And

$$E_{app,MV}^{0/,sw} = 0.5\left(E_{app,MB}^{0/,sw} + E_{app,NV}^{0/,sw}\right)$$

Using equations for acid dissociations, an equation for relating the experimental potential *E* to the formal potential for the overall reaction can be derived.

$$\Gamma_M + \Gamma_P + \Gamma_O = \Gamma_P\left(1 + \frac{H^+}{K_1} + \frac{K_3}{H^+}\right)$$

$$\Gamma_N + \Gamma_R + \Gamma_B = \Gamma_R\left(1 + \frac{H^+}{K_2} + \frac{K_4}{H^+}\right)$$

$$E = E_{app,MB}^{0/,sw} + \frac{RT}{F}\ln\left(\frac{\Gamma_P\left(1 + \frac{H^+}{K_1} + \frac{K_3}{H^+}\right)}{\Gamma_R\left(1 + \frac{H^+}{K_2} + \frac{K_4}{H^+}\right)}\right) = E_{app,MB}^{0/,sw} + \frac{RT}{F}\ln\left(\frac{\Gamma_P}{\Gamma_R}\right) + \frac{RT}{F}\ln\left(\frac{\left(1 + \frac{H^+}{K_1} + \frac{K_3}{H^+}\right)}{\left(1 + \frac{H^+}{K_2} + \frac{K_4}{H^+}\right)}\right)$$

$$E_2^{0/} = E - \frac{RT}{F}\ln\left(\frac{\Gamma_P}{\Gamma_R}\right)$$

Based on the Nernst equation:

Therefore, the expression for $E_{app,MB}^{0/,sw}$ is:

$$E_{app,MB}^{0/,sw} = E_2^{0/} - \frac{RT}{F}\ln\left(\frac{\left(1 + \frac{H^+}{K_1} + \frac{K_3}{H^+}\right)}{\left(1 + \frac{H^+}{K_2} + \frac{K_4}{H^+}\right)}\right) \tag{4.94}$$

Similarly:

$$E_{app,NV}^{0/,sw} = E_5^{0/} - \frac{RT}{F}\ln\left(\frac{\left(1 + \frac{H^+}{K_2} + \frac{K_4}{H^+}\right)}{\left(1 + \frac{H^+}{K_5} + \frac{K_6}{H^+}\right)}\right) \tag{4.95}$$

Then

$$2E_{app,MV}^{0/,sw} = \left(E_{app,MB}^{0/,sw} + E_{app,NV}^{0/,sw}\right) = E_5^{0/} + E_2^{0/} - \frac{RT}{F}\ln\left(\frac{\left(1 + \frac{H^+}{K_1} + \frac{K_3}{H^+}\right)}{\left(1 + \frac{H^+}{K_5} + \frac{K_6}{H^+}\right)}\right)$$

$$\ln\left(\frac{\left(1+\frac{H^+}{K_1}+\frac{K_3}{H^+}\right)}{\left(1+\frac{H^+}{K_5}+\frac{K_6}{H^+}\right)}\right)=\ln\left(\frac{K_5}{K_1}\right)+\ln\left(\frac{K_1[H^+]+[H^+]^2+K_1K_3}{K_5[H^+]+[H^+]^2+K_5K_6}\right)$$

Therefore:

$$E_{app,MV}^{0/,sw}=0.5(E_5^{0/}+E_2^{0/})-\frac{RT}{2F}\ln\left(\frac{K_5}{K_1}\right)-\frac{RT}{2F}\ln\left(\frac{K_1[H^+]+[H^+]^2+K_1K_3}{K_5[H^+]+[H^+]^2+K_5K_6}\right) \quad (4.96)$$

This 2e2H case can be treated as two 1e2H subcases. For the ladder defined by species M, P, O, N, R, B the following rare expressions apply.

$$Rate3=\frac{dM}{dt}=-k_{s,3}\Gamma_M\exp\left(-\alpha_3 f\eta_3\right)+k_{s,3}\Gamma_N\exp\left[\left(1-\alpha_3\right)f\eta_3\right]$$

$$Rate2=\frac{dP}{dt}=-k_{s,2}\Gamma_P\exp\left(-\alpha_2 f\eta_2\right)+k_{s,2}\Gamma_R\exp\left[\left(1-\alpha_2\right)f\eta_2\right]$$

$$Rate1=\frac{dO}{dt}=-k_{s,1}\Gamma_O\exp\left(-\alpha_1 f\eta_1\right)+k_{s,1}\Gamma_B\exp\left[\left(1-\alpha_1\right)f\eta_1\right]$$

$$Rate_{obs}=-k_{s,3}\Gamma_M\exp\left(-\alpha_3 f\eta_3\right)+k_{s,3}\Gamma_N\exp\left[\left(1-\alpha_3\right)f\eta_3\right]-k_{s,2}\Gamma_P\exp\left(-\alpha_2 f\eta_2\right)+$$
$$k_{s,2}\Gamma_R\exp\left[\left(1-\alpha_2\right)f\eta_2\right]-k_{s,1}\Gamma_O\exp\left(-\alpha_1 f\eta_1\right)+k_{s,1}\Gamma_B\exp\left[\left(1-\alpha_1\right)f\eta_1\right]$$

For these four proton transfer processes,

$$\Gamma_P=\frac{\Gamma_M[H^+]}{K_3} \qquad \Gamma_R=\frac{\Gamma_N[H^+]}{K_4}$$

$$\Gamma_O=\frac{\Gamma_M[H^+]^2}{K_1K_3} \qquad \Gamma_B=\frac{\Gamma_N[H^+]^2}{K_2K_4}$$

Eliminating Γ_P and Γ_O, the observed rate constant is

$$Rate_{obs}=-k_{s,3}\Gamma_M\exp\left(-\alpha_3 f\eta_3\right)+k_{s,3}\Gamma_N\exp\left[\left(1-\alpha_3\right)f\eta_3\right]-k_{s,2}\frac{\Gamma_M[H^+]}{K_3}\exp\left(-\alpha_2 f\eta_2\right)+$$
$$k_{s,2}\frac{\Gamma_N[H^+]}{K_4}\exp\left[\left(1-\alpha_2\right)f\eta_2\right]-k_{s,1}\frac{\Gamma_M[H^+]^2}{K_1K_3}\exp\left(-\alpha_1 f\eta_1\right)+k_{s,1}\frac{\Gamma_N[H^+]^2}{K_2K_4}\exp\left[\left(1-\alpha_1\right)f\eta_1\right] \quad (4.97)$$

As before, the cathodic component of the rate can be isolated

$$Rate_c=-k_{s,3}\Gamma_M\exp\left(-\alpha_3 f\eta_3\right)-k_{s,2}\frac{\Gamma_M[H^+]}{K_3}\exp\left(-\alpha_2 f\eta_2\right)-k_{s,1}\frac{\Gamma_M[H^+]^2}{K_1K_3}\exp\left(-\alpha_1 f\eta_1\right) \quad (4.98)$$

By convention, the current density from the cathodic current is negative. It arises from the reduction of all oxidized species Γ_{ox}

$$j = -nFk_c\Gamma_{ox} = nF * Rate_c$$

and $k_c = -\dfrac{Rate_c}{\Gamma_{ox}}$ (4.99)

After writing Γ_{ox} in terms of acid dissociation constants and the surface concentration of species, *M*,

The cathodic rate constant will be

$$k_{app,MB}^{sw,c} = \frac{k_{s,3}\exp(-\alpha_3 f\eta_3) + \frac{k_{s,2}[H^+]}{K_3}\exp(-\alpha_2 f\eta_2) + \frac{k_{s,1}[H^+]^2}{K_1K_3}\exp(-\alpha_1 f\eta_1)}{\left(1+\frac{[H^+]}{K_3}+\frac{[H^+]^2}{K_1K_3}\right)} \quad (4.100)$$

A similar process leads to the expression for the anodic rate constant

$$k_{app,MB}^{sw,a} = \frac{k_{s,3}\exp[(1-\alpha_3) f\eta_3] + \frac{k_{s,2}[H^+]}{K_4}\exp[(1-\alpha_2) f\eta_2] + \frac{k_{s,1}[H^+]^2}{K_2K_4}\exp[(1-\alpha_1) f\eta_1]}{1+\frac{[H^+]}{K_4}+\frac{[H^+]^2}{K_2K_4}} \quad (4.101)$$

.

The analysis for the ladder defined by N, R, B, S, T, and V is essentially identical:

$$k_{app,NV}^{sw,c} = \frac{k_{s,6}\exp(-\alpha_6 f\eta_6) + \frac{k_{s,5}[H^+]}{K_4}\exp(-\alpha_5 f\eta_5) + \frac{k_{s,4}[H^+]^2}{K_4K_2}\exp(-\alpha_4 f\eta_4)}{\left(1+\frac{[H^+]}{K_4}+\frac{[H^+]^2}{K_4K_2}\right)} \quad (4.102)$$

$$k_{app,NV}^{sw,a} = \frac{k_{s,6}\exp[(1-\alpha_6) f\eta_6] + \frac{k_{s,5}[H^+]}{K_6}\exp[(1-\alpha_5) f\eta_5] + \frac{k_{s,4}[H^+]^2}{K_5K_6}\exp[(1-\alpha_4) f\eta_4]}{1+\frac{[H^+]}{K_6}+\frac{[H^+]^2}{K_5K_6}} \quad (4.103)$$

Then the apparent rate constant $k_{app,MV}^{sw,c}$ and $k_{app,NV}^{sw,a}$ can be calculated using the following equations:

$$k_{app,MV}^{sw,a} = \frac{k_{app,MB}^{sw,a}k_{app,NV}^{sw,a}}{k_{app,MB}^{sw,a}+k_{app,NV}^{sw,c}} \qquad k_{app,MV}^{sw,c} = \frac{k_{app,MB}^{sw,c}k_{app,NV}^{sw,c}}{k_{app,MB}^{sw,a}+k_{app,NV}^{sw,c}}$$

Each ladder in a 2e2H scheme provides three possible limiting steps and therefore three possible routes. Assuming P and R are the starting species for each column, the

following expressions represent the six possible paths for the overall conversion of M to V

$$path1 = \frac{k_1}{k_3 + k_2 + k_1} = \frac{k_{POB}}{k_{PMN} + k_{PR} + k_{POB}} = \frac{\frac{k_{s,1}[H^+]}{K_3}\exp(-\alpha_1 f \eta_1)}{k_{s,3}\frac{K_3}{[H^+]}\exp(-\alpha_3 f \eta_3) + k_{s,2}\exp(-\alpha_2 f \eta_2) + \frac{k_{s,1}[H^+]}{K_3}\exp(-\alpha_1 f \eta_1)}$$

$$path2 = \frac{k_2}{k_3 + k_2 + k_1} = \frac{k_{PR}}{k_{PMN} + k_{PR} + k_{POB}} = \frac{k_{s,2}\exp(-\alpha_2 f \eta_2)}{k_{s,3}\frac{K_3}{[H^+]}\exp(-\alpha_3 f \eta_3) + k_{s,2}\exp(-\alpha_2 f \eta_2) + \frac{k_{s,1}[H^+]}{K_3}\exp(-\alpha_1 f \eta_1)}$$

$$path3 = \frac{k_3}{k_3 + k_2 + k_1} = \frac{k_{PMN}}{k_{PMN} + k_{PR} + k_{POB}} = \frac{k_{s,3}\frac{K_3}{[H^+]}\exp(-\alpha_3 f \eta_3)}{k_{s,3}\frac{K_3}{[H^+]}\exp(-\alpha_3 f \eta_3) + k_{s,2}\exp(-\alpha_2 f \eta_2) + \frac{k_{s,1}[H^+]}{K_3}\exp(-\alpha_1 f \eta_1)}$$

$$path4 = \frac{k_4}{k_6 + k_5 + k_4} = \frac{k_{RBV}}{k_{RNS} + k_{RT} + k_{RBV}} = \frac{\frac{k_{s,4}[H^+]}{K_2}\exp(-\alpha_4 f \eta_4)}{k_{s,6}\frac{K_4}{[H^+]}\exp(-\alpha_6 f \eta_6) + k_{s,5}\exp(-\alpha_5 f \eta_5) + \frac{k_{s,4}[H^+]}{K_2}\exp(-\alpha_4 f \eta_4)}$$

$$path5 = \frac{k_5}{k_6 + k_5 + k_4} = \frac{k_{RT}}{k_{RNS} + k_{RT} + k_{RBV}} = \frac{k_{s,5}\exp(-\alpha_5 f \eta_5)}{k_{s,6}\frac{K_4}{[H^+]}\exp(-\alpha_6 f \eta_6) + k_{s,5}\exp(-\alpha_5 f \eta_5) + \frac{k_{s,4}[H^+]}{K_2}\exp(-\alpha_4 f \eta_4)}$$

$$path6 = \frac{k_6}{k_6 + k_5 + k_4} = \frac{k_{RNS}}{k_{RNS} + k_{RT} + k_{RBV}} = \frac{k_{s,6}\frac{K_4}{[H^+]}\exp(-\alpha_6 f \eta_6)}{k_{s,6}\frac{K_4}{[H^+]}\exp(-\alpha_6 f \eta_6) + k_{s,5}\exp(-\alpha_5 f \eta_5) + \frac{k_{s,4}[H^+]}{K_2}\exp(-\alpha_4 f \eta_4)}$$

Subset of 2e3H reaction

The preceding discussion has summarized existing approaches for treating

multi-electron multi-proton stepwise PCET. Existing schemes in the literature have covered up to 2e2H PCET and, prior to this work, this was believed adequate to treat the electrochemical behavior of quinone derivatives. However, as shown in Chapter 3, the analysis of aminobenzoquinone monolayers has strongly hinted that there is an additional proton transfer in acidic electrolytes. In what follows, the 2e2H square scheme will be extended for asymmetric electron/proton transfer. Specifically a 12 membered scheme will be constructed that allows for the complete analysis of the conversion of aminobenzoquinone to ammonium-dihydroxybenzoquinone over a complete range of electrolyte acidities.

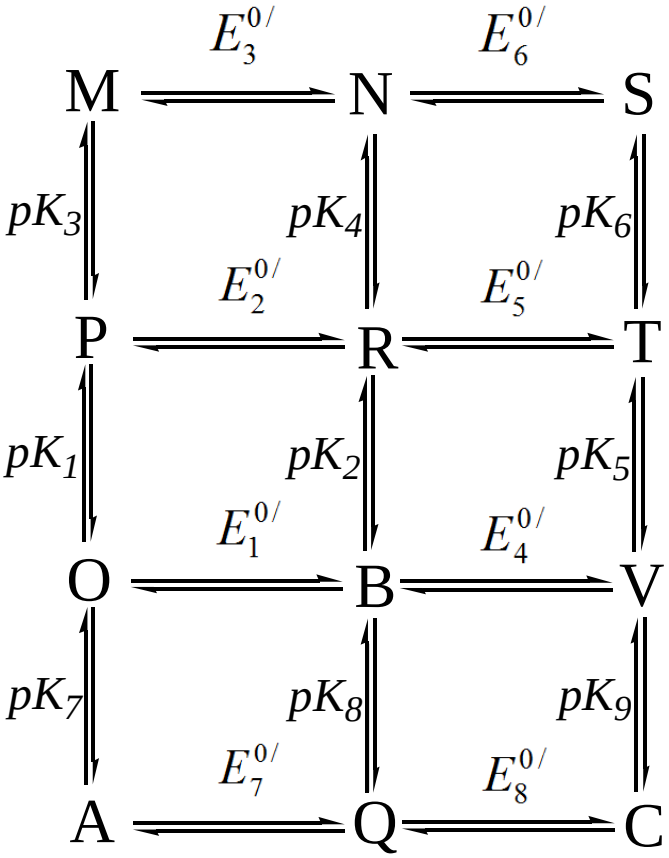

Scheme 4.1: 12 member scheme for two electrons, three proton transfer.

The following is the calculation of $E_{app,MC}^{0/,sw}$ for the overall process

$$M + 2e + 3H^+ \rightleftharpoons C$$

According to the Nernst equation:

$$E = E^{0/,sw}_{app,MQ} + \frac{RT}{F}\ln\left(\frac{\Gamma_M + \Gamma_P + \Gamma_O + \Gamma_A}{\Gamma_N + \Gamma_R + \Gamma_B + \Gamma_Q}\right) \text{and} \quad E = E^{0/,sw}_{app,NC} + \frac{RT}{F}\ln\left(\frac{\Gamma_N + \Gamma_R + \Gamma_B + \Gamma_Q}{\Gamma_S + \Gamma_T + \Gamma_V + \Gamma_C}\right)$$

Combining these expressions, one can obtain

$$2E = E^{0/,sw}_{app,MQ} + E^{0/,sw}_{app,NC} + \frac{RT}{F}\ln\left(\frac{\Gamma_M + \Gamma_P + \Gamma_O + \Gamma_A}{\Gamma_S + \Gamma_T + \Gamma_V + \Gamma_C}\right) \tag{4.104}$$

The Nernst for the overall 2e3H transfer reaction involves the sum of all oxidized and reduced species,

$$E = E^{0/,sw}_{app,MC} + \frac{RT}{F}\ln\left(\frac{\Gamma_M + \Gamma_P + \Gamma_O}{\Gamma_S + \Gamma_T + \Gamma_V}\right) \tag{4.105}$$

By combining Eqn. (4.104) with Eqn. (4.105), one obtains:

$$2E^{0/,sw}_{app,MC} = E^{0/,sw}_{app,MQ} + E^{0/,sw}_{app,NC} \tag{4.106}$$

Eqn. (4.106) can be rewritten as:

$$2E^{0/,sw}_{app,MC} = E^{0/,sw}_{app,MQ} + E^{0/,sw}_{app,NC} = E^{0/}_2 - \frac{RT}{F}\ln\left(\frac{\left(1+\frac{H^+}{K_1}+\frac{K_3}{H^+}+\frac{[H^+]^2}{K_1K_7}\right)}{\left(1+\frac{H^+}{K_2}+\frac{K_4}{H^+}+\frac{[H^+]^2}{K_2K_8}\right)}\right) + E^{0/}_5 - \frac{RT}{F}\ln\left(\frac{\left(1+\frac{H^+}{K_2}+\frac{K_8}{H^+}+\frac{[H^+]^2}{K_2K_8}\right)}{\left(1+\frac{H^+}{K_5}+\frac{K_6}{H^+}+\frac{[H^+]^2}{K_5K_9}\right)}\right) \tag{4.107}$$

$$= E^{0/}_2 + E^{0/}_5 - \frac{RT}{F}\ln\left(\frac{\left(1+\frac{H^+}{K_1}+\frac{K_3}{H^+}+\frac{[H^+]^2}{K_1K_7}\right)}{\left(1+\frac{H^+}{K_5}+\frac{K_6}{H^+}+\frac{[H^+]^2}{K_5K_9}\right)}\right)$$

Eqn. (4.107) can be rewritten as:

$$E^{0/,sw}_{app,MC} = 0.5\left(E^{0/}_2 + E^{0/}_5 - \frac{RT}{F}\ln\left(\frac{\left(K_7[H^+]^2 + K_1K_7[H^+] + K_1K_7K_3 + [H^+]^3\right)}{\left([H^+]^3 + K_5K_9[H^+] + K_9[H^+]^2 + K_5K_6K_9\right)}\right) - \frac{RT}{F}\ln\left(\frac{K_5K_9}{K_1K_7}\right)\right) \tag{4.108}$$

From electrostatic arguments for any chemical species in Scheme 4.1, the addition of each proton in a column makes subsequent proton transfer more disfavorable, conversely, proton transfer should be more favorable after the addition of one or more electron. So that one can conclude that

$$\begin{aligned} pK_6 &> pK_5 > pK_9 \\ pK_4 &> pK_2 > pK_8 \text{ ,} \\ pK_3 &> pK_1 > pK_7 \end{aligned}$$

This 2e transfer process can be separated into two 1e transfer process, and

$$k_{app,MC}^{sw,a} = \frac{k_{app,MQ}^{sw,a} k_{app,NC}^{sw,a}}{k_{app,MQ}^{sw,a} + k_{app,NC}^{sw,c}} \qquad k_{app,MC}^{sw,c} = \frac{k_{app,MQ}^{sw,c} k_{app,NC}^{sw,c}}{k_{app,MQ}^{sw,a} + k_{app,NC}^{sw,c}}$$

Following the same procedure outlined in the 1e3H case, the derived rate constant for MPOANRBQ:

$$k_{app,MQ}^{sw,c} = \frac{\frac{k_{s,3}K_3 \exp(-\alpha_3 f\eta_3)}{[H^+]} + \frac{k_{s,1}[H^+]}{K_1}\exp(-\alpha_1 f\eta_1) + \frac{k_{s,7}[H^+]^2}{K_1K_7}\exp(-\alpha_7 f\eta_7) + k_{s,2}\exp(-\alpha_2 f\eta_2)}{\left(1 + \frac{[H^+]}{K_1} + \frac{[H^+]^2}{K_1K_7} + \frac{K_3}{[H^+]}\right)} \quad (4.109)$$

$$k_{app,NC}^{sw,c} = \frac{\frac{k_{s,6}K_4 \exp(-\alpha_6 f\eta_6)}{[H^+]} + \frac{k_{s,4}[H^+]}{K_2}\exp(-\alpha_4 f\eta_4) + \frac{k_{s,8}[H^+]^2}{K_2K_8}\exp(-\alpha_8 f\eta_8) + k_{s,5}\exp(-\alpha_5 f\eta_5)}{\left(1 + \frac{[H^+]}{K_2} + \frac{[H^+]^2}{K_2K_8} + \frac{K_4}{[H^+]}\right)} \quad (4.110)$$

Similarily, for NRBQSTVC:

$$k_{app,NC}^{sw,a} = \frac{\frac{k_{s,6}K_6 \exp(-\alpha_6 f\eta_6)}{[H^+]} + \frac{k_{s,4}[H^+]}{K_5}\exp(-\alpha_4 f\eta_4) + \frac{k_{s,8}[H^+]^2}{K_5K_9}\exp(-\alpha_8 f\eta_8) + k_{s,5}\exp(-\alpha_5 f\eta_5)}{\left(1 + \frac{[H^+]}{K_5} + \frac{[H^+]^2}{K_5K_9} + \frac{K_6}{[H^+]}\right)} \quad (4.111)$$

$$k_{app,MQ}^{sw,a} = \frac{\frac{k_{s,3}K_4 \exp(-\alpha_3 f\eta_3)}{[H^+]} + \frac{k_{s,1}[H^+]}{K_2}\exp(-\alpha_1 f\eta_1) + \frac{k_{s,7}[H^+]^2}{K_2K_8}\exp(-\alpha_7 f\eta_7) + k_{s,2}\exp(-\alpha_2 f\eta_2)}{\left(1 + \frac{[H^+]}{K_2} + \frac{[H^+]^2}{K_2K_8} + \frac{K_4}{[H^+]}\right)} \quad (4.112)$$

Finally, for the full 2e3H case, there will be two columns, and each column gives four possible routes. The weight of each route determines the pathway of this process. Assuming both P and R are the starting species for each column, and using the same procedure as in the 1e1H case, it is possible to derive k_{PR}, k_{PMN}, k_{POB}, k_{POAQ}, k_{RT}, k_{RNS}, k_{RBV}, and k_{RBQC}.

Here are the expressions for each path.

$$path1 = \frac{k_1}{k_3 + k_1 + k_7 + k_2} = \frac{k_{POB}}{k_{PMN} + k_{POB} + k_{POAQ} + k_{PR}} =$$

$$\frac{\frac{k_{s,1}[H^+]}{K_1}\exp(-\alpha_1 f\eta_1)}{\frac{k_{s,3}K_3\exp(-\alpha_3 f\eta_3)}{[H^+]} + \frac{k_{s,1}[H^+]}{K_1}\exp(-\alpha_1 f\eta_1) + \frac{k_{s,7}[H^+]^2}{K_1K_7}\exp(-\alpha_7 f\eta_7) + k_{s,2}\exp(-\alpha_2 f\eta_2)}$$

$$path2 = \frac{k_2}{k_3 + k_1 + k_7 + k_2} = \frac{k_{PR}}{k_{PMN} + k_{POB} + k_{POAQ} + k_{PR}} =$$

$$\frac{k_{s,2}\exp(-\alpha_2 f\eta_2)}{\frac{k_{s,3}K_3\exp(-\alpha_3 f\eta_3)}{[H^+]} + \frac{k_{s,1}[H^+]}{K_1}\exp(-\alpha_1 f\eta_1) + \frac{k_{s,7}[H^+]^2}{K_1K_7}\exp(-\alpha_7 f\eta_7) + k_{s,2}\exp(-\alpha_2 f\eta_2)}$$

$$path3 = \frac{k_3}{k_3 + k_1 + k_7 + k_2} = \frac{k_{PMN}}{k_{PMN} + k_{POB} + k_{POAQ} + k_{PR}} =$$

$$\frac{\frac{k_{s,3}K_3\exp(-\alpha_3 f\eta_3)}{[H^+]}}{\frac{k_{s,3}K_3\exp(-\alpha_3 f\eta_3)}{[H^+]} + \frac{k_{s,1}[H^+]}{K_1}\exp(-\alpha_1 f\eta_1) + \frac{k_{s,7}[H^+]^2}{K_1K_7}\exp(-\alpha_7 f\eta_7) + k_{s,2}\exp(-\alpha_2 f\eta_2)}$$

$$path7 = \frac{k_7}{k_3 + k_1 + k_7 + k_2} = \frac{k_{POAQ}}{k_{PMN} + k_{POB} + k_{POAQ} + k_{PR}} =$$

$$\frac{\frac{k_{s,7}[H^+]^2}{K_1K_7}\exp(-\alpha_7 f\eta_7)}{\frac{k_{s,3}K_3\exp(-\alpha_3 f\eta_3)}{[H^+]} + \frac{k_{s,1}[H^+]}{K_1}\exp(-\alpha_1 f\eta_1) + \frac{k_{s,7}[H^+]^2}{K_1K_7}\exp(-\alpha_7 f\eta_7) + k_{s,2}\exp(-\alpha_2 f\eta_2)}$$

$$path4 = \frac{k_4}{k_6 + k_4 + k_8 + k_5} = \frac{k_{RBV}}{k_{RNS} + k_{RBV} + k_{RBQC} + k_{RT}} =$$

$$\frac{\frac{k_{s,4}[H^+]}{K_5}\exp(-\alpha_4 f\eta_4)}{\frac{k_{s,6}K_6\exp(-\alpha_6 f\eta_6)}{[H^+]} + \frac{k_{s,4}[H^+]}{K_5}\exp(-\alpha_4 f\eta_4) + \frac{k_{s,8}[H^+]^2}{K_5K_9}\exp(-\alpha_8 f\eta_8) + k_{s,5}\exp(-\alpha_5 f\eta_5)}$$

$$path5 = \frac{k_5}{k_6 + k_4 + k_8 + k_5} = \frac{k_{RT}}{k_{RNS} + k_{RBV} + k_{RBQC} + k_{RT}} = \frac{k_{s,5}\exp\left(-\alpha_5 f\eta_5\right)}{\frac{k_{s,6}K_6\exp\left(-\alpha_6 f\eta_6\right)}{[H^+]} + \frac{k_{s,4}[H^+]}{K_5}\exp\left(-\alpha_4 f\eta_4\right) + \frac{k_{s,8}[H^+]^2}{K_5K_9}\exp\left(-\alpha_8 f\eta_8\right) + k_{s,5}\exp\left(-\alpha_5 f\eta_5\right)}$$

$$path6 = \frac{k_6}{k_6 + k_4 + k_8 + k_5} = \frac{k_{RNS}}{k_{RNS} + k_{RBV} + k_{RBQC} + k_{RT}} = \frac{\frac{k_{s,6}K_6\exp\left(-\alpha_6 f\eta_6\right)}{[H^+]}}{\frac{k_{s,6}K_6\exp\left(-\alpha_6 f\eta_6\right)}{[H^+]} + \frac{k_{s,4}[H^+]}{K_5}\exp\left(-\alpha_4 f\eta_4\right) + \frac{k_{s,8}[H^+]^2}{K_5K_9}\exp\left(-\alpha_8 f\eta_8\right) + k_{s,5}\exp\left(-\alpha_5 f\eta_5\right)}$$

$$path8 = \frac{k_8}{k_6 + k_4 + k_8 + k_5} = \frac{k_{RBQC}}{k_{RNS} + k_{RBV} + k_{RBQC} + k_{RT}} = \frac{\frac{k_{s,8}[H^+]^2}{K_5K_9}\exp\left(-\alpha_8 f\eta_8\right)}{\frac{k_{s,6}K_6\exp\left(-\alpha_6 f\eta_6\right)}{[H^+]} + \frac{k_{s,4}[H^+]}{K_5}\exp\left(-\alpha_4 f\eta_4\right) + \frac{k_{s,8}[H^+]^2}{K_5K_9}\exp\left(-\alpha_8 f\eta_8\right) + k_{s,5}\exp\left(-\alpha_5 f\eta_5\right)}$$

4.3 Results and Discussion

Electrochemical techniques provide measured pH dependent apparent standard formal potentials, apparent standard rate constants and apparent transfer coefficients and have been provided in Chapter 3 for the aminobenzoquinone monolayer system. The behavior at pH>4.5 seems to be that predicted by the 2e2H subcase but the electrochemical behavior at low pH electrolyte require the work to be extended to the 2e3H case. Based on the theoretical model described above for the stepwise PCET mechanism, in a 2e3H framework, there are eight independent parameters controlling the apparent formal potential and nineteen independent parameters controlling the

apparent standard rate constant even with the assumption that all standard transfer coefficients equal 0.5. In the next section the capability of the above theoretical model will be shown in the determination of the charge transfer pathways of the aminobenzoquinone modified monolayer system.

4.3.1 Fitting for Apparent Formal Potentials and Apparent Standard Rate Constants

The voltammograms of the aminobenzoquinone modified monolayers indicate that a plot of apparent formal potentials versus pH shows two linear regions (Fig. 4.1). From 1.5<pH<4.5 the average slope is -88mV/pH and for 4.5<pH<8.5, the average slope is -58mV/pH. Usually, the redox behavior of quinone in aqueous buffer solution undergoes 2e2H transfer and thus the slope of -60mV/pH should be obtained from experiment. In polarographic studies of freely diffusing amino derivatives of benzoquinone and naphthoquinone, Driebergen *et al* reported -90 mV/pH< slopes < -84 mV/pH in certain pH regions. They inferred that this slope is from the additional protonation of the nitrogen atom on the reduced form of the quinone[42]. Similar behavior had previously been reported by Huntington and Davis as well as Cameron *et al*[43;44]. Eqn. (4.108) predicts a slope of -90mV/pH when the overall reaction results in an overall 2e3H transfer, which is close to the experimentally observed slope of -88mv/pH in highly acidic electrolytes. Furthermore, from Eqn. (4.108), the slope of -60mV/pH, which is close to -58mV/pH at high pH electrolyte, can be given for a 2e2H transfer at $pH<pK_9$.

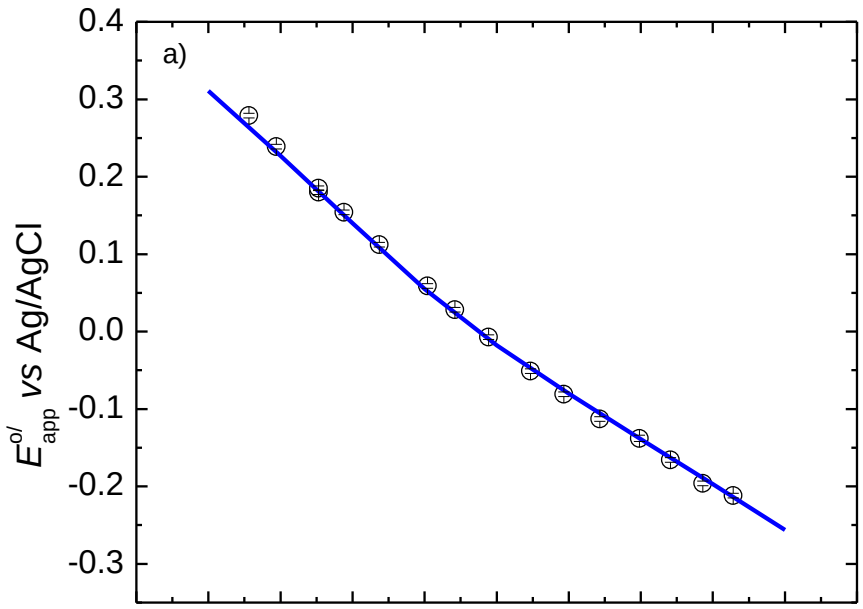

Figure 4.1: Apparent formal potential for the aminobenzoquinone monolayer system as a function of pH. Points with error bars are experimental values while solid lines are curves calculated from fitting analysis (Table 4.1).

Initial inspection of Scheme 4.1 reveals that there are a total of 17 thermodynamic parameters (nine dissociation constants and eight formal potentials). However, the formal potentials are not all independent parameters and the derivations above show that $E_1^{0/}$, $E_3^{0/}$, $E_4^{0/}$, $E_6^{0/}$, $E_7^{0/}$ and $E_8^{0/}$ are defined by $E_2^{0/}$, $E_5^{0/}$ and the acid dissociation constants. Thus, Eqn. (4.108) requires only two independent potentials and six acid dissociation constants for fitting analysis. Neverthless, these parameters require very careful selection of initial values in the fit analysis, and even then, it is not easy to ensure the accuracy of the fitting results as the minimum is most certainly a local minimum rather than the global minimum. Here the initial values of the acid dissociation constants and the standard formal potentials were obtained from reports in the literature for closely related benzoquinone species. The pK_a of 2-amino-1, 4-naphthohydroquinone has been measured to be 4[44;45], and was used for pK_a of the R-NH_2^+-Q functionality (pK_9). Additionally, Driebergen *et al* spectrophotometrically determined the pK_a of the amino group on the corresponding

naphthoquinone to be -1[42]. The shift in acidity of the exocyclic nitrogen for the two redox forms can be rationalized by the removal of the electron-withdrawing capabilities of the quinone on the amine's lone pair upon reduction to the hydroquinone. The initial values of the pK_a values of the carbonyl and hydroxyl groups in the quinone, semiquinone, and hydroxyquinone were taken from Laviron's work[19], although these values are expected to be slightly perturbed by the alkylamine substituent. In addition, it has been evidenced in experiment that when a molecule is immobilized on the electrode, its surface pK_a value will shift and its variation depends on the physical and chemical properties of the electrode[46-54]. The initial values of $E_2^{0/}$ and $E_5^{0/}$ were also taken from Laviron's work with underivatized 1, 4-benozquinone after conversion to the Ag/AgCl reference scale[19].

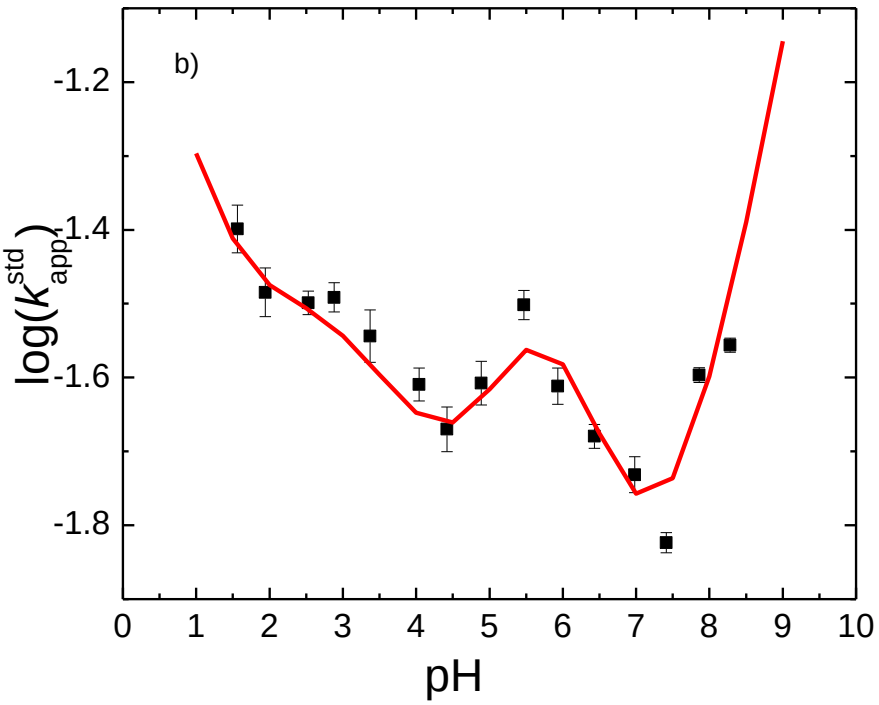

Figure 4.2: Apparent standard rate constant for the aminobenzoquinone monolayer system as a function of pH. Points with error bars are experimental values while solid lines are curves calculated from fitting analysis (Table 4.1).

Fitting was performed using the Solver functionality within Microsoft Excel for both pH dependent apparent formal potentials and apparent standard rate constants.

Besides the independent parameters for the fitting of pH dependent apparent formal potentials, the independent parameters for the fitting of apparent standard rate constants using Eqns. (4.111) and (4.112) also include eight standard rate constants even under the assumption of all standard transfer coefficients equaling to 0.5. For convenience, all standard rate constants are initially set to be $1s^{-1}$, although it is well known that each standard rate constant is strongly dependent on the species.

As for the fitting result for the kinetic data, there is more scatter in the k_{app}^{std} plot (Fig. 4.2) in contrast to that for apparent formal potential (Fig. 4.1), but the initial impression is of a distorted ‘‘W’’ plot typical for 2e2H SW-PCET. Ideally, experimental data over a broader pH range would reduce a lot of the error in the fitting, however, the instability of SAMs at high pH prevents this. Table 4.1 gives a summary of the initial parameter values as well as the results of the fitting analysis. Encouraging aspects of the fitting include the negative shift in the two formal potentials, consistent with previous reports of amino substituted benzoquinones. It is also likely that immobilization on the electrode may shift the acid dissociation constant of each chemical species, so it is unsurprising to see shifts in the pK_a values from known values. The results of the fitting results have been used to generate the solid lines in Figures 4.1 and 4.2 and also provide the chemical structures in the 12-member scheme which can now be drawn explicitly for the aminobenzoquinone system as shown in Figure 4.6. Figure 4.1 and 4.2 demonstrated that the agreement between experimental and calculated results is very good in the case of formal potential but less so for the apparent standard rate constant.

Table 4.1: Starting and fit parameters for the acid dissociation constants, standard rate constants, and formal potentials for the 12 member 2e3H redox system.

Parameter	Initial Value	Fit Result	Parameter	Initial Value	Fit Result
$E_2^{0/}$ (a)	0.552	0.235	$E_5^{0/}$ (a)	0.255	-0.372
pK_1	-7	-7.0	$k_{s,1}$ (b)	1	1
pK_2	2	2.8	$k_{s,2}$ (b)	1	2.0
pK_3	-1	0.5	$k_{s,3}$ (b)	1	0.2
pK_4	5	6.7	$k_{s,4}$ (b)	1	1.7
pK_5	9.9	11.1	$k_{s,5}$ (b)	1	0.9
pK_6	11.4	12.2	$k_{s,6}$ (b)	1	0.1
pK_7	-28	-28	$k_{s,7}$ (b)	1	1
pK_8	-1	-1.1	$k_{s,8}$ (b)	1	0.9
pK_9	4	4.5			

(a) V *vs* Ag/AgCl, (b) s^{-1}.

4.3.2 Fitting for Apparent Transfer Coefficients

The fitting discussed in section 4.3.1 arbitrarily assumed that the standard transfer coefficients for single electron transfer step are all equal to 0.5. This assumption needs to be proved reasonable for the mono-substituted aminobenzoquinone modified monolayer system. Finklea has shown that the Butler-Volmer expression can be used to faithfully reproduce Tafel plots predicted by Marcus DOS theory if a potential dependent transfer coefficient is used and described by a polynomial of the form $\alpha(\eta) = 0.5 + a\eta + b\eta^3 + c\eta^5$. Finklea has also provided values of the coefficients *a*, *b*, and *c* for different reorganization energies[3]. For the 1.4eV of benzoquinone's reorganization energy[55], the values of a, b, and c can be

assigned as 1.647×10^{-1}, -1.832×10^{-3}, and -4.239×10^{-4}.

Figure 4.3 demonstrates simulated $\log(k_{app}/k_{app}^{std})$ as a function of overpotential. One set of curves was obtained with the assumption that all the transfer coefficients (anodic and cathodic) are overpotential independent and equal to 0.5, while the other one is calculated from the overpotential dependent transfer coefficients, and the dependence is determined from Eqn. (1.16) with a reorganization energy, λ=1.4eV. Figure 4.3 shows that the difference between these two curves are only pronounced at the condition of large overpotential, so that it is reasonable to assume that the transfer coefficients equal 0.5 when studying large reorganization energy systems at small overpotential range.

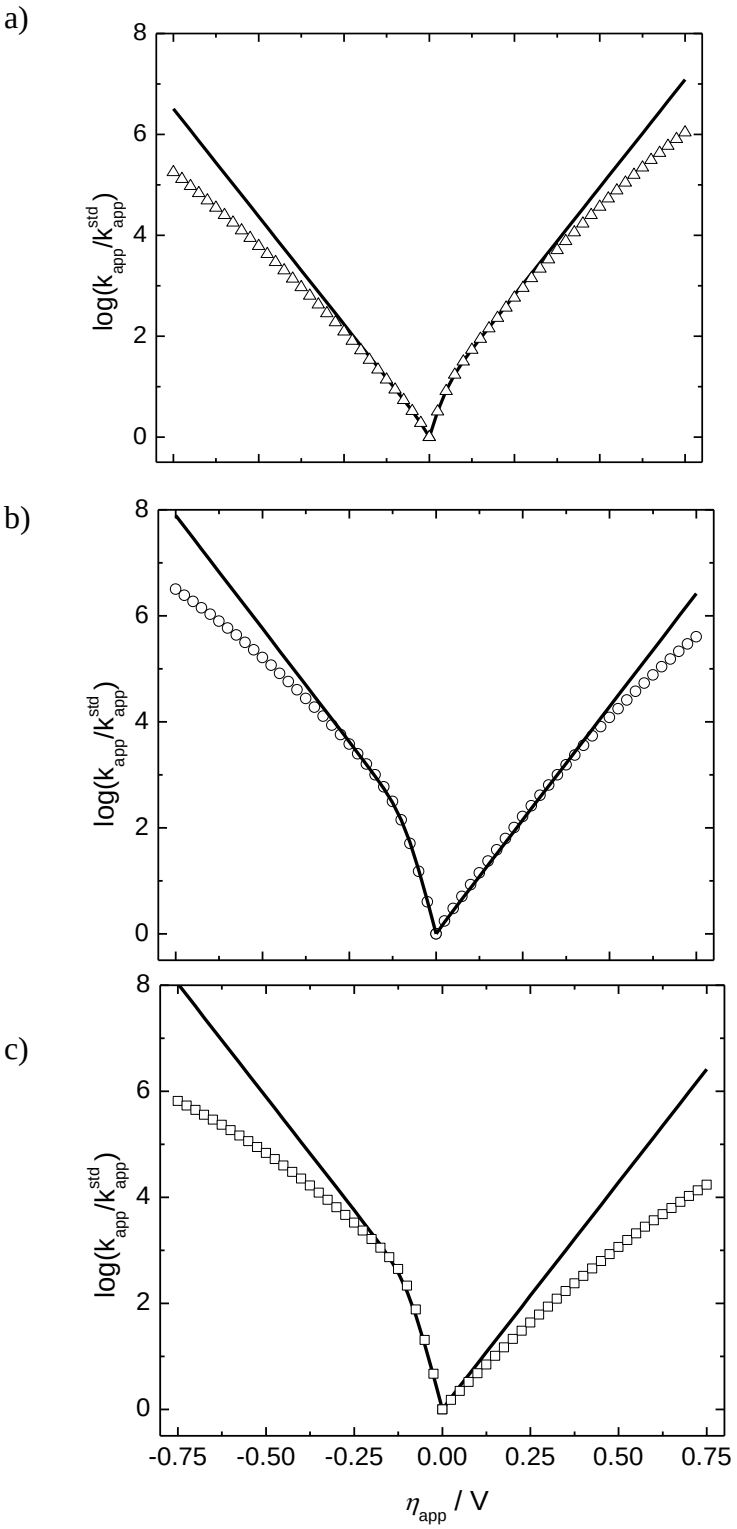

Figure 4.3: Simulated Tafel plots for a) pH 1 b) pH 5 and c) pH 9 using the kinetic expressions derived for the 12 member scheme. Solid lines: potential independent transfer coefficients. Points: potential dependent transfer coefficients with reorganization energy of 1.4 eV. Other thermodynamic and kinetic parameters used to generate the rate constants are described in the text.

Tafel plots ($\log(k_{app}^{c,a})$ versus overpotential η) have proved to be useful in the characterization of electron transfer kinetics. As described in Chapter 3, experimental Tafel plots for the aminobenzoquinone monolayer system can be constructed by measuring CVs at different scan rates. On the other hand, calculated Tafel plots can be generated using the theoretical model of 2e3H transfer described in this chapter and the fitting parameters including acid dissociation constants, standard formal potentials, and standard rate constants. Two sets of Tafel plots (experimental and calculated from fits to 2e3H stepwise PCET) for several different electrolyte acidities are plotted in Figure 4.4. In general, there is fair agreement between the experimental data (points) and the calculated plots (solid lines) which helps to further bolster the validity of the model and fitting analysis. As noted in Chapter 3, the measured overpotentials aren't large enough (because of experimental limitations) to display enough curvature from which the reorganization energy can be extracted. This is excellent justification that the transfer coefficients can be assumed as 0.5 since both sets of data in Figure 4.3 are nearly straight lines at low overpotential. Additionally, chronocoulometric measurements were attempted to track the apparent rate constant at low overpotentials, however, those low overpotentials can't be reached in the experiment due to the very large uncertainty predicted from the exponential in Eqn. (3.10a). It is interesting to remind the reader here that Figure 3.1 from Chapter 3 demonstrated the remarkable asymmetry between the cathodic and anodic branches, particularly at pH 4 and pH 7, is even easier to observe at larger scan rates, where the anodic (cathodic) branch of the Tafel plot is less (more) steep than its counterpart.

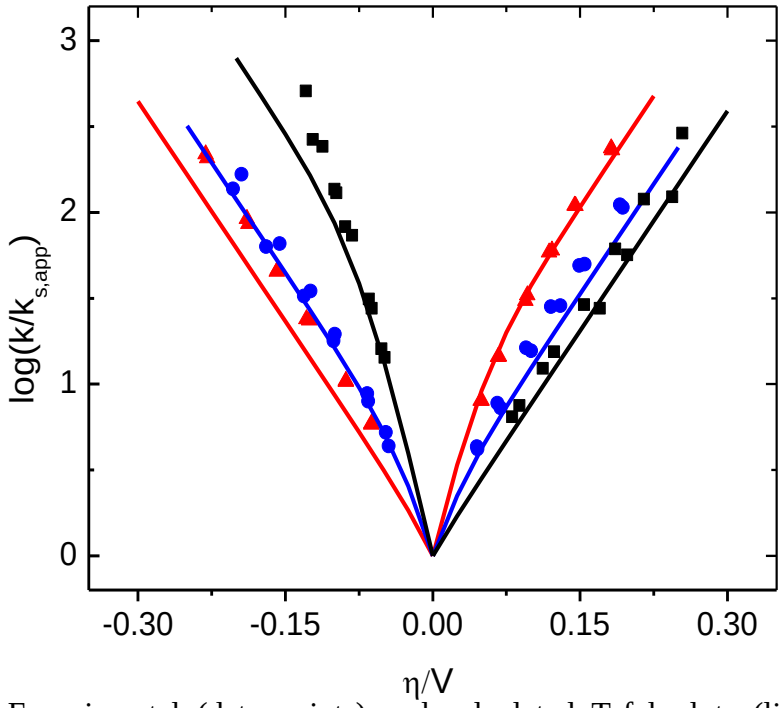

Figure 4.4: Experimental (data points) and calculated Tafel plots (lines) for the aminobenzoquinone monolayer system at pH 7 (■), pH 4.1 (▲), and pH 1.8 (●). Calculated curves were generated using the fitting results summarized in Table 4.1.

Besides the analysis of Tafel plots, the evaluation of the apparent transfer coefficient at zero overpotential is another useful means to assess the kinetic asymmetry in SW-PCET. According to the Butler-Volmer equation, for simple one electron transfer, the transfer coefficients can easily be obtained from the Tafel plot slopes. However, in the case of two consecutive one electron transfers, where the formal potential of the first oxidation is less than that of the second, the apparent transfer coefficient can't be obtained directly from Tafel plot and more importantly, it will be potential dependent even if the individual values are not. This is the case for the aminobenzoquinone modified monolayer system in aqueous buffer solution when multi-electron transfer pathways contribute to the overall reaction. By combining the fitting results provided in Table 4.1 with Eqn. (4.21), the plot of the cathodic and anodic transfer coefficient versus overpotential can be obtained at different pH, and from which, the apparent transfer coefficient at zero overpotential α_{app}^{std} can be

calculated. The resulting values as well as the experimental values of $\alpha_{app}(\eta = 0)$ versus pH are plotted in Figure 4.5. It has been shown in the previous section of this chapter that for a consecutive two electron transfer, the values of the apparent standard transfer coefficient can range between 0.25 and 0.75. Experimental results demonstrate that the apparent transfer coefficient at zero overpotential oscillates around 0.5 reaching a maximum value of 0.75 at the highest pH (8.5), and a minimum value of 0.4 at pH 4.1. Voltammograms should exhibit a relatively sharp anodic peak and a broader cathodic peak when $\alpha_{app}(\eta = 0) <$ ½ and *vice versa* when $\alpha_{app}(\eta = 0) >$ ½. Symmetric peaks should be observed in CVs when $\alpha_{app}(\eta = 0)$ is close to ½. The degree of asymmetry in the CVs shown in the previous chapter (viz. Figure 3.1) can be found to be in excellent accordance with the observed changes in $\alpha_{app}(\eta = 0)$.

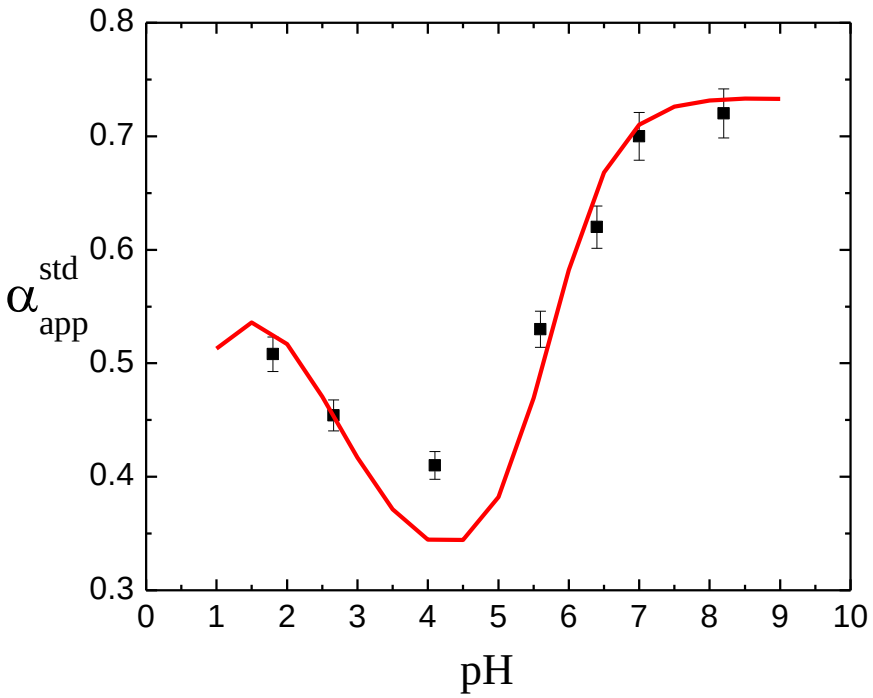

Figure 4.5: Experimental values of the apparent transfer coefficient at η = 0 (points with error bars) for the aminobenzoquinone monolayer system as a function of pH. The solid line is the calculated values determined from the fitting results.

4.3.3 Charge Transfer Pathways

As shown in Figure 4.6, the possible chemical structures for all involved species have been drawn using the fitting acid dissociation constants in the 12-member scheme. At pH>~12, the aminobenzoquinone system is predicted to undergo two electron transfer without any proton transfer and ends with dibenzoquinone anions if the measurement can be performed in sufficiently basic solution. In more slightly acid electrolyte, this system should undergo a 2e1H transfer reaction and the attached amino group doesn't participate in this process. A 2e2H transfer reaction has been observed over an experimentally accessible pH range between 4.5<pH<10 and the final product of this reaction is proposed to be amino-dihydroxybenzoquinone. In a modest range of electrolyte acidities (1 < pH < 4.5), the full 12-member scheme is operative as the amino-benzoquinone undergoes 2e3H transfer to yield the ammonium-dihydroxybenzoquinone. It is interesting to note that for the proposed two electron transfer steps with formal potential of $E_2^{0/}$ and $E_4^{0/}$, upon electron transfer, a proton undergoes a seemingly simultaneous intramolecular conversion. In this model, these two intramolecular proton transfers aren't considered to form stable intermediates, otherwise new species (constants) will be required and the 12-member scheme would need to be extended. Alternatively, these two so-called electron transfer steps could be treated as electron transfer coupled to concerted intramolecular proton transfer. From theoretical prediction, the system reverts to 2e2H at pH < 0.5, the subtle difference being that in such acidic conditions the majority species are the ammonium -benzoquinone and the ammonium –dihydroxybenzoquinone. Presumably, at even lower pH values, further subcases are operative but the analysis has not been extended below pH < -1.

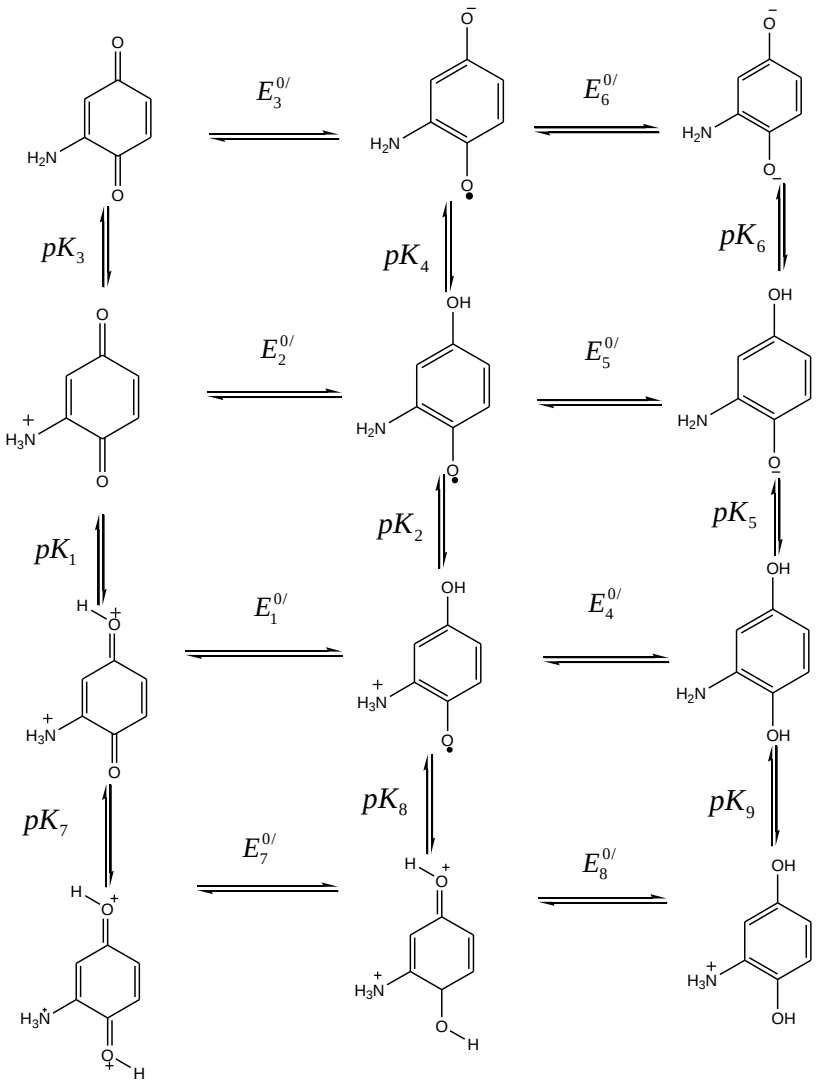

Figure 4.6: Possible chemical structures involved in the charge transfer process of an aminobenzoquinone modified monolayer system.

The path of cathodic charge transfer was also determined as a function of pH using Eqn. (4.22). In Figure 4.7b the changes in path are colour-mapped to also emphasize the changes in overall charge transference. For example, between 4.5 < pH < 10, where 2e2H involving only the benzoquinone group occurs, there is a transition at pH ~7.5 between eHHe (lower pHs) and eHeH (higher pHs), which is not surprising given that the amino group is not involved in the overall charge transfer in this pH region (see Figure 4.7a). There are two pathways for 2e3H at low pH electrolyte. The difference in those pathways is subtle and reflects an inversion in the order of the quantities transferred in the last two steps. The pHs at which the pathway

switches within the 2e2H and 2e3H regimes are ~7.5 and ~ 4.5. As might be expected, these are consistent with the largest measured values of $\alpha_{app}(\eta = 0)$ in Figure 4.5, and the most asymmetric observed Tafel plots, and the shapes of the voltammograms in Figure 3.1.

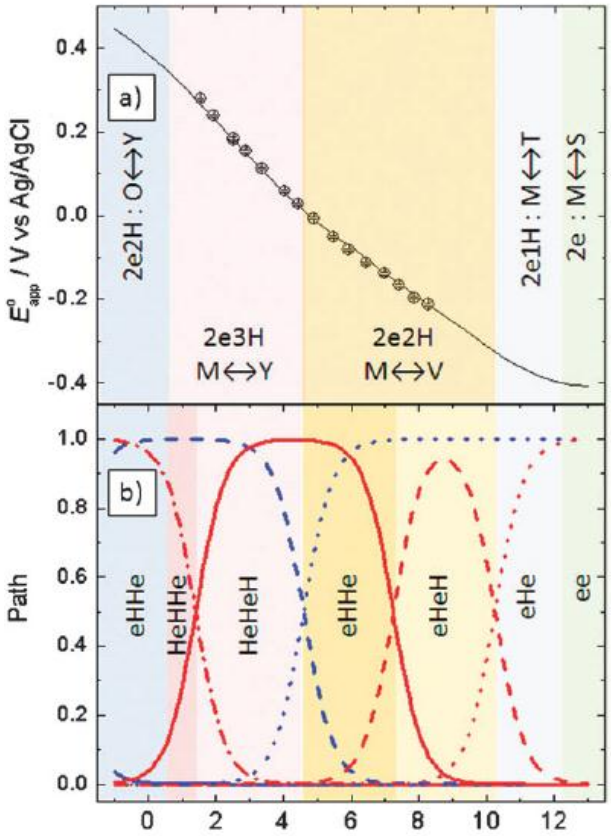

Figure 4.7: Summary of a) the predominate species participating in the overall charge transfer and b) the reaction pathway as a function of pH. The measured (data points) and calculated (line) formal potential dependence have been superimposed on panel *a* to help emphasize the demarcation between different regions.

4.4 Conclusions

In order to determine the PCET mechanisms of the aminobenzoquinone modified monolayer system, the theoretical models for different subcases (from 1e1H to 2e3H) have been revisited, refined and extended. The outlined theoretical framework is very important because it provides parameters that are experimental accessible. It also offers insight showing the difference between single electron and proton transfer and

multiple electron and proton transfer. The PCET pathways have been determined by using analytical expressions and the determined pathways indicate that not all the species are involved and thus the number of independent parameters for the kinetic analysis is smaller than nineteen.

The derived analytical expressions for the 12 member scheme predict that the slope of apparent formal potential versus pH can be -60mV/pH or -90mV/pH at different pH range of electrolytes, which is consistent with observations of the monolayer system shown in Chapter 3. Kinetic analysis for stepwise mechanism using this 12-member square scheme was able to explain the previous observation of deviation from the results predicted for the 2e2H model. These kinetic deviations arise because of the additional protonation/de-protonation of the amino group. Although the limited range of experimental pH values seems too small to provide truly reliable fitting for such a large number of unknowns, the fit results do provide reasonable results and demonstrate that the experimental results are entirely consistent with the stepwise 2e3H model. The measured and calculated Tafel plots, apparent transfer coefficients, and kinetic pathways are internally consistent and can qualitatively explain the asymmetry observed in kinetically controlled CVs. Because of the large reorganization energy of this system (1.4eV) and the inability to measure rate constants at large overpotential, this investigation can't differentiate between the predictions of classic Butler-Volmer and Marcus DOS kinetic behavior.

Stepwise PCET mechanism has been suggested for quinones especially in aqueous solution system, but there is still no direct evidence to deny that the concerted mechanism may also be active in the aminobenzoquinone modified monolayer system. To better ensure the charge transfer mechanism, careful measurement of apparent kinetic isotope effect as an experimental tool (KIE) (D_2O vs. H_2O as solvent) may be helpful. In the next chapter, the apparent kinetic isotope effect for the mono-substituted aminobenzoquinone modified monolayer system will be provided and more importantly, it can be explained by the isotopic effect induced changes of thermodynamic parameters, not kinetic parameters.

Reference List

(1) Finklea, H. O.; Haddox, R. M. *Phys.Chem.Chem.Phys.* **2001**, *3*, 3431-3436.

(2) Finklea, H. O. *J.Phys.Chem.B* **2001**, *105*, 8685-8693.

(3) Finklea, H. O. *J.Electroanal.Chem.* **2001**, *495*, 79-86.

(4) Haddox, R. M.; Finklea, H. O. *J.Electroanal.Chem.* **2003**, *550â€“551*, 351-358.

(5) Haddox, R. M.; Finklea, H. O. *J.Phys.Chem.B* **2004**, *108*, 1694-1700.

(6) Laviron, E. *J.Electroanal.Chem.* **1974**, *52*, 395-402.

(7) Laviron, E. *J.Electroanal.Chem.* **1979**, *101*, 19-28.

(8) Laviron, E. *J.Electroanal.Chem.* **1979**, *101*, 19-28.

(9) Laviron, E.; Roullier, L. *J.Electroanal.Chem.* **1980**, *115*, 65-74.

(10) Laviron, E. *J.Electroanal.Chem.* **1980**, *109*, 57-67.

(11) Laviron, E. *J.Electroanal.Chem.* **1981**, *122*, 37-44.

(12) Laviron, E. *J.Electroanal.Chem.* **1981**, *130*, 23-29.

(13) Laviron, E. *J.Electroanal.Chem.* **1981**, *124*, 9-17.

(14) Laviron, E. *J.Electroanal.Chem.* **1981**, *124*, 1-7.

(15) Laviron, E. *J.Electroanal.Chem.* **1983**, *146*, 1-13.

(16) Laviron, E. *J.Electroanal.Chem.* **1983**, *146*, 15-36.

(17) Laviron, E. *J.Electroanal.Chem.* **1984**, *169*, 23-28.

(18) Laviron, E. *J.Electroanal.Chem.* **1984**, *169*, 29-46.

(19) Laviron, E. *J.Electroanal.Chem.* **1984**, *164*, 213-227.

(20) Costentin, C.; Robert, M.; Savéant, J. M. *J.Electroanal.Chem.* **2006**, *588*, 197-206.

(21) Costentin, C.; Robert, M.; Savéant, J. M. *J.Am.Chem.Soc.* **2007**, *129*, 9953-9963.

(22) Costentin, C. *Chem.Rev.* **2008**, *108*, 2145-2179.

(23) Costentin, C.; Evans, D. H.; Robert, M.; Savéant, J. M.; Singh, P. S. *J.Am.Chem.Soc.* **2005**, *127*, 12490-12491.

(24) Costentin, C.; Robert, M.; Savéant, J. M. *J.Am.Chem.Soc.* **2006**, *128*, 8726-8727.

(25) Costentin, C.; Robert, M.; Savéant, J. M. *J.Am.Chem.Soc.* **2006**, *128*, 4552-4553.

(26) Costentin, C.; Robert, M.; Savéant, J. M. *J.Am.Chem.Soc.* **2007**, *129*, 5870-5879.

(27) Costentin, C.; Louault, C.; Robert, M.; Jean-Michel, S. *J.Am.Chem.Soc.* **2008**, *130*, 15817-15819.

(28) Rüttinger, W.; Dismukes, G. C. *Chem.Rev.* **1997**, *97*, 1-24.

(29) Yagi, M.; Kaneko, M. *Chem.Rev.* **2000**, *101*, 21-36.

(30) Yagi, M.; Syouji, A.; Yamada, S.; Komi, M.; Yamazaki, H.; Tajima, S. *Photochem.Photobiol.Sci.* **2009**, *8*, 139-147.

(31) Meyer, T. J.; Huynh, M. H. V.; Thorp, H. H. *Angew. Chem. Int. Ed.* **2007**, *46*, 5284-5304.

(32) Minguzzi, A.; Fan, F. R.; Vertova, A.; Rondinini, S.; Bard, A. J. *Chem.Sci.*

2012, *3*, 217-229.

(33) Nakagawa, T.; Bjorge, N. S.; Murray, R. W. *J.Am.Chem.Soc.* **2009**, *131*, 15578-15579.

(34) Kanady, J. S.; Tsui, E. Y.; Day, M. W.; Agapie, T. *Science* **2011**, *333*, 733-736.

(35) Liu, F.; Cardolaccia, T.; Hornstein, B. J.; Schoonover, J. R.; Meyer, T. J. *J.Am.Chem.Soc.* **2007**, *129*, 2446-2447.

(36) Liu, F.; Concepcion, J. J.; Jurss, J. W.; Cardolaccia, T.; Templeton, J. L.; Meyer, T. J. *Inorg.Chem.* **2008**, *47*, 1727-1752.

(37) Dau, H.; Limberg, C.; Reier, T.; Risch, M.; Roggan, S.; Strasser, P. *ChemCatChem* **2010**, *2*, 724-761.

(38) Gagliardi, C. J.; Vannucci, A. K.; Concepcion, J. J.; Chen, Z.; Meyer, T. J. *Energy Environ.Sci.* **2012**.

(39) Chen, Z.; Concepcion, J. J.; Jurss, J. W.; Meyer, T. J. *J.Am.Chem.Soc.* **2009**, *131*, 15580-15581.

(40) Chen, Z.; Concepcion, J. J.; Luo, H.; Hull, J. F.; Paul, A.; Meyer, T. J. *J.Am.Chem.Soc.* **2010**, *132*, 17670-17673.

(41) Bonin, J.; Costentin, C.; Robert, M.; Savéant, J. M. *Org.Biomol.Chem.* **2011**, *9*, 4064-4069.

(42) Driebergen, R. J.; Den Hartigh, J.; Holthuis, J. J. M.; Hulshoff, A.; van Oort, W. J.; Postma Kelder, S. J.; Verboom, W.; Reinhoudt, D. N.; Bos, M.; van der Linden, W. E. *Analytica Chimica Acta* **1990**, *233*, 251-268.

(43) Cameron, D. W.; Giles, R. G. F.; Pay, M. H. *Tetrahedron Lett。* **1970**, *11*, 2049-2050.

(44) Huntington, J. L.; Davis, D. G. *J. Electrochem. Soc.* **1971**, *118*, 57-63.

(45) F., L.; Fieser, M. *J.Am.Chem.Soc.* **1934**, *56*, 1565-1578.

(46) Burgess, I.; Seivewright, B.; Lennox, R. B. *Langmuir* **2006**, *22*, 4420-4428.

(47) Pillay, J.; Agboola, B. O.; Ozoemena, K. I. *Electrochem. Comm.* **2009**, *11*, 1292-1296.

(48) Rosendahl, S. M.; Burgess, I. J. *Electrochim. Acta* **2008**, *53*, 6759-6767.

(49) Rooth, M.; Shaw, A. M. *Phys.Chem.Chem.Phys.* **2006**, *8*, 4741-4743.

(50) Zhao, J.; Luo, L.; Yang, X.; Wang, E.; Dong, S. *Electroanalysis* **1999**, *11*, 1108-1113.

(51) Sugihara, K.; Shimazu, K.; Uosaki, K. *Langmuir* **2000**, *16*, 7101-7105.

(52) Smalley, J. F.; Chalfant, K.; Feldberg, S. W.; Nahir, T. M.; Bowden, E. F. *J.Phys.Chem.B* **1999**, *103*, 1676-1685.

(53) Gooding, J. J.; Hale, P. S.; Maddox, L. M.; Shapter, J. G. *J.Chem.Educ.* **2005**, *82*, 779.

(54) Bryant, M. A.; Crooks, R. M. *Langmuir* **1993**, *9*, 385-387.

(55) Park W.C.; Hong H.G. *Bull.Korean Chem.Soc.* **2006**, *27*, 381-385.

Chapter 5: Associated Concerted Pathways and Apparent Kinetic Isotope Effects in Proton Coupled Electron Transfer

Reproduced in part from [Zhang, W.; Burgess, I. J. *J. Electroanal. Chem.* **2012**, *668*, 66-72.]. With permission from Elsevier

5.1 Introduction

A nearly ideal aminobenzoquinone modified monolayer has been successfully prepared and apparent formal potential, apparent standard rate constant and apparent transfer coefficient at zero overpotential as a function of pH have been described in Chapters 3 and 4[1;2]. Combining the measured thermodynamic and kinetic information with the newly extended experimental accessible theoretical model presented in Chapter 4, the charge transfer pathways of this monolayer system have been determined with the assumption that the PCET follows the stepwise mechanism. In general, for any electrochemical PCET reaction, it has been proposed that there are two different principal mechanisms namely the stepwise (sw) mechanism and the concerted (cc) mechanism. The mechanisms have been discussed in detail in Chapter 4 and a brief review follows. In the sw PCET mechanism, it is generally assumed that any proton transfer steps are sufficiently fast enough that they can be treated as equilibrium processes and hence render the electron transfer processes as the rate determining steps. As a function of pH, potential pathways for this PCET process include exclusively sequential electron then proton transfer (ept), exclusively sequential proton then electron transfer (pet), and mixtures of both. In contrast to the sw PCET mechanism, both the proton transfer and the electron transfer occur in one kinetic step in the concerted PCET mechanism. A prototypical example of a concerted PCET transfer is the 1e1H oxidation of phenols in organic solvent systems[3-9]. As described in Chapter 1, a concerted process inherently requires a two-bodied

transition involving transfer of an electron between the redox center and the electrode as well as a simultaneous proton tunneling event between the redox center and the proton acceptor/donor. The simultaneous process is intrinsically disfavored relative to the sw process from a kinetic point of view. However, as the concerted process by-passes potentially high energy intermediates that must be formed in the sw transfer, it can be an energetically favored route for charge transfer.

It is important to distinguish both concerted mechanism and stepwise mechanism in terms of theory and experiment[3;10-15]. One main question of this concern is to find the interrelation between thermodynamic parameters, kinetic parameters and electrochemical PCET mechanisms. Experimental evidence has shown that the kinetics of the sw PCET process is inversely proportional to the difference in the acid dissociation constants of the oxidized and reduced forms of the redox probe[10]. In such cases the concerted pathway can become kinetically competitive with the sw pathway. Theoretical analyses using Butler-Volmer type equations to describe charge transfer kinetics verify such observations. However, theoretical studies that include the effect of the composition of the electrolyte on the concerted mechanism need to be extended and further developed. Experimental studies that attempt to discern between concerted and stepwise mechanisms are hampered by the observation of apparent rate constants rather than direct measures of individual charge transfer events, as well as the difficulty of direct experimental observation of the intermediates. The measurement of the hydrogen/deuterium apparent kinetic isotope effect (KIE) has been used as a convenient experimental tool to probe the existence of concerted PCET mechanisms[4;7;10-12;16-33]. Since simple electron transfer is always the rate determining step in the sw PCET mechanism, one would not expect to observe a KIE effect for PCET redox reactions under purely kinetic control in most cases. On the other hand, because the concerted PCET mechanism involves an atom tunneling event, a pronounced H/D kinetic isotope effect is theoretically predicted and has been observed in certain experimental systems. For instance in studying an osmium aquo monolayer system, Madhiri and Finklea observed that the apparent standard rate constant in D_2O is approximately a factor of two slower than in H_2O in high pH (pD)

electrolytes[24]. Subsequently, Costentin *et al* attributed this pH dependent apparent KIE as evidence of charge transfer under concerted control[10].

In this chapter, analytical expressions based on the Nernst equation and the Butler-Volmer formulism will be provided to model the apparent standard rate constants of a simple concerted 1e1H PCET process. These expressions, combined with expressions derived in Chapter 4 for the stepwise mechanism, allow for an analysis of the controlling parameters for the two different PCET mechanisms. In particular, the influence of the concentration and acidity of potential proton donating species present in the electrolyte is revealed. The affecting factors on the apparent kinetic isotope effect are discussed in terms of a thermodynamic contribution and an intrinsic contribution. In particular, owing to the difference in activities between protons and deuterons, pK_a values of acid donating/accepting species differ in D_2O and H_2O solvents. Using analytical expressions for apparent rate constants under complete sw and complete cc control it will be demonstrated that different proton/deuteron activity in electrolytes can induce kinetic isotope effects of comparable magnitude for both stepwise and concerted mechanisms. It is prudent to keep in mind that an underlying assumption in many literature reports is that the apparent kinetic isotope effect shouldn't be observed in the stepwise mechanism because the electron transfer step is the rate determining step. The results of this Chapter will demonstrate that this is not a correct assumption. In fact an apparent kinetic isotope effect can be measured for the aminobenzoquinone modified monolayer system, which the last two chapters have demonstrated follows the stepwise PCET mechanism. The observed apparent KIE can be successfully explained by the effect of H/D replacement on the thermodynamic parameters of the electrochemical system.

5.2 Model for one Electron, one Proton Transfer with Concerted Mechanism

To reveal the influences of thermodynamic and kinetic parameters on the concerted 1e1H mechanism, a typical electrochemical one electron one proton transfer (1e1H) of species M to form MH following the concerted mechanism is

shown in Scheme 5.1. In this reaction, HZ_j is the proton donor and Z_j is the corresponding proton acceptor. Although the ensuing analysis is constructed for the cathodic (reduction) process, equivalent conclusions are reached if one chooses to use the oxidation (anodic) process. It is assumed that the concerted mechanism involves an initial association of a transitory adduct $M{\cdot\cdot}HZ_j$, which participates in a rate limiting concerted charge transfer process (outlined by the dotted box in Scheme 5.1 and characterized by $E^0_{cpet,j}$ and $k^{cpet}_{s,j}$) followed by adduct dissociation. HZ_j and Z_j^- are the acidic forms and conjugate bases of either the solvent or the j^{th} component of the buffer system and are linked through the acid dissociation constant $K_{a,j}$. As there are several possible proton donors/acceptors it is possible to have multiple, mechanistically identical, pathways in a concerted 1e1H transfer. The equilibrium concentration of adducts before and after charge transfer are described by the formation constants $K_{I,j}$ and $K_{II,j}$ respectively. It has been discussed that there are two possible pathways (ept and pet) for the stepwise mechanism and the analytical expressions for apparent formal potential, apparent rate constant and apparent transfer coefficient as a function of pH have been derived, in Chapter 4. In the following section, concerted 1e1H PCET thermodynamics and kinetics will be treated in a fashion similar to the work of Costentin et al[10;12;18].

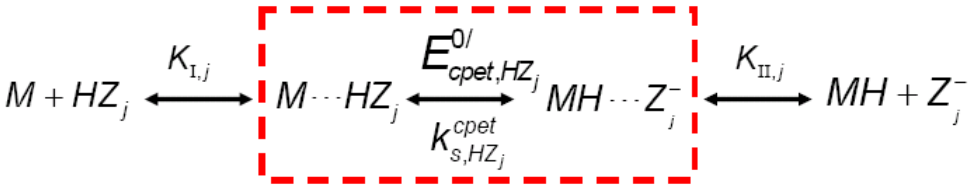

Scheme 5.1: Concerted pathway for a 1e1H proton coupled electron transfer process.

5.2.1 Concerted PCET Thermodynamics

When considering the concerted mechanism, the Nernst equation for the electron transfer step $(M\cdots HZ_j)+e^- \leftrightarrow (MH\cdots Z_j^-)$ is

$$E = E^{0/}_{cpet,HZ_j} + \frac{RT}{F}\ln\left(\frac{[M\cdots HZ_j]}{[MH\cdots Z_j^-]}\right) \tag{5.1}$$

Eqn. (5.1) can be combined with the definition of acid dissociation constant to provide

$$E^{0/}_{cpet,HZ_j} = E^{0/}_3 + \frac{RT}{F}\ln\left(\frac{K_{\mathrm{II},j}K_{a,j}}{K_{\mathrm{I},j}K_4}\right) \tag{5.2}$$

where $K_{\mathrm{a,j}}$ is the acid dissociation constant for the j^{th} proton donating species present in the electrolyte, $E^{0/}_3$ is the standard formal potential for the reduction of M, and K_4 is the acid dissociation constant for the protonation of M. In by-passing the potentially high energy intermediates M^- and MH^+ in favour of the adducts shown in Scheme 5.1, with the many possible proton acceptor/donor, the apparent formal potential of the concerted process is

$$E = E^{0/,cc}_{app,MR} + \frac{RT}{F}\ln\left(\frac{[M]+\sum_j[M\cdots HZ_j]}{[MH]+\sum_j[MH\cdots Z_j^-]}\right). \tag{5.3}$$

Based on the definition of acid dissociation constant for the different proton acceptors, Eqn. (5.3) can yield the following expression linking the apparent potential of the concerted process to its formal potential,

$$E^{0,cc}_{app,MR} = E^{0/}_3 + \frac{RT}{F}\ln\left(\frac{[H^+]}{K_4}\right) + \frac{RT}{F}\ln\left(\frac{1+\sum_j K_{II,j}[Z_j^-]}{1+\sum_j K_{I,j}[HZ_j]}\right) \tag{5.4}$$

Note, that in the limit of $pK_3 < \mathrm{pH} < pK_4$, $\sum_j K_{I,j}\left[\mathrm{HZ}_j\right] \ll 1$, and $\sum_j K_{II,j}\left[\mathrm{Z}_j^-\right] \ll 1$, Eqns. (4.26) and (5.4) provide the same -60 mV/pH slope of the apparent formal potential versus pH for both stepwise mechanism and concerted mechanism. Thus, as would be expected, the measurement of the apparent formal potential (a thermodynamic parameter) cannot be used to differentiate the mechanism of electrochemical PCET.

5.2.2 Concerted PCET Kinetics

The observed event is the rate of consumption of species M (or, alternatively, the rate of production of MH). However, as the charge transfer process is the rate limiting step in the cc mechanism, the observed rate of conversion of M to MH ($\equiv R$ in Chapter 4) is determined by the sum of the rates of reaction of the M··HZ$_j$ complexes

$$\frac{d[M]}{dt} = -k_{app,MR}^{cc,c}[M] + k_{app,MR}^{cc,a}[R] = \sum_j \frac{d[M\cdots HZ_j]}{dt} \tag{5.5}$$

where $k_{app,MR}^{cc,c}$ and $k_{app,MR}^{cc,a}$ represent the apparent, concerted cathodic and anodic rate constants, respectively.

Although there are several different approaches to describe the fundamental physics associated with the concerted charge transfer event, the phenomenological result is a Butler-Volmer type equation

$$\begin{aligned}\frac{d[M\cdots HZ_j]}{dt} = &-[M\cdots HZ_j]k_{s,j}^{cpet}\exp[-\alpha_{cpet,j}f\eta_{cpet,j}] \\ &+[MH\cdots Z_j^-]k_{s,j}^{cpet}\exp[(1-\alpha_{cpet,j})f\eta_{cpet,j}]\end{aligned} \tag{5.6}$$

where $\eta_{cpet,j} = E - E_{cpet,j}^o$. Detailed descriptions of a semi-classical interpretation of $k_{s,j}^{cpet}$ in an analogous fashion to Marcus-Hush-Levich theory are available in the literature but are not required in the development of this model.

By considering only the reduction process defined in Eqn. (5.6), one obtains the following expression for the apparent, concerted cathodic and anodic rate constants

$$k_{app,MR}^{cc,c} = \sum_j k_{s,j}^{cpet}K_{II,j}[HZ_j]\exp\left[-\alpha_{cpet,j}f\eta_{cpet,j}\right]. \tag{5.7}$$

$$k_{app,MR}^{cc,a} = \sum_j k_{s,j}^{cpet}K_{II,j}[Z_j]\exp\left[\left(1-\alpha_{cpet,j}\right)f\eta_{cpet,j}\right] \tag{5.8}$$

Analytical expressions derived for sw and cc mechanisms provide the foundation upon which arguments concerning the influence of solvent isotope variation can be constructed. In doing so, one must first determine which of the physical parameters will be altered by exchanging water for heavy water. For a concerted 1e1H transfer step, the transfer coefficient is the function of reorganization energy, overpotential, electronic coupling factor and other parameters[31;34]. To simplify the ensuing analysis,

it is assumed in this chapter that all standard transfer coefficients for both single electron transfer step and a concerted 1e1H transfer step are equal to ½ in both solvents (H_2O and D_2O) and are independent of applied potential which is applicable for high reorganization energy systems[34;35]. The individual stepwise standard heterogeneous rate constants $k_{s,3}$ and $k_{s,2}$ represent pure electron transfer events and, in accordance with the Butler-Volmer equation or the Marcus DOS theory, are not expected to depend on the isotopic composition of the solvent environment around the redox molecule. It is also assumed that the standard rate constants are isotope independent. The rate constant for the cc charge transfer inherently describes the rate of electron transfer in concert with proton transfer. For simplicity it is assumed that $k_{s,j}^{cpet}$ is two-fold smaller in D_2O compared to H_2O owing to the reduced tunneling probability of the heavier deuteron. This is a conservative estimate which will be revisited below. For simplicity the values of all standard heterogeneous rate constants are set to unity (0.5 for $k_{s,j}^{cpet}$ in D_2O) although in a real experimental system the values are not necessarily equal.

5.3 Results and Discussion

5.3.1 Influence of pH and Electrolyte Composition

As the standard rate constants $k_{s,3}$, $k_{s,2}$ and $k_{s,j}^{cpet}$ are experimentally inaccessible, only the apparent standard rate constants ($k_{app,MR}^{sw,std}$ for stepwise mechanism and $k_{app,MR}^{cc,std}$ for concerted mechanism) are available to evaluate the kinetics and determine the mechanism of PCET. Inspection of Eqn. (4.32) and (4.33) reveals that the two standard rate constants for pure electron transfer steps, the two acid dissociation constants of the proton transfer steps and the pH will influence the observed standard rate constant when the coupled charge transfer occurs exclusively through the sw mechanism. Eqn. (4.32) or (4.33) also provides a minimum in $k_{app,MR}^{sw,std}$

when $pH = (pK_3 + pK_4)/2$. At very low pH values the sw mechanism is dominated by the pet path, whereas at high pH only the ept pathway is operative. The measured rate constant corresponds to the simple electron transfers described by either $k_{s,3}$ or $k_{s,2}$. For $pK_3 < pH < pK_4$ there is a linear relationship between the logarithm of the apparent standard rate constant and pH with an absolute value of the slope equal to ½. These features are illustrated by curve 1 in Figure 5.1.

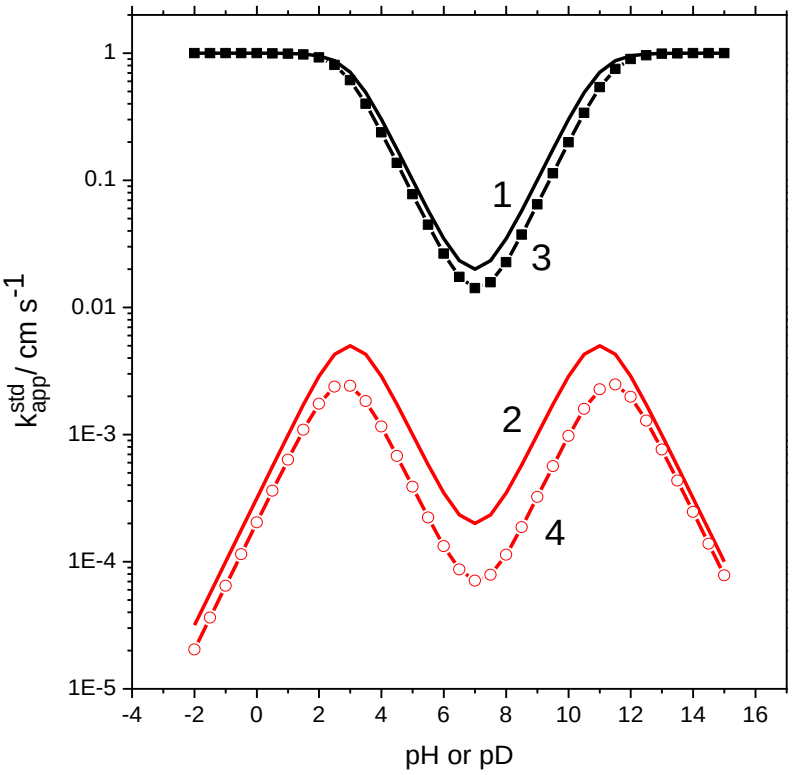

Figure 5.1: Simulated dependencies of the stepwise (curves 1 and 3) and concerted (curves 2 and 4) apparent standard rate constants as a function of electrolyte acidity. Curves 1 and 2 correspond to H_2O electrolytes and curves 3 and 4 correspond to D_2O electrolytes. Simulation parameters are described in the text.

On the other hand, when the concerted mechanism is exclusively operative, Equation (5.7) or (5.8) indicates that the apparent standard rate constant, $k_{app,MR}^{cc,std}$, depends on the electrolyte acidity explicitly through the argument for the overpotentials and implicitly through the concentration of the proton donating species

HZ_j. PCET studies are typically undertaken in complicated buffered electrolytes, so that it can be expected that the kinetic behavior of the concerted mechanism is related to the nature of the proton acceptor/donor. For example the Britton-Robinson buffer contains mixtures of boric acid, acetic acid, phosphoric acid, and their conjugate bases. The concentrations of all the potential proton donating species, excluding the solvent itself, will vary widely as the acidity of the electrolyte is varied. While all species concentrations can be readily evaluated, it is important to realize that in such complicated buffers it is quite likely that the identity of the proton donor in the concerted mechanism will differ in different pH regimes. In the modeling performed below, it was assumed that the buffer contains three, non-solvent, proton donor species that can participate in reactions I and II. Partial differentiation of Eqn. (5.7) or (5.8) with respect to proton concentration reveals that maxima in $k_{app,MR}^{cc,std}$ appear at each value of $K_{a,j}$. As expected from Equation (5.7) or (5.8), the slopes of the lines at the acid/base extremes equal the transfer coefficient for the concerted proton coupled electron transfer process. These general features can be better illustrated by simulating the response of the apparent standard rate constants in H_2O (Figure 5.1, curve 2) using the following thermodynamic parameters $E_3^{0/} = 0$, pK_3=3, pK_4=11, $pK_{a,1}$=3, and $pK_{a,2}$=11. Furthermore, the formal concentrations of proton donating species were all set to 10mM and all association equilibrium constants were made equal to 10^{-3}. Comparing curves 1 and 2 in Figure 5.1 reveals that the apparent standard rate constant of the concerted path is significantly smaller even at the minimum in the stepwise curve, which mathematically is caused by the low value of association equilibrium constants. In other words, only when the product of the association equilibrium constant and the concentration of proton species is large does the concerted mechanism become competitive with the stepwise mechanism. The kinetic differences would be even further exacerbated by large differences between the standard rate constants for simple electron transfer ($k_{s,3}$, $k_{s,2}$) and $k_{s,j}^{cpet}$. As the latter requires simultaneous transmission of both an electron and a proton through tunneling,

it might be expected that $k_{s,j}^{cpet}$ should be intrinsically much smaller[11]. In instances where the potential proton donating/acceptor species are known, comparison between experimental and simulated pH dependent apparent standard rate constants such as those shown in Figure 5.1 may provide mechanistic insight. For example, for a known 1e1H system the presence of a single minimum apparent standard rate constant strongly supports a stepwise mechanism, whereas multiple maxima and minima would indicate a concerted mechanism. Furthermore, as the apparent standard rate constant in the concerted mechanism is strongly dependent on the nature and concentration of the proton acceptor/donor species, the introduction of new proton acceptor/donor species such as pyridine could be used to support the existence of concerted mechanism[3].

5.3.2 Solvent Isotope Influence on Model Predictions (Intrinsic Contributions and Thermodynamic Contributions)

Inspection of Equations (5.7), (5.8) and Equations (4.32), (4.33) from Chapter 4 leads to the conclusion that for both the stepwise mechanism and the concerted mechanism, the apparent standard rate constants are strongly dependent on standard rate constants, standard formal potentials and the acid dissociation constants of the various species present in solution. The apparent kinetic isotope is defined as the ratio of the apparent standard rate constant in heavy water to that in normal water, and both the intrinsic contribution and the thermodynamic contribution need to be considered when discussing this established parameter. In general, the intrinsic contribution is from the changes of the standard rate constants under the replacement of solvent from H_2O to D_2O. The thermodynamic contribution is from the H/D replacement induced shifts of acid dissociation constants and standard formal potentials[30;36-40].

Both the standard rate constant and the standard formal potential have been shown to be dependent on deuterium exchange of the electrolyte in particular systems. Redox molecule-solvent interactions such as hydrogen bonding are often used to evaluate the effect of solvent replacement on the standard rate constants and standard

formal potentials. D_2O appears to have a greater trend to form hydrogen bonding in comparison with H_2O. For some transition metal redox couples containing aquo or amino ligands, the deuteration of ligands leads to about a two-fold decrease in the standard rate constant for electron transfer processes and the standard formal potential usually shifts to more positive values[38-40].

H/D replacement induced pK_a shifting has been introduced explicitly in Chapter 2. When simulating the isotopic dependence of measured rate constants, all acid dissociation constants defined in the model (pK_1, pK_2, $pK_{a,j}$) should be subjected to Eqn. (2.12).

Recalculation of $k_{app,MR}^{sw,std}$ as a function of pD for *sw* 1e1H results leads to curve 3 in Figure 5.1 and upon comparison to its analog for H_2O based electrolytes (curve 1) a displacement along the abscissa for the two solvents is noticeable. This can be explained by the larger difference between pK^{D_2O} and pK^{H_2O} for pK_2 compared to pK_1. The apparent kinetic isotope effect (KIE) of the solvent is presented in Figure 5.2 as the ratio $k_{app,MR}^{sw,std}(H_2O) / k_{app,MR}^{sw,std}(D_2O)$. As expected, the ratio approaches unity when the electrolyte acidity is below pK_1 and above pK_2 as the overall reaction in these regions is no longer a proton coupled electron transfer process. A remarkable apparent KIE effect is observed when the electrolyte acidity is between pK_1 and pK_2, with lower kinetics observed in D_2O. The apparent KIE spans from a factor of 1 to a value greater than 1.5, which, although less than an order of magnitude in scale, should be measurable within acceptable error in an experimental system. It is important to note that in the absence of the solvent isotope dependence on the acid dissociation constants, such behavior would not be expected and a KIE of unity should be observed at all electrolyte acidities. The results in Figure 5.2 clearly demonstrate that upon consideration of Equation (2.12), a stepwise mechanism can result in an appreciable apparent KIE, a concept which has not been previously fully appreciated in the mechanistic studies of electrochemical PCET.

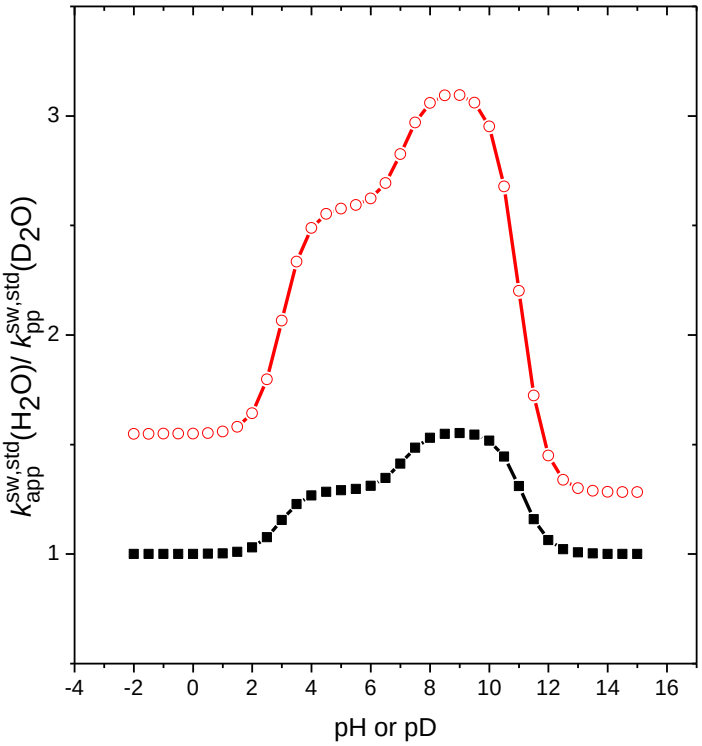

Figure 5.2: Simulated solvent isotope variation induced kinetic effect for stepwise (squares) and concerted mechanism (circle). Simulation parameters are described in the text.

Similar procedures to those described above for 1e1H stepwise PCET can be applied for multiple electron/proton transfer processes in order to evaluate how solvent mitigated changes in pK_a values induce an apparent kinetic isotope effect. The relevant expressions for the kinetic rate constants in the 2e2H case have been developed in Chapter 4 (section 4.2.2). Similar to the results of 1e1H case, a remarkable apparent KIE can be predicted by the application of Eqns. (4.100), (4.101), (4.102) and (4.103) with only the variation in the acid dissociation constants. As another interesting simulative result, it is easy to draw a conclusion from Eqns. (4.32) and (4.33) that for a 1e1H sw PCET process, only pK_a variation can induce an apparent kinetic isotope effect. However, for a proton coupled multi-electron transfer reaction, the apparent kinetic isotope effect could be caused because both pK_a and $E^{0/}$ values vary upon H/D substitution. It can be predicted from the theoretical discussion in section 4.2.2 that for the PCET process of M converting to V (Scheme 4.1), an

increased value of $(E_2^{0/} - E_5^{0/})$ caused by H/D replacement can give an increase in the apparent standard rate constant and *vice versa*.

A similar analysis of the effect of solvent isotope variation can be performed for the 1e1H concerted mechanism. Curve 4 in Figure 5.1 shows the logarithm of the apparent standard rate constant as a function of pD and, as is the case for the sw simulations, the D_2O and H_2O curves are very qualitatively similar. Closer inspection reveals a consistent decrease of kinetics in D_2O compared to that in H_2O. Figure 5.3 demonstrates that in the concerted mechanism, the apparent KIE is lower by a factor of two in both highly acidic and highly basic electrolytes. This result is caused by larger D_2O /H_2O pK_a shifts for weaker acids which partially offset the intrinsically lower value of $k_{s,j}^{cpet}$ in D_2O compared to H_2O due to different proton/deuteron tunneling transmission probabilities. Apparent KIE factors ranging from about 1.5 to nearly 3.2 are observed. The smallest apparent KIE values are observed either in solutions much more acidic than the K_a of the strongest proton donating species or when pH (pD) is greater than the pK_a of the weakest proton donating species. Of particular interest is the fact that the apparent KIEs observed for the concerted mechanism is around two times larger than those for sw mechanisms, which may be ascribed from the intrinsic two-fold difference between k_{s,D_2O}^{cpet} and k_{s,H_2O}^{cpet}.

The data in Figure 5.3 arise from one set of simulation conditions and variation of the thermodynamics and kinetic parameters can lead to major qualitative and quantitative differences in the predicted kinetic isotope effect. Nevertheless, in general, both the concerted and stepwise mechanisms have regions of pH (pD) where they exhibit large kinetic isotope effects as well as regions where the KIE approaches unity. It is suggested that the presence or absence of an apparent KIE alone should not be used as a definite criterion to differentiate between stepwise and associated concerted PCET mechanisms, particularly, as is the case for many real systems, where only a limited region of electrolyte acidities is experimentally accessible. In most of the previously reported experimental systems[12-14], the apparent kinetic isotope effect was only explained by the intrinsic contribution and the observation of a KIE value

led the authors, perhaps erroneously, to conclude the concerted mechanism. The above descriptions suggest that supporting information to differentiate stepwise mechanism and concerted mechanism should include the discussion of apparent standard rate constants versus pH and the effect of varying the nature of the proton donor/acceptor.

5.3.3 Apparent Kinetic Isotope Effects in the Aminobenzoquinone Modified Monolayer System

The aminobenzoquinone (aBQ) modified monolayer[1;2] is an excellent model to understand how changes in the microenvironment affect electrochemical PCET behavior, and the changes discussed in this chapter are from exchanging the isotopic composition of the electrolyte solvent as well as changing the diluent from octanethiol (OT) to 8-mercapto-octanoic acid (MOA) in order to investigate the influence of local environment on the PCET kinetics. As was described in detail in Chapters 3 and 4, aBQ can be grafted onto a pre-assembled mixed monolayer of octanethiol (OT) and 11-amino-1-undecanethiol (AUT). This system is simplified as the OT/AUT system. If the diluting OT component of the monolayer is replaced by 8-mercapto-octanoic acid (MOA) the resulting monolayer is referred to as a MOA/AUT system. The voltammograms, as demonstrated in Figure 5.3a for the MOA/AUT system, indicate a 2e2H PCET in high pH electrolyte and a 2e3H PCET in low pH electrolyte. Meanwhile, as shown in Figure 5.3b, the curve of apparent standard rate constant *versus* pH for the MOA/AUT system is remarkably different from that for the OT/AUT system (Fig. 5.4), and it indicates the consistent increase in the apparent standard rate constant with decreasing acidity, which is consistent with the voltammograms shown in Figure 5.3a. Comparison of apparent standard rate constant for both the OT/AUT and the MOA/AUT system reveals that changes of local environment can dramatically affect the PCET kinetics of the aBQ monolayer system.

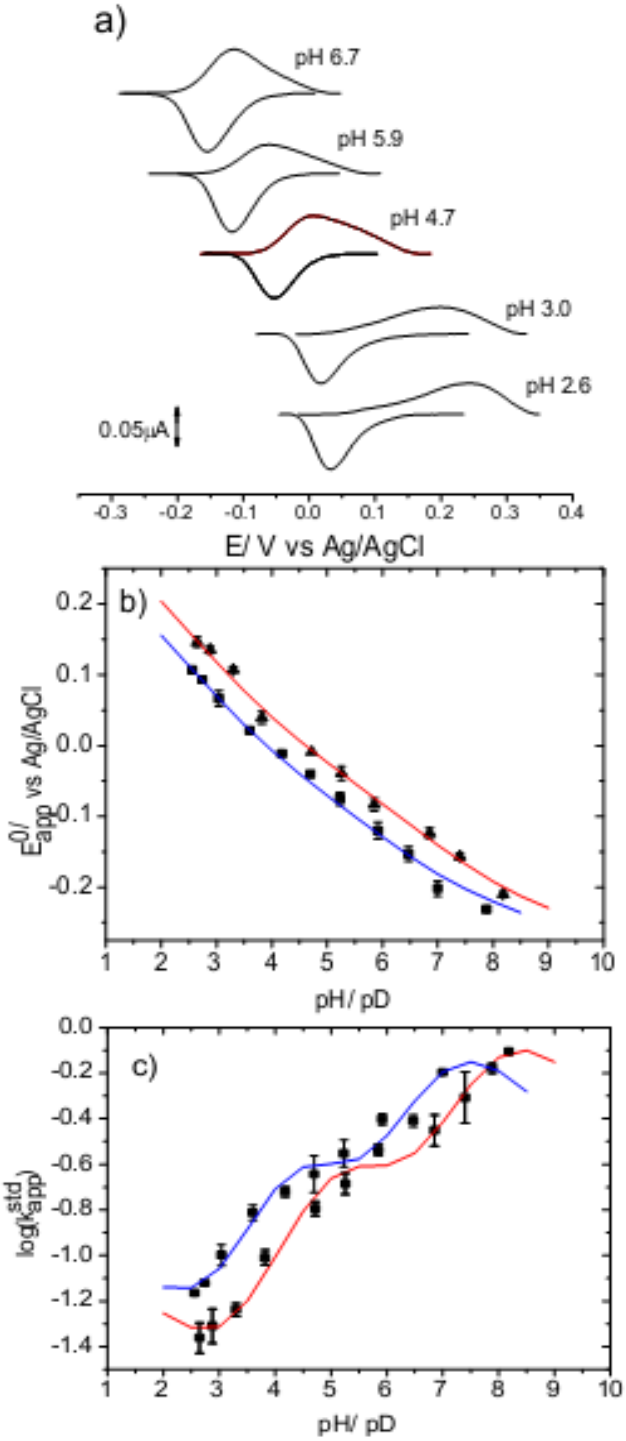

Figure 5.3: a) pH dependent, background corrected, voltammograms recorded at 20 mV/s b) apparent formal potential c) $\log(k^{std}_{app})$ versus pH or pD for a MOA/AUT system from the voltammograms of 10 mV/s. Points with error bars are experimental values in H_2O (squares) and D_2O (triangles) while solid lines are the corresponding fitting curves.

To measure the apparent kinetic isotope more conveniently, the Britton-Robinson buffer was used as the electrolyte instead of sodium phosphate buffer. The difference in the apparent standard rate constants measured in the two different buffers was observed to be subtle. For both the OT/AUT and the MOA/AUT systems, as shown in Figure 5.3c and Figure 5.4b, the apparent standard rate constants in D_2O are approximately a factor of two smaller than those in H_2O. Since the stepwise 2e3H framework PCET mechanism has been proved to be appropriate for both the OT/AUT system and the MOA/AUT system, it can be said that an apparent kinetic isotope effect can be observed in this multiple proton/electron reaction, which is consistent with the previous discussion in the theoretical section.

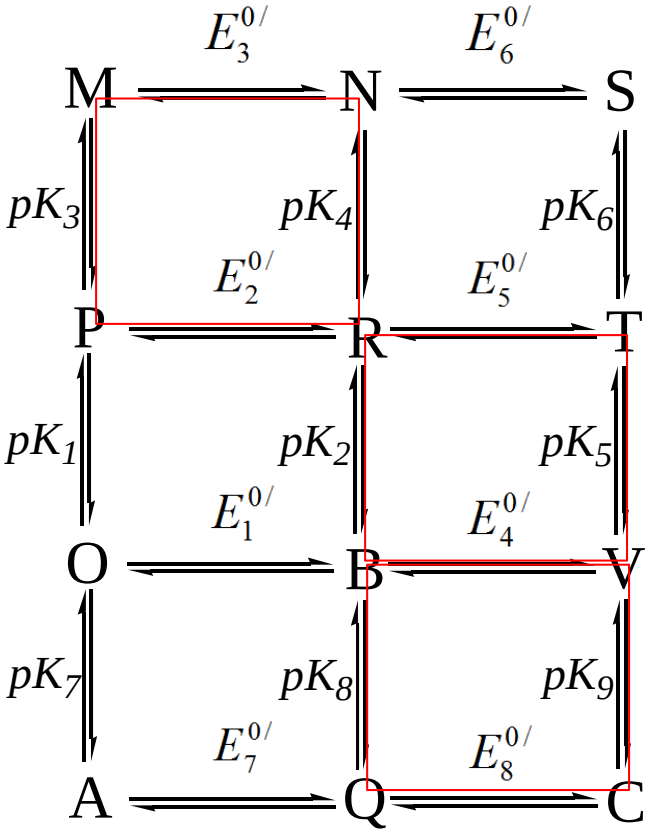

Scheme 5.2: Pathways for an aminobenzoquinone modified monolayer system. The lines indicate the single steps involved.

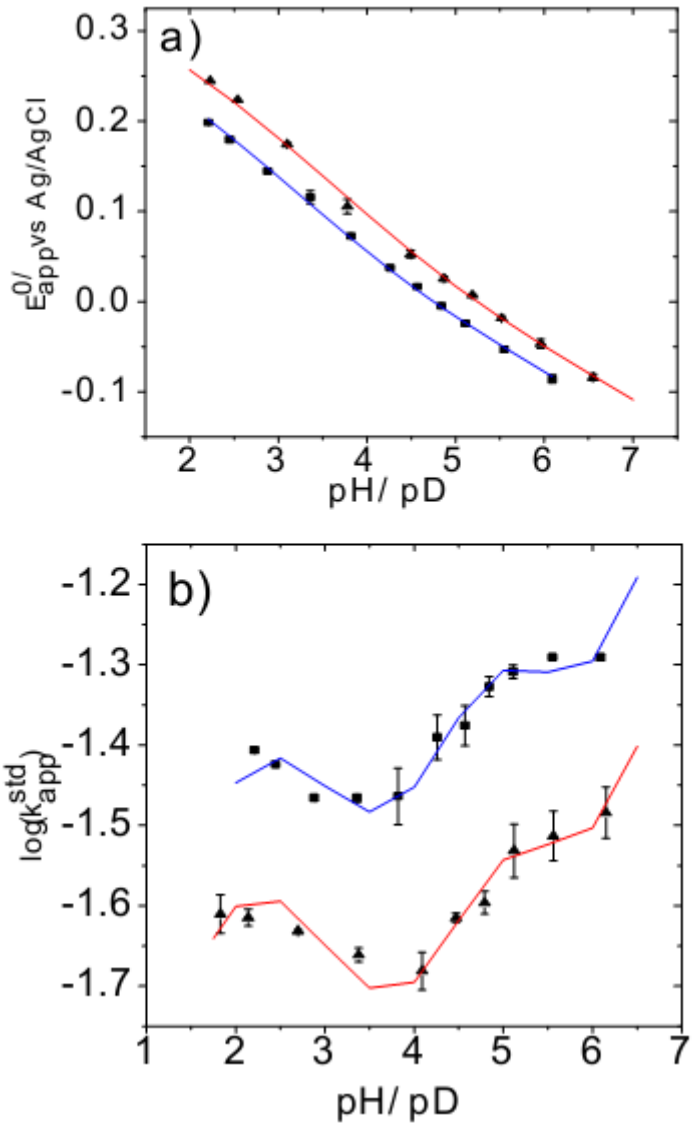

Figure 5.4: (a) apparent formal potential (b) $\log(k_{app}^{std})$ versus pH or pD for an OT/AUT system from 2 mV/s voltammograms. Points with error bars are experimental values in H_2O (squares) and D_2O (triangles) while solid lines are the corresponding fitting curves.

Table 5.1 shows the fit results of acid dissociation constants and standard formal potentials for both systems at H_2O and D_2O solvents. The provided values will be used for the discussion of the solvent isotope effect including the apparent kinetic isotope effect.

Using the analytical procedure provided in Chapter 4, one can reveal that within

the investigated pH range, the steps in the PCET reaction of both the OT/AUT and MOA/AUT systems only involve a subset of the twelve possible chemical species (see Scheme 5.2). It is therefore not surprising to notice in Table 5.1 that the changes of pK_1, pK_6 and pK_7 aren't reflected by measurements of the apparent standard rate constant and the apparent formal potential in H_2O and D_2O. It can also be observed in the same table that the introduction of the carboxylic acid group in replace of a methyl group at the terminus of the diluent component in the monolayer shifts the pK_a of the neighbor quinones to more negative values. As for the isotope exchange induced $E^{0/}$ variation, there is basically no change in either independent formal potential ($E_2^{0/}$ and $E_5^{0/}$) in the OT/AUT system. However in the MOA/AUT system, although $E_5^{0/}$ is remains in invariant upon solvent variation, $E_2^{0/}$ is seen to shift to more positive values. This may be caused by intramolecular proton transfer according to the chemical structures provided in Scheme 5.3. As was discussed in Section 5.3.2 of this chapter, $E^{0/}$ variation should be taken into account when explaining the apparent KIE of the proton coupled two electron transfer reaction, and this will complicate the apparent KIE analysis of the MOA/AUT system. For the sake of simplicity, only the apparent KIE of the OT/AUT system will be discussed in the following section.

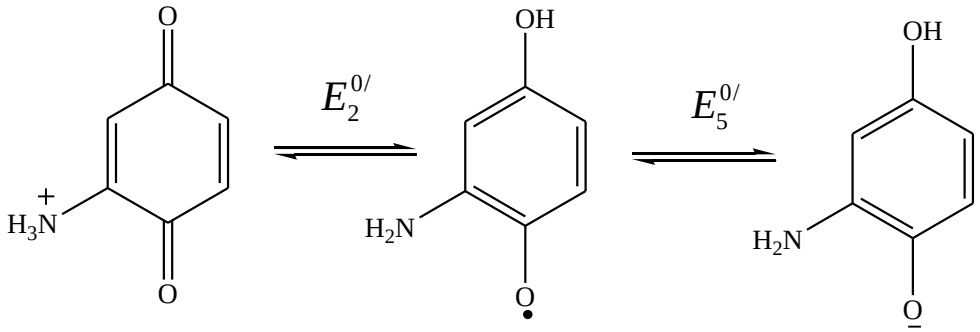

Scheme 5.3: Extracted electron transfer steps with chemical structures from Figure 4.6.

One main concern in this chapter is to prove that the remarkable apparent kinetic isotope effect should be observed in the stepwise PCET mechanism even with the

assumption that the electron transfer standard rate constant is isotope independent. In doing so, fit results of pK_a (H_2O) versus pK_a (D_2O) for the OT/AUT system have been plotted in Figure 5.5 and reveal a linear dependence. The theoretical relationship between $pK_a(D_2O)$ and $pK_a(H_2O)$ is given by Eqn. (2.12) and is plotted as a solid line in Figure 5.5 using the values of *a* and *b* reported by Krezel and Bal for 0.1M electrolytes[36]. It must be emphasized that the solid line in Figure 5.5 is not a best-fit line but rather the result predicted from theory. The very good agreement between the predicted (solid) and experimental (points) strongly supports the contention that H/D replacement induced pK_a causes the apparent kinetic isotope effect in the OT/AUT system under stepwise PCET control.

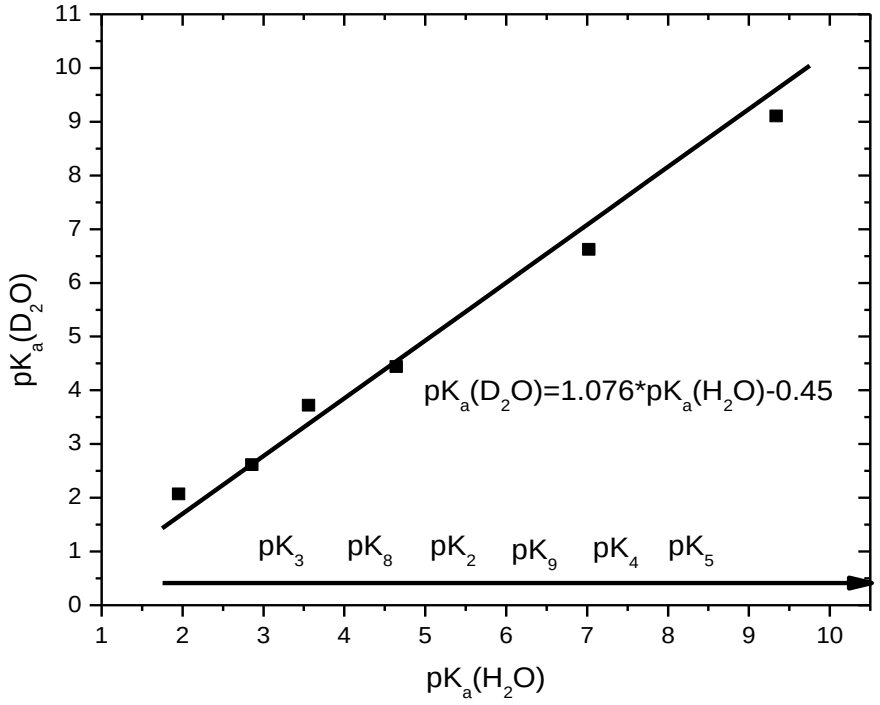

Figure 5.5: pK_a (D_2O) vs pK_a (H_2O). Points are from fitting curves and solid line is from theoretical relation for solvent dependent pK_a variation in 0.1M electrolyte.

Table 5.1: Fit results of acid dissociation constants and standard formal potentials for both OT/AUT and MOA/AUT systems.

System	pK_1	pK_2	pK_3	pK_4	pK_5	pK_6	pK_7	pK_8	pK_9	E_2^0 (V)	E_s^0 (V)
OT/AUT(H_2O)	-7	3.7	2.1	6.6	9.1	12.4	-28	2.6	4.4	-0.122	-0.23
MOA/AUT(H_2O)	-7	2.8	0.05	5.6	7.15	12.4	-28	-1.9	3.75	0.236	-0.215
OT/AUT(D_2O)	-7	3.56	1.95	7.0	9.34	12.4	-28	2.86	4.64	-0.122	-0.23
MOA/AUT(H_2O)	-7	3.5	-0.34	6.66	8.0	12.4	-28	-1.88	3.79	0.313	-0.228

5.4 Conclusions

To extend the understanding of the interrelationship between observable thermodynamic parameters, kinetic parameters and electrochemical PCET mechanisms, this chapter, has outlined simple expressions a concerted charge transfer model which proceeds through the formation of an analyte-proton donor (acceptor) complex. The refined expressions for a 1e1H case reveal that the observed kinetic parameters for the concerted process are strongly influenced by the composition of the electrolyte, particularly the concentration and acidity of potential proton donating species. The apparent standard rate constants for the associated mechanism are also highly sensitive to complexation equilibrium constants with stronger association leading to accelerated concerted kinetics. The measurement of an apparent kinetic isotope effect has previously been used as a good experimental tool to distinguish between the stepwise and the concerted mechanisms. Previous to this work it was unexpected that both the associated concerted and the stepwise mechanism can lead to kinetic isotope effects of comparable magnitude. The prediction of an observed KIE for the stepwise mechanism is shown by the fact that acid dissociation constants measured in water shift in D_2O, and the magnitudes of these shifts increase with increasing pK_a. Upon accounting for these shifts, a strong kinetic isotope effect is predicted for the stepwise mechanism even with the assumption that the fundamental standard electron transfer coefficients are independent of the isotopic composition of

the electrolyte. This same effect can mitigate the intrinsic sensitivity of the associated concerted standard rate constant to proton/deuteron isotope exchange. As a consequence, the measurement of an apparent kinetic isotope as an experimental tool to differentiate the stepwise mechanism and the concerted mechanism while studying the electrochemical PCET reaction should be used with great caution.

Experimentally, an apparent kinetic isotope effect in the OT/AUT system (which Chapter 4 showed most likely follows the stepwise PCET mechanism) has been measured and reasonably explained by H/D replacement induced shifts in acid dissociation constants, which is slightly different from that in the MOA/AUT system. This appears to be the first experimental system to show a relationship between stepwise mechanism and apparent kinetic isotope effect. Furthermore, studies where the nature of the proton donor and acceptor in the electrolyte are strongly varied at constant pH (or pD) should provide more meaningful insight into PCET mechanisms. Attempts should be made to evaluate the complex formation equilibrium constants. In instances where these values are low (< ca. 10^{-3}) it is unlikely that the buffer species of an electrolyte would be present in sufficient concentration to adequately strengthen the associated concerted pathway relative to a competing stepwise mechanism. On the other hand, the concentrations of proton donating species in the form of co-solvents would be expected to be sufficiently large and variation of solvent composition could greatly alter the extent the associated concerted pathway plays in the PCET mechanism even in instances where K_I and K_{II} are small.

Reference List

(1) Zhang, W.; Rosendahl, S. M.; Burgess, I. J. *J.Phys.Chem.C* **2010**, *114*, 2738-2745.

(2) Zhang, W.; Burgess, I. J. *Phys.Chem.Chem.Phys.* **2011**, *13*, 2151-2159.

(3) Bonin, J.; Costentin, C.; Robert, M.; Savéant, J. M. *Org.Biomol.Chem.* **2011**, *9*, 4064-4069.

(4) Costentin, C.; Robert, M.; Savéant, J. M. *J.Am.Chem.Soc.* **2006**, *128*, 4552-4553.

(5) Costentin, C.; Louault, C.; Robert, M.; Savéant, J. M. *Proc. Natl. Acad. Sci.* **2009**, *106*, 18143-18148.

(6) Costentin, C.; Robert, M.; Savéant, J. M. *Phys.Chem.Chem.Phys.* **2010**, *12*, 11179-11190.

(7) Markle, T. F.; Rhile, I. J.; Mayer, J. M. *J.Am.Chem.Soc.* **2011**, *133*, 17341-17352.

(8) Rhile, I. J.; Mayer, J. M. *J.Am.Chem.Soc.* **2004**, *126*, 12718-12719.

(9) Rhile, I. J.; Markle, T. F.; Nagao, H.; DiPasquale, A. G.; Lam, O. P.; Lockwood, M. A.; Rotter, K.; Mayer, J. M. *J.Am.Chem.Soc.* **2006**, *128*, 6075-6088.

(10) Anxolabehere-Mallart, E.; Costentin, C.; Policar, C.; Robert, M.; Saveant, J. M.; Teillout, A. L. *Faraday Discuss.* **2011**, *148*, 83-95.

(11) Costentin, C. *Chem.Rev.* **2008**, *108*, 2145-2179.

(12) Costentin, C.; Robert, M.; Savéant, J. M.; Teillout, A. L. *ChemPhysChem* **2009**, *10*, 191-198.

(13) Finklea, H. O.; Haddox, R. M. *Phys.Chem.Chem.Phys.* **2001**, *3*, 3431-3436.

(14) Haddox, R. M.; Finklea, H. O. *J.Phys.Chem.B* **2004**, *108*, 1694-1700.

(15) Huynh, M. H.; Meyer, T. J. *Chem.Rev.* **2007**, *107*, 5004-5064.

(16) Costentin, C.; Evans, D. H.; Robert, M.; Savéant, J. M.; Singh, P. S. *J.Am.Chem.Soc.* **2005**, *127*, 12490-12491.

(17) Costentin, C.; Robert, M.; Savéant, J. M. *J.Am.Chem.Soc.* **2006**, *128*, 8726-8727.

(18) Costentin, C.; Robert, M.; Savéant, J. M.; Teillout, A. L. *Proc. Natl. Acad. Sci.* **2009**, *106*, 11829-11836.

(19) Costentin, C.; Robert, M.; Savéant, J. M.; Tard, C. *Phys.Chem.Chem.Phys.* **2011**, *13*, 5353-5358.

(20) Edwards, S. J.; Soudackov, A. V.; Hammes-Schiffer, S. *J.Phys.Chem.A* **2009**, *113*, 2117-2126.

(21) Huynh, M. H.; Meyer, T. J. *Proc. Natl. Acad. Sci.* **2004**, *101*, 13138-13141.

(22) Iordanova, N.; Hammes-Schiffer, S. *J.Am.Chem.Soc.* **2002**, *124*, 4848-4856.

(23) Johannissen, L. O.; Irebo, T.; Sjödin, M.; Johansson, O.; Hammarström, L. *J.Phys.Chem.B* **2009**, *113*, 16214-16225.

(24) Madhiri, N.; Finklea, H. O. *Langmuir* **2006**, *22*, 10643-10651.

(25) Makarycheva-Mikhailova, A. V.; Stanbury, D. M.; McKee, M. L. *J.Phys.Chem.B* **2007**, *111*, 6942-6948.

(26) Markle, T. F.; Rhile, I. J.; DiPasquale, A. G.; Mayer, J. M. *Proc. Natl. Acad. Sci.* **2008**, *105*, 8185-8190.

(27) Shafirovich, V.; Dourandin, A.; Luneva, N. P.; Geacintov, N. E. *J.Phys.Chem.B* **1999**, *104*, 137-139.

(28) Sjödin, M.; Styring, S.; Wolpher, H.; Xu, Y.; Sun, L.; Hammarström, L. *J.Am.Chem.Soc.* **2005**, *127*, 3855-3863.

(29) Tüchsen, E.; Hansen, P. E. *Inter. J. Biol. Macromol.* **1991**, *13*, 2-8.

(30) Tobias, R. S.; Yasuda, M. *J.Phys.Chem.* **1964**, *68*, 1820-1828.

(31) Venkataraman, C.; Soudackov, A. V.; Hammes-Schiffer, S. *J.Phys.Chem.C* **2008**, *112*, 12386-12397.

(32) Zhang, M. T.; Irebo, T.; Johansson, O.; Hammarström, L. *J.Am.Chem.Soc.* **2011**, *133*, 13224-13227.

(33) Zhang, M. T.; Hammarström, L. *J.Am.Chem.Soc.* **2011**, *133*, 8806-8809.

(34) Ludlow, M. K.; Soudackov, A. V.; Hammes-Schiffer, S. *J.Am.Chem.Soc.* **2010**, *132*, 1234-1235.

(35) Finklea, H. O. *J.Electroanal.Chem.* **2001**, *495*, 79-86.

(36) Krezl, A.; Bal, W. *J. Inorg. Biochem.* **2004**, *98*, 161-166.

(37) Li, N. C.; Tang, P.; Mathur, R. *J.Phys.Chem.* **1961**, *65*, 1074-1076.

(38) Buhks, E.; Bixon, M.; Jortner, J. *J.Phys.Chem.* **1981**, *85*, 3763-3766.

(39) Weaver, M. J.; Tyma, P. D.; Nettles, S. M. *J.Electroanal.Chem.* **1980**, *114*, 53-72.

(40) Weaver, M. J.; Nettles, S. M. *Inorg.Chem.* **1980**, *19*, 1641-1646.

Chapter 6: Electrochemical Proton Coupled Electron Transfer Studies of a Nitroxyl Radical Modified Bilayer System

6.1 Introduction

A theoretical framework composed of a series of analytical expressions has been built in Chapter 4 and 5 to describe how various parameters control electrochemical PCET mechanisms. It also offers the means to devise new experimental approaches that can differentiate concerted and stepwise mechanisms[1;2]. For an electrochemical one proton, one electron system one can predict from theory that larger pK_a differences between the reduced and oxidized species will increase the energy of intermediates produced in stepwise routes and therefore favour the concerted mechanism. Studies of $Os^{II}(OH_2)/Os^{III}(OH)$ and $Os^{III}(OH)/Os^{IV}(O)$ couples have provided an illustrative verification of this prediction[3], and such PCET experimental systems are attractive due to the possible existence of concerted PCET mechanism.

PCET thermochemistry (acid dissociation constants, standard formal potentials and bond dissociation free energies) of different proton coupled electron transfer reagents partially guides the design of new reactions involving proton transfer and electron transfer[4]. The thermochemical data of species that are known to participate in PCET reactions such as phenols, nitroxyl radicals, alcohols, transition metal complexes, and others have been summarized in an excellent review[4]. In previous studies of electrochemical PCET, the oxidation of phenols is treated as a model system in part because of their general applications in the fields of biosynthesis[5], biological energy production[6-12], and food preservation[13]. The concerted 1e1H transfer mechanism has been observed in this model system, which has been qualitatively analyzed on the basis of thermochemical data. It has been speculated that nitroxyl radicals and their 1e1H reduced partners[14-16], i.e. hydroxylamine, can provide concerted 1e1H pathways instead of stepwise pathways due to low O-H bond strengths[17;18]. However, the above speculation for the concerted mechanism in nitroxyl radicals in the field of electrochemistry still lacks strong experimental

evidence. TEMPO (2, 2'-6, 6'-tetramethylpiperidine-1-oxyl radical) and related derivatives of the most popular species of nitroxyl radicals, have been widely used as spin labels, spin traps, free radical polymerization promoters and especially as "green oxidation catalysts" for the oxidation of primary alcohols to carboxylic acids[19]. Most interesting because of its highly stability in the aqueous solution, this free radical can be chosen as a suitable PCET reagent in the field of electrochemistry.

Combining thermochemical data with the theoretical model provided in Chapter 5 indicates that the stepwise mechanism is unlikely to be favoured over the concerted mechanism. The TEMPO system would therefore seem like an ideal system to investigate in hopes of finding strong evidence of the concerted mechanism. However, the TEMPO system is known to participate in a variety of confounding additional reactions including disproportionation and additional acid-base chemistry[20-22]. To minimize the contributions of these reactions (particularly the disproportionation), it is desirable to once again create a monolayer system with immobilized redox centers. In this chapter, two different techniques are described as means to assemble TEMPO onto gold electrodes. The resulting surface TEMPO systems (a covalently bonded TEMPO monolayer and a TEMPO bilayer formed through physisorption) show different electrochemical behavior. In addition, preliminary analysis of the latter system is provided in terms of thermodynamic and kinetic aspects.

6.2 Experimental

Two techniques have been developed to assemble TEMPO molecules onto gold electrode surfaces. The first technique is similar to the one used in the preparation of aminobenzoquinone modified monolayers as the TEMPO molecule is covalently bonded to the electrode surface. The second one is one where a bilayer system is assembled on an electrode surface with the assistance of hydrophobic forces and physisorption bonds. This experimental section describes the procedures used to assemble the two surface systems as well as a description of the synthesis used to produce a TEMPO surfactant.

6.2.1 Covalent Bond Based TEMPO Monolayer Formation

As suggested by Finklea and Mahidri[23], a surface coupling reaction can be used to build a TEMPO modified monolayer system. This reaction involves the initial assembly of a carboxyl-acid terminated SAM followed by the covalent bonding of aminoTEMPO through the formation of an amide bond (Scheme 6.1). Alternatively, a priori TEMPO derivative thiols can be synthesized using similar chemistry and directly assembled on gold surfaces. In either case, the resulting systems have been previously used as model systems in the study of electron transfer reactions[23]. In those studies the only redox event that was reported was the simple electron transfer corresponding to the oxidation of the TEMPO radical to form the nitrosonnium ion (i.e. a non-PCET event). The procedures followed in this chapter to form a covalently bound TEMPO monolayer basically follow the work done by Finklea and Mahidri[23], only with a subtle difference in the composition of substrate for the coupling reaction. As briefly described in Scheme 6.1, the freshly cleaned gold bead electrode was initially incubated in an ethanolic solution of 0.1M octanethiol (OT) and 0.02M 11-mercaptoundecanoic acid (MUA) for one hour followed by ethanol rinsing in order to remove physisorbed thiols. The as-formed, two component SAM modified gold electrode was subsequently transferred into a 10mM amino-TEMPO dichloromethane solution with 50mM 1-ethyl-3-(3-dimethylaminopropyl) carbodiimide (EDC) as a coupling reagent. After half an hour surface coupling reaction, the resulting functionalized electrode is rinsed thoroughly with water and then placed in the electrolyte solution for electrochemical characterization.

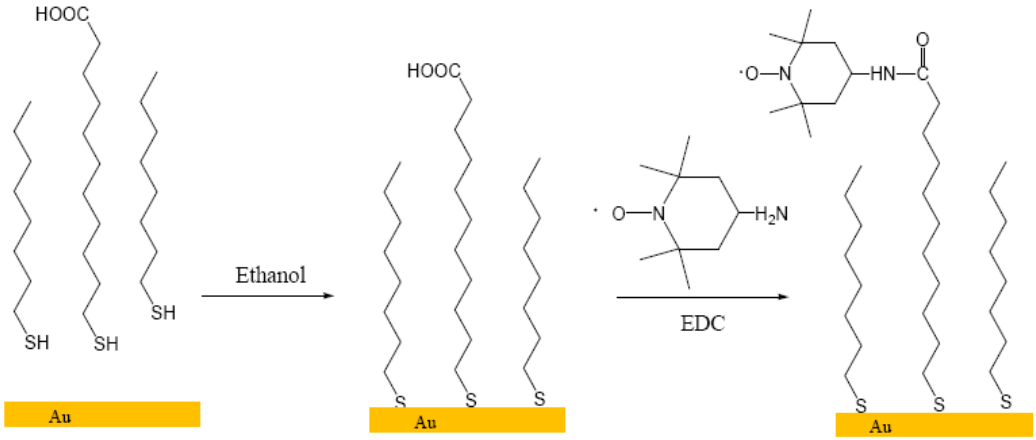

Scheme 6.1: Formation of TEMPO modified monolayer with surface amide coupling reaction.

6.2.2 Synthesis of C_{18}TEMPO

The synthesis of C_{18}TEMPO in this chapter follows a procedure first reported by Majda et al[24-28]. The main coupling reaction is performed in an organic solvent environment. 0.011 mol of 4-aminoTEMPO and 0.01 mol of stearic acid were dissolved in 50 mL of methyl chloride, and 0.01 mol of EDC was then added as a coupling agent. After stirring overnight under nitrogen, the cloudy orange mixture was slowly converted to a clear orange solution. The resulting solution was washed twice with saturated $NaHCO_3$ to remove extra stearic acid and then dried with $MgSO_4$ to remove the produced H_2O. The bottom organic layer was collected and purified on a silica column with methyl chloride as the eluting solvent. To check the purity of the product, thin-layer chromatography (TLC) was used which proved that C_{18}TEMPO is the major product in the collected organic solution. After removing methyl chloride by evaporation under nitrogen gas, the orange powder obtained is the final product which is termed C_{18}TEMPO (Scheme 6.2).

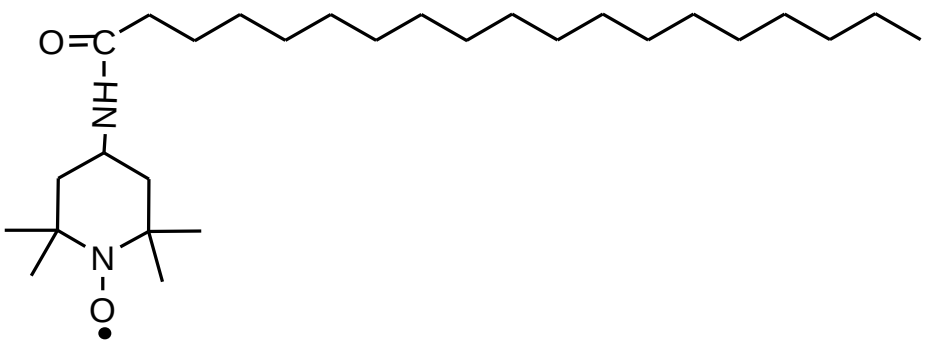

Scheme 6.2: Chemical structure of C_{18}TEMPO.

6.2.3 Physisorbed TEMPO Bilayer Formation

This method using one hydrophobic substrate and one biological molecule with a hydrophobic tail as building blocks to form a bilayer system have attracted attention over many decades in bioelectrochemistry[29-31]. As described in Scheme 6.3, the formation of a TEMPO bilayer is achieved by two main steps. Briefly, the mechanically polished and cleaned gold electrode was first modified by a monolayer of hydrophobic thiols (Octanethiol (OT), Hexanethiol (HT), or Ethanethiol (ET)). The resulting SAM-modified electrode was rinsed with ethanol and then placed on the water surface with well-organized C_{18}TEMPO at the air/H_2O interface (~1g/cm^2) for about one minute. Finally the as prepared electrode (TEMPO bilayer modified electrode) was transferred to an electrochemical cell and a hanging meniscus was created to afford electrochemical characterization.

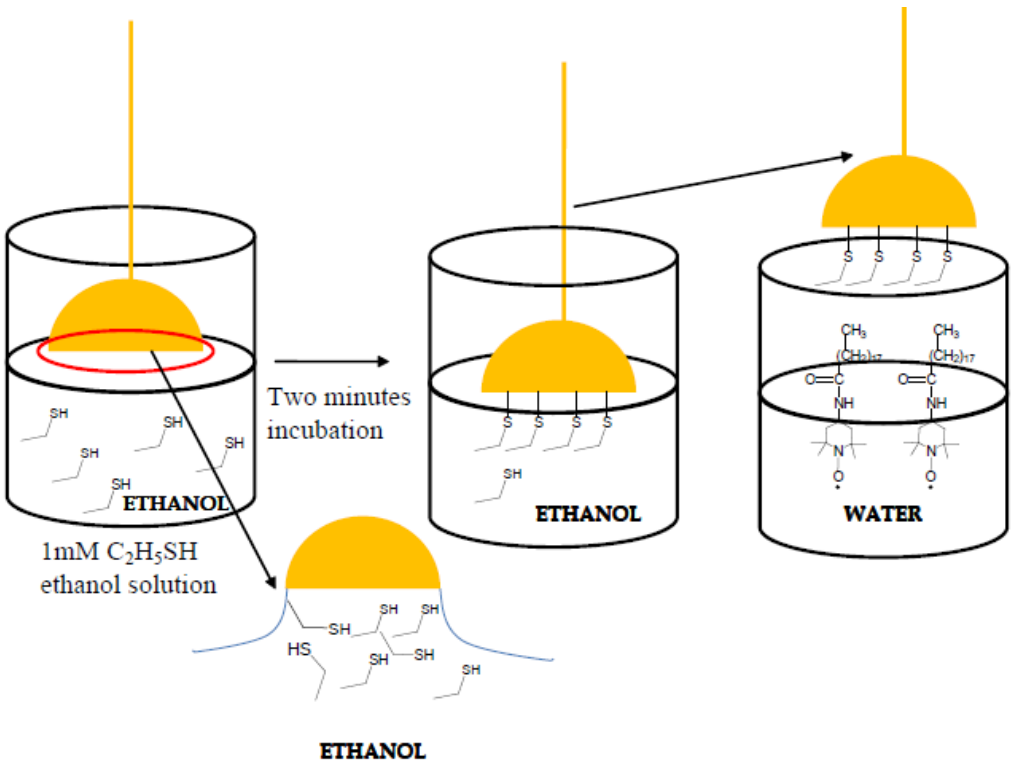

Scheme 6.3: Hydrophobic force based nitroxyl radical modified bilayer formation.

6.3 General Cyclic Voltammetry Features

The electrochemical behavior of TEMPO in the aqueous solution (i.e not immobilized to an electrode surface) has been obtained using cyclic voltammetry measurements with glassy carbon[14;16] and hanging mercury[32] electrodes. It was found that TEMPO can be oxidized to $TEMPO^+$ by removing one electron. Meanwhile, TEMPO can be reduced to TEMPOH with the transfer of one proton and one electron. Usually the oxidation reaction occurs around 700mV with respect to the Ag/AgCl reference electrode[23], and it shows a reversible voltammogram. The reduction process attracts special attention in this chapter since it involves one electron coupled one proton transfer. It was proved in experiment that rate constants of this reduction reaction are dependent on the nature of the working electrodes. For example, the 1e1H transfer rate constant of 4-Hydroxy-2, 2'-6, 6'-tetramethylpiperidine-N-oxyl (TEMPOL) on glassy carbon electrode is much lower than that on hanging mercury electrode[14;16;32]. Although the reduction reaction of TEMPO has been studied in

solution for several years, it was rarely investigated when the TEMPO molecule was assembled onto an electrode surface.

Figure 6.1 depicts a typical voltammogram of this system, a redox couple with a formal potential of 700mV is observed and reveals reversible kinetics. It is reasonable to assign these two peaks as the oxidation process of the TEMPO modified monolayer based on the value of formal potential. According to voltammetry of TEMPO in aqueous solution systems, it would be expected that a reduction reaction should also be observed within the potential domain of this voltammogram. However, no additional redox peaks are observed. It is possible that the disappearance of peaks for the reduction reaction is caused by slow coupled electron/proton transfer kinetics of this TEMPO modified monolayer, or the potential of this reduction reaction is more negative than the potential of hydrogen evolution.

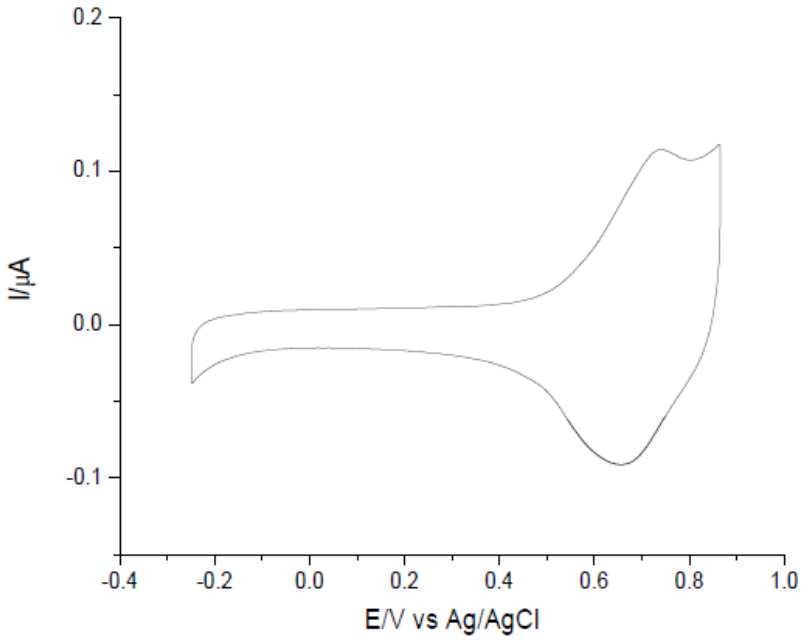

Figure 6.1: 5 mV/s voltammograms of a nitroxyl radical modified monolayer at pH 6.8.

Suspecting that very slow electron transfer kinetics prevents the observation of PCET reaction peaks in the voltammograms, shorter thiols were used as spacer layer. It is well known that the heterogeneous electron transfer kinetics has an inverse

exponential dependence on the distance between the electrode and the immobilized electroactive center[34]. When 4-mercaptobenzoic acid (MBA) was used instead of MUA/OT to form the initial monolayer it was found that the surface coupling of amino-TEMPO was also successful. The resulting TEMPO modified monolayer was also characterized by cyclic voltammetry but unfortunately, similar to the voltammograms of the MUA/OT based TEMPO modified monolayer system, the voltammograms of this new TEMPO modified monolayer system still didn't reveal the peaks for the reduction reaction. The absence of PCET peaks may be caused by the slow kinetics of the reduction reactions in these two TEMPO modified monolayer systems, which needs to be further proven in future work.

In order to observe the PCET peak for electrochemical investigation, a different technique was sought to graft TEMPO molecules onto the electrode surface. Majda and co-workers have been able to synthesize TEMPO surfactants and investigate their electron transfer behavior (oxidation reaction) at the air/water interface[25-28]. Their contributions provided insightful input on how TEMPO surfactants can be assembled onto the gold electrode surface without the formation of covalent Au-S bonds. To achieve this, C_{18}TEMPO, an insoluble redox molecule, was synthesized for the purpose of forming a tethered bilayer. Direct assembly of C_{18}TEMPO on the bare gold electrode proved unsuccessful at first, as evidenced by the very weak oxidation reaction peaks in the voltammograms. This was caused by very poor adherence of the C_{18}TEMPO to the bare gold surface. In order to immobilize more C_{18}TEMPO molecules on the electrode surface, the gold electrode was initially modified by the formation of a SAM of hydrophobic alkanethiols. It was suspected that the hydrophobic tails of the C_{18}TEMPO molecules would have high affinity for the SAM-modified gold via strong hydrophobic (van der Waals) forces, and in principle, it would result in a high loading of C_{18}TEMPO on the electrode surface. Three alkanethiols with different carbon chain lengths (octanethiol (OT), hexanedithiol (HT), and ethanethiol (ET) were tested for this purpose.

The preparation procedures for the OT/C_{18}TEMPO, HT/C_{18}TEMPO and ET/C_{18}TEMPO bilayer systems has been described in the experimental section, and

the as prepared bilayer systems were mainly characterized by cyclic voltammetry. Fig. 6.2 describes typical voltammograms of OT/C_{18}TEMPO and HT/C_{18}TEMPO bilayer systems. Peaks for the TEMPO oxidation reaction are clearly observed for both bilayer systems and the measured formal potentials for these oxidation reactions are around 700mV, which is close to the value observed for TEMPO monolayers previously described. In addition, the loading of TEMPO in the OT/C_{18}TEMPO bilayer is much larger than that in the HT/C_{18}TEMPO bilayer, which can be crudely explained by differences in the strength of hydrophobic forces. It is generally accepted that the longer the chain length of an alkanethiol, the larger the strength of the van der Waal forces. It should be expected from the same reasoning, that the loading of TEMPO molecules in OT/C_{18}TEMPO is more than that in HT/C_{18}TEMPO, and this is proven to be the case upon integration of either the cathodic or anodic peak corresponding to the TEMPO oxidation reaction. As shown in Figure 6.2, the reduction reaction provides a much more complicated voltammetric response in comparison with the oxidation reaction. In Figure 6.2a for the OT/C_{18}TEMPO bilayer system in pH 4.3 electrolyte, a broad wave is observed at E ~ -0.3V in the negative-going scan. It is speculated that this signal represents TEMPO reduction overlapping with hydrogen evolution, which can be observed when sweeping the potential to -300mV in the absence of C_{18}TEMPO. On the return (positive-going) scan a very sharp peak with intensity higher than that of the TEMPO radical oxidation peak is observed.

As compared to the voltammogram collected in an OT/C_{18}TEMPO bilayer system, the peak of conversion for a HT/C_{18}TEMPO bilayer system from TEMPO to TEMPOH occurs with a 100mV shifting to more positive, as well as with a more defined shape. More complicated situations were observed for the process of TEMPOH converting back to TEMPO with the potential scanning to positive values. As Figure 6.2 demonstrated, there are two main differences of both bilayer systems. Firstly, the intensity of that very sharp peak decrease remarkably when OT was replaced by HT and this is three times difference in this case. On the other hand, the decreasing intensityof the very sharp peak is followed by the appearance of a new

bump, which can be observed at a more negative potential in comparison with the sharp peak. It can be speculated in both systems that the overall process of TEMPOH to TEMPO may involve not only the simple 1e1H transfer reaction but also some other conformation changes.

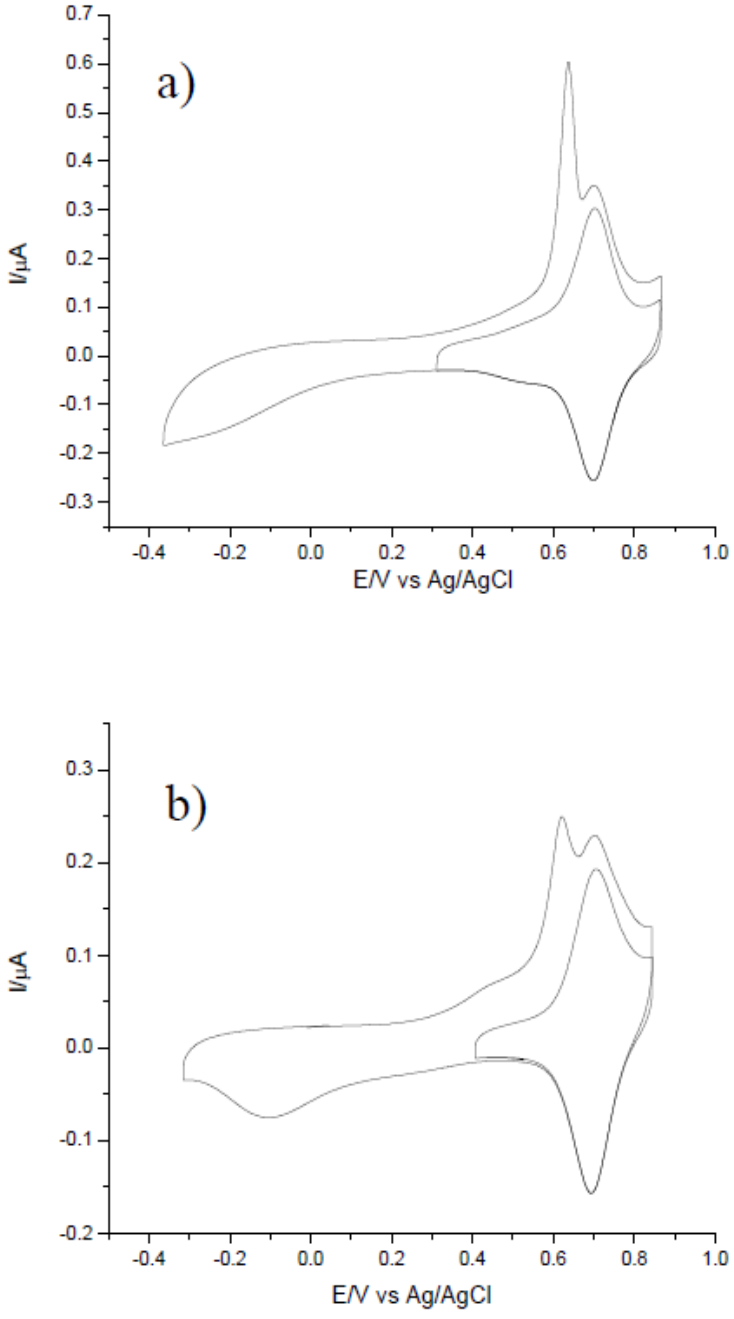

Figure 6.2: 5 mV/s voltammograms of a) OT/C_{18}TEMPO; b) HT /C_{18}TEMPO bilayer system at pH 4.3.

A typical voltammogram of an ET/C_{18}TEMPO bilayer system at pH 4.4 is shown in Fig. 6.3. It can be determined from the integration of the oxidation peaks that the loading of TEMPO molecules in this system is much smaller than that in the above two systems due to its smaller hydrophobic force strength. A very promising result observed in Fig. 6.4 is the voltammetric evidence of the reduction reaction in this TEMPO bilayer modified electrode. The first interesting result is that the sharp peaks observed in the OT/C_{18}TEMPO system as well as the HT/C_{18}TEMPO system unexpectedly disappear in the voltammograms for the ET/C_{18}TEMPO system. This unexpected result still remains to be further explained. Meanwhile, a redox couple is observed at more negative potentials. Evidence that this signal arises from a PCET process is forthcoming from the fact that the more negative redox couple shifts along the potential axis with changing electrolyte pH (viz. Fig. 6.5) whereas the positive potential pair is essentially pH invariant.

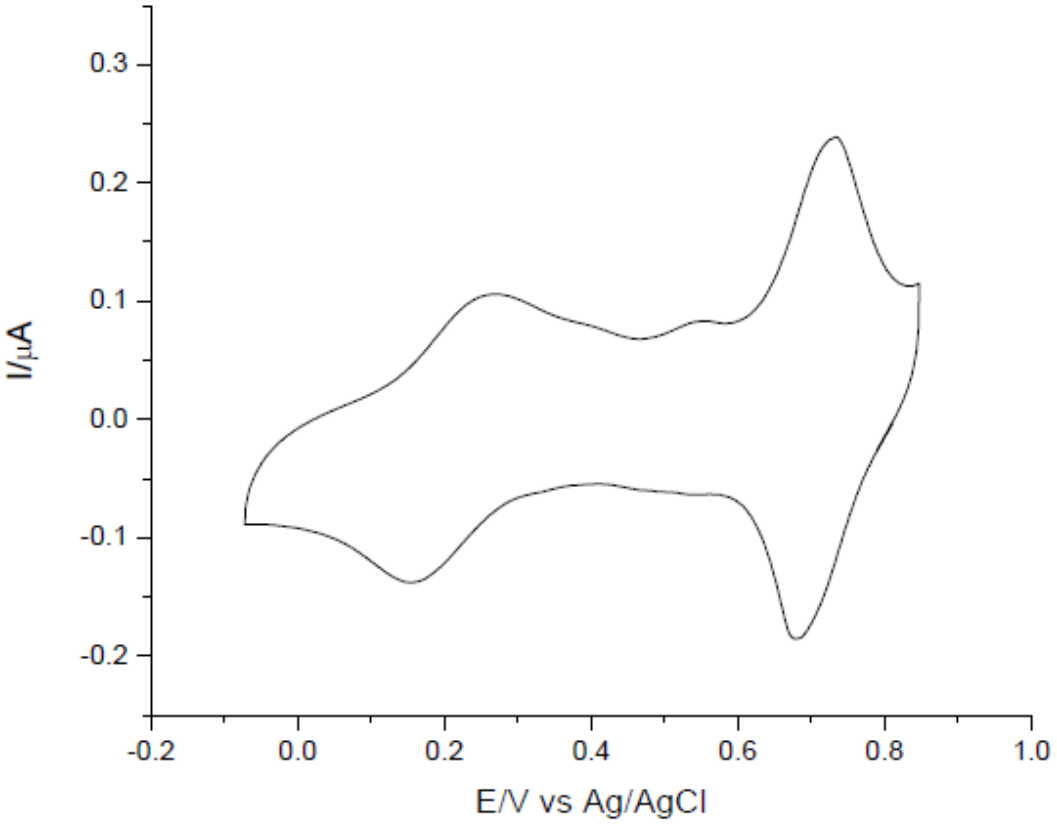

Figure 6.3: 5 mV/s voltammograms of an ET/C_{18}TEMPO bilayer system at pH 4.4.

Ensuring the stability of a redox molecule modified electrode is a very important issue in the field of mechanistic study of charge transfer process due to the requirement of experimental reproducibility. As was described in Chapter 3, the removal of intermolecular effects between electroactive centers can minimize the complexity of kinetic analysis. The ideal electrochemical system would be one where intermolecular interactions are negligible. Chronocoulometric measurements have been successfully employed for the aminobenzoquinone modified monolayer system in order to test its ideality, and this technique requires at least one hour of electrochemical interrogation of this monolayer. In other words, any instability in the modifying layer(s) prevents the assessment of the ideality test of the system. Figure 6.4 depicts two voltammograms for the reduction reaction occurring in an ET/C_{18}TEMPO bilayer system, one voltammogram is for the first potential cycle, and the other one is collected after twenty cycles. It would be a stable electrochemical system if the shapes, intensities and potentials of the voltammograms keep constant with continuous potential cycling. Unfortunately Fig. 6.4 provides clear evidence that the ET/C_{18}TEMPO bilayer system suffers from imperfect stability. After 20 potential cycles the potential separation between the anodic peak potential and cathodic peak potential of the reduction reaction increases and both peak intensities decrease remarkably. The decreasing peak intensity can be ascribed to the loss of TEMPO molecules from the electrode surface. It can be summarized that the inherent instability of an ET/C_{18}TEMPO bilayer system prohibits the ideality test using the chronocoulometric measurements. An alternative, qualitative method in the analysis of ideality of this bilayer system will be described below in detail.

.

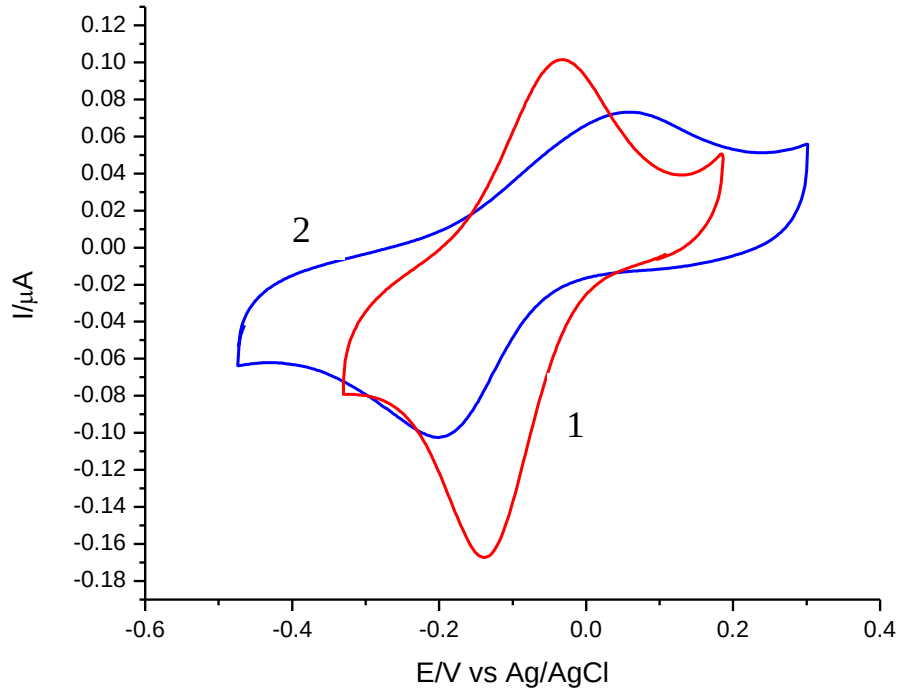

Figure 6.4: 5 mV/s voltammograms of reduction process of an ET/C_{18}TEMPO bilayer recorded at pH9. First cycle: 1, and after 20 cycles: 2.

6.4 Results and Discussion of an ET/C_{18}TEMPO Bilayer System

Although charge measurements can't be performed to determine the ideality of the presumed 1e1H transfer in the ET/C_{18}TEMPO bilayer system, a qualitative alternative is provided through analysis of FWHM values from the voltammetric peaks in combination with the theoretical description of voltammetry, which is provided in Chapter 2. For a redox molecule modified monolayer system undergoing one electron transfer, it can be observed from the CV simulation that the values of the FWHM depend on the standard rate constants and scan rates, For instance, if the standard rate constant is assumed to be relatively slow, say $0.01s^{-1}$, and the scan rate is 5mV/s, the FWHM from the theoretical provided voltammogram is about 130mV, which is larger than 90mV for the ideal 1e transfer process. This is a reflection of the fact that the CV was performed under a rate of potential perturbation that exceeds the intrinsic rate at which electrons can exchange between the redox center and the

electrode. In other words, the experimental conditions do not allow for a Nernstian response from the system.

Fig. 6.5 gives background subtracted voltammograms collected at 5mV/s, and their FWHM values are around 140mV at pH > 6 and approximately 160mV between pH 3.5 and pH 6. Meanwhile, as will be shown in the following section, the calculated rate constants of the TEMPO reduction reaction are around $0.01s^{-1}$. By using the information provided by the simulation and experiment, it can be postulated that the ET/C_{18}TEMPO bilayer system behaves nearly ideally, especially in high pH electrolyte.

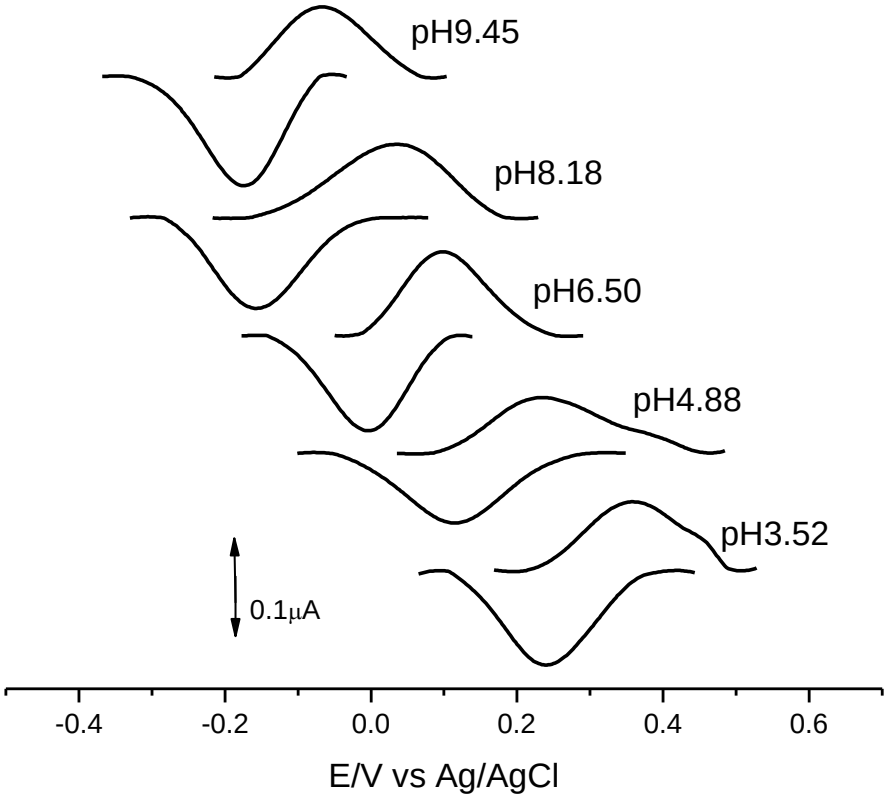

Figure 6.5: Baseline corrected 5 mV/s voltammograms of an ET/C_{18}TEMPO bilayer system at different pHs.

6.4.1 Influence of pH on Apparent Formal Potential

It is generally accepted in previous electrochemical studies of TEMPO in aqueous solution that the reduction process of TEMPO involves the transfer of one proton and one electron[16]. In Chapter 4, the thermodynamic relationship between pH and formal potential for a 1e1H transfer process was developed and revealed that the Pourbaix diagram should provide a linear line with a slope of 60mV/pH. Figure 6.6 provides such a plot for the ET/C_{18}TEMPO bilayer system. Between pH 3 and pH 10 there are two linear regions with a slope of -87mV/pH at low pH electrolyte and a slope of -58mV/pH at high pH. It is therefore reasonable to believe that there is a 1e1H transfer at pHs between 5.8 and 9.5. However, the slope at low pH electrolyte isn't consistent with either that of 1e1H (-60mV/pH) or that of 1e2H (-120mV/pH). It has been reported that in aqueous solution, the reduction process of TEMPO is usually followed by some chemical reactions like disproportion reaction or dimerization to form a hydrogen bond dimer[20-22]. It would seem that an unexpected electrochemical followed by a homogeneous chemical reaction gives rise to the observed slope of -87mV/pH at low pH electrolyte. This unusual slope may be induced by the chemical reaction followed by the 1e1H transfer reaction, and the type of this chemical reaction may need to be identified with the assistance of electrochemical combined spectroscopic techniques.

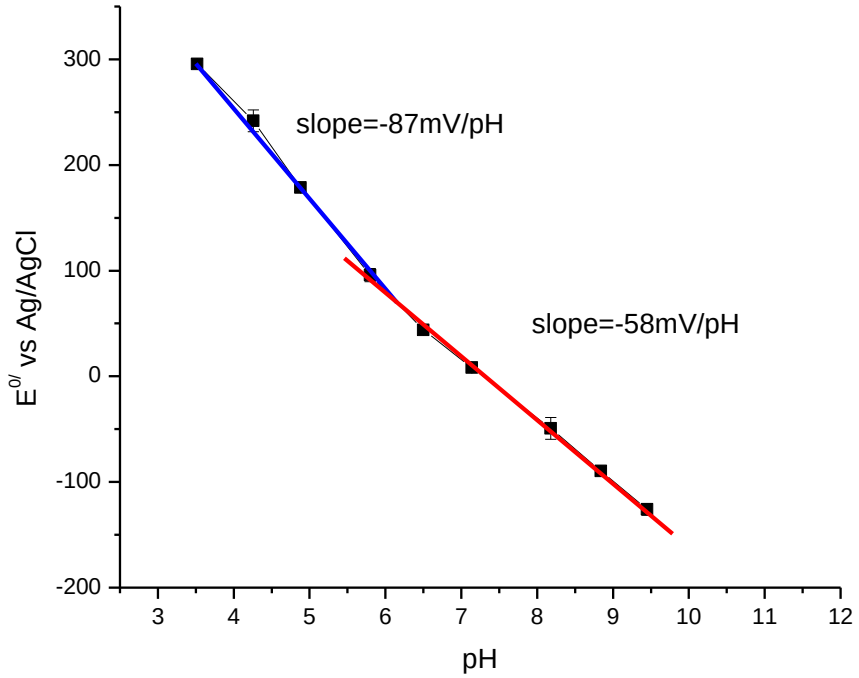

Figure 6.6: Apparent formal potential for an ET/C_{18}TEMPO bilayer system as a function of pH. Points with error bars are experimental values and the solid line is the fitting result.

6.4.2 Influence of pH on Apparent Standard Rate Constant

The 1e1H reduction reaction at relative high pH range is the main concern in this chapter. Similar to the electrochemical study of the aminobenzoquinone modified monolayer system, the plot of potential separation versus pH is very useful in the qualitative analysis of apparent standard rate constants as a function of pH. In general, the larger potential separation between the cathodic peak potential and the anodic peak potential indicates lower values of the apparent standard rate constant for the 1e1H reaction. As demonstrated in Figure 6.7, potential separations are between 75 mV and 200 mV depending on pH and the curve shows an inverted "V" shape with a maximum point located at pH 8, which imply the quasi "V" shape of apparent standard rate constants versus pH. As demonstrated in Figure 6.8b, with the

decreasing of acidity concentration, 1e1H transfer standard rate constants first decrease and then increases with a minimum value around pH 8.

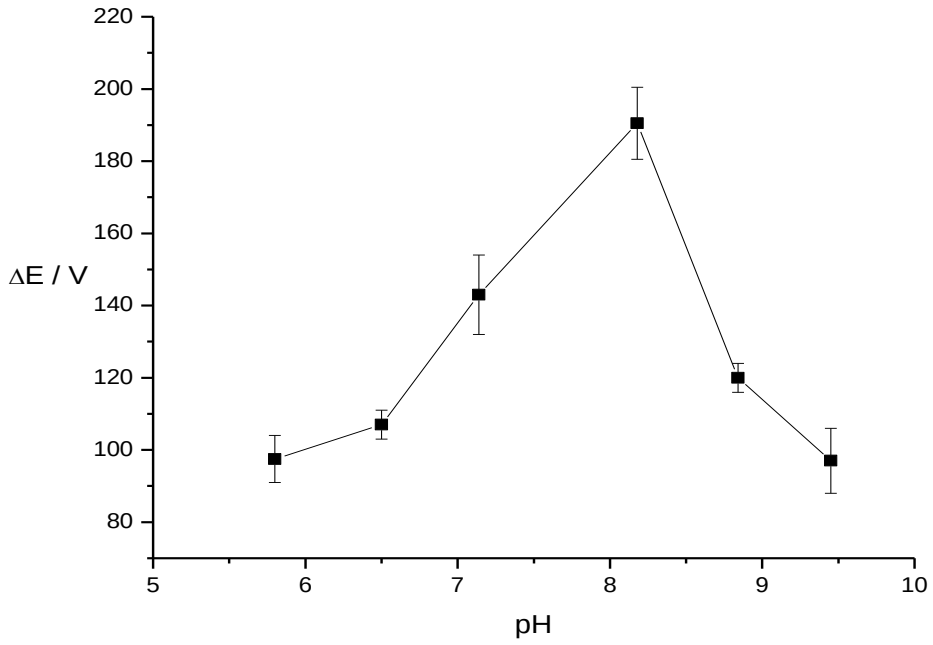

Figure 6.7: Potential separation vs pH for the ET/C_{18}TEMPO bilayer system.

6.4.3 Charge Transfer Pathways

It can be derived from the theoretical model described in Chapter 4 that for 1e1H transfer with stepwise mechanism, the plot of apparent standard rate constants vs pH provides a "V" shape and the maximum standard rate constant should be at least ten orders larger than the minimum one depending on different setting parameters. This is obvious contradict with the result shown in Figure 6.8b for an ET/C_{18}TEMPO bilayer system, which shows a two times difference in standard rate constants within the studied pH range, therefore it is more reasonable to assume that at the studied pH range, nitroxyl radicals assembled onto the gold electrode undergo some combination of the stepwise and concerted mechanism instead of only the stepwise mechanism. In comparison with the reduction reaction of an aminobenzoquinone modified monolayer system, which includes many possible PCET pathways, there are only

three pathways in the reduction process of an ET/C_{18}TEMPO bilayer system. Specifically, these three pathways are proton transfer followed by electron transfer (pet), electron transfer followed by proton transfer (ept), and proton transfer and electron transfer occurring in the same kinetic step (cpet). The first two pathways are ascribed to the stepwise mechanism and the last one is a concerted mechanism. To determine the exact 1e1H transfer pathways of this ET/C_{18}TEMPO bilayer system from pH 5.8 to pH 9.5, the fitting between experimental results and theoretical model should be provided with a reasonable agreement. In doing so, all possible charge transfer routes are shown in Scheme 6.4, and the PCET reagent is represented by a nitroxyl radical group. For the sake of simplification, all standard transfer coefficients for single electron transfer step as well as concerted 1e1H transfer step are assumed to be 0.5. For the ept and pet pathways in the stepwise mechanism (Scheme 6.4a), the independent parameters include two standard rate constants (electron transfer steps), two standard formal potentials (electron transfer steps), and two acid dissociation constants (proton transfer steps). Based on the Nernst equation, the two standard formal potentials involved, $E_3^{0/}$ and $E_2^{0/}$, are related to each other and the induced expression of apparent formal potential also includes the two acid dissociation constants (see Chapter 4 for details). As for the two acid dissociation constants, the initial values used in the fitting procedure are the same as the reported values of TEMPO measured in aqueous solution system[14;16;20-22]. Scheme 6.4b shows the concerted 1e1H mechanism, in which water is assumed to be the proton donor and OH^- is the corresponding proton acceptor with an inherent acid dissociation constant equal to 14 for the sake of simplicity. Meanwhile, the formation constants $K_{I,j}$ and $K_{II,j}$ describing the intermediates were both assumed as 1. The discussion now can be limited to the process outlined by the dotted line in Scheme 6.4b, where the independent parameters are one standard rate constant $k_{s,cpet}$, and one standard formal potential E_{cpet}^0. Similar to the stepwise mechanism, $k_{s,cpet}$ is assumed to be $1s^{-1}$, and as discussed in Chapter 5, E_{cpet}^0 can be calculated from other parameters and thus isn't

independent. It is interesting to note that the fitting for an ET/C_{18}TEMPO bilayer system requires only six independent parameters, which is much less than the nineteen independent parameters for the analysis of an aminobenzoquinone modified monolayer system.

a)

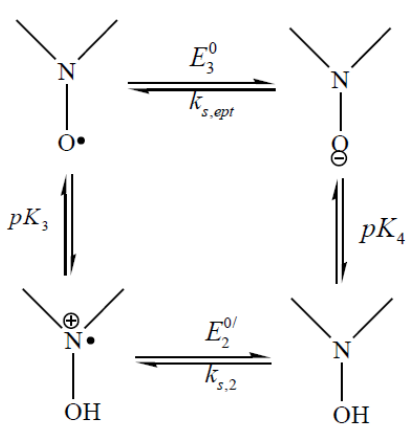

b)

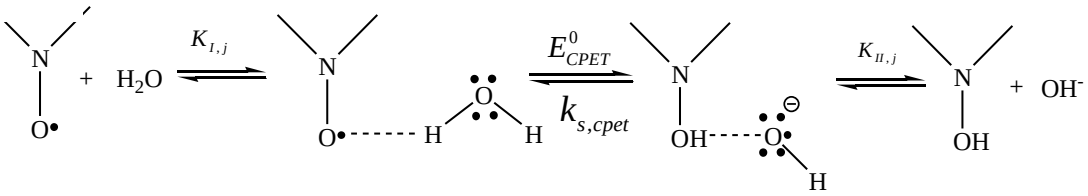

Scheme 6.4: Schematic view of the one proton coupled one electron transfer reaction for a nitroxyl radical group, a) stepwise mechanism; b) concerted mechanism.

The analytical expressions for both the apparent formal potential and the apparent rate constant for the stepwise and the concerted mechanism can be simply obtained from the theoretical discussion in Chapters 4 and 5.

$$E_{app}^{0/} = E_3^{0/} + \frac{RT}{F}\ln\left(\frac{1+\left[H^+\right]/K_4}{1+\left[H^+\right]/K_3}\right) \tag{6.1}$$

$$k_{app}^{c} = \frac{k_{s,3}\exp(-\alpha_3 f\eta_3) + k_{s,2}\dfrac{[H^+]}{K_3}\exp(-\alpha_2 f\eta_2) + k_{s,cpet}[HZ]\exp(-\alpha_{cpet} f\eta_{cpet})}{1+\dfrac{[H^+]}{K_3}} \tag{6.2a}$$

$$k_{app}^{a} = \frac{k_{s,3}\frac{K_4}{[H^+]}\exp[(1-\alpha_3) f\eta_3] + k_{s,2}\exp[(1-\alpha_2) f\eta_2] + k_{s,cpet}[Z^-]\exp[(1-\alpha_{cpet}) f\eta_{cpet}]}{1+\frac{K_4}{[H^+]}} \quad (6.2b)$$

The apparent standard rate constant should be strongly dependent on the charge transfer pathway, and the expressions for the cathodic and anodic reaction (1e1H) are shown in Eqn. (6.2a) and (6.2b). In comparison with those previously derived for an exclusively stepwise mechanism, Eqns. (6.2a) and (6.2b) include new terms for the concerted 1e1H pathway. The experimental, pH dependent, apparent formal potentials and apparent standard rate constants were fit to Equations (6.1) and (6.2) and the results are shown in Fig. 6.8. The fitting of apparent formal potential requires three independent parameters from Equation (6.1) and it shows reasonable fitting behavior as shown in Figure 6.8a, while the fitting for the apparent standard rate constants as a function pH shows more scatter (Figure 6.8b). This relative worse fitting behavior for apparent standard rate constant may be caused by the instability of this experimental system, which make the data collection of the apparent standard rate constants for this bilayer system not as accurate as that for the aminobenzoquinone modified monolayer system, even though the required independent parameters for this fitting is much less. The fit values of standard rate constants, standard formal potential and acid dissociation constants are shown in Table 6.1. In comparison with the values measured in aqueous solution, these obtained values for the surface system don't show remarkable changes. The fitting for acid dissociation constants indicate that it is easier to get protonated for both nitroxyl radical and its reduced form grafted onto the gold electrode surface other than those in aqueous solution, and this can be explained by the electrostatic force since the gold electrode may be treated as a source of electrons attracting positive charge of protons. More accurate analysis is hard to perform, especially when it involves the dramatic change in the chemical structures from TEMPO to ET/C_{18}TEMPO hybrid. Generally it can be concluded that these values are reasonable comparing with the initial values and thus can be used for the determination of charge transfer pathways based on Equation (6.3), which are easily derived from the method reported in Chapter 4.

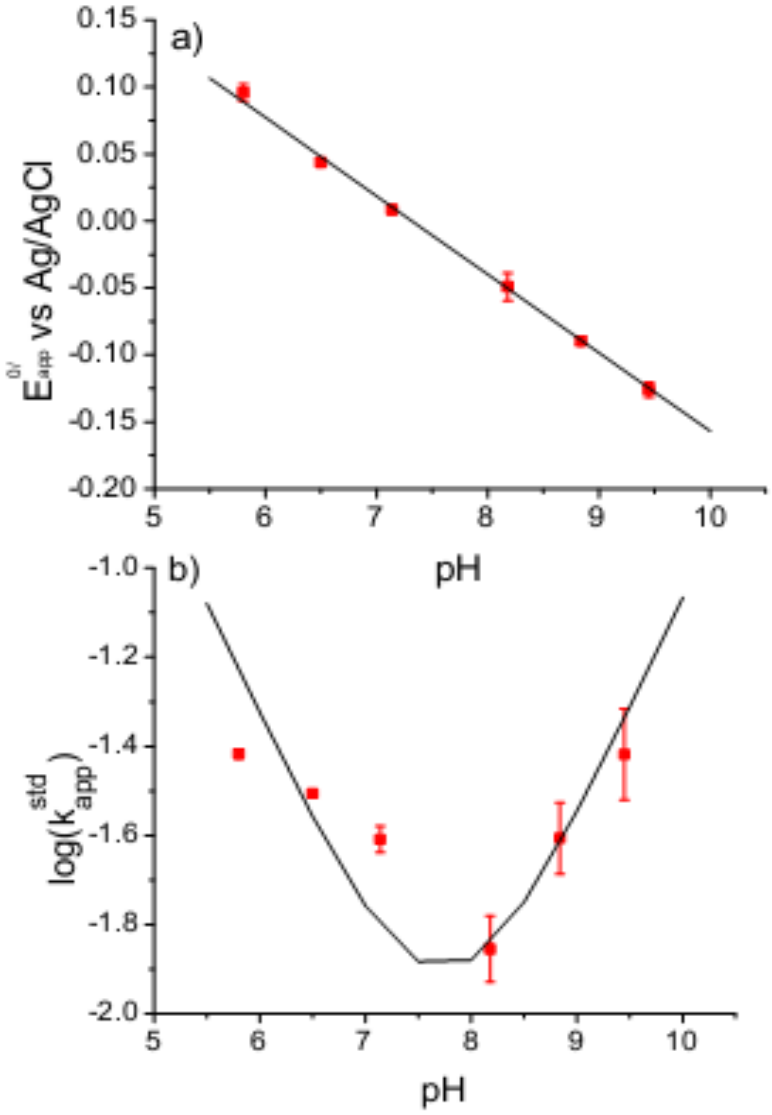

Figure 6.8: Apparent formal potential (a) and apparent standard rate constant (b) for the ET/C_{18}TEMPO bilayer system as a function of pH. Points with error bars are experimental values and solid curve was obtained from fitting analysis.

Table 6.1: Initial and resulting best-fit parameters for acid dissociation constants, standard formal potentials and standard rate constants for the TEMPO 1e1H redox system.

Parameter	Initial Value	Fit Result
pK_3	-1.0	2.45
pK_4	15.0	16.0
$E_3^{0\prime\,(a)}$	-0.213	-0.511
$k_{s,2}^{(b)}$	1	3.25
$k_{s,3}^{(b)}$	1	1
$k_{s,cpet}^{(b)}$	1	0.56

(a) V vs Ag/AgCl

(b) s^{-1}

The transfer pathways of 1e1H transfer in an ET/C_{18}TEMPO bilayer system can be determined from Eqns. (6.3a), (6.3b) and (6.3c), and the resulting pathways in the investigated pH range are shown in Figure 6.9. As shown, there is no contribution of ept pathway at the investigated pH range. At relatively low pH, the nitroxyl radical gets reduced to the hydroxylamine in a stepwise fashion, i.e. it first accepts one proton following which the protonated radical accepts one electron. With decreasing electrolyte acidity the kinetic analysis indicates that the electron tends to transfer in concert with the proton. This reveals that the concerted pathway begins to dominate the charge transfer pathway with increasing pH. The transition between pet and cpet occurs around pH 8, which corresponds to the lowest apparent standard rate constant (see Figure 6.9). It has been shown in both theory and experiment that for systems that undergo 1e1H PCET transfer, a large pK_a difference between the oxidized and reduced halves of the redox couple leads to favoured concerted 1e1H pathways.

$$Path_{ept} = \frac{k_{s,3}\exp\left(-\alpha_3 f\eta_3\right)}{k_{s,3}\exp\left(-\alpha_3 f\eta_3\right)+k_{s,2}\dfrac{[H^+]}{K_3}\exp\left(-\alpha_2 f\eta_2\right)+k_{s,cpet}[HZ]\exp\left(-\alpha_{cpet} f\eta_{cpet}\right)} \quad (6.3a)$$

$$Path_{pet} = \frac{k_{s,2}\dfrac{[H^+]}{K_3}\exp\left(-\alpha_2 f\eta_2\right)}{k_{s,3}\exp\left(-\alpha_3 f\eta_3\right)+k_{s,2}\dfrac{[H^+]}{K_3}\exp\left(-\alpha_2 f\eta_2\right)+k_{s,cpet}[HZ]\exp\left(-\alpha_{cpet} f\eta_{cpet}\right)} \quad (6.3b)$$

$$Path_{cpet} = \frac{k_{s,cpet}[HZ]\exp\left(-\alpha_{cpet} f\eta_{cpet}\right)}{k_{s,3}\exp\left(-\alpha_3 f\eta_3\right)+k_{s,2}\dfrac{[H^+]}{K_3}\exp\left(-\alpha_2 f\eta_2\right)+k_{s,cpet}[HZ]\exp\left(-\alpha_{cpet} f\eta_{cpet}\right)} \quad (6.3c)$$

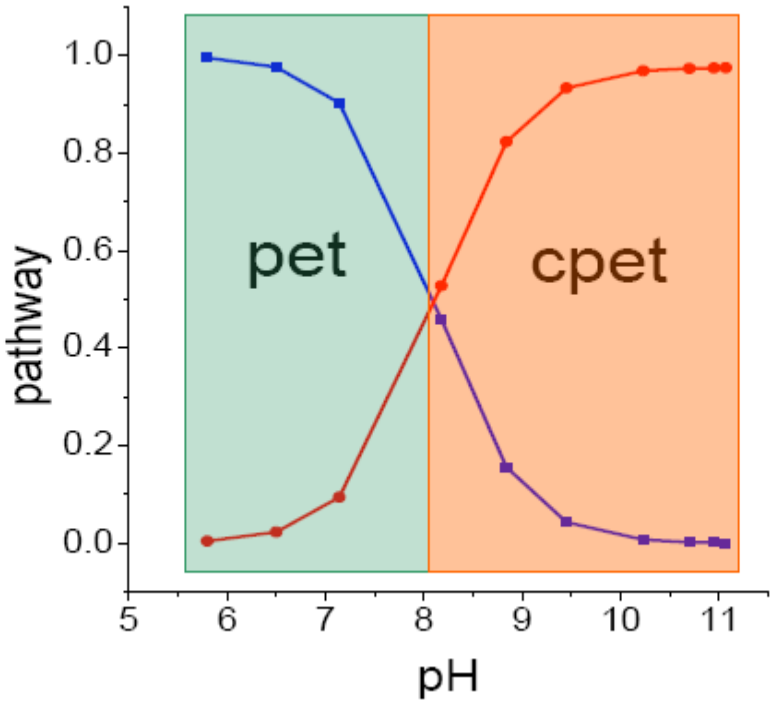

Figure 6.9: Charge transfer pathways as a function of pH for the reduction reaction of an ET/C_{18}TEMPO bilayer system.

6.5 Conclusions

Analytical procedures have been provided in the last chapters to determine the charge transfer mechanism of an electrochemical PCET reaction. An aminobenzoquinone modified monolayer system has been prepared and then used as a

model system in experiment. The relationship between thermodynamic parameters, kinetic parameters and PCET mechanisms from the aspect of theoretical model can offer insight in designing new systems with the pre-requested mechanism. To follow the above idea, TEMPO, as a PCET reagent showing the potential concerted mechanism from its thermochemistry date was successfully modified onto electrode surfaces. Superficially, it is a much simpler system with fewer fitting parameters. The decrease in complexity should help make it possible to see contributions from the concerted pathway. Furthermore, on consideration of thermodynamic concepts there is further justification that TEMPO reduction may include concerted contributions.

An ET/C_{18}TEMPO bilayer system has been proved to be experimentally accessible in providing pH dependent apparent formal potentials and apparent standard rate constants. However, one weakness of this system is its instability, which induces some uncertainty in the experimental results, especially when measuring the apparent standard rate constant. Based on the fitting between apparent formal potential, apparent standard rate constant and theoretical model for the associated concerted and stepwise mechanism, the charge transfer pathways in this 1e1H case were determined and found out to change from pet to cpet with increasing pH under the assumption of water as the proton donor. Mechanistic studies of electrochemical 1e1H transfer in the TEMPO modified bilayer system indicate that the thermochemical data did offer insight into the charge transfer mechanism since the pK_as of TEMPO can predict the possible existence of concerted mechanism in this bilayer system. This strengthens the principle of designing the purpose-built PCET systems from the thermochemistry data of the related PCET reagents.

In this chapter, preliminary analysis on the 1e1H reduction reaction of TEMPO modified electrode has been provided. Due to its instability, an ET/C_{18}TEMPO bilayer system can’t be fully discussed as much as an aminobenzoquinone modified monolayer system. A stable TEMPO modified electrode with the well-defined voltammogram will be required for the further study, to do so, a nitroxyl radical modified monolayer system using delocalized bridge (e.g. oligo(phenylene ethynylene) instead of saturated bridge (e.g. alkane) should be suggested to be built in

the future. It was found out that for the quinone modified monolayer on gold electrode systems that the charge transfer reaction is much faster when the quinone is attached via a delocalized oligo(phenylene ethynylene) bridge in comparison with a saturated alkane chain[33].

Reference List

(1) Zhang, W.; Rosendahl, S. M.; Burgess, I. J. *J.Phys.Chem.C* **2010**, *114*, 2738-2745.

(2) Zhang, W.; Burgess, I. J. *Phys.Chem.Chem.Phys.* **2011**, *13*, 2151-2159.

(3) Anxolabehere-Mallart, E.; Costentin, C.; Policar, C.; Robert, M.; Savéant, J. M.; Teillout, A. L. *Faraday Discuss.* **2011**, *148*, 83-95.

(4) Warren, J. J.; Tronic, T. A.; Mayer, J. M. *Chem.Rev.* **2010**, *110*, 6961-7001.

(5) Stubbe, J.; Nocera, D. G.; Yee, C. S.; Chang, M. C. Y. *Chem.Rev.* **2003**, *103*, 2167-2202.

(6) Feher, G.; Allen, J. P.; Okamura, M. Y.; Rees, D. C. *Nature* **1989**, *339*, 111-116.

(7) Barber, J. *Inorg.Chem.* **2008**, *47*, 1700-1710.

(8) Berry, E. A.; Guergova-Kuras, M.; Huang, L. s.; Crofts, A. R. *Annu.Rev.Biochem.* **2000**, *69*, 1005-1075.

(9) Mayer, J.; Rhile, I.; Larsen, F.; Mader, E.; Markle, T.; DiPasquale, A. *Photosynth.Res.* **2006**, *87*, 3-20.

(10) Okamura, M. Y.; Paddock, M. L.; Graige, M. S.; Feher, G. *Biochim.Biophys.Acta* **2000**, *1458*, 148-163.

(11) Liu, F.; Concepcion, J. J.; Jurss, J. W.; Cardolaccia, T.; Templeton, J. L.; Meyer, T. J. *Inorg.Chem.* **2008**, *47*, 1727-1752.

(12) Feher, G.; Allen, J. P.; Okamura, M. Y.; Rees, D. C. *Nature* **1989**, *339*, 111-116.

(13) Ingold, K. U. *Chem.Rev.* **1961**, *61*, 563-589.

(14) Kato, Y.; Shimizu, Y.; Yijing, L.; Unoura, K.; Utsumi, H.; Ogata, T. *Electrochim.Acta* **1995**, *40*, 2799-2802.

(15) Baur, J. E.; Wang, S.; Brandt, M. C. *Anal.Chem.* **1996**, *68*, 3815-3821.

(16) Fish, J. R.; Swarts, S. G.; Sevilla, M. D.; Malinski, T. *J.Phys.Chem.* **1988**, *92*, 3745-3751.

(17) Mahoney, L. R.; Mendenhall, G. D.; Ingold, K. U. *J.Am.Chem.Soc.* **1973**, *95*, 8610-8614.

(18) Mader, E. A.; Manner, V. W.; Markle, T. F.; Wu, A.; Franz, J. A.; Mayer, J. M. *J.Am.Chem.Soc.* **2009**, *131*, 4335-4345.

(19) Rappoport, Z. L. J. F. *The Chemistry of Hydroxylamines, Oximes and Hydroxamic Acids*; Wiley: West Sussex, U.K.: 2009; pp 705-750.

(20) Israeli, A.; Patt, M.; Oron, M.; Samuni, A.; Kohen, R.; Goldstein, S. *Free Radic.Biol.Med.* **2005**, *38*, 317-324.

(21) Sen, V. D.; Golubev, V. A. *J.Phys.Org.Chem.* **2009**, *22*, 138-143.

(22) Janiszewska, A. M.; Grzeszczuk, M. *Electroanalysis* **2004**, *16*, 1673-1681.

(23) Finklea, H. O.; Madhiri, N. *J.Electroanal.Chem.* **2008**, *621*, 129-133.

(24) Malec, A. D.; Wu, D. G.; Louie, M.; Skolimowski, J. J.; Majda, M. *Langmuir* **2004**, *20*, 1305-1310.

(25) Wu, D. G.; Malec, A. D.; Head-Gordon, M.; Majda, M. *J.Am.Chem.Soc.* **2005**, *127*, 4490-4496.

(26) Glandut, N.; Malec, A. D.; Mirkin, M. V.; Majda, M. *J.Phys.Chem.B* **2006**, *110*, 6101-6109.

(27) Johnson, M. J.; Majmudar, C.; Skolimowski, J. J.; Majda, M. *J.Phys.Chem.B* **2001**, *105*, 9002-9010.

(28) Johnson, M. J.; Anvar, D. J.; Skolimowski, J. J.; Majda, M. *J.Phys.Chem.B* **2000**, *105*, 514-519.

(29) Helm, C. A.; Israelachvili, J. N.; McGuiggan, P. M. *Biochemistry* **1992**, *31*, 1794-1805.

(30) Kwiat, M.; Elnathan, R.; Kwak, M.; de Vries, J. W.; Pevzner, A.; Engel, Y.; Burstein, L.; Khatchtourints, A.; Lichtenstein, A.; Flaxer, E.; Herrmann, A.; Patolsky, F. *J.Am.Chem.Soc.* **2011**, *134*, 280-292.

(31) Donaldson, S. H.; Lee, C. T.; Chmelka, B. F.; Israelachvili, J. N. *Proc.Natl.Acad.Sci.* **2011**, *108*, 15699-15704.

(32) Kishoka, S. Y.; Umeda, M.; Yamada, A. *Analytical Sciences* **2002**, *18*, 1379-1381.

(33) Trammell, S. A.; Lowy, D. A.; Seferos, D. S.; Moore, M.; Bazan, G. C.; Lebedev, N. *J.Electroanal.Chem.* **2007**, *606*, 33-38.

(34) Hong, H. G.; Park, W.; Yu, E. *J.Electroanal.Chem.* **1999**, *476*, 177-181.

Chapter 7: Summary and Conclusions

7.1 Summary of Thesis

Owing to their importance in applications like energy-harvesting and fundamental interests, mechanistic studies of electrochemical PCET reactions have attracted intensive attention for several years. Nevertheless, this field is still very young, and there remain lots of challenges in both theory and experiment. The contributions to this thesis in furthering the understanding of electrochemical PCET reactions can be summarized under two headings: 1) the development of analytical procedures for fabricating and characterizing a multi-electron, multi-proton transfer monolayer system with the stepwise mechanism (Chapters 3 and 4)[1;2] and 2) outlining the relationship between thermochemical characteristics and PCET mechanism (Chapter 5 and 6)[3].

In order to extend the understanding of quinone and its derivatives in biological reactions, an aminobenzoquinone modified monolayer was prepared and used as a model system for mechanistic studies of electrochemical multiple electron and proton transfer. This model system shows nearly ideal electrochemical behavior and high stability and it can be characterized using non-destructive electrochemical techniques like cyclic voltammetry and chronocoulometry (Chapter 3). The dependence of the observed apparent standard formal potential on electrolyte pH shows two linear regions and indicates that this monolayer system undergoes a 2e3H transfer under acidic conditions and 2e2H transfer in neutral to basic solutions. In order to understand the kinetics of this system, apparent rate constants as well as apparent transfer coefficients at different pH have been measured by employing both cyclic voltammetry and chronocoulometry and the resulting graph of apparent standard rate constant versus pH shows a distorted “W” curve, which is different from the theoretical simulation results published elsewhere for the 2e2H transfer of benzoquinone freely dissolved in aqueous solution.

In Chapter 4, a 12-member square scheme has been built, theoretically treated, and analyzed to fully describe the 2e3H PCET reaction of the aminobenzoquinone modified monolayer system. This scheme basically shows all the possible single electron transfer and single proton transfer steps. An assumption was made that only the stepwise mechanism is considered for this monolayer system, which greatly simplifies the discussion of the kinetic data. It has been demonstrated through analysis of the scheme that the independent parameters for the discussion of the aminobenzoquinone modified monolayer system at the investigated pH are nine acid dissociation constants, six standard formal potentials and six standard rate constants. Analytical expressions for the apparent standard rate constant, apparent formal potential and apparent standard transfer coefficient as a function of pH have been derived in terms of these fundamental parameters.

The significance of these analytical expressions for the thesis is the capability to test experimentally accessible parameters (e.g. apparent rate constants, apparent formal potentials) to test the validity of the proposed model. From the fitting between experimental results described in Chapter 3 and the analytical expressions from the 12-member scheme, the thermochemical data (acid dissociation constants, standard formal potentials) and kinetic data (standard rate constants) of this aminobenzoquinone modified monolayer system are obtained and thus the charge transfer pathways can be determined. In addition, the derived charge transfer pathways of benzoquinone modified on the gold electrode surface have been proved to be similar to the pathways of benzoquinone in aqueous buffer solution. An analytical procedure has been provided and successfully applied for the mechanistic study of an aminobenzoquinone modified monolayer system, and it can expected that this method can work for other electrochemically driven multi-electron, multi-proton transfer reactions.

In general, the controlling parameters of stepwise mechanism versus concerted mechanism can be classified into two aspects: thermodynamic parameters, namely acid dissociation constants and standard formal potentials; and kinetic parameters,

namely standard rate constant and standard transfer coefficients. Despite the efforts of researchers such as Costentin and his colleagues, the relationship between the relative magnitudes of these controlling parameters and electrochemical PCET mechanism (stepwise versus concerted) remains the subject of considerable debate. Chapter 5 refined and extended Costentin's work, especially on the influence of thermodynamic parameters on both stepwise and concerted mechanisms. The measurement of apparent kinetic isotope effects has often been used by electrochemical experimentalists as a meaningful metric to differentiate the contributions of stepwise concerted charge-transfer paths to electrochemical PCET experiments. However, the correlated theory behind the values of apparent KIE was not fully considered prior to this thesis. The main concern of Chapter 5 was to probe this correlated theory and determine the validity of prior conclusions that had been reached based on observed kinetic isotope effects in PCET systems. In addition, for the first time, values of apparent KIE, which were measured from the aminobenzoquinone modified monolayer system, were successfully explained in terms of purely thermodynamic contributions. An important result that was established in Chapter 5 was demonstration that both the stepwise and concerted mechanisms can give rise to an observed kinetic isotope effect in the experimentally measurable apparent standard rate constants. This fact has never been illustrated in previous studies of electrochemical PCET and challenges the notion that strong kinetic dependence upon isotopic variation of the solvent indicates an operative concerted mechanism. In other words, the apparent KIE should not be used as the primary criterion to distinguish the stepwise mechanism from the concerted mechanism. However, the measurement of apparent KIE can still be used as an experimental tool to probe the PCET mechanism but it requires more in-depth consideration and further experiments where the nature of the proton acceptor/donor are varied.

The conditions that favour the concerted mechanism can be determined by careful consideration of the analytical expressions provided in Chapter 5. One of the conditions is a large pK_a difference upon oxidation/reduction in a 1e1H PCET

reaction. In an effort to correlate the theoretical prediction with experimental evidence, several means of fabricating a TEMPO modified electrode were described in Chapter 6. One of these systems, the ET/C_{18}TEMPO bilayer system, provided an accessible 1e1H transfer reaction although cyclic voltammetry studies demonstrated that it unfortunately suffered from poor stability. Nonetheless, experiments could be performed and after applying the same analytical procedure as that for the aminobenzoquinone modified monolayer system, this ET/C_{18}TEMPO bilayer system was shown to include a concerted 1e1H transfer pathway in high pH electrolytes. The instability of this bilayer prohibited the full determination of its PCET mechanism, and more work in designing a more robust TEMPO modified electrode will be required in the future.

Lastly, it should be noted that research devoted to determining the relationship between thermochemical data and PCET mechanism is still very far from complete and much more work, especially in the design and analysis of suitable experimental systems, needs to be performed. The final goal for the mechanistic study of PCET reaction should be that for any given PCET reagent, charge transfer pathways can be predicted from its structure and the corresponding environment. This thesis has made some important steps in this direction. It is hoped that the material described herein can spur further development in both theory and experiment as a means to build definitive and predictive models for coupled proton-electron transfer.

7.2 Scope of Future Research

This thesis has provided a semi-empirical and experimentally accessible model with implications for further research in electrochemical PCET reactions. For example, theoretical discussions on the relationship between thermodynamic parameters, kinetic parameters and charge transfer mechanisms should be extended from the very simple (and very rare in nature) 1e1H case to other more complicated cases such as 2e2H, 3e3H *etc* that are far more ubiquitous in nature. This is vitally important for applications of PCET to energy-harvesting applications since many

PCET reactions aren't simply one electron one proton transfer processes[4-11]. It is well known that the standard rate constant is dependent on many independent parameters such as reorganization energies and coupling factors[12-19], so the assumption that all standard rate constants in a multi-electron process are equal is clearly oversimplified. A more fundamental understanding of electrochemical PCET mechanism based on parameters such as reorganization energies and coupling factors instead of standard rate constant will be required in the future. In comparison with electrochemical PCET reaction (or heterogeneous PCET reaction), homogeneous PCET reactions have attracted more attention to date, most likely due to its occurrence in biological systems. However, electrochemical PCET are inherently more easily studied as they allow for systematic studies of charge-transfer rates as a function of a continuum of adjustable driving forces (i.e. application of electrochemical potentials). In the future, the models that are derived from electrochemical PCET will need to be successfully adapted to describe homogeneous PCET. These efforts would be entirely analogous to the adaption of Marcus theory for homogenous and electrode-driven electron transfer.

One big challenge in work such as that described in this thesis is the modification of the PCET center so that it can be attached to electrode surfaces. Compared with so many PCET reagents studied in aqueous solution or organic solvent systems, there have been very few reports of monolayer derived PCET systems. This imbalance should be corrected for both fundamental interest reasons and industrial applications reasons, especially for the design of electrocatalysts for important processes like water splitting. Previous experimental systems including this aminobenzoquinone modified monolayer system are basically to self-assembled monolayer technologies; thus there are still lots of unexploited techniques to prepare PCET modified electrode system. Since the 1970s[20;21], semiconductor materials have been explored as working electrodes for applications as solar cells, waste water remediation and energy storage and uncoupled electron transfer mechanism onto semiconductor electrode has been fully probed. Thus extension of PCET studies will be possibly accomplished and will

then largely enrich the field of semiconductor electrochemistry in fundamental understanding as well as technological purposes.

To sum up, the studies of PCET, as a fundamental physical chemical process, will continue to be one of hot topics in many research areas owing to its importance in fundamental interest and technological applications, especially in the field of energy conversion that contributed a lot in industry for economic interest. The contribution of this thesis to electrochemical PCET, which is regarded as an important subclass of PCET, is small but important in the development of fundamental interest of PCET studies, it as well offer insight to obtain new knowledge of the PCET process in theory and technical applications.

Reference List

(1) Zhang, W.; Rosendahl, S. M.; Burgess, I. J. *J.Phys.Chem.C* **2010**, *114*, 2738-2745.

(2) Zhang, W.; Burgess, I. J. *Phys.Chem.Chem.Phys.* **2011**, *13*, 2151-2159.

(3) Zhang, W.; Burgess, I. J. *J.Electroanal.Chem.* **2012**, *668*, 66-72.

(4) Barber, J. *Inorg.Chem.* **2008**, *47*, 1700-1710.

(5) Chen, Z.; Concepcion, J. J.; Jurss, J. W.; Meyer, T. J. *J.Am.Chem.Soc.* **2009**, *131*, 15580-15581.

(6) Cook, T. R.; Dogutan, D. K.; Reece, S. Y.; Surendranath, Y.; Teets, T. S.; Nocera, D. G. *Chem.Rev.* **2010**, *110*, 6474-6502.

(7) Gust, D.; Moore, T. A.; Moore, A. L. *Acc.Chem.Res.* **2009**, *42*, 1890-1898.

(8) Hammes-Schiffer, S. *Acc.Chem.Res.* **2009**, *42*, 1881-1889.

(9) Huynh, M. H.; Meyer, T. J. *Chem.Rev.* **2007**, *107*, 5004-5064.

(10) Liu, F.; Concepcion, J. J.; Jurss, J. W.; Cardolaccia, T.; Templeton, J. L.; Meyer, T. J. *Inorg.Chem.* **2008**, *47*, 1727-1752.

(11) Mayer, J.; Rhile, I.; Larsen, F.; Mader, E.; Markle, T.; DiPasquale, A. *Photosynth.Res.* **2006**, *87*, 3-20.

(12) Costentin, C.; Robert, M.; Savéant, J. M. *J.Electroanal.Chem.* **2006**, *588*, 197-206.

(13) Costentin, C.; Robert, M.; Savéant, J. M. *Acc.Chem.Res.* **2010**, *43*, 1019-1029.

(14) Costentin, C.; Robert, M.; Savéant, J. M. *Phys.Chem.Chem.Phys.* **2010**, *12*, 13061-13069.

(15) Ludlow, M. K.; Soudackov, A. V.; Hammes-Schiffer, S. *J.Am.Chem.Soc.* **2010**, *132*, 1234-1235.

(16) Marcus, R. A. *Can.J.Chem.* **1959**, *37*, 155-163.

(17) Marcus, R. A. *Annu.Rev.Phys.Chem.* **1964**, *15*, 155-196.

(18) Marcus, R. A. *J.Electroanal.Chem.* **1997**, *438*, 251-259.

(19) Venkataraman, C.; Soudackov, A. V.; Hammes-Schiffer, S. *J.Phys.Chem.C* **2008**, *112*, 12386-12397.

(20) Gerischer, H. *Journal of Electroanalytical Chemistry and Interfacial Electrochemistry* **1977**, *82*, 133-143.

(21) Gerischer, H. *Electrochimica Acta* **1990**, *35*, 1677-1699.